ACOUSTIC SCATTERING IN CIRCULAR CYLINDRICAL SHELLS: A MODAL APPROACH BASED ON A GENERALISED ORTHOGONALITY RELATION

A thesis submitted for the degree of Doctor of Philosophy

by

Ryan Michael Pullen

Department of Mathematics
College of Engineering, Design and Physical Sciences
Brunel University

Abstract

During the past 60 years fluid-structure interaction in a wide range of three dimensional circular cylinder problems have been studied. Initial problems considered a rigid wall structure which were solved using impedance model comparisons. Soon after, further solution techniques were used, such as computer simulation, transfer matrix methods and finite element techniques. However such problems were only valid for low frequencies when compared with experiments, this was because that did not include higher order modes. The importance of higher order modes was then established and studies have since included these modes. More recently, mode matching methods have been used to find the amplitudes of waves in structures comprising two or more ducts. This has been done with using an orthogonality relation to find integrals which occur from the application this method. This methodology is demonstrated in as background information and is applied to prototype problems formed of rigid ducts.

The rigid duct theory led to the consideration of elastic shells, of which several shell modelling equations were available from the vibration theory. In this thesis, the Donnell-Mustari equations of motion are used to model thin, elastic, fluid-loaded shells of circular cross-section. It is demonstrated that generalised orthogonality relations exist for such shells. Two such relations are found: one for shells subject to axisymmetric motion and one for shells subject to non-axisymmetric motion. These generalised orthogonality relations are new to the field of acoustics and are specific to shells modelled with the Donnell-Mustari equations of motion. The mode matching method is used to find the amplitudes of waves propagating in prototype problems and the generalised orthogonality relations are used to find integrals which occur through this method. Expressions for energy for all considered structure types are used to find the resulting energy for each prototype problem and results for equivalent problems are compared. In addition, verification of the resulting amplitudes is done by ensuring that the matching conditions are suitably satisfied.

It is anticipated that the method will have application to the understanding and control of the vibration of cylindrical casings such as those enclosing turbo-machinery. Another application of the method would be the tuning of cylindrical casings, such as those featured on car exhaust systems or HVAC (heating, ventilation and air conditioning) systems.

Contents

Chapter 1

Literature Review

In modern society the reduction of noise pollution is important as it has been proved to be detrimental to the health of humans and animals. A major source of outdoor noise pollution comes from the exhaust systems of motor vehicles. This motivates the study and design of systems which minimise the vibration of the structures and acoustic noise passing through them. Most exhaust systems are fitted with a silencer, which is typically a section with perforations that allow the emissions to dissipate into a surrounding chamber before exiting the system. Unwanted indoor noise can occur in heating, ventilation and air conditioning (HVAC) systems. These are systems that use waveguides to transport air in order to heat, ventilate or cool a room. The air is moved by a fan which can generate unwanted noise and additional noise can enter the waveguide from outside and propagate within. These waveguides often have rectangular cross sections but it is not uncommon for them to be circular. Consequently the study of the vibration and acoustic propagation in circular cylindrical shells is of continued interest to the field of engineering and applied mathematics. In particular the effects of discontinuities on propagating waves.

The simplest circular cylindrical structure is one with a rigid wall, which means it does not support vibrations and it does not absorb acoustic waves. One of the first studies involving acoustic scattering in a rigid, cylindrical duct was presented by Miles [1]. The research considered a plane wave propagating in an infinite, rigid, cylindrical duct and investigated the effect of evanescent modes formed by an abrupt change in radius. The radiation of the plane wave at the junction was determined by solving the boundary value problem for an analogous electrical system. The research derived the fundamental governing equations for acoustic propagation near a discontinuity and found a systematic method to derive expressions for the reflected and transmitted coefficients.

At much the same time, Levine and Schwinger [2] obtained an explicit solution for the reflection coefficient in a semi-infinite, rigid, cylindrical duct. The solution was found through an integral formulation using the Wiener-Hopf technique and the resulting reflection coefficient was evaluated numerically. The magnitude of reflection was compared against the dimensional radius of the duct and it was found that the amount of reflected

energy was increased for smaller duct radii. The results were valid for the range of the first dominant mode as the analysis was restricted to plane wave propagation.

The sound radiating due to a plane piston located at one end of a finite, rigid, open, cylindrical duct was investigated by Ingard [3]. The problem was solved by considering the effects on the acoustic pressure field at the open end of the duct. Higher order modes were included in the analysis. The radiation impedance and pressure distribution were presented together with an element analysis for equivalent impedance circuits. The calculations were verified by comparing results of those obtained from a cylinder closed by a rigid plate.

Karal [4] considered a zeroth order mode propagating in an infinite, rigid, cylindrical system and examined the analogous impedance introduced by an abrupt change of radius and by a constriction between two ducts. The impedance was found solving the boundary value problem for the analogous electrical systems and was plotted for different ratios of duct radii. The results showed that the constriction impedance was equivalent to the sum of the impedance for each discontinuity considered separately. The analysis was restricted to the use of volume flow (the amount of fluid that passes through the junction area per unit time) and therefore this research was valid only for very low frequencies.

The sound transmission at the sudden area of expansion formed by two semi-infinite sections of rigid, cylindrical duct was studied by Cummings [5]. The purpose of this work was to determine which of two velocity profiles was more suitable for predicting the reflection coefficient. The actual velocity profile was compared with a profile introduced by Ronneberger [6] which fills the entire cross-section of the larger duct and also compared with a velocity profile which maintains a cross section equal to the smaller duct. The results showed that of these two profiles, the reflection coefficient at an area expansion is predicted best when the velocity profile has a cross section equal to the smaller duct.

A method for evaluating elements of rigid, cylindrical, exhaust silencers with mean flow was studied by Munjal [7]. The aim was to develop an expression for the attenuation of the silencer. The work was formulated in terms of the convective pressure and convective mass velocity. Transfer matrices for seven geometric elements of a silencer were derived, these included a uniform duct (for which the transfer matrix is the identity matrix) and a sudden expansion/contraction of the duct radius. The transfer matrices were formed from basic relations of energy, mass and momentum. It was observed that some of the transfer matrices were similar to the ones obtained from zero mean flow with stationary variables.

The four poles of a transfer matrix for a rigid, cylindrical silencer were found by Peat [8]. The poles are essentially elements of a matrix which represent measured values before and after the silencer. This work required the solution to three duct geometries: a sudden decrease in radius, an expansion chamber and an intake duct. The poles for each geometry were determined by using the finite element method with two sets of boundary

conditions that identified the required region of the duct. It was shown that there was a good agreement with the results for the sudden decrease in radius and for the expansion chamber.

The transfer matrix method was used by Munjal and Prasad [9] to study the propagation of a plane wave in the presence of hot mean flow inside an infinite, rigid, uniform duct. The variation of temperature inside the duct was described by a decreasing linear gradient. A four-pole transfer matrix was formed by matching acoustic pressure and acoustic volume velocity and was solved by use of Green's function. The transfer matrix was shown to yield the known transfer matrices for the following simple cases: no mean flow and no temperature gradient, mean flow and no temperature gradient and linear temperature gradient with no mean flow. For the special case of linear temperature gradient with no mean flow it was noted that it did not match the matrix obtained by Young [10]. Investigation into Young's work found that the wave equation used was the basic equation with only sound speed as a variable, which implicity assumed that the medium density would remain constant with temperature.

The transfer matrix method was used by Peat [11] for a rigid, cylindrical, uniform duct with a linear temperature gradient. This paper identified that the four-pole transfer matrices presented by Munjal and Prasad [9] had wrongly omitted terms involving the gradient of mean density and velocity along the duct. The formation of the four-pole transfer matrix by Peat was done by analysis into the mean flow of the fluid and the resulting matrix differed to those in earlier literature by the first order terms of the temperature gradient. The method required the solution to the governing equation and it was shown to be simpler than the Green's function approach. The results were validated against experimental measurements and it was found that there was little practical benefit to modelling temperature variations in further detail.

Expressions for the four-pole matrix for a rigid, circular cylindrical duct of mean temperature gradient was presented by Sujith [12]. These expressions were valid for large temperature gradients, whereas transfer matrices in earlier literature were valid only for small temperature gradients. The expressions were derived for both a linear and an exponential temperature profile. The paper serves as a useful benchmark for checking program results, however its noted that this paper contains errors in the signs used in the method.

Cargill [13] considered a cylindrical duct with a wall property changing from rigid to vortex sheet and investigated its effect on a propagating plane wave. This work used the Wiener-Hopf technique to include identified higher order modes and it gave an explicit formula for the far field radiation and the reflected sound. It was shown how the presence of a mean flow causes a reduction in the reflection coefficient near the duct axis. The results were valid to the second order in the ratio of duct diameter to wavelength and were shown to be in excellent agreement with the numerical computations stated by Munt [14].

It was noted that to proceed beyond the second order approximation would be of little benefit to the physical understanding and would also produce very complicated formulae.

The effect of higher order modes produced by a rigid-walled expansion chamber was studied by Ih and Lee [15]. This work developed an analytical solution to the problem by modelling it as a lossless, piston-driven rigid duct. The pressure at the inlet was expressed as a combination of the inlet volume velocity and the impedance of the chamber. A general expression for the output pressure was found for the whole chamber by using a Fourier-Bessel expansion. The characteristics of the chamber were described using four pole-parameters to show the plane wave interaction with transverse waves at different points. The results of the study were found to be in good agreement to those found using the four-pole parameters and also with the results found by previous authors. In addition, the four-pole parameters were also used to estimate the transmission loss for an expansion chamber with common centres and with an offset inlet and outlet, the results were found to be in good agreement with past experiments.

Noise attenuation in a rigid, expansion chamber with a side inlet and end outlet was studied by Yi and Lee [16]. The influences of higher order modes were investigated using a theoretical method in which the chamber is considered as a piston driven circular cylinder. Also the characteristics of the chamber where investigated with respect to the location of the inlet or outlet and the length of the chamber. The theory was verified with various experiments and it was found that the theoretical method agrees with the experimental results for the low frequency range, but not for the case where the end outlet was offset. The transmission loss was estimated by using the derived four pole parameters which used the same method as [15].

The higher order modes generated at a discontinuity between two sections of rigid, cylindrical duct were investigated by Peat [17]. An equivalent impedance circuit was used to identify an evanescent mode and assess whether to include it. This work considered the effects of superimposed mean flow and the effects of high frequencies up to the cut off. The results found that mean flow effects were negligible but the variation of impedance with frequency was necessary.

Lawrie and Abrahams [18] discussed the radiation of sound waves formed between two rigid, coaxial, cylindrical ducts. The ducts were semi-infinite with the left-hand duct having a radius less than the right-hand one and an arbitrary gap was formed between them. Forcing was by a wave incident towards the gap and the resulting reflected and transmitted wave fields were calculated. Two approximate solutions were presented, one valid for small gaps or a large diameter ratio and the other valid for when the dimensionless gap is much less than 1. The first method introduced a new type of entire function, this was expanded to give solutions valid for small gaps between cylinders or for large ratio diameters. The second approximate solution method involving a modified Wiener-Hopf technique which assumed a matrix form. It was found that these two

methods were only suitable for a small minority of cases as the integral representation of the factors presented numerical difficulties due to singularities. The final solution of the Wiener-Hopf problem was represented as a double integral which made numerical computation extremely slow.

Evanescent modes in rigid, cylindrical ducts with a sudden expansion and with a sudden contraction were analysed by Sahasrabudhe and Munjal [19]. This research derived a simple, accurate and comprehensive expression for the Karal correction factor. This was found by using three-dimensional finite element analysis and the resulting correction factor became a function of radius ratio, frequency and offset distance. The finite element analysis was also used to verify the results of earlier researchers such as Ingard [3], Karal [4] and Peat [17]. It was found that for smaller ducts, the results obtained by the finite element method were of similar order to those obtained by analytical methods. From this it was concluded that it is acceptable to model only plane wave motion in small ducts. The revised Karal correction factor was found to be useful in indicating the accuracy of plane wave analysis for frequencies up to the cut-on for the first higher order mode. However it was noted that for such analysis to be performed on an expansion chamber, the model was required to have chambers of sufficient length.

An appropriate method of modelling automotive dissipative silencers was identified by Kirby [20]. This work looked at the computational efficiently of two numerical methods compared with equivalent analytic methods. The numerical methods considered were a mode matching method and a hybrid finite element method. The system comprised a perforated cylindrical shell contained within an expansion chamber lined with a porous material. The walls of the inlet and outlet ducts and the expansion chamber were assumed to be rigid. It was found that there was an excellent agreement between the results of the analytic and numerical method provided a sufficient number of propagating modes were retained. The numerical mode matching method was proved to be the fastest method, significantly outperforming the equivalent analytic technique. In addition, it was found that the hybrid finite element method was as fast as the equivalent analytic technique. This research showed that both numerical techniques deliver fast and accurate predictions and are capable of outperforming equivalent analytic methods for a dissipative silencer.

The re-expansion method was used by Homentcovschi and Miles [21] to analyse wave scattering at discontinuities of rigid cylindrical ducts. This was done by expanding the velocity in the plane of the discontinuities in terms of functions which accounted for singularities at the edges. The research investigated two types of configuration: a cylindrical duct with an abrupt change of radius and a cylindrical expansion chamber. The effect of changing the radius of the duct and the obstacles were investigate and the resulting reflection and transmission amplitudes for the first mode were presented. In addition, an explicit formula for the transmission loss coefficient was formed.

A method for finding the reflection and transmission amplitudes for plane waves in

discontinuous piping systems was presented by Föller and Polifke [22]. This method considers a large eddy simulation (a mathematical model used for turbulence [23]) with a single change of radius in a cylindrical duct. The simulation externally excites acoustic waves at either end of the discontinuity simultaneously. The interactions between acoustic waves are captured in detail and the problem is solved to find the amplitudes of the waves scattered at the discontinuity. The results of the simulation are compared to many analytic methods and show good agreement with the experimental data.

Perrey-Debain *et al* [24] dealt with strategies for efficiently computing the propagation of sound waves in ducts containing acoustic cavities. A numerical technique was devised that exploits the benefit of the finite element and boundary element method in order to predict the sound transmission through such systems. This was done by creating a numerical impedance matrix to compute a set of eigenmodes within the cavity. The matrix connects the pressure and the acoustic velocity at the duct wall interface. The acoustic pressure in the main duct could then be expressed as its integral representation. An appropriate Green's function was used to restrict the integration to the duct-cavity interface alone. This allowed for the accurate computation of the scattering matrix for a system that has a complexity that increases slightly with frequency.

For flexible shells, the motion of the shell has an effect on waves that are internally propagating. Therefore appropriate equations of motion which describe the flexible wall should be used. There are several proposed theories for describing cylindrical shell vibration, many of which are compared by Leissa [25].

Burroughs [26] derived an equation for the acoustic radiation from a point-driven cylindrical shell reinforced with doubly periodic ring supports. The motion of the shell was based on the thin shell equations provided by Kennard [27] and the fluid loading interactions between the ring supports were analysed. The predictions were compared with measured data collected from a finite experimental model with similar properties and the results showed good agreement.

A semi-infinite flexible shell rigidly bonded to a hollow cylindrical shell surrounded by an inviscid, compressible fluid with plane wave forcing was investigated by Lawrie [28]. A mixed-boundary value problem was formed to described the coupled motion between the fluid and the flexible shell. An exact solution was formulated in terms of contour integrals by using the Wiener-Hopf technique. The limit of heavy fluid loading and long waves reduced the kernel to that of a semi-infinite rigid duct obtained by Levine and Schwinger [2].

Lawrie [29] considered an infinite flexible cylindrical shell where the shell had a finite number of ring constraints and the system was totally surrounded by an inviscid compressible fluid. The vibrations of the flexible shell were modelled using the Donnell-Mushtari equations of motion as stated by Junger and Feit [30]. A single ring constraint was considered first and the exact solution was found by forming the boundary value

problem and solving the resulting linear system. For two ring constraints the problem was expressed as a symmetric and antisymmetric problem, which led to the uncoupling of terms, the exact solution could then be found by solving the two resulting linear systems.

The time-dependant pressure for a fluid filled, finite, open ended, cylindrical shell was investigated by Stepanishen and Tougas [31]. A piston source located at the inner closed end of the shell was used to force the fluid in the system. The piston was considered to have a gated sine wave acceleration which followed a spatial profile. The solution was found by using a time-space Green's function to form a boundary value problem. The solution of the boundary value problem produced a transfer function that described the duct. This transfer function was then used in another transfer function that described the duct outlet in order to determine the resulting output sound field.

A modified Wiener-Hopf technique was used by Zhang and Abrahams [32] to examine the sound radiated from a finite fluid-loaded finite cylindrical shell. The shell was freely submerged in a compressible stationary fluid and its vibrations were modelled using the Donnell-Mushtari equations of motion for a thin, cylindrical shell. Fluid forcing was formed by an axisymmetric ring force located between the open ends of the shell.

An infinite flexible cylindrical shell immersed in a compressible fluid was considered by Skelton [33]. The shell displacement was found as the sum of circumferential modes evaluated by considering the asymptotic limit of heavy exterior fluid-loading. The asymptotic expression were trigonometric functions of the shell and fluid parameters and they showed excellent agreement to numerical results for a wide frequency range.

The Donnell-Mushtari equations of motions were used by Skelton [34] to model a finite cylindrical shell, reinforced by two internal rigid plates. Circumferential mode expansion was used to obtain numerical results of the scattering caused by the reaction force of the internal plates. The internal rigid plates were firstly considered to intersect at the longitudinal axis and then to lie parallel to the longitudinal axis and each other. The predictions showed good agreement with the results obtained by numerical evaluation of the infinite sums for the reaction forces. They also showed that the presence of internal rigid plates in an flexible shell have a significant effect on the scattered sound field due to the additional constraints.

Brambley and Peake [35] considered the scattering of waves formed by a sudden change of shell boundary, from a rigid cylindrical duct to an flexible cylindrical shell. The flexible cylindrical shell was modelled using Flügge's equations and forcing was by an inbound acoustic wave in the rigid duct. The solution was given analytically as a sum of shell modes.

The low frequency behaviour and radiated sound of a submarine hull vibrating axisymmetrically was considered by Caresta and Kessissoglou [36]. The hull was modelled as a finite flexible cylindrical shell closed at each end by a rigid plate, the shell was reinforced with internal bulkheads and ring-stiffeners. The vibrational behaviour of the

cylindrical shell was defined by Flügges equations as they were seen to be more accurate for low frequency vibrations and a smeared approach was used to model the ring-stiffeners. Because of the reinforcements the pressure of the system was reduced to that due to the radial displacement of the cylindrical shell. The results from the analytic model were compared to computational results from finite element and boundary element models.

The effects of a viscoelastic coating applied to a cylindrical shell with a defect was investigated by Kirby *et al* [37]. The shell walls were considered to be coated in bitumen and the wall properties were considered to be thick and flexible. This led to the use of Navier's equation for the governing equation for the propagation of flexible waves in the pipe. Many axisymmetric defects were considered and the resulting reflection coefficients for each were compared.

An impedance mobility approach was used by Xie *et al* [38] to predict the response of a fluid filled cylindrical shell. The vibrations of the underlying shell were modelled using the equations of motion provided by Cao [39]. The method coupled the stiffness of the structure to the velocity of the fluid and was solved to find the amplitude of pressure and radial velocity. The method was compared to a finite element analysis approach which found the pressure for each segment. The results showed good agreement between the methods and the impedance mobility approach was considerable faster to carry out. In addition the transmission loss was shown for both a water filled and an air filled cylindrical shell.

The Donnell-Mushtari equations were used by Lee and Kwak [40] to find the natural frequencies for an flexible cylindrical shell. This was done by creating a dynamic model using the Raleigh-Ritz method to approximate the eigenvalues and eigenvectors. The strain displacements from Donnell-Mushtari theory were then altered in order to apply the method to other shell theories. In all cases the axisymmetric circumferential mode was neglected as those natural frequencies were deemed to be too high. The results showed that the Donnell-Mushtari theory for non-axisymmetric vibrations did not yield sufficiently accurate natural shell frequencies. It was stated that this was due to a lack of terms in the circumferential and shear strains. However, the Donnell-Mushtari equations used in this study do not match those used by Leissa [25] and Junger and Feit [30].

The aim of this thesis is to find and analyse the energy radiated due to a piston or wave at the junction of flexible circular cylindrical shells. Results of these problems are already available in the literature, but the approach considered herein is novel in that it uses mode matching method based on a generalised orthogonality relation. The generalised orthogonality relations derived here are new to the research area and are specific to flexible shells modelled using the Donnell-Mushtari equations of motion. This research builds on the mode matching method, the orthogonality relations simplify equations which occur in the method thus reducing computation time.

To achieve this aim the equations which govern the fluid and describe the motion of

the waveguide are to be found and used to derive a dispersion relation. This relation will in turn describe the form of the velocity potential and identify the associated wavenumbers for each section of waveguide. Also the dispersion relation will be used to derive an appropriate orthogonality relation/ generalised orthogonality relation. The mode matching method is applied through continuity of the normal component of velocity at the junction and where necessary the continuity of pressure. Those integrals which occur through the application of these conditions will be evaluated with the orthogonality relation/ generalised orthogonality relation or reduced to the appropriate limit. For problems which involve a flexible waveguide it is necessary to include edge conditions to describe the connection of the finite end. These edge conditions are to be found in literature and are required to determine constants which will arise from evaluating with the generalised orthogonality relation. This method will provide the amplitudes of the waves present in the velocity potential that are required for determining the radiated energy. The energy equations are to be formed from the equation of power (which will be the same as energy as harmonic time dependance will be assumed).

Chapter two will serve as background information which focuses on wave propagation in rigid waveguides. The research in this chapter is already available in the literature, but it is presented here as it serves as suitable foundation for the work which follows in later chapters. The governing equation and motion equation, dispersion relation and orthogonality relation for a rigid shell are all known (see for example Miles [1] and Ambramowitz and Stegun [41]). However, the separation method used to derive the velocity potential and a method for deriving the orthogonality relation shall be presented as a guide for deriving these for the flexible waveguide. Prototype problems are introduced to show the application of the mode matching method to problems featuring a piston and a change of radius. Also to show how a problem comprising an expansion chamber between two equal radius waveguides can be broken into subproblems. A transfer matrix method will be applied to this problem to obtain a low frequency estimate for the radiated power in order to ensure there is a good agreement with the results from the mode matching method. The amplitudes obtained from the mode-matching method will be used to determine the energy radiated at the waveguide junction. The results are presented and analysed for comparison to later equivalent problems with flexible shells.

The research in Chapter three will consider wave propagation in flexible walled shells and will proceed on the assumption of axisymmetric motion. As seen in the work of Leissa [25] there are several proposed theories for describing the vibrations of a cylindrical shell. Donnell-Mushtari theory of motion will be considered as it uses the simplest differential equations. However as Lee [40] found this theory to be inaccurate due to insufficient terms, the Donnell-Mushtari theory presented in Junger and Feit [30] will be used as it includes additional terms. The velocity potential in the fluid will be governed by the same equation for a rigid duct and hence will have the same form. The form of the velocity

potential with the equations of motion will be used to derive dispersion relation for flexible shells which vibrate axisymmetrically. The method used for deriving the rigid wall orthogonality relation will be employed in this chapter to find a generalised orthogonality relation for velocity potentials propagating in flexible shells with axisymmetric motion. The mode matching method with continuity of the normal component of velocity will be used to solve some semi-infinite problems which feature a rigid end plate or a piston plane. The energy radiated at the junction shall be presented compared with the equivalent problems in chapter two.

Flexible walled problems with axisymmetric motion and a change of radius are considered in chapter four. The mode matching method is applied through matching the continuity of the normal component of velocity and the continuity of pressure at the change of radius. Problems comprising an expansion chamber between two shells of equal radius are to be considered and it is hoped they can be broken down into two sub-problems similarly to the rigid expansion problem of Chapter two. The energy radiated at the junction shall be presented and compared with the equivalent problems in Chapter two.

The governing equations and a generalised orthogonality relation for a flexible shell with non-axisymmetric motion are to be derived in Chapter five. Problems involving a rigid end plate and an abrupt increase in radius will be considered. Again the energy radiated at the junction of these problems are to be compared with the results obtained from rigid and axisymmetric equivalent problems in Chapters two, three and four.

The purpose of Chapter six is to discuss the results from the solved problems and compare the orthogonality relation for propagation in rigid ducts to the generalised orthogonality relations for propagation in flexible shells.

Finally two additional problems are presented in Chapter seven as recommended further work which would both build on the research presented in this thesis.

This research should serve useful to engineers looking to simulate the energy radiated in flexible cylindrical shells featuring a piston or abrupt change of radius. Of key interest are the cut-on modes and their behaviour, which would be useful towards the design of systems aimed at minimising or maximising transmitted or reflected noise.

Chapter 2

Background Information

2.1 Introduction

The work presented in this chapter focuses on acoustic propagation in rigid cylindrical ducts. This research is already available in the literature, but it serves as a suitable foundation for the work which follows in later chapters. The governing equations are presented and some prototype problems are solved. This introduces the notation and demonstrates the methodology for applying the mode matching technique that will be used to solve problems in later chapters. Also, the results of these problems will be useful to compare with those results obtained from later problems. Four prototype problems are presented in this chapter: acoustic response due to a plane piston; acoustic response due to a plane piston and forcing wave; the energy radiated due to a forcing wave at an abrupt increase in radius and the energy transmitted through an expansion chamber situated between two ducts. Forcing is introduced in the form of plane piston and/or a wave and the resulting energy is analysed for each problem.

2.1.1 Governing equation and dispersion relation

The problems in this chapter consider a circular, cylindrical duct described in cylindrical polar co-ordinates $(\bar{r}, \bar{\theta}, \bar{z})$ (where the overbar here and henceforth indicates a dimensional quantity). The wall of the duct has the rigid property, which results in an axisymmetric system (with axisymmetric wave forcing assumed), therefore the $\bar{\theta}$ co-ordinate is dropped. The interior region contains a compressible fluid of sound speed c and density ρ. A harmonic time factor, $e^{-i\omega t}$, is assumed throughout where t is time and $\omega = ck$, with k being the fluid wavenumber. The governing equation for the interior region is given by the Helmholtz equation (see Crighton *et al* [42])

$$\left\{ \frac{\partial^2}{\partial \bar{r}^2} + \frac{1}{\bar{r}} \frac{\partial}{\partial \bar{r}} + \frac{\partial^2}{\partial \bar{z}^2} + k^2 \right\} \bar{\phi} = 0, \tag{2.1}$$

where $\bar{\phi}$ is the dimensional fluid velocity potential. This velocity potential is a scalar function which had a gradient equal to the velocity of the fluid. It can be used to express the pressure in terms of the potential as:

$$\bar{p} = i\omega\rho\bar{\phi}, \tag{2.2}$$

where $\bar{p}$ is the dimensional pressure. It is useful to non-dimensionalise the dimensional variables with respect to ω^{-1} and k^{-1} as typical time and length scales. The dimensional variables in terms of their non-dimensionalised counterparts are thus

$$k\bar{r} = r,\ k\bar{z} = z,\ k^2\bar{\phi} = \omega\phi. \tag{2.3}$$

Hence the non-dimensionalised governing equation is

$$\left\{\frac{\partial^2}{\partial r^2} + \frac{1}{r}\frac{\partial}{\partial r} + \frac{\partial^2}{\partial z^2} + 1\right\}\phi = 0, \tag{2.4}$$

where ϕ is the non-dimensional fluid velocity potential. The method of separation of variables is used to find the velocity potential, which is dependant on r and z and thus assumes the form

$$\phi = R(r)Z(z). \tag{2.5}$$

This form of ϕ is substituted into (2.4) which is divided through by RZ to give the separated equation

$$\left\{\frac{1}{R}\frac{\mathrm{d}^2R}{\mathrm{d}r^2} + \frac{1}{rR}\frac{\mathrm{d}R}{\mathrm{d}r} + 1\right\} = -\frac{1}{Z}\frac{\mathrm{d}^2Z}{\mathrm{d}z^2}. \tag{2.6}$$

The right-hand side of (2.6) must have a negative separation constant as waves should oscillate in the z direction, which gives

$$-\frac{1}{Z}\frac{\mathrm{d}^2Z}{\mathrm{d}z^2} = s^2, \tag{2.7}$$

where s is the separation constant. This has the solution

$$Z(z) = Ce^{isz} + De^{-isz}, \tag{2.8}$$

where C and D are arbitrary constants. However on selecting $C = 1$ and $D = 0$, the velocity potential comprises only waves propagating in the positive direction. The solution

$$Z(z) = e^{isz} \tag{2.9}$$

is substituted into (2.6) and the resulting expression is multiplied through by r^2R to give

$$r^2\frac{\mathrm{d}^2R}{\mathrm{d}r^2} + r\frac{\mathrm{d}R}{\mathrm{d}r} + r^2(1-s^2)R = 0. \tag{2.10}$$

The above expression is recognised as Bessel's differential equation (see Abramowitz and Stegun [41]) which is known to have a solution in the form

$$R(r) = AJ_0(\kappa r) + BY_0(\kappa r), \tag{2.11}$$

where $J_0(\cdot)$ and $Y_0(\cdot)$ are Bessel functions of the first and second kind respectively, $\kappa^2 = (1-s^2)^{1/2}$ and A, B are constants. There is a singularity in $Y_0(\kappa_n r)$ as $r \to 0$, therefore B is selected as zero and A now denotes the wave amplitude. Thus the velocity potential is given as

$$\phi = \sum_{n=0}^{\infty} A_n J_0(\kappa_n r)e^{is_n z}, \tag{2.12}$$

where A_n is the amplitude of the nth wave, s_n is the wavenumber of the mode and satisfies the dispersion relation $K(s) = 0$ which is presented below and $\kappa_n = (1-s_n^2)^{1/2}$. It is assumed that the velocity potential is formed of an infinite number of discrete waves. The velocity potential in (2.12) must also satisfy the rigid wall condition which is

$$\frac{\partial\phi}{\partial r}(a,0) = 0, \tag{2.13}$$

where a is the dimensionless radius of the duct (with $a = \bar{a}k$). From this condition the characteristic equation, $K(s)$, can be formed by substituting in a single mode of (2.12), which gives

$$K(s) = \frac{\partial}{\partial r}J_0(\kappa r)|_{r=a} = -\kappa J_1(\kappa a) = 0, \tag{2.14}$$

the roots of which give the wavenumbers s_n. The wavenumbers are ordered sequentially with the largest real value first, then by increasing imaginary part. There will always be one fundamental root $s_0 = 1$, $\kappa_0 = 0$ as $J_1(0) = 0$. The remaining roots are evanescent and these become real when they cut-on. These roots are approximated by identifying the large approximation formula for Bessel functions given in [41] as

$$J_\nu(z) \approx \sqrt{\frac{2}{\pi z}}\cos\left(z - \frac{\nu\pi}{2} - \frac{\pi}{4}\right), \tag{2.15}$$

where ν here is the order of the Bessel function (in this problem $\nu = 1$). Thus the evanescent roots are approximately located at $s_n = [1-\pi^2/a^2(n+1/4)^2]^{1/2}$, $n = 0, 1, 2, \ldots$.

2.1.2 Orthogonality relation

In any given problem the aim will be to determine the amplitude of the radiated waves through the application of the mode matching method. This method creates systems of equations involving summations with infinite modes. These are integrated and the orthogonality relation gives the solution to these integrals. The orthogonality relation for rigid ducts is the orthogonality relation for Bessel functions, which is already available in the literature, see for example Brown and Churchill [47]. The orthogonality relation is derived by considering the difference relation

$$K(s_n)J_0(\kappa_m a) - K(s_m)J_0(\kappa_n a) = 0, \tag{2.16}$$

where s_n and s_m are the aforementioned wavenumbers for a duct of radius a and $\kappa_n = (1 - s_n^2)^{1/2}$. This relation can be expressed as follows

$$\left[\left\{\kappa_n J_0'(\kappa_n r)J_0(\kappa_m r) - \kappa_m J_0'(\kappa_m r)J_0(\kappa_n r)\right\} r\right]_{r=0}^{a} = 0, \tag{2.17}$$

where the left-hand side is an integrand evaluated at $r = 0$ and $r = a$. This is expressed as an integral by differentiating it with respect to r to give

$$\begin{aligned}\int_0^a \Bigg[&\frac{\mathrm{d}}{\mathrm{d}r}\left\{\kappa_n J_1(\kappa_n r)\right\} J_0(\kappa_m r) + \kappa_n J_1(\kappa_n r)\frac{\mathrm{d}}{\mathrm{d}r}J_0(\kappa_m r)\\ &- \frac{\mathrm{d}}{\mathrm{d}r}\left\{\kappa_m J_1(\kappa_m r)\right\} J_0(\kappa_n r) + \kappa_m J_1(\kappa_m r)\frac{\mathrm{d}}{\mathrm{d}r}J_0(\kappa_n r)\Bigg]\,\mathrm{d}r = 0.\end{aligned} \tag{2.18}$$

The derivative formula for Bessel functions of order ν is given in Abramowitz and Stegun [41] as

$$\left(\frac{1}{z}\frac{\mathrm{d}}{\mathrm{d}z}\right)^k \left\{z^\nu J_\nu(z)\right\} = z^{\nu-k}J_{\nu-k}(z),\ k = 0, 1, 2, \ldots. \tag{2.19}$$

This formula is used to simplify (2.18) to

$$\int_0^a \left\{\kappa_n^2 J_0(\kappa_n r)J_0(\kappa_m r)r - \kappa_m^2 J_0(\kappa_m r)J_0(\kappa_n r)r\right\}\,\mathrm{d}r = 0. \tag{2.20}$$

It follows that

$$(s_n^2 - s_m^2)\frac{1}{a}\int_0^a J_0(\kappa_n r)J_0(\kappa_m r)r\,\mathrm{d}r = K(s_n)J_0(\kappa_m a) - K(s_m)J_0(\kappa_n a). \tag{2.21}$$

Provided the roots κ_n and κ_m are not equal, the results of the orthogonality relation is zero. For the case of equal roots (i.e. $\kappa_n = \kappa_m$) the value of the integral is found by

considering the limit

$$\int_0^a J_0^2(\kappa_n r) r \, \mathrm{d}r = \lim_{s_m \to s_n} \frac{a\{J_0(\kappa_m a)K(s_n) - J_0(\kappa_n a)K(s_m)\}}{s_m^2 - s_n^2}. \tag{2.22}$$

If $\kappa_n = \kappa_m$ the fraction gives the indeterminate form. This is bypassed using l'Hôpital's rule by computing the limit of the derivatives of both the numerator and denominator, that is

$$\int_0^a J_0^2(\kappa_n r) r \, \mathrm{d}r = \lim_{s \to s_n} \frac{a\left\{\frac{\mathrm{d}}{\mathrm{d}s}[J_0(\kappa a)]K(s_n) - J_0(\kappa_n a)K'(s)\right\}}{2s}. \tag{2.23}$$

Given that $K(s_n) = 0$, the limit is found to be

$$\int_0^a J_0^2(\kappa_n r) r \, \mathrm{d}r = -\frac{a J_0(\kappa_n a)K'(s_n)}{2s_n}. \tag{2.24}$$

Thus the orthogonality relation is

$$\int_0^a J_0(\kappa_n r) J_0(\kappa_m r) r \, \mathrm{d}r = \delta_{nm} C_n, \tag{2.25}$$

where δ is the Kronecker delta and

$$C_n = -\frac{a J_0(\kappa_n a)K'(s_n)}{2s_n} = \frac{a^2 J_0^2(\kappa_n a)}{2}. \tag{2.26}$$

Similarly, the orthogonality relation for a rigid duct of radius b is given by

$$\int_0^b J_0(\gamma_n r) J_0(\gamma_m r) r \, \mathrm{d}r = \delta_{nm} D_n, \tag{2.27}$$

where γ_n and γ_m are the wavenumbers for a duct of radius b, $\eta_n = (1 - \gamma_n^2)^{1/2}$ and

$$D_n = -\frac{b J_0(\gamma_n b)K'(\eta_n)}{2\eta_n} = \frac{b^2 J_0^2(\gamma_n b)}{2}. \tag{2.28}$$

Note that although the method of derivation is unorthodox, it is performed in this way such that it can later be used to derive those generalised orthogonality relations for flexible walled shells.

2.2 Energy in a cylindrical waveguide

To determine how the energy is reflected and/or transmitted at a discontinuity, an expression for the energy propagating in a rigid duct is required. As rigid walls cannot carry energy, only the energy in the fluid is considered. The dimensional power $\bar{\mathcal{E}}$ is given by integrating the pressure multiplied by the complex conjugate of the velocity over the

cross section, thus

$$\bar{\mathcal{E}} = 2\pi\omega\rho \text{Real}\left[\int_0^{\bar{a}} i\bar{\phi}\left(\frac{\partial\bar{\phi}}{\partial\bar{z}}\right)^* \bar{r}\ \mathrm{d}\bar{r}\right], \tag{2.29}$$

where the super-script asterisk identifies a complex conjugate. The equation for energy in this case is the same as that for power due to the assumption of harmonic time. The equivalent non-dimensional variables in (2.3) are used to non-dimensionalise this equation, which gives

$$\bar{\mathcal{E}} = \frac{2\pi c^3\rho}{k^2}\text{Real}\left[\int_0^{a} i\phi\left(\frac{\partial\phi}{\partial z}\right)^* r\ \mathrm{d}r\right]. \tag{2.30}$$

Thus the non-dimensionalised energy, may be defined as

$$\bar{\mathcal{E}} = \frac{2\pi c^3\rho}{k^2}\mathcal{E}. \tag{2.31}$$

It follows that

$$\mathcal{E} = \text{Real}\left[\int_0^{a} i\phi\left(\frac{\partial\phi}{\partial z}\right)^* r\ \mathrm{d}r\right]. \tag{2.32}$$

On using (2.32) the energy carried by an individual propagating mode of (2.12) can be determined. Consider

$$\phi_n = A_n J_0(\kappa_n r)e^{is_n z}, \tag{2.33}$$

where s_n is real. On substituting this into (2.32) it is found that

$$\mathcal{E}_n = \text{Real}\left[\int_0^{a} iA_n J_0(\kappa_n r)e^{is_n z}\left\{is_n A_n J_0(\kappa_n r)e^{is_n z}\right\}^* r\ \mathrm{d}r\right], \tag{2.34}$$

which can be expressed as

$$\mathcal{E}_n = \text{Real}\left[s_n|A_n|^2\int_0^{a} J_0^2(\kappa_n r) r\ \mathrm{d}r\right], \tag{2.35}$$

as κ_n is real for s_n real. The energy carried for an individual propagating mode is then found by evaluating the integral using the orthogonality relation in (2.25) to give

$$\mathcal{E}_n = |A_n|^2 s_n C_n, \tag{2.36}$$

where C_n is given in (2.26). This expression can be used to find the energy contribution from the input forcing wave, which is composed of the first mode of (2.12). For all rigid problems $\kappa_0 = 0$ and $s_0 = 1$, thus the forcing mode is

$$\phi_{\mathrm{F}} = Fe^{iz}, \tag{2.37}$$

where F is the amplitude of the forcing wave and will be chosen such that the energy carried by this mode is unity. The forcing wave is substituted into (2.32) and it follows from (2.36) that

$$\mathcal{E}_{\mathrm{F}} = \frac{a^2}{2}|F|^2, \tag{2.38}$$

as $C_0 = a^2/2$. Thus, in order for the forcing energy to be unity the amplitude is chosen as

$$F = \frac{\sqrt{2}}{a}. \tag{2.39}$$

A field of waves propagating in the positive z-direction in a duct of radius a is given in (2.12). The direction of travel is changed by using a negative exponent thus representing a field of reflected waves, that is

$$\phi = \sum_{n=0}^{\infty} A_n J_0(\kappa_n r) e^{-is_n z}, \tag{2.40}$$

where A_n are the amplitudes of the reflected field. On using (2.32) the energy contribution for a field of reflected waves is given by

$$\mathcal{E}_{\mathrm{A}} = \mathrm{Real}\left[\sum_{m=0}^{M} |A_m|^2 s_m C_m\right], \tag{2.41}$$

where $M+1$ is the number of considered modes. Note that C_m is given in (2.26) and by definition is related to the derivative of the dispersion relation $K(s)$ in (2.14). Expression (2.41) is a standard result that has been derived for various different waveguides. It holds both for rigid ducts and ducts comprising membrane or plate walls see Warren *et al* [43], Lawrie [44] and Nawaz and Lawrie [45]. In the former case the energy is transmitted only in the fluid, but in the latter case the energy can also be carried in the flexible wall. Thus the result in (2.41) is valid for both situations. An analogous expression is found for the energy contribution for a field of transmitted waves propagating in a duct of radius b

$$\mathcal{E}_{\mathrm{B}} = \mathrm{Real}\left[\sum_{m=0}^{M} |B_m|^2 \eta_m D_m\right], \tag{2.42}$$

where B_m are the amplitudes of the transmitted waves, η_m are the wavenumbers, $\gamma_m = (1-\eta_m^2)^{1/2}$ and D_m is given in (2.28).

2.3 Acoustic response due to a plane piston

The purpose of this section is to find the reflected energy and the impedance radiated by an oscillating plane piston into a semi-infinite duct (see Figure 2.1). This is to pave

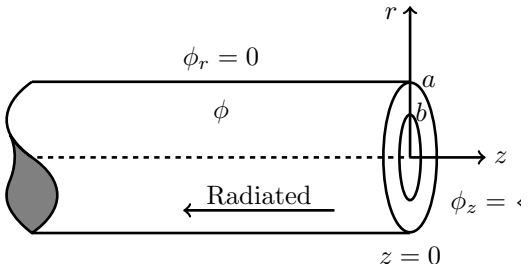

Figure 2.1: Physical configuration of the semi-infinite duct with piston problem.

the way for later problems which involve area expansion. The duct is located in the region $z \leq 0,\ 0 \leq r \leq a$ and is closed at one end by a rigid annular disc with a plane piston of radius $r = b$ in its centre with $a \geq b$. The annular disc is located in the region $z = 0,\ b \leq r \leq a$ and the plane piston is located at $z = 0,\ 0 \leq r \leq b$. The piston is the sound source for the system and it forces in the negative z direction. This problem configuration is essentially the same as the first problem considered in Ingard [3].

The velocity potential for this system comprises the waves radiated by the sound source

$$\phi = \sum_{n=0}^{\infty} A_n J_0(\kappa_n r) e^{-is_n z},\ 0 \leq r \leq a,\ z \leq 0, \tag{2.43}$$

where A_n is the amplitude of the nth radiated wave, s_n is the nth wavenumber and $\kappa_n^2 = (1 - s_n^2)^{1/2}$. The piston is assumed to have a symmetrical axial velocity distribution $u = u(r)$, with

$$u(r) = \begin{cases} U_0, & 0 \leq r \leq b \\ 0, & b \leq r \leq a \end{cases}, \tag{2.44}$$

where U_0 is a constant.

The normal component of velocity is matched with the velocity distribution for the sound source at the closed end. That is at $z = 0$

$$\frac{\partial \phi}{\partial z}(r, 0) = u(r),\ 0 \leq r \leq a. \tag{2.45}$$

The velocity potential in (2.43) is substituted into (2.45) to give

$$-i \sum_{n=0}^{\infty} A_n s_n J_0(\kappa_n r) = u(r),\ 0 \leq r \leq a. \tag{2.46}$$

On multiplying (2.46) by $J_0(\kappa_m r) r$ and integrating with respect to $r,\ 0 \leq r \leq a$, it is found that

$$-i \sum_{n=0}^{\infty} A_n s_n \int_0^a J_0(\kappa_n r) J_0(\kappa_m r) r \, \mathrm{d}r = \int_0^a u(r) J_0(\kappa_m r) r \, \mathrm{d}r. \tag{2.47}$$

The orthogonality relation in (2.25) is used to evaluate the integral on the left-hand side and (2.44) is substituted into the right-hand side to give

$$-i\sum_{n=0}^{\infty} A_n s_n \delta_{nm} C_m = U_0 \int_0^b J_0(\kappa_m r) r \, \mathrm{d}r. \tag{2.48}$$

It follows that

$$A_m = \frac{iU_0 b J_1(\kappa_m b)}{\kappa_m s_m C_m}. \tag{2.49}$$

The dimensional radiation impedance of the piston given in Ingard [3] is

$$\bar{Z} = \frac{\bar{P}/A}{\bar{U}}, \tag{2.50}$$

where $\bar{P}/A$ is the dimensional force on the piston, with A being the area of the piston $A = \pi \bar{b}^2$ and $\bar{U}$ is the dimensional velocity of the piston given by

$$\bar{U} = cU_0. \tag{2.51}$$

The definition for the dimensional pressure over the piston surface given in Ingard [3] is

$$\bar{P} = 2\pi \int_0^{\bar{b}} \bar{p}(\bar{r}, 0)\bar{r} \, \mathrm{d}\bar{r}, \tag{2.52}$$

where $\bar{p}$ is the dimensional pressure

$$\bar{p} = i\omega\rho\bar{\phi}. \tag{2.53}$$

The dimensional variables in (2.52) are replaced with the non-dimensional equivalent variables in (2.3) to obtain

$$\bar{P} = 2\pi i \frac{\omega^2 \rho}{k^4} \int_0^b \phi(r, 0) r \, \mathrm{d}r. \tag{2.54}$$

The dimensional impedance is then

$$\bar{Z} = \frac{2ic\rho}{b^2 U_0} \int_0^b \phi(r, 0) r \, \mathrm{d}r. \tag{2.55}$$

The non-dimensional radiation impedance Z is chosen as

$$\bar{Z} = c\rho Z. \tag{2.56}$$

It follows that

$$Z = \frac{2i}{b^2 U_0} \int_0^b \phi(r,0) r \, \mathrm{d}r. \tag{2.57}$$

The velocity potential in (2.43) is substituted into (2.57), with $U_0 = 1$, to express the impedance in terms of the radiated amplitude

$$Z = \frac{2i}{b^2} \sum_{n=0}^{\infty} A_n \int_0^b J_0(\kappa_n r) r \, \mathrm{d}r, \tag{2.58}$$

which gives

$$Z = \frac{2i}{b^2} \sum_{n=0}^{\infty} \frac{A_n b J_1(\kappa_n b)}{\kappa_n}. \tag{2.59}$$

The amplitude of the radiated wave in (2.49) is substituted into the above impedance equation, with $U_0 = 1$, to express the impedance as

$$Z = -2 \sum_{n=0}^{\infty} \frac{J_1^2(\kappa_n b)}{s_n C_n \kappa_n^2}. \tag{2.60}$$

The results show the energy radiated by the piston given in equation (2.41) and the radiation impedance given in equation (2.60). These are both plotted against frequency from $5 - 4000$Hz with the energy plot presented in a) and the impedance plot presented in b). The energies are found in Matlab with the code presented in Appendix A, where the radius of the duct is $\bar{a} = 0.2$m throughout. Note that this code is not perfect as the root finder does not give an accurate value for one of the identified roots in the 300Hz to 600Hz range. As a result, the energy plots presented in this chapter may show some noise in this range. The roots are checked by checking that they satisfy the dispersion relation. Also the number of obtained roots is checked through the application of the argument principle theorem which counts the number of zeros that occur in the half circle.

In the first configuration it is considered that the radius of the plane piston is equal to that of the rigid duct, where $\bar{a} = \bar{b} = 0.2$m. The resulting radiated energy and radiation impedance are shown in Figure 2.2. The reflected energy increases with frequency due to the constant energy input of the piston. The absolute impedance is seen to be one throughout, this can be derived from equation (2.60), as all but the $n = 0$ terms vanish when $a = b$. The impedance for this configuration becomes

$$Z = -2 \frac{J_1^2(\kappa_0 a)}{s_0 C_0 \kappa_0^2}, \tag{2.61}$$

where $s_0 = 1$, $\kappa_0 = 0$ and $C_0 = a^2 J_0^2(\kappa_0 a)/2$. Thus the impedance can be obtained by finding the limit

$$Z = -\lim_{\kappa \to 0} \frac{4 J_1^2(\kappa a)}{a^2 \kappa^2 J_0^2(\kappa a)}. \tag{2.62}$$

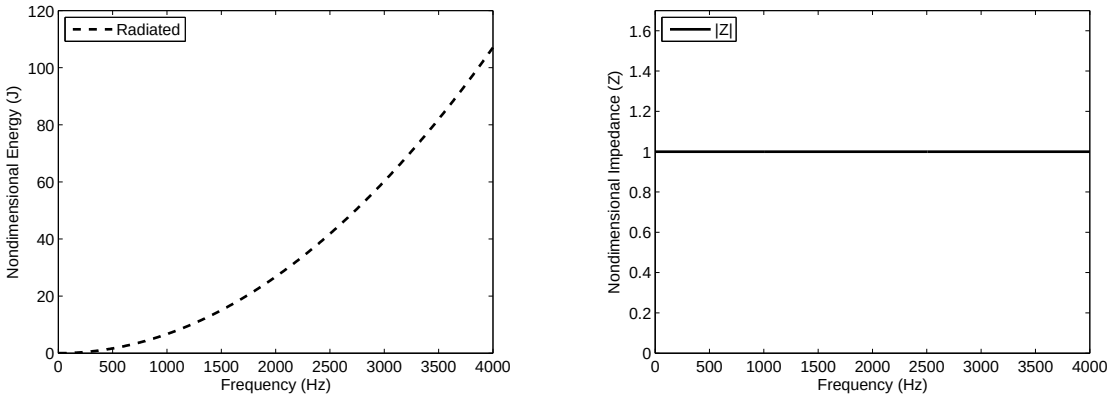

a) b)

Figure 2.2: At the closed end of a piston forced semi-infinite duct with $\bar{a} = 0.2$m and $\bar{b} = 0.2$m: a) Radiated energy, b) Radiation impedance.

It follows from l'Hôpital's rule that

$$Z = -\lim_{\kappa \to 0} \left\{ \frac{2J_1(\kappa a)}{aJ_0(\kappa a)\kappa} \right\}^2 = -\frac{aJ_0(\kappa a)}{aJ_0(\kappa a) - a^2 J_1(\kappa a)\kappa} = -1, \tag{2.63}$$

which confirms the results of Figure 2.2b.

The second considered configuration assumes the plane piston to be half the radius of the duct, where $\bar{a} = 0.2$m and $\bar{b} = 0.1$m. The resulting radiated energy and impedance are shown in Figure 2.3. Again the constant energy input of the piston causes the reflected energy to increase with frequency. The reflected energy is roughly a quarter of that found in the previous configuration owing to the radius of the piston. By having the piston radius less than the duct radius the reflected energy (and absolute impedance) spike up at specific frequencies. This phenomena is known as a cut-on, which is where an evanescent mode becomes real valued, thus contributing to the energy. For a shell of radius $\bar{a} = 0.2$m, these occur when $\kappa < 1$, thus yielding a real valued s. The cut-on frequencies can be approximated by $f > (n + 0.25)c/a$ $n = 0, 1, \ldots$, where n are mode numbers, this formula gives 1073Hz, 1932Hz, 2791Hz, 3650Hz. For comparison, the true cut-on frequencies shown in Figure 2.3 (and 2.4 below) are 1048Hz, 1918Hz, 2781Hz and 3643Hz. For verification, note that the impedance plot shown here is essentially the same as Figure 6a) produced by Ingard [3]. However, in that article the non-dimensional impedance is plotted against $f\bar{a}/c$ as opposed to f.

Lastly, the radius of the piston is considered as being significantly smaller compared to the radius of the duct, where $\bar{a} = 0.2$m and $\bar{b} = 0.06$m. The resulting radiated energy and impedance are shown in Figure 2.4. This time the radiated energy is half of the previous configuration ($\bar{a} = 0.2$m and $\bar{b} = 0.1$m). Again the cut-ons are present here as the radius of the piston is less than that of the duct radius (which allows for evanescent mode excitation). These cut-ons occur at the exact same frequencies as the

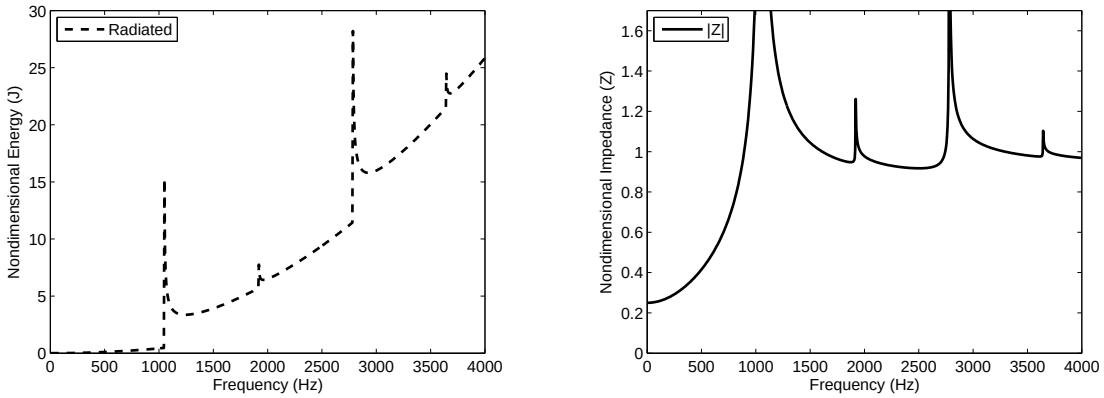

a) b)

Figure 2.3: At the closed end of a piston forced semi-infinite duct with $\bar{a} = 0.2$m and $\bar{b} = 0.1$m: a) Radiated energy, b) Radiation impedance.

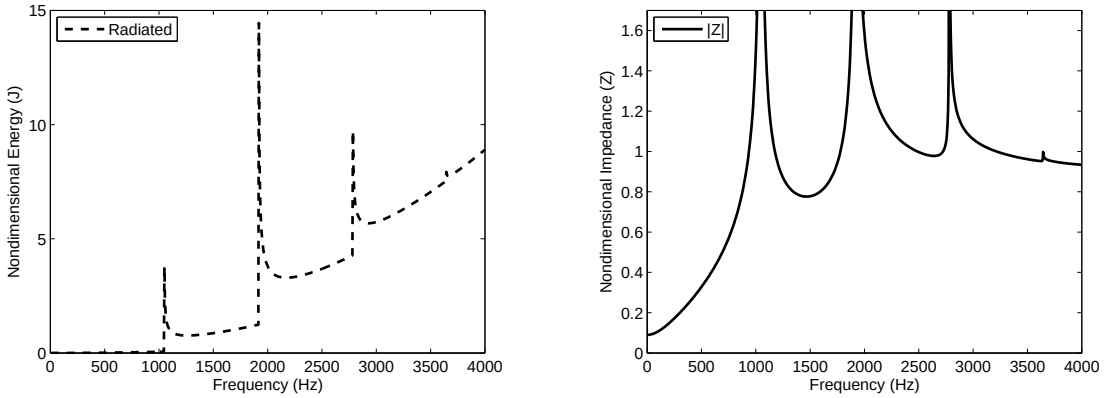

a) b)

Figure 2.4: At the closed end of a piston forced semi-infinite duct with $\bar{a} = 0.2$m and $\bar{b} = 0.06$m: a) Radiated energy, b) Radiation impedance.

previous configuration as they are dependant on the radius of the duct (the piston has no influence on when a cut-on occurs).

2.4 Acoustic response due to a plane piston and wave forcing

The purpose of this section is to find the energy radiation by an oscillating plane piston and wave forcing into a semi-infinite shell. The problem is essentially the same as considered in Section 2.3, but with the inclusion of a forcing wave incident towards the piston as shown in Figure 2.5.

The velocity potential now incorporates the wave forcing as well as waves radiated by

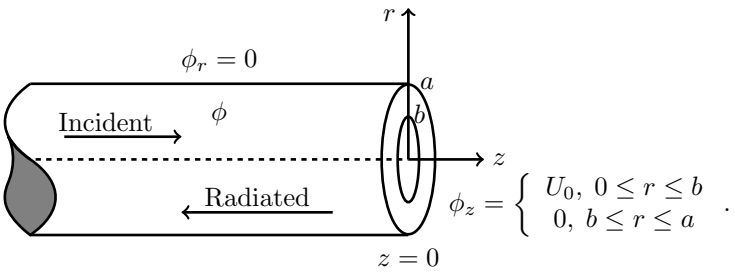

Figure 2.5: Physical configuration of the semi-infinite duct with piston and wave forcing.

the plane piston

$$\phi = Fe^{iz} + \sum_{n=0}^{\infty} A_n J_0(\kappa_n r) e^{-is_n z},\ 0 \le r \le a,\ z \le 0, \tag{2.64}$$

where F is the amplitude for the forcing wave which is given by (2.39), A_n is the amplitude of the nth radiated wave, s_n is the nth wavenumber and $\kappa_n^2 = (1 - s_n^2)^{1/2}$. The piston is assumed to have a symmetrical axial velocity distribution $u = u(r)$, with

$$u(r) = \begin{cases} U_0 & 0 \le r \le b \\ 0 & b \le r \le a \end{cases}, \tag{2.65}$$

where U_0 is a constant.

The normal component of velocity is matched with the velocity distribution of the piston at the closed end. That is at $z = 0$

$$\frac{\partial \phi_z}{\partial z}(r, 0) = u(r),\ 0 \le r \le a. \tag{2.66}$$

The velocity potential in (2.64) is substituted into (2.66) to give

$$iF - i\sum_{n=0}^{\infty} A_n s_n J_0(\kappa_n r) = u(r),\ 0 \le r \le a. \tag{2.67}$$

On multiplying (2.67) by $J_0(\kappa_m r)r$ and integrating with respect to r, $0 \le r \le a$, it is obtained that

$$iF \int_0^a J_0(\kappa_m r) r \, \mathrm{d}r - i\sum_{n=0}^{\infty} A_n s_n \int_0^a J_0(\kappa_n r) J_0(\kappa_m r) r \, \mathrm{d}r = \int_0^a u(r) J_0(\kappa_m r) r \, \mathrm{d}r. \tag{2.68}$$

The orthogonality relation in (2.25) is used to find the integrals on the left-hand side and (2.65) is used such that the right-hand side can be integrated. It follows that

$$A_m = F\delta_{0m} + \frac{iU_0 b J_1(\kappa_m b)}{\kappa_m s_m C_m}. \tag{2.69}$$

The velocity potential in (2.64) is used in the impedance formula given in (2.57) with $U_0 = 1$, to yield

$$Z = \frac{2i}{b^2}\left\{\frac{FbJ_1(\kappa_0 b)}{\kappa_0} + \sum_{n=0}^{\infty}\frac{A_n bJ_1(\kappa_n b)}{\kappa_n}\right\}. \tag{2.70}$$

The amplitude for the radiated waves in (2.69) is substituted into the above equation to give

$$Z = \frac{2i}{b^2}\left\{\frac{2FbJ_1(\kappa_0 b)}{\kappa_0} + i\sum_{n=0}^{\infty}\frac{b^2 J_1^2(\kappa_n b)}{\kappa_n^2 s_n C_n}\right\}. \tag{2.71}$$

It follows that

$$Z = \frac{4iFJ_1(\kappa_0 b)}{b\kappa_0} - 2\sum_{n=0}^{\infty}\frac{J_1^2(\kappa_n b)}{\kappa_n^2 s_n C_n}. \tag{2.72}$$

The results comprise of the energy radiated by the piston given by the formula in (2.41) and the radiation impedance given in (2.72). These are both plotted against frequency from $5 - 4000$Hz with the energy presented in plot a) and the impedance presented in plot b). The energy and impedance are created in Matlab with the code presented in Appendix A, where the radius of the duct is $\bar{a} = 0.2$m throughout. The cut-ons in a duct of radius $\bar{a} = 0.2$m are as given in Section 2.3 and are stated again for convenience: 1041Hz, 1918Hz, 2781Hz and 3643Hz.

The first configuration considered assumes the radius of the plane piston to be equal to that of the rigid duct, where $\bar{a} = \bar{b} = 0.2$m. The resulting radiated energy and radiation impedance are shown in Figure 2.6. As with the equivalent no wave forcing problem, the constant energy from the piston causes the reflected energy to increase over frequency. The radius of the piston being the same as the duct only allows for the fundamental mode to propagate, therefore no evanescent mode cut-ons occur. The impedance shown here is different to the equivalent no forcing wave impedance in that it is not constant one. This is due to the inclusion of the wave forcing, which increases the absolute impedance for low frequencies. However, as the frequency increases, the forcing wave has less of an impact on the absolute impedance and so it converges towards one.

The second considered configuration assumes the radius of the piston to be half the radius of the duct, where $\bar{a} = 0.2$m and $\bar{b} = 0.1$m. The resulting radiated energy and impedance are shown in Figure 2.7. The reflected energy appears to be the same as the equivalent no wave forcing problem, but it is actually one non-dimensional Joule higher due to the unit energy of the forcing wave. This is roughly half the radiated energy shown in the previous configuration. The absolute impedance begins high, due to the wave forcing and it then converges towards one, while sharply peaking at the cut-on frequencies.

Lastly, the radius of the piston is assumed to be significantly smaller compared to the radius of the duct, where $\bar{a} = 0.2$m and $\bar{b} = 0.06$m. The resulting radiated energy

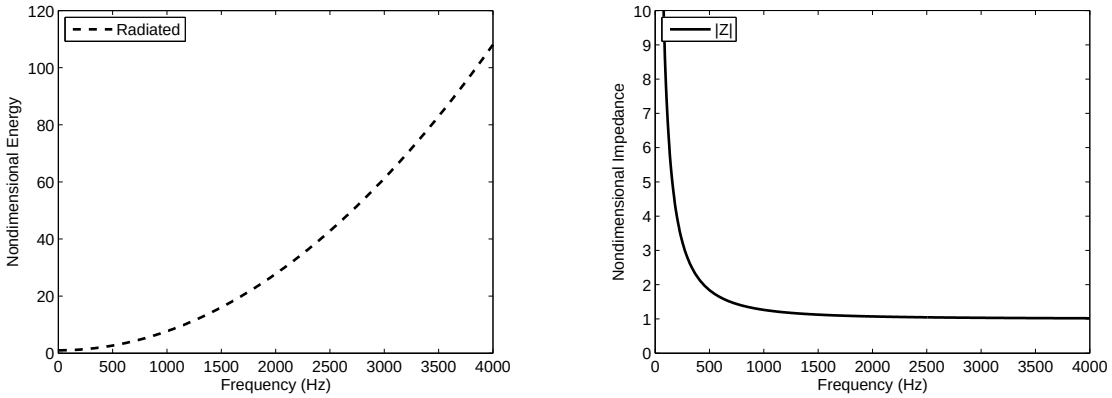

a) b)

Figure 2.6: At the closed end of a semi-infinite duct with piston and wave forcing $\bar{a} = 0.2$m, $\bar{b} = 0.2$m: a) Radiated energy, b) Radiation impedance.

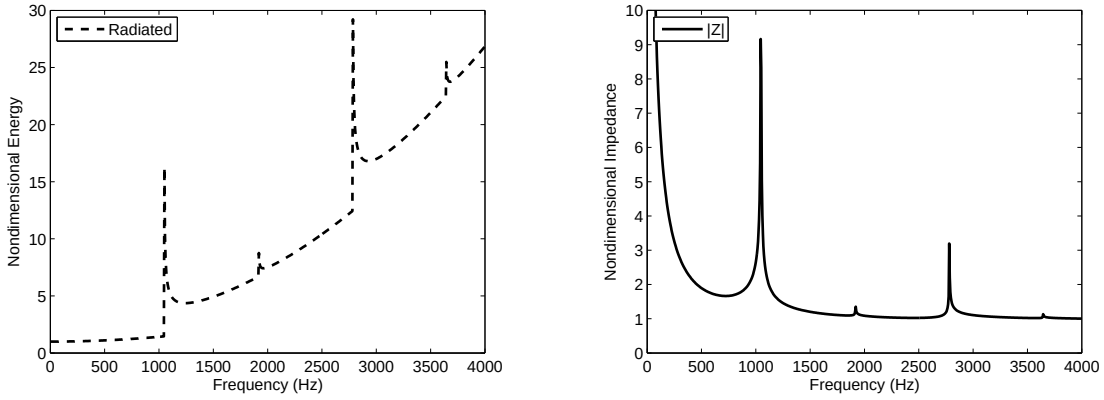

a) b)

Figure 2.7: At the closed end of a semi-infinite duct with piston and wave forcing $\bar{a} = 0.2$m,$\bar{b} = 0.1$m: a) Radiated energy, b) Radiation impedance.

and impedance are shown in Figure 2.8. The radiated energy is half of the previous configuration ($\bar{a} = 0.2$m and $\bar{b} = 0.1$m). Also the cut-ons are present here because the radius of the piston a allows for evanescent mode excitation. These cut-ons occur at the exact same frequencies as the previous configuration as they are dependant on the radius of the duct.

2.5 Energy radiated due to a forcing wave at an abrupt increase in radius

The aim of this section is to determine the energy reflected and transmitted due to a forcing wave at an abrupt increase in radius. The problem comprises two semi-infinite ducts: the left-hand duct occupies $0 \leq r \leq a,\ z \leq 0$ and the right-hand duct occupies $0 \leq r \leq b,\ z \geq 0$, where $a \leq b$ as shown in Figure 2.9. The waveguide is closed by a rigid

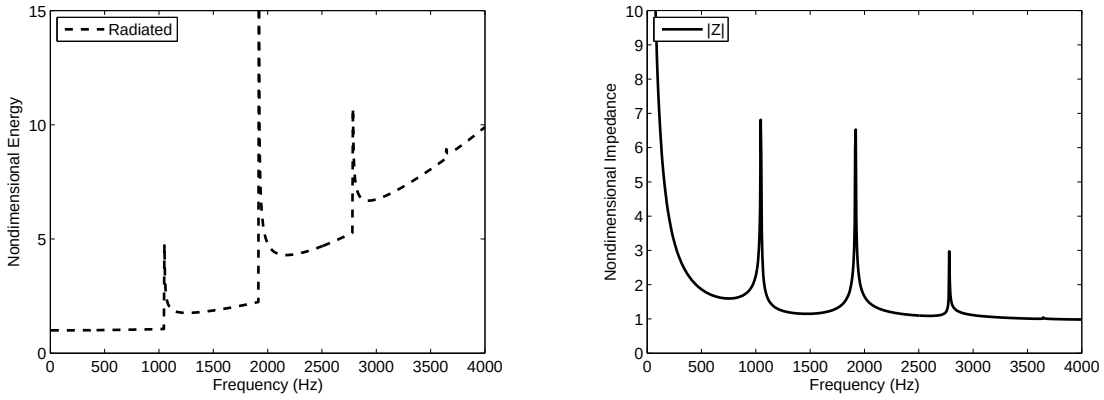

a) b)

Figure 2.8: At the closed end of a semi-infinite duct with piston and wave forcing $\bar{a} = 0.2$m, $\bar{b} = 0.06$m: a) Radiated energy, b) Radiation impedance.

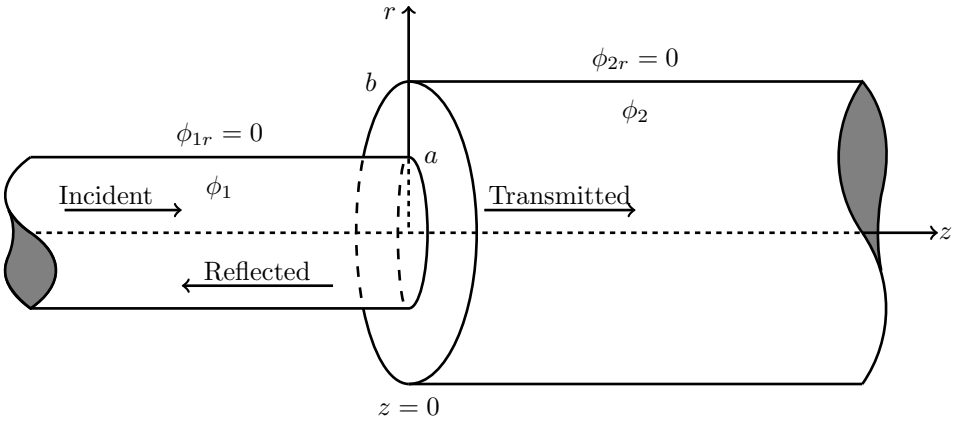

Figure 2.9: Physical configuration of the abrupt increase in radius problem.

annular disc occupying $a \leq r \leq b,\ z = 0$ and forcing is by a wave propagating in the positive z direction towards the abrupt increase in radius. This problem has been studied numerous times in literature, see for example Homentcovschi and Miles [21]. However this section demonstrates how the orthogonality relation is used to simplify the mode matching method applied to problems with an abrupt change in radius.

The velocity potential for the left-hand duct ϕ_1 comprises the forcing wave and the reflected sound field, which leads to

$$\phi_1 = Fe^{iz} + \sum_{n=0}^{\infty} A_n J_0(\kappa_n r) e^{-is_n z},\ 0 \leq r \leq a,\ z \leq 0, \tag{2.73}$$

where F is the amplitude of the forcing wave given in (2.39), A_n is the amplitude of the nth reflected wave, s_n are the wavenumbers and $\kappa_n = (1 - s_n^2)^{1/2}$. The velocity potential

ϕ_2 for the right-hand duct is comprised of the transmitted sound field

$$\phi_2 = \sum_{n=0}^{\infty} B_n J_0(\gamma_n r) e^{i\eta_n z},\ 0 \le r \le b,\ z \ge 0, \tag{2.74}$$

where B_n is the nth amplitude of the transmitted wave, η_n are the wavenumbers and $\gamma_n = (1 - \eta_n^2)^{1/2}$. The amplitudes of the reflected and transmitted fields are found by matching the fluid pressure and the normal component of velocity between the ducts. At the junction, the fluid pressure and normal component of velocity are continuous within the fluid, while the latter vanishes on the rigid annular disc. That is at $z = 0$

$$\phi_1(r, 0) = \phi_2(r, 0),\ 0 \le r \le a, \tag{2.75}$$

$$\frac{\partial \phi_2}{\partial z}(r, 0) = \begin{cases} \frac{\partial \phi_1}{\partial z}(r, 0), & 0 \le r \le a \\ 0, & a \le r \le b \end{cases}. \tag{2.76}$$

The velocity potentials (2.73) and (2.74) are substituted into (2.75) to give

$$F + \sum_{n=0}^{\infty} A_n J_0(\kappa_n r) = \sum_{n=0}^{\infty} B_n J_0(\gamma_n r),\ 0 \le r \le a. \tag{2.77}$$

On multiplying (2.77) by $J_0(\kappa_m r) r$ and integrating with respect to r, $0 \le r \le a$ it is found that

$$F \int_0^a J_0(\kappa_m r) r \, \mathrm{d}r + \sum_{n=0}^{\infty} A_n \int_0^a J_0(\kappa_n r) J_0(\kappa_m r) r \, \mathrm{d}r = \sum_{n=0}^{\infty} B_n \int_0^a J_0(\gamma_n r) J_0(\kappa_m r) r \, \mathrm{d}r. \tag{2.78}$$

This is done so that the orthogonality relation in (2.25) can be used to evaluate the integrals on the left-hand side. Similarly, (2.77) could have been multiplied by $J_0(\gamma_m r) r$ and integrated and the orthogonality relation in (2.27) would instead be used. It follows from evaluating the left-hand integrals that

$$A_m = -F\delta_{0m} + \frac{1}{C_m} \sum_{n=0}^{\infty} B_n R_{mn}, \tag{2.79}$$

where C_m is given in (2.26) and

$$R_{mn} = \int_0^a J_0(\kappa_m r) J_0(\gamma_n r) r \, \mathrm{d}r. \tag{2.80}$$

For $\kappa_m \neq \gamma_n$, R_{mn} simplifies to

$$R_{mn} = \frac{a \left\{ \kappa_m J_1(\kappa_m a) J_0(\gamma_n a) - \gamma_m J_1(\gamma_m a) J_0(\kappa_m a) \right\}}{\kappa_m^2 - \gamma_n^2}. \tag{2.81}$$

When $\kappa_m = \gamma_n$ expression (2.80) is (2.26) with $m = n$. It follows

$$R_{mm} = \frac{a^2 J_0^2(\kappa_m a)}{2}. \tag{2.82}$$

A second expression is obtained by multiplying (2.76) by $J_0(\gamma_m r)r$ and integrating with respect to r, $0 \leq r \leq b$. As the right-hand side is zero on (a, b), it follows that

$$\int_0^b \frac{\partial \phi_2}{\partial z}(r, 0) J_0(\gamma_m r) r \, \mathrm{d}r = \int_0^a \frac{\partial \phi_1}{\partial z}(r, 0) J_0(\gamma_m r) r \, \mathrm{d}r. \tag{2.83}$$

Note that as with the pressure condition, multiplying by $J_0(\kappa_m r)r$ and integrating would also be possible. However, this would require a new integral (similar to R_{mn}) to be defined and this would increase the complexity of the problem. The velocity potentials (2.73) and (2.74) are substituted into the above equation to give

$$iB_n\eta_n \int_0^b J_0(\gamma_n r) J_0(\gamma_m r) r \, \mathrm{d}r = F \int_0^a J_0(\gamma_m r) r \, \mathrm{d}r - i \sum_{n=0}^{\infty} A_n s_n \int_0^a J_0(\kappa_n r) J_0(\gamma_m r) r \, \mathrm{d}r. \tag{2.84}$$

The orthogonality relation in (2.27) is used to evaluate the integral on the left-hand side. It follows that

$$B_m = \frac{F R_{0m}}{\eta_m D_m} - \frac{1}{\eta_m D_m} \sum_{n=0}^{\infty} A_n s_n R_{nm}. \tag{2.85}$$

The amplitudes for the reflected and transmitted fields are thus found by truncating and solving the coupled equations (2.79) and (2.85). The respective energies are calculated by using these amplitudes in the energy equations (2.41) and (2.42). These are stated below for convenience: The energy for the reflected field is given by

$$\mathcal{E}_{\mathrm{A}} = \mathrm{Real}\left[\sum_{m=0}^{M} |A_m|^2 s_m C_m\right], \tag{2.86}$$

where A_m are the amplitudes of the reflected waves and the energy for the transmitted field is

$$\mathcal{E}_{\mathrm{B}} = \mathrm{Real}\left[\sum_{m=0}^{M} |B_m|^2 \eta_m D_m\right], \tag{2.87}$$

where B_m are the amplitudes of the transmitted waves. The amplitudes and energies are calculated in Matlab with the code presented in Appendix B and the plots are presented below. This has been done using 100 modes to calculate the amplitudes of the propagating waves. It is shown in the next subsection that this is more than sufficient for calculating accurate results. The frequency range used is 5Hz-1200Hz, it is possible to plot the energy beyond this frequency but 1200Hz is selected as the upper range as later equivalent problems are limited to this maximum frequency.

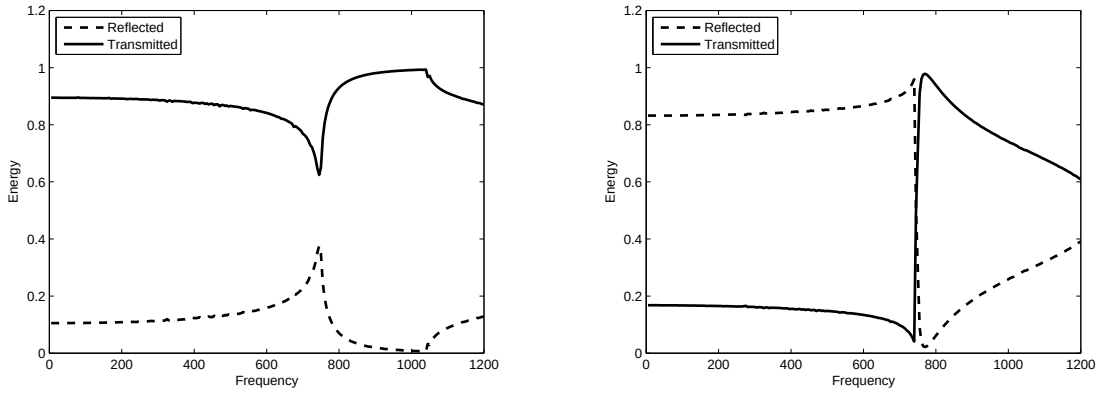

a) b)

Figure 2.10: Energy reflected and transmitted at an abrupt increase in radius with a) $\bar{a} = 0.2\text{m}$, $\bar{b} = 0.28\text{m}$; b) $\bar{a} = 0.06\text{m}$, $\bar{b} = 0.28\text{m}$.

The first considered configuration has the radius of the left-hand duct to be equal to the radius of the right-hand duct, which reduces the problem to an infinite duct. The left-hand radius is $\bar{a} = 0.2\text{m}$ and the right-hand radius is $\bar{b} = 0.2\text{m}$. For a duct of radius $\bar{a} = 0.2\text{m}$ the first cut-on occurs at 1041Hz (while other cut-ons occur outside the chosen frequency range). For this problem the energy is totally transmitted and the cut-ons present in both ducts have no impact on the energy. This is because there is no junction to disrupt the energy from being transferred from the left-hand to the right-hand duct.

The next considered configuration has the radius of the right-hand shell to be increase to $\bar{b} = 0.28\text{m}$ while the radius of the left-hand duct is maintained at $\bar{a} = 0.2\text{m}$. For a duct of radius $\bar{b} = 0.28\text{m}$ the first cut-on occurs at 744Hz (while other cut-ons occur outside the chosen frequency range). The energies are plotted in against frequency for $5 - 1200\text{Hz}$ and presented in Figure 2.10a. It is seen that the majority of energy is transmitted. A large dip in transmitted energy occurs at 744Hz, this is a result of the mode cut-on occurring in the larger duct. A second drop in transmitted energy occurs at 1041Hz which is when the cut-on in the smaller duct occurs. Note that the noise mentioned in the piston problem is more evident here.

The final configuration considers the radius of the left-hand duct to be significantly smaller compared to the right-hand duct. The radius of the left-hand duct is reduced to $\bar{a} = 0.06\text{m}$ and the radius of the right-hand duct is kept at $\bar{b} = 0.28\text{m}$. For a duct of radius 0.06m there are no cut-ons which occur in the considered range of frequencies. The resulting plot of energy is shown in Figure 2.10b. For frequencies below the first cut-on at 744Hz it is seen that the majority of energy is reflected. This is in keeping with the well known result (see for example Levine and Schwinger [2]) that the energy is totally reflected as $k\bar{a} = a \to 0$. After the first cut-on there is a sharp inversion of the energies and the majority of energy is then transmitted.

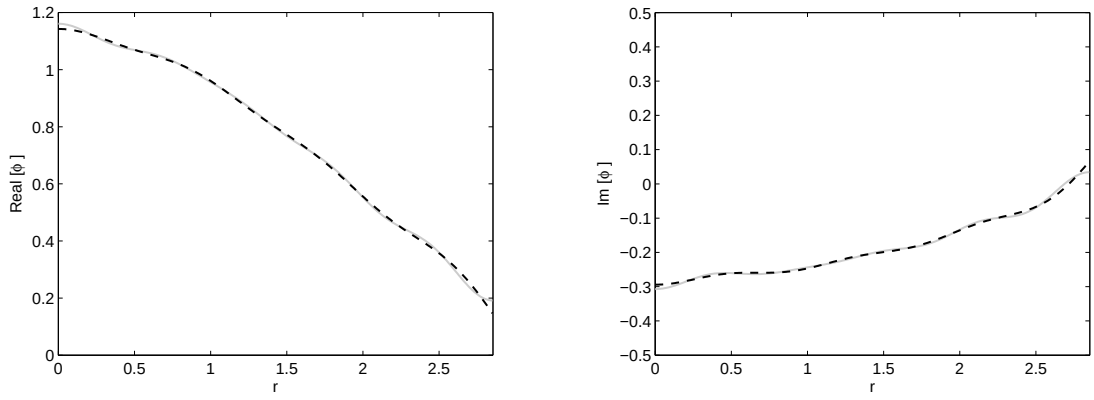

a) b)

Figure 2.11: The two sides of the pressure matching condition for 10 modes with $\bar{a} = 0.2$m, $\bar{b} = 0.28$m (dashed line: left side of the condition, solid line: right side of the condition) a) Real; b) Imaginary.

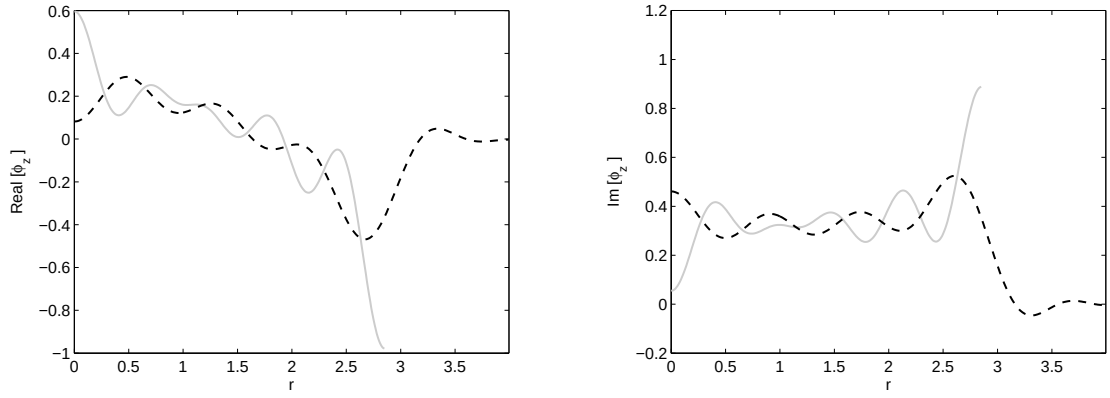

a) b)

Figure 2.12: The two sides of the normal component of velocity matching condition for 10 modes with $\bar{a} = 0.2$m, $\bar{b} = 0.28$m a) Real; b) Imaginary.

2.5.1 Verification of results

To verify the results, the matching conditions are plotted in order to ensure that they converge and to check that sufficient modes have been included. This is done for a configuration with $\bar{a} = 0.2$m, $\bar{b} = 0.28$m at 780Hz. The matching condition for pressure is (2.78) which is presented against the non-dimensional radius of the duct in Figure 2.11 for 10 modes. The results show that there is a good agreement on the two sides of the pressure condition, but it drifts apart in the center and at the edges of the duct. The matching condition for the normal component of velocity is (2.84) which is presented against the non-dimensional radius of the duct for the real and imaginary parts for 10 modes in Figure 2.12. The results show a agreement between the normal component of velocity from the two sides of the junction. This is due to a singularity at which the normal component of velocity jumps from continuity in the fluid to zero on the rigid

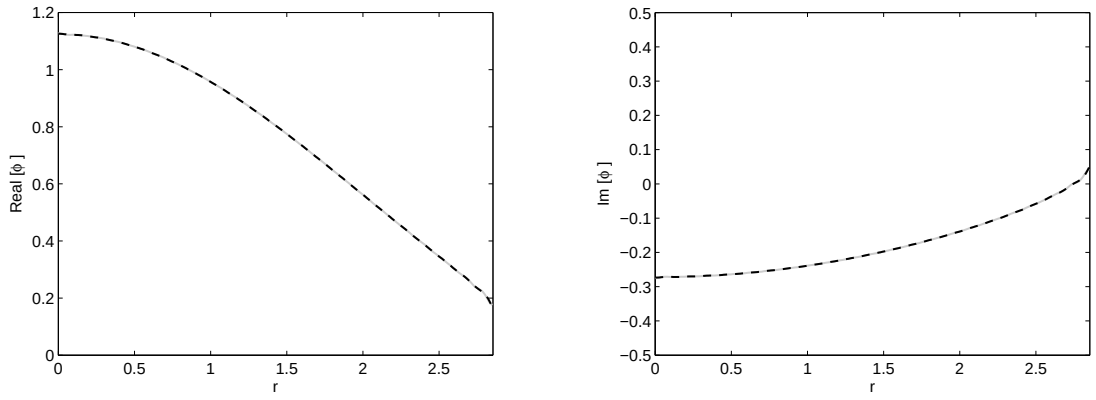

a) b)

Figure 2.13: The two sides of the pressure matching condition for 60 modes with $\bar{a} = 0.2$m, $\bar{b} = 0.28$m (dashed line: left side of the condition, solid line: right side of the condition) a) Real; b) Imaginary.

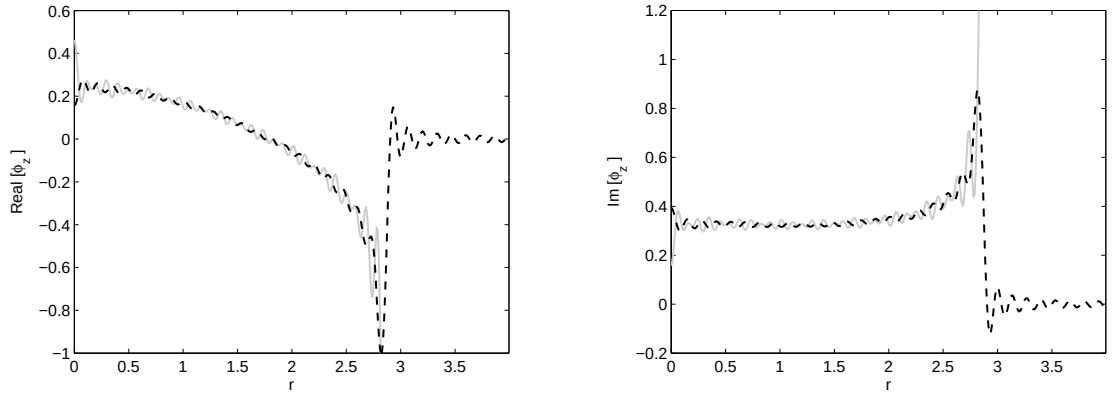

a) b)

Figure 2.14: The two sides of the normal component of velocity matching condition for 60 modes with $\bar{a} = 0.2$m, $\bar{b} = 0.28$m (dashed line: left side of the condition, solid line: right side of the condition) a) Real; b) Imaginary.

annulus. From these results it is seen that the amplitudes obtained with 10 modes are not sufficiently accurate, thus additional modes are required. The real and imaginary results of the matching condition for pressure is now found for 60 modes and are shown in Figure 2.13. There is an improvement in the match in the pressure from each side of the junction and they do not drift at the center or towards the edge of the duct. Therefore 60 modes finds sufficiently accurate amplitudes for satisfying the condition for matched pressure. The amplitudes used to find energy results were formed using 100 modes, which is more than enough modes to satisfy the matched pressure condition. The normal component of velocity condition is now presented for each side with 60 modes and is presented in Figure 2.14. There is a much closer match between the two normal components of velocity for $\bar{r} \leq 0.2$m, however it is not one-to-one due to the oscillatory behaviour. These plots better demonstrate the behaviours occurring from the abrupt

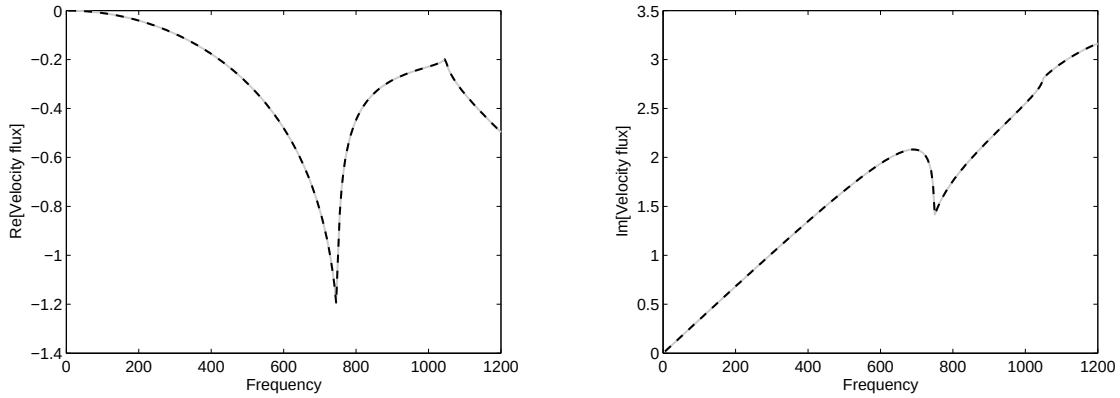

a) b)

Figure 2.15: The two sides of the velocity flux for 10 modes with $\bar{a} = 0.2$m, $\bar{b} = 0.28$m (dashed line: left side of the condition, solid line: right side of the condition) a) Real; b) Imaginary.

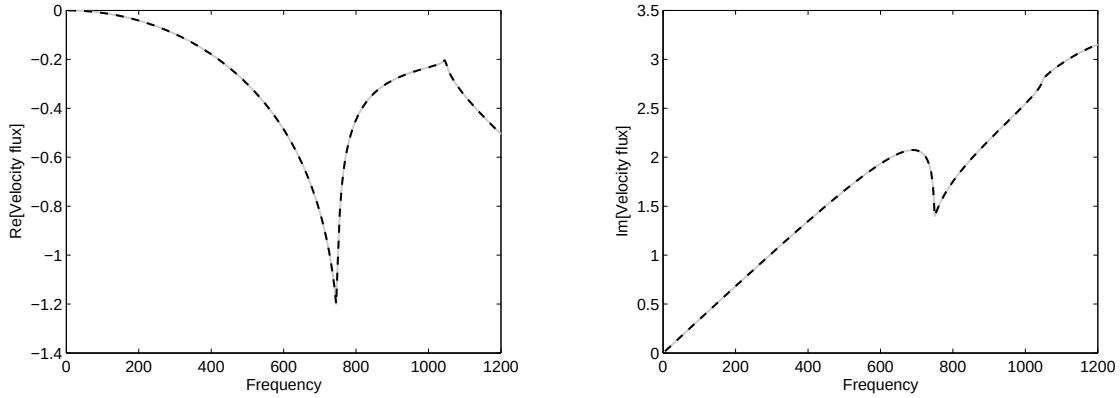

a) b)

Figure 2.16: The two sides of the velocity flux for 60 modes with $\bar{a} = 0.2$m, $\bar{b} = 0.28$m (dashed line: left side of the condition, solid line: right side of the condition) a) Real; b) Imaginary.

change in the normal component of velocity (known as Gibb's phenomenon). These plots show that with 60 modes the amplitudes have a better agreement with the normal component of velocity condition, but is not perfect due to its piecewise nature. A better validation for this matching condition would be to show the matched velocity flux. The velocity flux is the average velocity over the region, achieved through integration, thus the matched velocity flux is

$$\frac{ia^2(F - A_0)}{2} - i\sum_{n=1}^{\infty} A_n \int_0^a J_0(\kappa_n r) r \, \mathrm{d}r = \frac{ib^2}{2} + i\sum_{n=1}^{\infty} B_n \int_0^b J_0(\gamma_n r) r \, \mathrm{d}r. \tag{2.88}$$

Note that the modes involving A_0 and B_0 have been integrated separate to the remainder of the summation as $s_0 = \eta_0 = 1$ and $\kappa_0 = \gamma_0 = 0$. The two sides of (2.88) (real and imaginary) are presented in Figure 2.15 with 10 modes and Figure 2.16 with 60 modes. It is seen that there is a one-to-one agreement between the two sides of (2.88) with 100

modes used to form the amplitudes. There is a dip in both the real and imaginary parts at 745Hz which is in keeping with the first cut-on in the larger duct. Also there is a peak in the real part (with a slight increase in the imaginary part) at 1045Hz which is due to the first cut-on in the smaller duct. The plots in this subsection show that 10 modes is more than sufficient to formulate the amplitudes with and they validate that the method has been applied correctly.

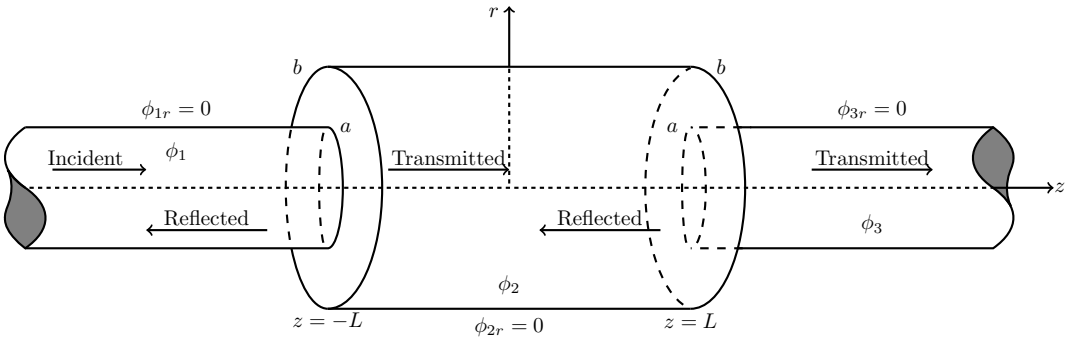

Figure 2.17: Physical configuration of the rigid expansion chamber problem.

2.6 Energy transmitted through a rigid expansion chamber situated between two ducts

This section considers the energy leaving an expansion chamber situated between two ducts. The problem comprises two semi-infinite ducts with a finite chamber of non-dimensional half-length L between them (where $L = \bar{L}k$) as shown in Figure 2.17. The inlet duct is located in the region $0 \leq r \leq a,\ z \leq -L$, the outlet duct is located in the region $0 \leq r \leq a,\ z \geq L$, and the expansion chamber occupies the space between them, $0 \leq r \leq b,\ -L \leq z \leq L$. The waveguide is closed by rigid annular discs located at $a \leq r \leq b,\ z = \pm L$.

The velocity potential for the left-hand duct ϕ_1 comprises the incident wave and the field reflected at the first junction, which leads to

$$\phi_1 = FJ_0(\kappa_0 r)e^{is_0(z+L)} + \sum_{n=0}^{\infty} A_n J_0(\kappa_n r)e^{-is_n(z+L)},\ 0 \leq r \leq a,\ z \leq -L, \tag{2.89}$$

where F is the amplitude of the forcing wave given in (2.39), A_n is the amplitude of the nth mode, s_n are the wavenumbers for the inlet and outlet ducts and $\kappa_n = (1 - s_n^2)^{1/2}$. Note that the arguments of the exponentials have been manipulated such that they will later simplify. The velocity potential for the expansion chamber is made of the waves reflected by the second junction and those which pass through the first junction. This gives the velocity potential ϕ_2 as

$$\phi_2 = \sum_{n=0}^{\infty} \left\{P_n e^{-i\eta_n z} + Q_n e^{i\eta_n z}\right\} J_0(\gamma_m r),\ 0 \leq r \leq b,\ -L \leq z \leq L, \tag{2.90}$$

where P_n and Q_n are the amplitudes of the nth reflected and transmitted modes respectively, η_n are the wavenumbers for the expansion chamber and $\gamma_n = (1 - \eta_n^2)^{1/2}$. The velocity potential for the right-hand duct ϕ_3 contains those waves transmitted through

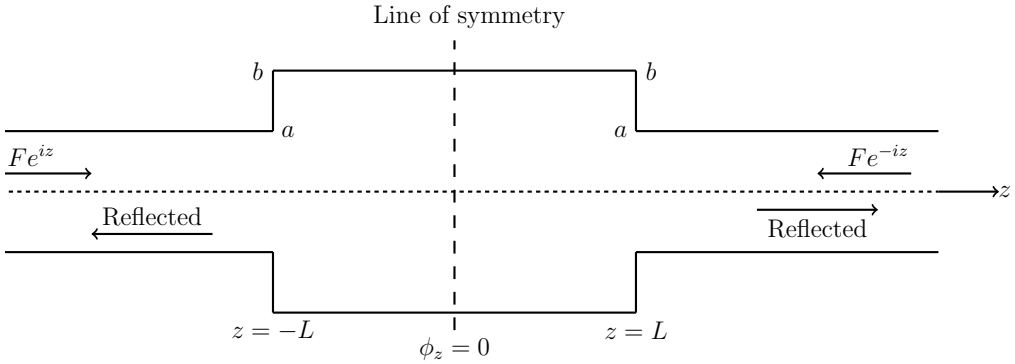

Figure 2.18: The symmetric subproblem.

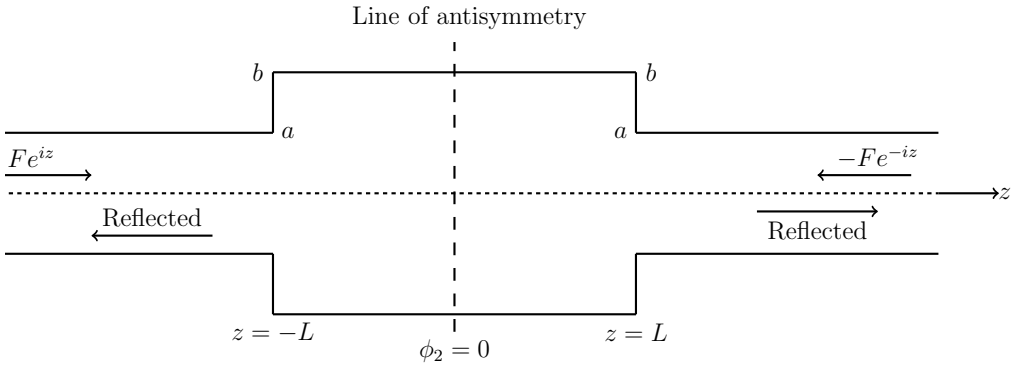

Figure 2.19: The antisymmetric subproblem.

the second junction, that is

$$\phi_3 = \sum_{n=0}^{\infty} B_n J_0(\kappa_n r) e^{is_n(z-L)},\ 0 \leq r \leq a,\ z \geq L, \tag{2.91}$$

where B_n amplitude of the nth transmitted mode.

The problem can be broken down into a symmetric and an antisymmetric subproblem. This is done by introducing a second forcing wave located in the right-hand duct. This travels in the negative z direction for both problems. For the antisymmetric subproblem the additional forcing wave has a phase shift of π, which by Euler's identity results in a negative forcing amplitude. These subproblems are illustrated in Figure 2.18 and Figure 2.19.

These subproblems are simpler to solve as they have a line of symmetry/antisymmetry allowing them to be reduced to a problem with an abrupt increase in radius. The reflected amplitudes from these systems can then be used to find the reflected and transmitted amplitudes for the full problem.

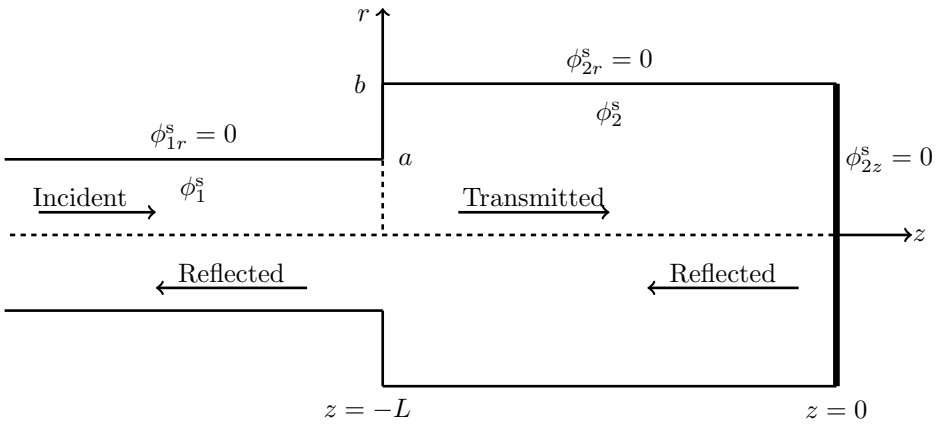

Figure 2.20: Physical configuration of the symmetric subproblem.

2.6.1 Symmetric subproblem

The nature of the symmetric subproblem enables it to be reduced to an equivalent semi-infinite problem with an abrupt increase in radius and a rigid end plate as shown in Figure 2.20. The purpose of this subsection is to determine the acoustic field reflected due to a forcing wave at an abrupt increase in radius. The problem comprises one semi-infinite duct and one finite duct. The semi-infinite duct is on the left-hand side and occupies $0 \leq r \leq a,\ z \leq -L$ and the finite duct is on the right-hand side and occupies $0 \leq r \leq b,\ -L \leq z \leq 0$. The waveguide is closed by a rigid annular disc occupying $a \leq r \leq b,\ z = -L$ and a rigid plate occupying $0 \leq r \leq b,\ z = 0$. Forcing is by a wave propagating in the positive z direction towards the abrupt increase in radius.

The velocity potential for the left-hand duct ϕ^{s}_1 comprises the plane wave and the reflected field, which is

$$\phi^{\mathrm{s}}_1 = Fe^{i(z+L)} + \sum_{n=0}^{\infty} A^{\mathrm{s}}_n J_0(\kappa_n r) e^{-is_n(z+L)},\ 0 \leq r \leq a,\ z \leq -L, \tag{2.92}$$

where the superscript denotes the symmetric subsystem and $A^{\mathrm{s}}_n,\ n = 0, 1, 2, \ldots$ are the amplitudes of the reflected modes for the symmetric system. The velocity potential for the right-hand duct ϕ^{s}_2 comprises the field reflected by the rigid disc and the field which passes through the junction, thus

$$\phi^{\mathrm{s}}_2 = \sum_{n=0}^{\infty} \left\{ P^{\mathrm{s}}_n e^{-i\eta_n z} + Q^{\mathrm{s}}_n e^{i\eta_n z} \right\} J_0(\gamma_n r),\ 0 \leq r \leq b,\ -L \leq z \leq 0, \tag{2.93}$$

where P^{s}_n and Q^{s}_n are the amplitudes of the nth reflected and transmitted modes respec-

tively. The property of the rigid end plate is

$$\frac{\phi_2^{\rm s}}{\partial z}(r,0) = i\sum_{n=0}^{\infty}\left\{-P_n^{\rm s}+Q_n^{\rm s}\right\}\eta_n J_0(\gamma_n r) = 0,\ 0\le r\le b. \tag{2.94}$$

From the large argument approximation for Bessel functions it is seen that in order for $J_0(\gamma_n r) = 0$ the roots $\gamma_n r = (m+1)\pi/2\ , m = 0,1,2,\ldots$. However, as the roots are defined as $\gamma_n a = (m+1/4)\pi/2\ , m = 0,1,2,\ldots$ (from the characteristic equation) the above equation is only satisfied when $P_n^{\rm s} = Q_n^{\rm s}$. It follows that $\phi_2^{\rm s}$ reduces to

$$\phi_2^{\rm s} = 2\sum_{n=0}^{\infty} P_n^{\rm s}\cos(\eta_n z)J_0(\gamma_n r),\ 0\le r\le b,\ -L\le z\le 0. \tag{2.95}$$

The system is solved by matching the fluid pressure and the normal component of velocity at the junction. These are continuous in the fluid, while the normal component of velocity vanishes on the rigid annular disc. That is at $z = -L$

$$\phi_1^{\rm s}(r,-L) = \phi_2^{\rm s}(r,-L),\ 0\le r\le a, \tag{2.96}$$

$$\frac{\partial\phi_2^{\rm s}}{\partial z}(r,-L) = \begin{cases} \frac{\partial\phi_1^{\rm s}}{\partial z}(r,-L), & 0\le r\le a \\ 0, & a\le r\le b \end{cases}. \tag{2.97}$$

From (2.96) it is found that

$$F + \sum_{n=0}^{\infty} A_n^{\rm s} J_0(\kappa_n r) = 2\sum_{n=0}^{\infty} P_n^{\rm s}\cos(\eta_n L)J_0(\gamma_n r). \tag{2.98}$$

Equation (2.98) is multiplied by $J_0(\kappa_m r)r$ and integrated with respect to $r,\ 0\le r\le a$, to give

$$\begin{aligned} &F\int_0^a J_0(\kappa_m r)r\ {\rm d}r + \sum_{n=0}^{\infty} A_n^{\rm s}\int_0^a J_0(\kappa_n r)J_0(\kappa_m r)r\ {\rm d}r \\ &= 2\sum_{n=0}^{\infty} P_n^{\rm s}\cos(\eta_n L)\int_0^a J_0(\gamma_n r)J_0(\kappa_m r)r\ {\rm d}r. \end{aligned} \tag{2.99}$$

The orthogonality relation in (2.25) is used to evaluate those integrals on the left-hand side. It follows that

$$A_m^{\rm s} = -F\delta_{\ell m} + \frac{2}{C_m}\sum_{n=0}^{\infty} P_n^{\rm s}\cos(\eta_n L)R_{mn}. \tag{2.100}$$

where R_{mn} is as given in (2.80) and C_m is as given in (2.26). A second expression is found by multiplying (2.97) by $J_0(\gamma_m r)r$ and integrating with respect to $r,\ 0\le r\le b$. It

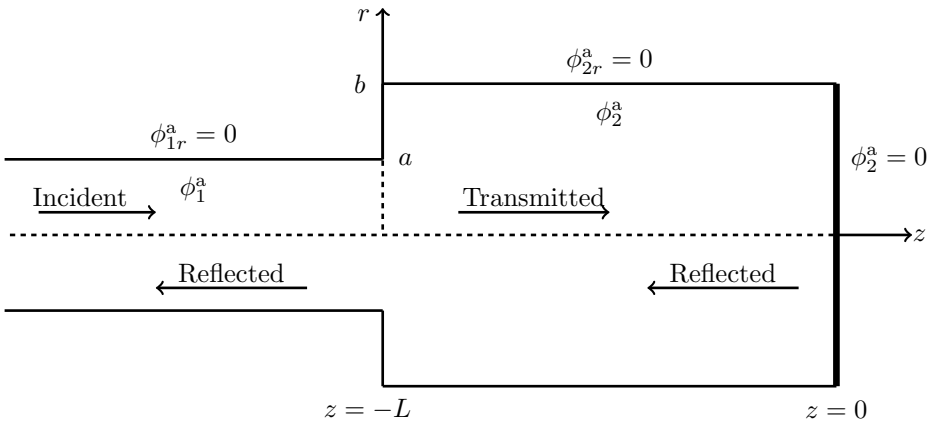

Figure 2.21: Physical configuration of the antisymmetric subproblem.

is noted that the right-hand side is zero on (a, b) and the orthogonality relation in (2.27) is used to evaluate the left-hand side to give

$$P^{\mathrm{s}}_m = \frac{iFs_\ell R_{\ell m}}{4D_m\eta_m \sin(\eta_m L)} - \frac{i}{2D_m\eta_m \sin(\eta_m L)} \sum_{n=0}^{\infty} A^{\mathrm{s}}_n s_n R_{nm}, \tag{2.101}$$

where R_{mn} is given in (2.80) and D_m is given in (2.28). The reflected and transmitted amplitudes of the symmetric system are thus found by solving the coupled equations (2.98) and (2.101), where the number of modes in each summation is truncated to 100 modes.

2.6.2 Antisymmetric subproblem

The nature of the antisymmetric subproblem enables it to be reduced to a semi-infinite system with an abrupt increase in radius and an acoustically soft end plate (see Figure 2.21). The system comprises two sections of duct: the left-hand duct occupies $0 \le r \le a,\ z \le -L$ and the right-hand duct occupies $0 \le r \le b,\ -L \le z \le 0$. It is closed by a rigid annular disc occupying $a \le r \le b,\ z = -L$ and an acoustically soft end plate occupying $0 \le r \le b,\ z = 0$. Forcing is by a wave located in the left-hand duct propagating in the positive z direction towards the abrupt increase in radius.

The velocity potential for the left-hand duct ϕ^{a}_1 comprises the incident wave and the reflected field

$$\phi^{\mathrm{a}}_1 = Fe^{i(z+L)} + \sum_{n=0}^{\infty} A^{\mathrm{a}}_n J_0(\kappa_n r) e^{-is_n(z+L)},\ 0 \le r \le a,\ z \le -L, \tag{2.102}$$

where the superscript denotes an antisymmetric subsystem and $A^{\mathrm{a}}_n,\ n = 0, 1, 2, \ldots$ are the amplitudes for the reflected field. The velocity potential for the right-hand duct ϕ^{a}_2 comprises the field reflected by the acoustically soft disc and the field which passes

through the junction

$$\phi_2^{\mathrm{a}} = \sum_{n=0}^{\infty} \left\{ P_n^{\mathrm{a}} e^{-i\eta_n z} + Q_n^{\mathrm{a}} e^{i\eta_n z} \right\} J_0(\gamma_n r),\ 0 \le r \le b,\ -L \le z \le 0, \tag{2.103}$$

where P_n^{a} and Q_n^{a} are the amplitudes of the nth reflected and transmitted modes respectively. The property of the acoustically soft end plate is

$$\phi_2^{\mathrm{a}}(r,0) = \sum_{n=0}^{\infty} \left\{ P_n^{\mathrm{s}} + Q_n^{\mathrm{s}} \right\} J_0(\gamma_n r) = 0,\ 0 \le r \le b, \tag{2.104}$$

which implies that $P_n^{\mathrm{a}} = -Q_n^{\mathrm{a}}$, which reduces ϕ_2^{a} to

$$\phi_2^{\mathrm{a}} = 2 \sum_{n=0}^{\infty} P_n^{\mathrm{a}} \sin(\eta_n z) J_0(\gamma_n r),\ 0 \le r \le b,\ -L \le z \le 0, \tag{2.105}$$

The method of solution is analogous to that of the symmetric subproblem. The first expression is found by applying the pressure condition, which on completing the steps described above, gives

$$A_n^{\mathrm{a}} = -F_\ell \delta_{\ell m} - \frac{2}{aC_m} \sum_{n=0}^{\infty} P_n^{\mathrm{a}} \sin(\eta_n L) R_{nm}, \tag{2.106}$$

where R_{nm} is given in (2.80) and C_m is given in (2.26). The second expression is found by applying the condition for the normal component of velocity condition, which leads to

$$P_m^{\mathrm{a}} = \frac{iF_\ell s_\ell R_{\ell m}}{2bD_m \eta_m \cos(\eta_m L)} - \frac{i}{2bD_m \eta_m \cos(\eta_m L)} \sum_{n=0}^{\infty} A_n^{\mathrm{a}} s_n R_{nm}, \tag{2.107}$$

where R_{nm} is as in (2.80) and D_m is as in (2.28). The reflected and transmitted amplitudes are found by truncating and solving the coupled equations (2.106) and (2.107).

With the reflected amplitudes of the symmetric and antisymmetric subproblems, the amplitudes for the full expansion chamber problem can be found. These are given by

$$A_m = \frac{A_m^{\mathrm{s}} + A_m^{\mathrm{a}}}{2},\ B_m = \frac{A_m^{\mathrm{s}} - A_m^{\mathrm{a}}}{2}, \tag{2.108}$$

where A_m are the amplitudes of the reflected field and B_m are the amplitudes of the transmitted field. Energy balance is achieved when the total energy input is equal to the total energy output. For this problem there is one source of energy entering the system $\mathcal{E}_{\mathrm{F}}$ and two sources of energy leaving the system. Those sources leaving the system are the reflected $\mathcal{E}_{\mathrm{A}}$ and transmitted energy $\mathcal{E}_{\mathrm{B}}$. Therefore the energy balance for the problem is given by $\mathcal{E}_{\mathrm{F}} = \mathcal{E}_{\mathrm{A}} + \mathcal{E}_{\mathrm{B}}$.

The amplitudes A_m and B_m are used in the (2.41) and (2.42) to give the reflected and transmitted energies respectively. These are stated below for convenience: The energy for the reflected field is given by

$$\mathcal{E}_{\mathrm{A}} = \mathrm{Real}\left[\sum_{m=0}^{M} |A_m|^2 s_m C_m\right], \tag{2.109}$$

where A_m are the amplitudes of the reflected waves and the energy for the transmitted field is

$$\mathcal{E}_{\mathrm{B}} = \mathrm{Real}\left[\sum_{m=0}^{M} |B_m|^2 \eta_m D_m\right], \tag{2.110}$$

where B_m are the amplitudes of the transmitted waves. The amplitudes and energies are calculated in Matlab with the code presented in Appendix C and the plots are presented below. This has been done using 100 modes to calculate the amplitudes of the propagating waves. It is shown in the next subsection that this is more than sufficient for calculating accurate results.

The radius of the inlet and outlet ducts are firstly considered to be equal to the radius of the expansion chamber, thus forming an infinite duct. The radius of the inlet and outlet ducts are $\bar{a} = 0.2$m and the radius of the expansion chamber is $\bar{b} = 0.2$m. For a duct of radius $\bar{a} = 0.2$m the first cut-on occurs at 1041Hz (and further modes cut-on outside the frequency range). In both case of $\ell = 0$ and $\ell = 1$ forcing modes it is seen that the energy is totally transmitted, this is due to there being no discontinuity to scatter the incident wave.

The next configuration considers the radii of the inlet and outlet ducts to be kept at $\bar{a} = 0.2$m while the radius of the expansion chamber is increased to $\bar{b} = 0.28$m. An expansion chamber of half length $\bar{L} = 0.25$m is considered in Figure 2.22a and the results show that the expansion chamber causes the energies to oscillate over frequency. This behaviour is due to the trigonometric factor present in both the reflected and transmitted amplitudes. The troughs of the reflected energy (and likewise peaks of the transmitted energy) can be predicted while the energy is carried by the fundamental mode. As $\eta_0 = 1$ the drops occur when $\sin(\eta L) = 0$, which is when $k\bar{L} = n\pi,\ n = 0, 1, 2, \ldots$, which is when $f = nc/(4\bar{L}),\ n = 0, 1, 2, \ldots$ (as $k = f2\pi/c$). This accounts for the troughs in the reflected energy at 0Hz, 343.5Hz and 687Hz. At 744Hz the cut-on mode from the expansion chamber causes the reflected energy to peak sharply. After this cut-on the energy is mostly reflected and it drops again at the cut-on at from the inlet and outlets ducts at 1041Hz. Note the noise mentioned in the piston problem is more evident in this plot.

Increasing the length of the expansion chamber to $2\bar{L} = 1$m the energies are found as shown in Figure 2.22b. The oscillations now occur twice as often due to the increase

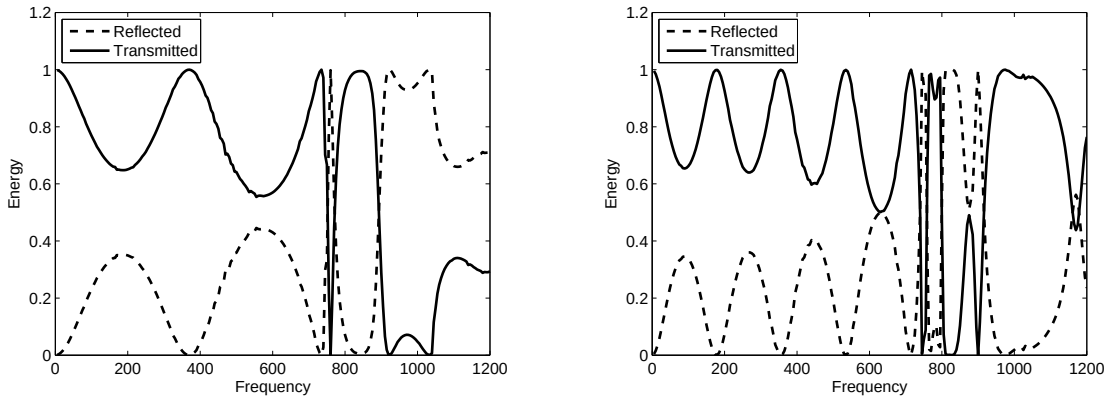

a) b)

Figure 2.22: Energy output from an expansion chamber with: a) $\bar{a} = 0.2$m, $\bar{b} = 0.28$m, $\bar{L} = 0.25$m; b) $\bar{a} = 0.2$m, $\bar{b} = 0.28$m, $\bar{L} = 0.5$m.

chamber length. The predicted dips in reflected energy are at 0Hz, 171.75Hz, 343.5Hz, 515Hz and 687Hz. At 744Hz the cut-on mode from the expansion chamber causes the reflected energy to peak sharply. Between 800Hz and 900Hz the energy is mostly reflected, after which the transmitted energy dominates again. The cut-on from the inlet and outlets ducts at 1041Hz cause a minor disturbance in the transmitted energy, which then proceeds to decrease.

The radius of the inlet and outlets ducts are now reduced to $\bar{a} = 0.06$m while keeping the radius of the expansion chamber at $\bar{b} = 0.28$m. The energies for an expansion chamber of length $2\bar{L} = 0.5$m are shown in Figure 2.23a). It is seen that the reflected energy drops in reflected energy occur at the same frequencies approximated for the previous configuration, however the dips here are much sharper with the reflected energy being zero at these frequencies. The cut-on from the expansion chamber at 744Hz causes an inversion in the energies and after this frequency the transmitted energy is dominant up until approximately 880Hz.

Increasing the length of the expansion chamber to $2\bar{L} = 1$m produces results seen in Figure 2.23b. It is again seen that with a chamber twice as long, the energy oscillations occur twice as frequent. The energy is mostly reflected below the first cut-on, however beyond here the energy flips between mostly reflected and mostly transmitted.

2.6.3 Transfer matrix method

The transfer matrix method used in Munjal and Prasad [7] and Peat [8] can be applied to the rigid expansion chamber system. This is a low frequency approach using only plane waves. Thus the normal component of velocity is not an appropriate matching condition because it contains no information about the change in radius. Therefore the transfer matrix will instead be formed by matching the fluid pressure and velocity flux.

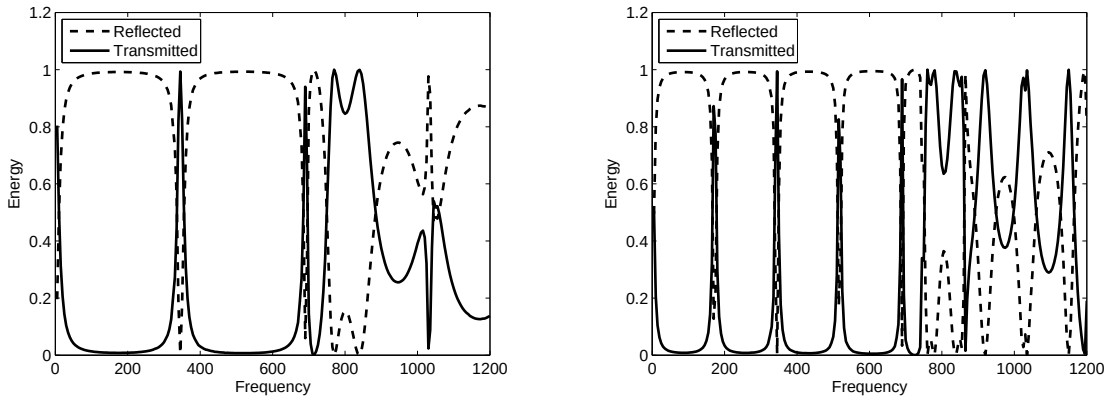

a) b)

Figure 2.23: Energy output from an expansion chamber with: a) $\bar{a} = 0.06$m, $\bar{b} = 0.28$m, $\bar{L} = 0.25$m; b) $\bar{a} = 0.06$m, $\bar{b} = 0.28$m, $\bar{L} = 0.5$m.

As mentioned above, this method uses only the first mode of each velocity potential and thus the potentials are approximated as

$$\tilde{\phi}_1(z) = Fe^{i(z+L)} + A_0 e^{-i(z+L)}, \tag{2.111}$$

$$\tilde{\phi}_2(z) = P_0 e^{-iz} + Q_0 e^{iz}, \tag{2.112}$$

$$\tilde{\phi}_3(z) = B_0 e^{i(z-L)}. \tag{2.113}$$

Equations which relate the velocity potentials at the first junction are found by matching the fluid pressure and the velocity flux. These conditions are applied at $z = -L$ and are given by

$$\tilde{\phi}_1(-L) = \phi_2(r, -L),\ 0 \leq r \leq a, \tag{2.114}$$

$$\int_0^{2\pi}\int_0^a \frac{\partial\tilde{\phi}_1}{\partial z}(-L)r\ \mathrm{d}r\mathrm{d}\theta = \int_0^{2\pi}\int_0^b \frac{\partial\tilde{\phi}_2}{\partial z}(-L)r\ \mathrm{d}r\mathrm{d}\theta. \tag{2.115}$$

The velocity potentials in (2.111) and (2.112 are substituted into the above conditions and expressed in matrix form as:

$$\begin{bmatrix} \tilde{\phi}_1(-L) \\ \frac{\partial\tilde{\phi}_1}{\partial z}(-L) \end{bmatrix} = \begin{bmatrix} e^{iL} & e^{-iL} \\ -ib^2e^{iL}/a^2 & ib^2e^{-iL}/a^2 \end{bmatrix} \begin{bmatrix} P_0 \\ Q_0 \end{bmatrix}. \tag{2.116}$$

The matrix which relates pressures and velocity across the first junction is

$$M_1 = \begin{bmatrix} e^{iL} & e^{-iL} \\ -ib^2e^{iL}/a^2 & ib^2e^{-iL}/a^2 \end{bmatrix}. \tag{2.117}$$

A second matrix is found by matching the pressure and velocity flux at the second junc-

tion. That is, at $z = L$

$$\tilde{\phi}_3(L) = \tilde{\phi}_2(L),\ 0 \leq r \leq a, \tag{2.118}$$

$$\int_0^{2\pi}\int_0^a \frac{\partial\tilde{\phi}_3}{\partial z}(L) r\ \mathrm{d}r\mathrm{d}\theta = \int_0^{2\pi}\int_0^b \frac{\partial\tilde{\phi}_2}{\partial z}(L) r\ \mathrm{d}r\mathrm{d}\theta. \tag{2.119}$$

The velocity potentials in (2.113) and (2.111 are substituted into the above conditions and they are expressed in matrix form as:

$$\begin{bmatrix} \tilde{\phi}_3(L) \\ \frac{\partial\tilde{\phi}_3}{\partial z}(L) \end{bmatrix} = \begin{bmatrix} e^{-iL} & e^{iL} \\ -ib^2e^{-iL}/a^2 & ib^2e^{iL}/a^2 \end{bmatrix} \begin{bmatrix} P_0 \\ Q_0 \end{bmatrix}. \tag{2.120}$$

The matrix at the second junction is thus given by

$$M_2 = \begin{bmatrix} e^{-iL} & e^{iL} \\ -ib^2e^{-i\eta_0 L}/a^2 & ib^2e^{iL}/a^2 \end{bmatrix}. \tag{2.121}$$

In order to form the transfer matrix for the expansion chamber, the expressions for each junction must be combined. This is done by eliminating $[P_0\ Q_0]$ between (2.116) and (2.120) to give

$$\begin{bmatrix} \tilde{\phi}_1(-L) \\ \frac{\partial\tilde{\phi}_1}{\partial z}(-L) \end{bmatrix} = M_1M_2^{-1} \begin{bmatrix} \tilde{\phi}_3(L) \\ \frac{\partial\tilde{\phi}_3}{\partial z}(L) \end{bmatrix}, \tag{2.122}$$

where the inverse of M_2 is

$$M_2^{-1} = \frac{1}{2ib^2} \begin{bmatrix} ib^2e^{iL}/a^2 & -e^{iL} \\ ib^2e^{-iL}/a^2 & e^{-iL} \end{bmatrix}. \tag{2.123}$$

The matrix multiplication of matrix M_1 with the inverse of the transfer matrix M_2 lead to the equations for the entire system as

$$\begin{bmatrix} \tilde{\phi}_1(-L) \\ \frac{\partial\tilde{\phi}_1}{\partial z}(-L) \end{bmatrix} = \frac{1}{2} \begin{bmatrix} e^{2iL} + e^{-2iL} & ia^2(e^{2iL} - e^{-2iL})/b^2 \\ -ib^2(e^{2iL} - e^{-2iL})/a^2 & e^{2iL} + e^{-2iL} \end{bmatrix} \begin{bmatrix} \tilde{\phi}_3(L) \\ \frac{\partial\tilde{\phi}_3}{\partial z}(L) \end{bmatrix}. \tag{2.124}$$

From here it can be seen that the transfer matrix for the entire system is

$$\begin{bmatrix} \cos(2L) & -a^2\sin(2L)/b^2 \\ b^2\sin(2L)/a^2 & \cos(2L) \end{bmatrix} \tag{2.125}$$

Now the transfer matrix has been obtained, it is left to solve the following equations to

obtain the reflected and transmitted coefficients

$$F + A_0 = B_0 \left\{ \cos(2L) - \frac{ia^2 \sin(2L)}{b^2} \right\}, \tag{2.126}$$

$$i(F - A_0) = B_0 \left\{ \frac{b^2 \sin(2L)}{a^2} + i\cos(2L) \right\}. \tag{2.127}$$

With the transfer matrix method the approximations for the first mode amplitudes of the reflected and transmitted waves are

$$A_0 = \frac{F(a^4 - b^4)\sin(2L)}{2ia^2b^2\cos(2L) + (a^4 + b^4)\sin(2L)}, \tag{2.128}$$

$$B_0 = \frac{2iFa^2b^2}{2ia^2b^2\cos(2L) + (a^4 + b^4)\sin(2L)}. \tag{2.129}$$

The amplitudes A_m and B_m are used in the (2.41) and (2.42) to give the reflected and transmitted energies respectively. These are stated below for convenience: The energy for the reflected field is given by

$$\mathcal{E}_{\mathrm{A}} = \mathrm{Real}\left[\sum_{m=0}^{M} |A_m|^2 s_m C_m \right], \tag{2.130}$$

where A_m are the amplitudes of the reflected waves and the energy for the transmitted field is

$$\mathcal{E}_{\mathrm{B}} = \mathrm{Real}\left[\sum_{m=0}^{M} |B_m|^2 \eta_m D_m \right], \tag{2.131}$$

where B_m are the amplitudes of the transmitted waves. The amplitudes and energies are calculated in Matlab with the code presented in Appendix C and they are compared with those obtained from the mode matching method in the results that follow. This has been done using 100 modes to calculate the amplitudes of the propagating waves. The thinner solid line is the approximated transmitted energy and the thinner dashed line is the approximated reflected energy. Note that the transfer matrix is only valid up until the first cut-on as only the fundamental mode is considered in the velocity potentials.

Expansion chambers with outer radius $\bar{a} = 0.2$m and chamber radius $\bar{b} = 0.28$m are firstly considered. With an expansion chamber of half length $\bar{L} = 0.25$m (see Figure 2.24a), it is seen that up until 200Hz the transfer matrix method provides a very good approximation for the reflected and transmitted energy. From this point the approximated energies begin to drift increasingly further away from those found from the mode matching method.

The radius of the outer ducts are now considered to be equal to the radius of the expansion chamber with $\bar{a} = 0.2$m and $\bar{b} = 0.2$m. With an expansion chamber half length of $\bar{L} = 0.25$m, the transfer matrix energies are in full agreement with the energies

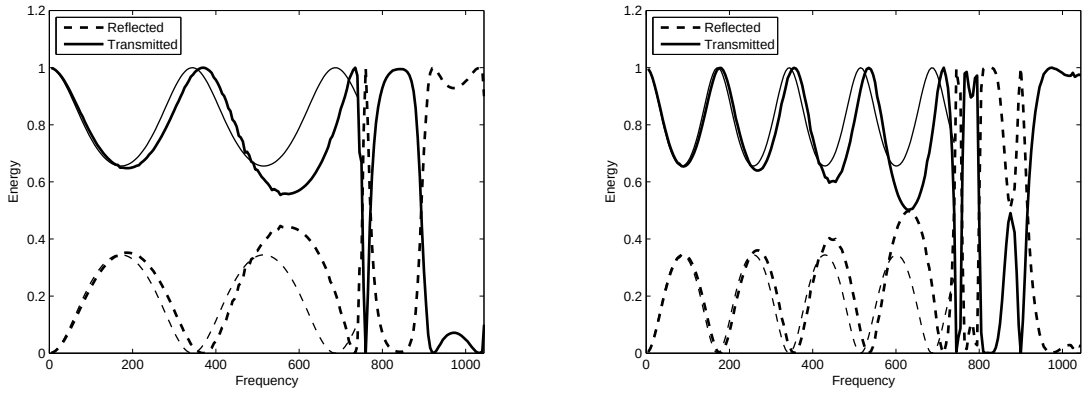

a) b)

Figure 2.24: Energy output from an expansion chamber with: a) $\bar{a} = 0.2$m, $\bar{b} = 0.28$m, $\bar{L} = 0.25$m; b) $\bar{a} = 0.2$m, $\bar{b} = 0.28$m, $\bar{L} = 0.5$m.

obtained from the mode matching method for the entire valid frequency range as the energy is totally transmitted.

With a longer chamber half length of $\bar{L} = 0.5$m (see Figure 2.24b), the transfer matrix approximation is valid for a wider frequency range. It is not until around 300Hz that the approximation begins to drift away from the energies obtained from the mode matching method. In addition, the error difference does not appear to be as big as it is with the shorter length chamber.

The second set of results are for the case when the radius of the outer ducts are reduced to $\bar{a} = 0.6$m while keeping the radius of the expansion chamber at $\bar{b} = 0.28$m. When the half length of the expansion chamber is $\bar{L} = 0.25$m (see 2.25a), the approximated energies form the transfer matrix method almost entirely agree with those obtained from the mode matching method. The approximated energies do begin to drift away after 600Hz, but the error difference is not as significant in this region when compared with the wider outer duct radius results.

Increasing the half of the expansion chamber to $\bar{L} = 0.5$m (see Figure 2.25b), shows an even better agreement between the energies from the transfer and the mode matching energies. The energies do still drift from the mode matching energies a tiny amount after 600Hz, but the error difference is not as large.

From these results it is seen that the transfer matrix method provides a good approximation for to the energy output for low frequencies. The frequency range of accurate approximations is wider for problems where the outer radius is significantly smaller compared to the radius of the expansion chamber.

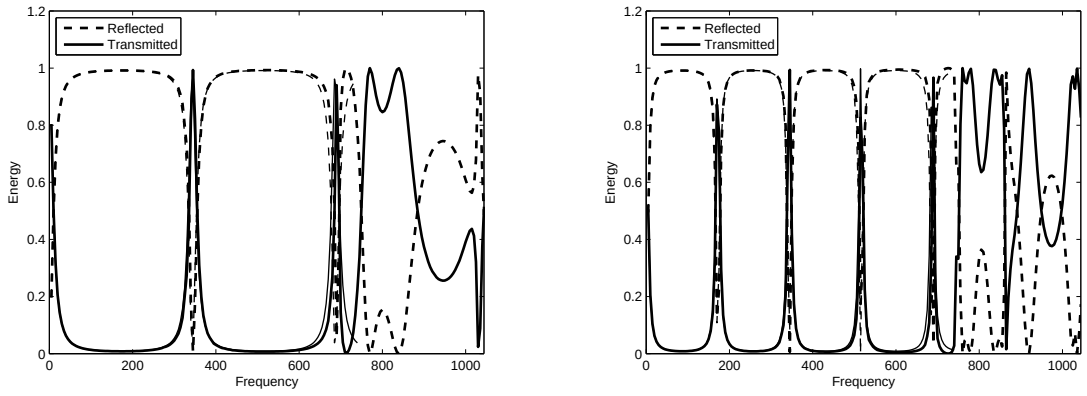

a) b)

Figure 2.25: Energy output from an expansion chamber with: a) $\bar{a} = 0.06$m, $\bar{b} = 0.28$m, $\bar{L} = 0.25$m; b) $\bar{a} = 0.06$m, $\bar{b} = 0.28$m, $\bar{L} = 0.5$m.

Chapter 3

Energy radiated in shells subject to axisymmetric motion

This chapter focuses on acoustic propagation in thin, circular, cylindrical shells with flexible walls. Equations are found for the flexible shell with axisymmetric motion and used to find the energy radiated in some simple problems involving propagation in a semi-infinite shell. A generalised orthogonality relation for the flexible shell with axisymmetric motion is derived and used with the mode-matching method to find the amplitudes. The generalised orthogonality relation is new to the research area. The results produced in this chapter are compared with those obtained from equivalent problems in Chapter two. Three problems are presented: Energy reflected due to a rigid plate, acoustic response due to a plane piston and acoustic response due to a plane piston and forcing wave.

3.1 Governing equations and dispersion relation

A thin, flexible-walled cylindrical shell described in cylindrical polar co-ordinates $(\bar{r}\,\bar{\theta}, \bar{z})$ is now considered. The interior region of the shell contains a compressible fluid of sound speed c and density ρ whilst the exterior region is in-vacuo. A harmonic time factor, $e^{-i\omega t}$, is assumed throughout where t is time and $\omega = ck$, with k being the fluid wavenumber. For this chapter and Chapter four, the flexible shells are subject to axisymmetric motion. Non-axisymmetric motion is considered later in Chapter five. These two types of motion are illustrated in Figure 3.1, where the dotted circles shows the maximum position of motion and the dashed circles represent the minimum position of motion. The value n shown in this figure relates to the order of the Bessel function used which creates this motion. This may not be evident in this Chapter as $n = 0$, but it will be more apparent in Chapter five when $n = 1$.

The fluid has the same properties as the fluid considered in Chapter two. Hence it is governed by the same Helmholtz equation stated in (2.4) which gives the solution for the

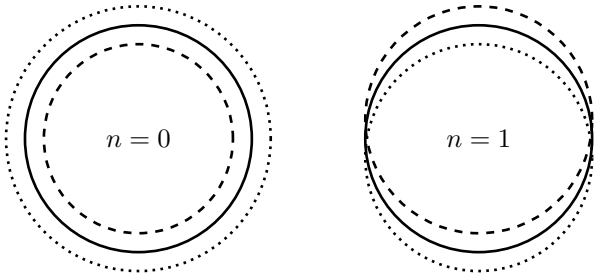

Figure 3.1: Illustration of axisymmetric (n=0) and non-axisymmetric vibrations (n=1).

velocity potential as

$$\phi_n = A_n J_0(\kappa_n r) e^{is_n z}, \tag{3.1}$$

where A_n is the amplitude of the nth wave, s_n is the wavenumber of the mode and satisfies the flexible-walled characteristic equation $K(s) = 0$ which is presented below and $\kappa_n^2 = (1 - s_n^2)^{1/2}$.

There are several different sets of equations which describe the motion of a flexible shell, many of which have been analysed in Leissa [25]. In this chapter (and in those chapters that follow), the Donnell-Mushtari equations of motion stated by Junger and Feit [30] will be used. This theory assumes that the displacements are small when compared to the thickness of the shell. Furthermore, that the thickness of the shell is small when compared to the radius of the shell. For a shell of thickness h, radius $\bar{a}$ and density ρ_s these assumptions translate to the limitations $hk \ll 1$ and $h/\bar{a} \ll 1$. The Donnell-Mushtari equations of motion for a cylindrical shell are:

$$\frac{\partial^2 \bar{u}}{\partial \bar{z}^2} + \frac{1-\nu}{2\bar{a}^2}\frac{\partial^2 \bar{u}}{\partial \theta^2} + \frac{1+\nu}{2\bar{a}}\frac{\partial^2 \bar{v}}{\partial \bar{z}\partial \theta} + \frac{\nu}{\bar{a}}\frac{\partial \bar{w}}{\partial \bar{z}} + \frac{\omega^2 \bar{u}}{{c_s}^2} = 0, \ \bar{r} = \bar{a}, \tag{3.2}$$

$$\frac{1+\nu}{2\bar{a}}\frac{\partial^2 \bar{u}}{\partial \bar{z}\partial \theta} + \frac{1-\nu}{2}\frac{\partial^2 \bar{v}}{\partial \bar{z}^2} + \frac{1}{\bar{a}^2}\frac{\partial^2 \bar{v}}{\partial \theta^2} + \frac{1}{\bar{a}^2}\frac{\partial \bar{w}}{\partial \theta} + \frac{\omega^2 \bar{v}}{c_s^2} = 0, \quad \text{at } \bar{r} = \bar{a}, \tag{3.3}$$

$$\frac{\nu}{\bar{a}}\frac{\partial \bar{u}}{\partial \bar{z}} + \frac{1}{\bar{a}^2}\frac{\partial \bar{v}}{\partial \theta} + \frac{\bar{w}}{\bar{a}^2} + \frac{h^2}{12}\frac{\partial^4 \bar{w}}{\partial \bar{z}^4} + \frac{2h^2}{12\bar{a}^2}\frac{\partial^4 \bar{w}}{\partial \bar{z}^2 \partial \theta^2} + \frac{h^2}{12\bar{a}^4}\frac{\partial^4 \bar{w}}{\partial \theta^4} - \frac{\omega^2 \bar{w}}{{c_s}^2} - \frac{\bar{p}(\bar{a}, \bar{z})}{{c_s}^2 \rho_s h} = 0, \ \bar{r} = \bar{a}, \tag{3.4}$$

where $\bar{u}$, $\bar{v}$ and $\bar{w}$ are the longitudinal, circumferential and radial shell displacements, respectively, ν is Poisson's ratio, $\bar{p}(\bar{a}, \bar{z})$ is the internal fluid pressure acting on the shell and c_s is the in-vacuo sound speed in the shell given by

$$c_s = \sqrt{\frac{E}{(1-\nu^2)\rho_s}}, \tag{3.5}$$

where E is Young's modulus. Note that the region exterior to the cylinder is in-vacuo. The pressure $\bar{p}$ and the circumferential shell displacement $\bar{w}$ can be expressed in terms

of the velocity potential $\bar{\phi}$ as follows:

$$\bar{p} = i\omega\rho\bar{\phi}, \tag{3.6}$$

$$\bar{w} = \frac{i}{\omega}\frac{\partial\bar{\phi}}{\partial\bar{r}}. \tag{3.7}$$

The non-dimensional variables given in (2.3) are used to non-dimensionalise the Donnell-Mushtari equations of motion as follows:

$$\frac{\partial^2 u}{\partial z^2} + \frac{1-\nu}{2a^2}\frac{\partial^2 u}{\partial\theta^2} + \frac{1+\nu}{2a}\frac{\partial^2 v}{\partial z\partial\theta} + \frac{i\nu}{a}\frac{\partial^2\phi}{\partial r\partial z} + \beta^2 u = 0, \quad \text{at } r = a, \tag{3.8}$$

$$\frac{1+\nu}{2a}\frac{\partial^2 u}{\partial z\partial\theta} + \frac{1-\nu}{2}\frac{\partial^2 v}{\partial z^2} + \frac{1}{a^2}\frac{\partial^2 v}{\partial\theta^2} + \frac{i}{a^2}\frac{\partial^2\phi}{\partial r\partial\theta} + \beta^2 v = 0, \quad \text{at } r = a, \tag{3.9}$$

$$\begin{aligned} &- i\nu a\frac{\partial u}{\partial z} - i\frac{\partial v}{\partial\theta} + \frac{\partial\phi}{\partial r} + \frac{1}{\tau_1}\frac{\partial^5\phi}{\partial r\partial z^4} + \frac{2}{\tau_1 a^2}\frac{\partial^5\phi}{\partial r\partial z^2\partial\theta^2} + \frac{1}{\tau_1 a^4}\frac{\partial^5\phi}{\partial r\partial\theta^4} - a^2\beta^2\frac{\partial\phi}{\partial r} \\ &- \frac{a^2\beta^2\rho}{\rho_s hk}\phi = 0, \quad \text{at } r = a, \end{aligned} \tag{3.10}$$

where $\beta = \omega/(c_s k)$ and $\tau_1 = 12/(k^2h^2a^2)$. For axisymmetric motion all θ- dependant displacements can be neglected, which reduces the equations of motion to

$$\frac{\partial^2 u}{\partial z^2} + \frac{i\nu}{a}\frac{\partial^2\phi}{\partial r\partial z} + \beta^2 u = 0, \quad \text{at } r = a, \tag{3.11}$$

$$-i\nu a\frac{\partial u}{\partial z} + \frac{\partial\phi}{\partial r} + \frac{1}{\tau_1}\frac{\partial^5\phi}{\partial r\partial z^4} - a^2\beta^2\frac{\partial\phi}{\partial r} - \frac{a^2\beta^2\rho}{\rho_s hk}\phi = 0, \quad \text{at } r = a. \tag{3.12}$$

On substituting the form of the velocity potential (3.1) into (3.11) the function for the longitudinal displacement is found as

$$u_n(a,z) = \frac{\nu s_n\kappa_n J_1(\kappa_n a)}{a(s_n^2 - \beta^2)}e^{is_n z}. \tag{3.13}$$

Similarly the form of the velocity potential (3.1) is substituted into $\bar{w}$ in (3.7) and non-dimensionalised to give

$$w_n(a,z) = \kappa_n J_1(\kappa_n a)e^{is_n z}. \tag{3.14}$$

The functional form for the longitudinal displacement is used in (3.12) to obtain the characteristic equation

$$K(s,a) = \tau_1\nu^2 s^2 - (s^2 - \beta^2)\left\{s^4 - \mu^4 + \alpha\frac{J_0(\kappa a)}{\kappa J_1(\kappa a)}\right\} = 0, \tag{3.15}$$

where $\mu^4 = \tau_1(a^2\beta^2 - 1)$ and $\alpha = 12\beta^2\rho/(\rho_s h^3 k^3)$. This function defines the wavenumbers

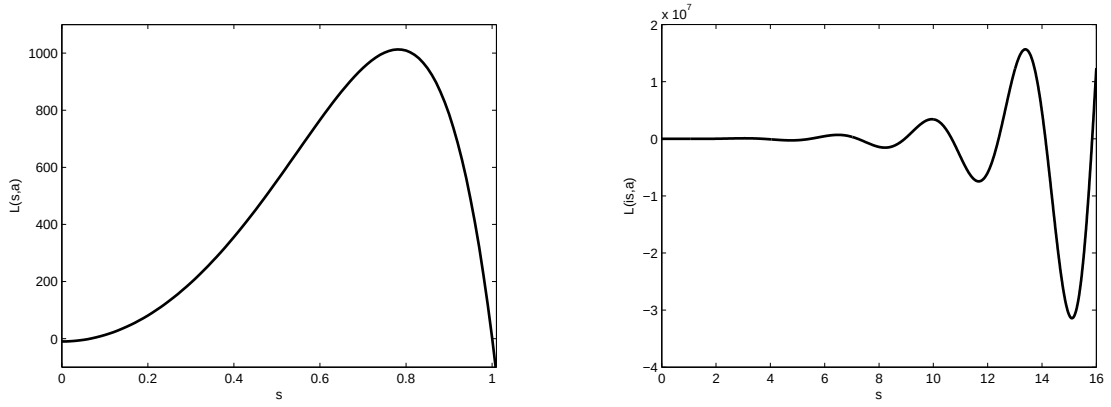

a) b)

Figure 3.2: Plot of the characteristic function for $\bar{a} = 0.2$m, $f = 500$Hz: a) Real valued input; b) Imaginary valued input.

of the fluid-coupled propagating waves travelling within the shell. Note that as $a \to \infty$, $\tau_1 \to 0$ the characteristic equation reduces to that for a thin plate.
For simplicity the characteristic function in (3.15) is multiplied through by $-\kappa J_1(\kappa a)$ to give the dispersion function

$$L(s,a) = -\tau_1 \nu^2 s^2 \kappa J_1(\kappa a) + \left(s^2 - \beta^2\right)\left(s^4 - \mu^4\right)\kappa J_1(\kappa a) + \left(s^2 - \beta^2\right)\alpha J_0(\kappa a) = 0. \quad (3.16)$$

For the problems presented herein the shells are to be representative of ductwork which appears in HVAC systems. However, these are commonly made of steel, which is not the best material to represent a flexible shell. Instead an aluminium shell, of thickness $h = 0.002$m and of density $\rho_s = 2700\text{kg m}^{-3}$ is considered. In addition, the required values of Young's modulus and Poisson's ratio are $E = 7.2 \times 10^{10}\text{Nm}^{-2}$ and $\nu = 0.34$; whilst the fluid is air with sound speed $c = 343.5\text{ms}^{-1}$ and density $\rho = 1.2\text{kg m}^{-3}$.

A plot of the characteristic function $L(s,a)$ is shown in Figure 3.1 for a radius of $\bar{a} = 0.2$m, where plot a) shows a real valued input and plot b) shows an imaginary valued input. It is seen that as $s \to \infty$, the imaginary part of the function oscillates more frequently, meaning the imaginary roots form closer together. It is the roots s_n, $n = 0, 1, 2, \ldots$ of this function that are required for the wavenumbers for the velocity potential. Those that are either positive real or have a positive imaginary part are required as these correspond to a waves that propagate in the positive z direction or decay as $z \to \infty$. To find these roots the Newton-Raphson method is used, this is an iterative technique for root finding in continuous functions. It requires a starting value z_0 that is close to the wanted root and iterates the equation until the desired accuracy is found. The

Newton-Raphson equation is

$$z_{n+1} = z_n - \frac{L(z_n, a)}{L'(z_n, a)}, \tag{3.17}$$

where z_{n+1} is the improved root value. This method has quadratic convergence and so within a few iterations the desired accuracy can be achieved. There are some limitations of this method which will be mentioned later. Starting root approximations for each of the roots need to be found, this is done by firstly approximating the characteristic function by its dominant term. For $|s| > 1$, the characteristic equation can be approximated to the dominant term

$$L(s, a) \approx \left(s^2 - \beta^2\right)\left(s^4 - \mu^4\right)\kappa J_1(\kappa a) = 0. \tag{3.18}$$

With this approximation, it can be seen that there are three possible ways that a root can develop. Thus the first root approximations are given by $s \approx \pm\beta$, $s \approx \pm\mu$ and $s \approx \pm i\mu$. It is left to solve $J_1(\kappa a) = 0$, which is done by approximating the Bessel function as follows

$$J_1(\kappa a) \approx \sqrt{\frac{2}{\pi\kappa a}} \cos\left(\kappa a - \frac{3\pi}{4}\right) = 0. \tag{3.19}$$

The roots of this function give the remaining approximations for the initial values as

$$s \approx \left[1 - \left\{\frac{\pi}{a}\left(m + \frac{5}{4}\right)\right\}^2\right]^{1/2}, \; m = 0, 1, 2 \ldots, \tag{3.20}$$

which suggests that there are an infinite number of evanescent modes. Note that for each m such that $a \geq \pi(m + 5/4),\ m = 0, 1, 2 \ldots$ an imaginary root becomes real, this is when an evanescent mode starts to propagate, this phenomena is known as a cut-on. These roots are ordered sequentially with real roots first and then by increasing imaginary part. Hence, s_0 is always the largest real root and remaining roots are ordered accordingly. There are two fundamental real roots. The first root is $s_0 \approx 1$, this corresponds to a fluid-borne mode as $\phi_0 = J_0(0)e^{iz}$ is a plane wave. The second root is $s_1 \approx \beta$, this is a solution of the equation created by considering $a \to \infty$ in (3.8) which leads to

$$\frac{\partial^2 u}{\partial z^2} + \beta^2 u = 0. \tag{3.21}$$

Thus, s_1 corresponds to a structure-borne mode as it is the mode propagating in this direction for large a. It is possible for a pair of complex roots to exist for certain ranges of frequency, these are found at $s \approx \pm i\mu$. A plot of the first 13 roots of the characteristic equation for a shell of radius 0.2m at a frequency of 500Hz is shown in Figure 3.3. Appendix D shows Matlab code which finds the roots of the characteristic equation with

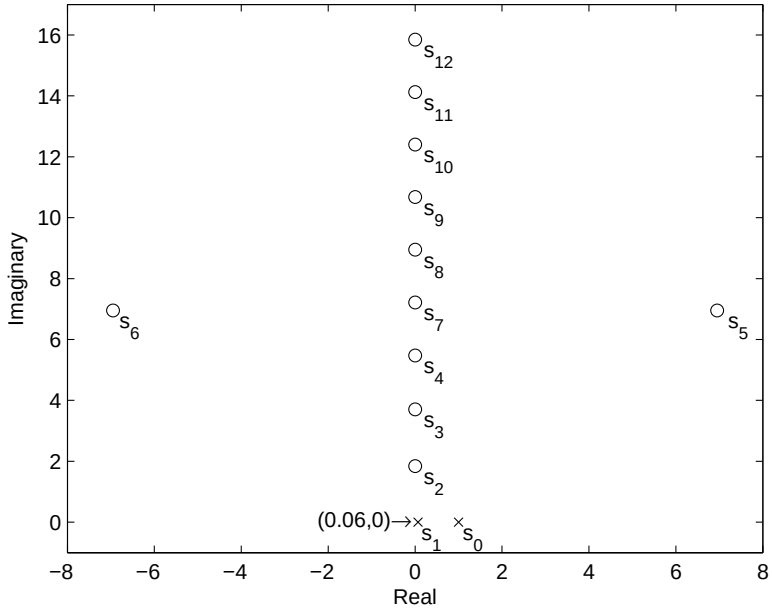

Figure 3.3: The first 13 roots of the characteristic equation at 500Hz with $\bar{a} = 0.2$m.

the approximations discussed above as initial values. This has been done using 100 modes to calculate the amplitudes of the propagating waves. However there are some limitations to using this method, firstly it fails around each cut-on due to the jump in continuity from the approximated imaginary to the real axis. This is avoided by instead using the range $(0, 1)$ with intervals of 0.1 and then use filtering techniques to identify unique roots that satisfy the dispersion function. The other limitation is that the starting values for the Newton-Raphson method have to be suitably close to desired root, this becomes a problem with higher frequencies as the roots become closer together. To avoid this, attention is restricted to the case of three or fewer real roots, which means that for each shell the non-dimensional radius should be $a \leq 13.34$. In order to ensure that all roots have been found the Cauchy integral theorem is used. This theorem states that if a function f is analytic and is non zero on an within a circle C, then the number of zeros $N_0(\cdot)$ (counting multiplicities) inside C is given by

$$N_0(f) = \frac{1}{2\pi i} \oint_C \frac{f'(z)}{f(z)} \, \mathrm{d}z. \tag{3.22}$$

The roots of the characteristic equation where $Re(s_n) > 0$ and/or $\mathrm{Im}(s_n) > 0$ are required. In order to perform the integration a change of variables $g(\theta) = re^{i\theta}$ is used, which gives

$$N_0(L) = \frac{1}{4\pi i} \int_0^{2\pi} \frac{L'(g(\theta), a)}{L(g(\theta), a)} g'(\theta) \, \mathrm{d}\theta, \tag{3.23}$$

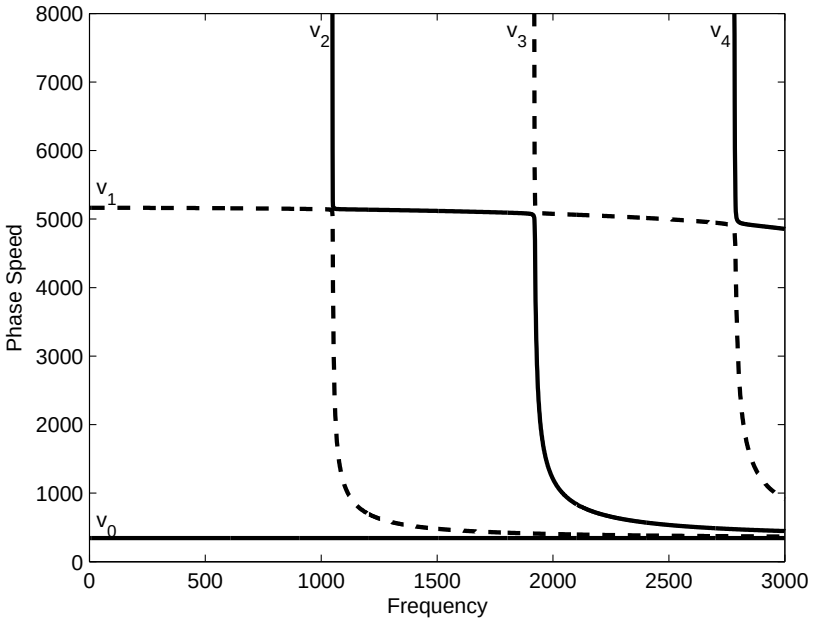

Figure 3.4: The phase speeds of the characteristic equation for $\bar{a} = 0.2$m.

where the r is the radius of the circle.

The phase velocities $v_n = c/s_n$, $n = 0, 1, 2, 3, 4$ for a shell of radius $\bar{a} = 0.2$m with frequencies $5 - 3000$Hz are illustrated in Figure 3.4. It is seen that for each root cut-on, the phase velocity of the previously leading root drops towards the sound speed of the fluid ($c = 343.5\text{ms}^{-1}$).

3.2 Edge conditions

For a shell of finite length it is necessary to specify edge conditions to describe the behaviour at each edge of the shell. Two sets of edge conditions for a shell of length $2\bar{L}$ (where $L = \bar{L}k$) are found in Junger and Feit [30]. For a shell that is clamped, the conditions are

$$\bar{u} = \bar{v} = \bar{w} = \frac{\partial \bar{w}}{\partial \bar{z}} = 0, \quad \text{at } \bar{z} = \pm\bar{L},\ \bar{r} = \bar{a}, \tag{3.24}$$

where $\bar{v}$ is the torsional direction, retained here for later non-axisymmetric problems. As the name suggests, the edge is clamped in place and no displacement can occur in any direction. For a shell that is pin-jointed, the conditions are

$$\bar{w} = \frac{\partial^2 \bar{w}}{\partial \bar{z}^2} = \bar{v} = \frac{\partial \bar{u}}{\partial \bar{z}} = 0, \quad \text{at } \bar{z} = \pm\bar{L},\ \bar{r} = \bar{a}. \tag{3.25}$$

This creates a hinge-like joint, where the shell can pivot on the fixing point. These edge conditions are non-dimensionalised using the non-dimensional counterparts given in (2.3)

to find the clamped edge conditions

$$u = v = \frac{\partial \phi}{\partial r} = \frac{\partial^2 \phi}{\partial r \partial z} = 0, \quad \text{at } z = \pm L,\ r = a, \tag{3.26}$$

and the pin-jointed conditions

$$\frac{\partial \phi}{\partial r} = \frac{\partial^3 \phi}{\partial r \partial z^2} = v = \frac{\partial u}{\partial z} = 0, \quad \text{at } z = \pm L,\ r = a, \tag{3.27}$$

where (3.7) has been used to express w in terms of ϕ.

3.3 The generalised orthogonality relation

To form the generalised orthogonality relation, the following equation involving $L(s, a)$ in (3.16) is considered:

$$\frac{L(s_n, a)\kappa_m J_1(\kappa_m a)}{s_n^2 - \beta^2} - \frac{L(s_m, a)\kappa_n J_1(\kappa_n a)}{s_m^2 - \beta^2} = 0, \tag{3.28}$$

where $s_n,\ n = 0, 1, 2, \ldots$ are the aforementioned roots and $\kappa_n = (1 - s_n^2)^{1/2}$. It is easily seen that this relation holds true for all roots and $s_n \neq \beta$ for $n = 0, 1, 2, \ldots$. On substituting the characteristic function (3.16) into this relation, it is obtained that

$$\begin{aligned} &\left\{ \frac{-\tau_1 \nu^2 \beta^2 (s_n^2 - s_m^2)}{(s_n^2 - \beta^2)(s_m^2 - \beta^2)} - s_n^4 + s_m^4 \right\} \kappa_n J_1(\kappa_n a) \kappa_m J_1(\kappa_m a) \\ &+ \frac{\alpha}{a} \Big[\Big\{ J_0(\kappa_n r)\kappa_m J_0'(\kappa_m r) - J_0(\kappa_m r)\kappa_n J_0'(\kappa_n r) \Big\} r \Big]_{r=0}^{a} = 0. \end{aligned} \tag{3.29}$$

The term in the square brackets is differentiated and expressed in integral form

$$\begin{aligned} &\frac{\alpha}{a} \int_0^a J_0(\kappa_m r) \big\{ \kappa_n^2 J_0''(\kappa_n r) r + \kappa_n J_0'(\kappa_m r) \big\} - J_0(\kappa_n r) \big\{ \kappa_m^2 J_0''(\kappa_m r) r + \kappa_m J_0'(\kappa_m r) \big\} \, \mathrm{d}r \\ &- \left\{ \frac{-\tau_1 \nu^2 \beta^2 (s_n^2 - s_m^2)}{(s_n^2 - \beta^2)(s_m^2 - \beta^2)} - s_n^4 + s_m^4 \right\} \kappa_n J_1(\kappa_n a) \kappa_m J_1(\kappa_n a). \end{aligned} \tag{3.30}$$

On using Bessel's equation, it is found that

$$\begin{aligned} &\big(s_m^2 - s_n^2\big) \frac{\alpha}{a} \int_0^a J_0(\kappa_m r) J_0(\kappa_n r) r \, \mathrm{d}r \\ &= -(s_m^2 - s_n^2) \left\{ \frac{\tau_1 \nu^2 \beta^2}{(s_n^2 - \beta^2)(s_m^2 - \beta^2)} + s_n^2 + s_m^2 \right\} \kappa_n J_1(\kappa_n a) \kappa_m J_1(\kappa_m a). \end{aligned}$$

The above equation was generated from the relation in (3.28); therefore it is correct to state

$$\frac{\alpha}{a}\int_0^a J_0(\kappa_m r)J_0(\kappa_n r)r\,\mathrm{d}r = \frac{L(s_n,a)\kappa_m J_1(\kappa_m a)}{\left(s_m^2-s_n^2\right)(s_n^2-\beta^2)} - \frac{L(s_m,a)\kappa_n J_1(\kappa_n a)}{\left(s_m^2-s_n^2\right)(s_m^2-\beta^2)}$$
$$-\left\{\frac{\tau_1\nu^2\beta^2}{(s_n^2-\beta^2)(s_m^2-\beta^2)}+2-\kappa_n^2-\kappa_m^2\right\}\kappa_n J_1(\kappa_n a)\kappa_m J_1(\kappa_m a). \tag{3.31}$$

The case of equal ($\kappa_n = \kappa_m$) and unequal ($\kappa_n \neq \kappa_m$) roots are considered separately. For $n = m$ this reduces to

$$\frac{\alpha}{a}\int_0^a J_0^2(\kappa_n r)r\,\mathrm{d}r = C_n - \left\{\frac{\tau_1\nu^2\beta^2}{(s_n^2-\beta^2)^2}+2-2\kappa_n^2\right\}\kappa_n^2 J_1^2(\kappa_n a), \tag{3.32}$$

where C_n is a non-zero constant, given by

$$C_n = \frac{\kappa_n J_1(\kappa_n a)}{\beta^2-s_n^2}\lim_{s\to s_n}\frac{L(s_n,a)-L(s,a)}{s^2-s_n^2}. \tag{3.33}$$

From l'Hôpital's rule it follows that

$$C_n = \frac{L'(s_n,a)\kappa_n J_1(\kappa_n a)}{2s_n(s_n^2-\beta^2)}, \tag{3.34}$$

where the prime denotes differentiation with respect to s. For $n \neq m$ the value of C_n is zero due to the relation in (3.28). Hence the generalised orthogonality relation is

$$\frac{\alpha}{a}\int_0^a J_0(\kappa_m r)J_0(\kappa_n r)r\,\mathrm{d}r = \delta_{nm}C_n$$
$$-\left\{\frac{\tau_1\nu^2\beta^2}{(s_n^2-\beta^2)(s_m^2-\beta^2)}+2-\kappa_n^2-\kappa_m^2\right\}\kappa_n J_1(\kappa_n a)\kappa_m J_1(\kappa_m a). \tag{3.35}$$

where δ is the Kronecker delta. This generalised orthogonality relation is new to the research area and is specific to shells with axisymmetric motion modelled on the Donnell-Mushtari equations of motion. Similarly, for a shell of radius b, the equivalent generalised orthogonality relation is

$$\frac{\alpha}{b}\int_0^b J_0(\gamma_n r)J_0(\gamma_m r)r\mathrm{d}r$$
$$=\delta_{mn}D_n - \left\{\frac{\tau_2\nu^2\beta^2}{(\eta_n^2-\beta^2)(\eta_m^2-\beta^2)}+2-\gamma_m^2-\gamma_n^2\right\}\gamma_n J_1(\gamma_n b)\gamma_m J_1(\gamma_m b), \tag{3.36}$$

where $\tau_2 = 12/(h^2k^2b^2)$, η_n are the equivalent wavenumbers, $\gamma_n = (1-\eta_n^2)^{1/2}$ and

$$D_n = \frac{L'(\eta_n,b)\gamma_n J_1(\gamma_n b)}{2\eta_n(\eta_n^2-\beta^2)}. \tag{3.37}$$

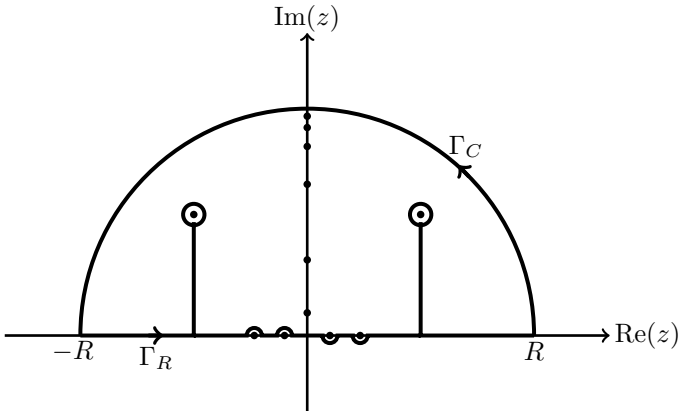

Figure 3.5: The path of integration used for Cauchy's residue theorem.

These generalised orthogonality relations will be used in the following chapters to find integrals which arise from the application of the mode matching method. The non-zero constant C_n (or equivalently D_n) is a useful parameter arising in various identities which involve the characteristic equation.

3.3.1 Properties of the eigensystem

The eigensystem comprising (2.4), (3.11) and (3.12) has many interesting properties. In particular, it can be shown that the eigenfunctions are linearly dependent. This is demonstrated through the existence of a number of identities comprising summations of the eigenfunctions. It is shown in Lawrie [46] that the number of such identities depends on the order of the boundary conditions. This number is the same as the number of edge conditions required (or alternatively half the order of the characteristic equation). In this case there are three such identities and these are given by $I_1(r)$, $I_2(r)$ and $I_3(r)$. These identities are constructed by considering contour integrals with odd integrands. On applying Cauchy's residue theorem an identity is obtained. The first identity is derived by considering the integral

$$I_1(r) = \frac{1}{2\pi i}\int_{-\infty}^{\infty} \frac{2s(s^2-\beta^2)J_0(\kappa r)}{L(s,a)}\,\mathrm{d}s, \quad 0 \le r \le a, \tag{3.38}$$

where the path of integration is indented above any poles on the negative real axis and below any poles on the positive real axis as shown in Figure 3.5. Contour integration can be used to express the integral as a sum of residues and thus obtain an identity. Cauchy's residue theorem gives

$$I_1(r) + \frac{1}{2\pi i}\int_{\Gamma_c} \frac{2s(s^2-\beta^2)J_0(\kappa r)}{L(s,a)}\,\mathrm{d}s = \sum_{n=0}^{\infty} \varrho_n, \ 0 \le r \le a, \tag{3.39}$$

where ϱ_n are the residues at $s = s_n$. That is

$$\varrho_n = \lim_{s\to s_n} \frac{2s(s-s_n)(s^2-\beta^2)J_0(\kappa r)}{L(s,a)} = \frac{2s_n(s_n^2-\beta^2)J_0(\kappa_n r)}{L'(s_n,a)},\ 0 \le r \le a, \tag{3.40}$$

where l'Hôpital's rule has been applied. Note that as $|s| \to \infty$ the integrand can be approximated by

$$\frac{2s(s^2-\beta^2)J_0(\kappa_n r)}{L(s,a)} \approx \frac{2J_0(isr)}{is^4 J_1(isa)}. \tag{3.41}$$

Hence, as $R \to \infty$

$$\int_{\Gamma_c} \frac{2s(s^2-\beta^2)J_0(\kappa r)}{L(s,a)}\,\mathrm{d}s \to 0,\ 0 \le r \le a. \tag{3.42}$$

The first identity is now obtained using (3.34). That is

$$\sum_{n=0}^{\infty} \frac{\kappa_n J_1(\kappa_n a)J_0(\kappa_n r)}{C_n} = 0,\ \ 0 \le r \le a. \tag{3.43}$$

A further two identities can be found by following the same process with the integrals

$$I_2(r) = \frac{1}{2\pi i}\int_{-\infty}^{\infty} \frac{2sJ_0(\kappa r)}{L(s,a)}\,\mathrm{d}s,\ \ 0 \le r \le a, \tag{3.44}$$

$$I_3(r) = \frac{1}{2\pi i}\int_{-\infty}^{\infty} \frac{2s\kappa^2 J_0(\kappa r)}{L(s,a)}\,\mathrm{d}s,\ \ 0 \le r \le a. \tag{3.45}$$

In both cases the integrands are odd functions, therefore $I_2(r)$ and $I_3(r)$ are zero. The same procedure is used to obtain identities two and three as

$$\sum_{n=0}^{\infty} \frac{2s_n J_0(\kappa_n r)}{L'(s_n,a)} = \sum_{n=0}^{\infty} \frac{\kappa_n J_1(\kappa_n a)J_0(\kappa_n r)}{(s_n^2-\beta^2)C_n} = 0,\ \ 0 \le r \le a, \tag{3.46}$$

$$\sum_{n=0}^{\infty} \frac{2s_n J_0(\kappa_n r)}{L'(s_n,a)} = \sum_{n=0}^{\infty} \frac{\kappa_n^3 J_1(\kappa_n a)J_0(\kappa_n r)}{(s_n^2-\beta^2)C_n} = 0,\ \ 0 \le r \le a. \tag{3.47}$$

Some additional identities can be found by using the Bessel function $J_1(\kappa a)$ in the integrand. To obtain further identities, the following integrals are considered:

$$I_4 = \frac{1}{2\pi i}\int_{-\infty}^{\infty} \frac{2s(s^2-\beta^2)\kappa J_1(\kappa a)}{L(s,a)}\,\mathrm{d}s, \tag{3.48}$$

$$I_5 = \frac{1}{2\pi i}\int_{-\infty}^{\infty} \frac{2s\kappa J_1(\kappa a)}{L(s,a)}\,\mathrm{d}s, \tag{3.49}$$

$$I_6 = \frac{1}{2\pi i}\int_{-\infty}^{\infty} \frac{2s^3(s^2-\beta^2)\kappa J_1(\kappa a)}{L(s,a)}\,\mathrm{d}s, \tag{3.50}$$

These integrals were chosen such that the integrand is an odd function of s, thereby ensuring that the result is zero. From using the same procedure implemented for $I_1(r)$, it follows that the identities given by I_4 and I_5 are

$$\sum_{n=0}^{\infty} \frac{2s_n(s_n^2-\beta^2)\kappa_n J_1(\kappa_n a)}{L'(s_n,a)} = \sum_{n=0}^{\infty} \frac{\{\kappa_n J_1(\kappa_n a)\}^2}{C_n} = 0, \tag{3.51}$$

$$\sum_{n=0}^{\infty} \frac{2s_n\kappa_n J_1(\kappa_n a)}{L'(s_n,a)} = \sum_{n=0}^{\infty} \frac{\{\kappa_n J_1(\kappa_n a)\}^2}{(s_n^2-\beta^2)C_n} = 0. \tag{3.52}$$

For integral I_6 it is seen that as $R \to \infty$ the contribution from C_{R^+} is non-zero. In order to find this contribution the integrand is approximated for large $|s|$ by:

$$\frac{2s^3(s^2-\beta^2)\kappa J_1(\kappa a)}{L(s,a)} \approx \frac{2s^3(s^2-\beta^2)\kappa J_1(\kappa a)}{s^4(s^2-\beta^2)\kappa J_1(\kappa a)} = \frac{2}{s}. \tag{3.53}$$

With the parameterisations $s = Re^{i\theta}$ and $ds/d\theta = iRe^{i\theta}$, the integral over the arc is found as

$$\frac{1}{2\pi i}\int_{C_{R^+}} \frac{2s^3(s^2-\beta^2)\kappa J_1(\kappa a)}{L(s,a)}\,\mathrm{d}s \approx \frac{1}{2\pi i}\int_0^{\pi} -2i\,\mathrm{d}\theta = -1. \tag{3.54}$$

Cauchy's residue theorem is used to obtain

$$\begin{aligned}&\frac{1}{2\pi i}\int_{C_{R^+}} \frac{2s^3(s^2-\beta^2)\kappa J_1(\kappa a)}{L(s,a)}\,\mathrm{d}s + \frac{1}{2\pi i}\int_{-R}^{R} \frac{2s^3(s^2-\beta^2)\kappa J_1(\kappa a)}{L(s,a)}\,\mathrm{d}s \\ &= \sum_{n=0}^{\infty} \frac{s_n^2\{\kappa_n J_1(\kappa_n a)\}^2}{C_n}.\end{aligned} \tag{3.55}$$

It follows that

$$\sum_{n=0}^{\infty} \frac{\kappa_n^2\{\kappa_n J_1(\kappa_n a)\}^2}{C_n} = -1. \tag{3.56}$$

A final identity can be found by multiplying the characteristic equation $L(s_n,a)$ by $\kappa_n J_1(\kappa_n a)/\{(s_n^2-\beta^2)C_n\}$ and summing to give

$$\begin{aligned}&-\tau_1\nu^2\sum_{n=0}^{\infty}\frac{\{\kappa_n J_1(\kappa_n a)\}^2}{C_n} - \tau_1\nu^2\beta^2\sum_{n=0}^{\infty}\frac{\{\kappa_n J_1(\kappa_n a)\}^2}{(s_n^2-\beta^2)C_n} + \sum_{n=0}^{\infty}\frac{(s_n^4-\mu^4)\{\kappa_n J_1(\kappa_n a)\}^2}{C_n} \\ &+\alpha\sum_{n=0}^{\infty}\frac{\kappa_n J_1(\kappa_n a)J_0(\kappa_n a)}{C_n} = 0.\end{aligned} \tag{3.57}$$

With the identities obtained from $I_1(a)$, I_4, I_5 and I_6 in the above equation, it is found that

$$\sum_{n=0}^{\infty} \frac{\kappa_n^4\{\kappa_n J_1(\kappa_n a)\}^2}{C_n} = -2. \tag{3.58}$$

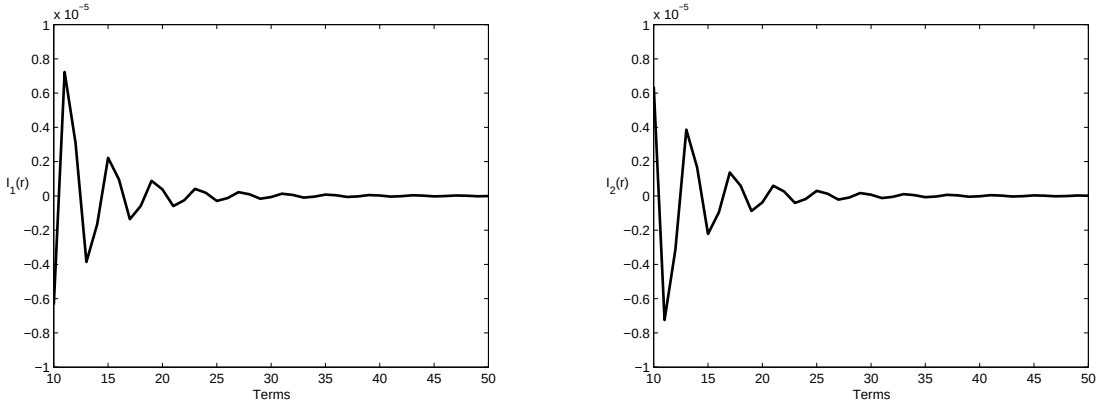

a) b)

Figure 3.6: Identities one and two.

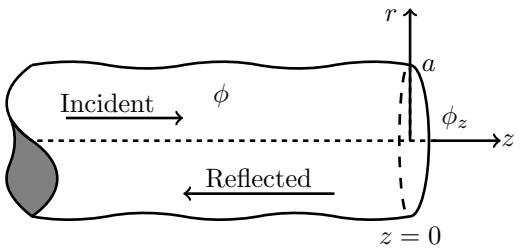

Figure 3.7: Physical configuration of the semi-infinite system closed by a rigid plate.

The roots of the characteristic equation (3.16) from a shell of radius $\bar{a} = 0.2$m at 500Hz were used to plot the value of each identity against the number of considered modes. The results of identities 1 and 2 in Figure 3.6 show that the identities are satisfied to 5 decimal places from 10 modes and continue to converge to zero. The results of identities 3, 4 and 5 are all zero to at least 6 decimal places when 10 modes are considered.

3.4 Energy reflected by a rigid plate

The aim of this section is to find the energy reflected by a rigid plate at the end of a semi-infinite shell. The system comprises a single shell located in the region $0 \leq r \leq a,\ z \leq 0$ closed by a rigid plate occupying $0 \leq r \leq a,\ z = 0$ (see Figure 3.7). Forcing wave propagating in the positive z direction towards the end plate, this will be done for both a fluid-borne and a structure-borne wave. The velocity potential ϕ comprises the incident wave and the reflected field

$$\phi(r, z) = F_\ell J_0(\kappa_\ell r) e^{is_\ell z} + \sum_{n=0}^{\infty} A_n J_0(\kappa_n r) e^{-is_n z},\ z \leq 0, \tag{3.59}$$

where ℓ indicates the chosen fundamental mode to force with ($\ell = 0$ or $\ell = 1$), F_ℓ is the amplitude of the forcing wave, A_n is the amplitude of the nth reflected wave, s_n is the wavenumber and $\kappa_n = (1 - s_n^2)^{1/2}$. In order for the forcing wave to have unit energy, it follows from (2.36) that

$$F_\ell = \sqrt{\frac{\alpha}{a s_\ell C_\ell}}. \tag{3.60}$$

The eigenfunction expansion forms of the longitudinal and radial displacements given in (3.13) and (3.14) are

$$u(a,z) = \frac{\nu F_\ell s_\ell \kappa_\ell J_1(\kappa_\ell a)}{a(s_\ell^2 - \beta^2)} e^{is_\ell z} - \frac{\nu}{a}\sum_{n=0}^{\infty} \frac{A_n s_n \kappa_n J_1(\kappa_n a)}{s_n^2 - \beta^2} e^{-is_n z},\ z < 0, \tag{3.61}$$

$$w(a,z) = -F_\ell \kappa_\ell J_1(\kappa_\ell a) e^{is_\ell z} - \sum_{n=0}^{\infty} A_n \kappa_n J_1(\kappa_n a) e^{-is_n z},\ z < 0. \tag{3.62}$$

At the end plate, the normal component of velocity vanishes. That is at $z = 0$

$$\frac{\partial \phi}{\partial z}(r,0) = 0,\ 0 \le r \le a. \tag{3.63}$$

From (3.63) it is found that

$$F_\ell s_\ell J_0(\kappa_\ell r) - \sum_{n=0}^{\infty} A_n s_n J_0(\kappa_n r) = 0,\ \ 0 \le r \le a. \tag{3.64}$$

On multiplying (3.64) by $J_0(\kappa_m r) r/a$, integrating with respect to r, $0 \le r \le a$, and using (3.35), it is found that

$$A_m = F_\ell \delta_{m\ell} + \frac{\kappa_m J_1(\kappa_m a)}{s_m C_m (s_m^2 - \beta^2)} E_0 + \frac{(2 - \kappa_m^2)\kappa_m J_1(\kappa_m a)}{s_m C_m} E_1 - \frac{\kappa_m J_1(\kappa_m a)}{s_m C_m} E_2, \tag{3.65}$$

where

$$E_0 = \tau_1 \nu^2 \beta^2 \left\{ \sum_{n=0}^{\infty} \frac{A_n \kappa_n s_n J_1(\kappa_n a)}{s_n^2 - \beta^2} - \frac{F_\ell \kappa_\ell s_\ell J_1(\kappa_\ell a)}{s_\ell^2 - \beta^2} \right\}, \tag{3.66}$$

$$E_1 = \sum_{n=0}^{\infty} A_n \kappa_n s_n J_1(\kappa_n a) - F_\ell \kappa_\ell s_\ell J_1(\kappa_\ell a), \tag{3.67}$$

$$E_2 = \sum_{n=0}^{\infty} A_n \kappa_n^3 s_n J_1(\kappa_n a) - F_\ell \kappa_\ell^3 s_\ell J_1(\kappa_\ell a). \tag{3.68}$$

The constants $E_0 - E_2$ are found by applying edge conditions which describe how the shell edge is connected to the end plate.

The reflected energy

$$\mathcal{E}_{\mathrm{A}} = \frac{a}{\alpha}\mathrm{Real}\left[\sum_{n=0}^{M}|A_n|^2 C_n s_n\right], \tag{3.69}$$

is plotted against frequency. Note: as discussed in Chapter two, expression (3.69) incorporates both the fluid and structure borne components of energy. The results are created in Matlab with the code presented in Appendix E. This has been done using 100 modes to calculate the amplitudes of the propagating waves.

3.4.1 Clamped edge

The displacements given in (3.62) are used with the clamped edge conditions given in (3.26) to find the eigenfunction expansions of the edge conditions as

$$\sum_{m=0}^{\infty}\frac{A_m\kappa_m s_m J_1(\kappa_m a)}{s_m^2-\beta^2} - \frac{F_\ell\kappa_\ell s_\ell J_1(\kappa_\ell a)}{s_\ell^2-\beta^2} = 0, \tag{3.70}$$

$$\sum_{m=0}^{\infty}A_m\kappa_m J_1(\kappa_m a) + F_\ell\kappa_\ell J_1(\kappa_\ell a) = 0, \tag{3.71}$$

$$\sum_{m=0}^{\infty}A_m\kappa_m s_m J_1(\kappa_m a) - F_\ell\kappa_\ell s_\ell J_1(\kappa_\ell a) = 0. \tag{3.72}$$

From edge conditions (3.70) and (3.72) it is seen that for a clamped edge $E_0 = E_1 = 0$. Hence equation (3.65) reduces to

$$A_m = F_\ell\delta_{m\ell} - \frac{\kappa_m J_1(\kappa_m a)}{s_m C_m}E_2, \tag{3.73}$$

Edge condition (3.71) is applied by multiplying (3.73) by $\kappa_m J_1(\kappa_m a)$ and summing over m, to give

$$E_2 = 2F_\ell\kappa_\ell J_1(\kappa_\ell a)/\sum_{m=0}^{\infty}\frac{\kappa_m^2 J_1^2(\kappa_m a)}{s_m C_m}. \tag{3.74}$$

The method of edge condition application can be generalised by recognising that the edge conditions take the form:

$$\sum_{m=0}^{\infty}A_m\psi_{mn}^{(\mathrm{a})} + F_\ell\psi_n^{(\mathrm{f})} = 0, \text{ for } n = 0,1,2, \tag{3.75}$$

where $\psi_{mn}^{(\mathrm{a})}$ are the terms in the edge condition which multiply A_m, $\psi_n^{(\mathrm{f})}$ are the constants corresponding to F_ℓ and n identifies which of the three edge conditions to apply. For

clamped edge conditions, the definitions for these come from (3.70)-(3.72), to give

$$\begin{aligned}
\psi_{m0}^{(\mathrm{a})} &= s_m\kappa_m J_1(\kappa_m a)/(s_m^2-\beta^2), & \psi_0^{(\mathrm{f})} &= -s_\ell\kappa_\ell J_1(\kappa_\ell a)/(s_\ell^2-\beta^2),\\
\psi_{m1}^{(\mathrm{a})} &= \kappa_m J_1(\kappa_m a), & \psi_1^{(\mathrm{f})} &= \kappa_\ell J_1(\kappa_\ell a),\\
\psi_{m2}^{(\mathrm{a})} &= s_m\kappa_m J_1(\kappa_m a), & \psi_2^{(\mathrm{f})} &= -s_\ell\kappa_\ell J_1(\kappa_\ell a).
\end{aligned} \tag{3.76}$$

The results for a shell of radius $\bar{a} = 0.2$m, the edge of which is clamped to the rigid disc are found. Both for a fluid-borne forcing mode and a structure-borne forcing mode, the output energy $\mathcal{E}_\mathrm{A}$ is totally reflected. This is because it is a closed system and the energy can only be reflected.

3.4.2 Pin-jointed edge

The pin-jointed edge conditions given in (3.27) can be expressed as

$$\sum_{m=0}^{\infty} \frac{A_m\kappa_m s_m^2 J_1(\kappa_m a)}{s_m^2-\beta^2} - \frac{F_\ell\kappa_\ell s_\ell^2 J_1(\kappa_\ell a)}{s_\ell^2-\beta^2} = 0, \tag{3.77}$$

$$\sum_{m=0}^{\infty} A_m\kappa_m J_1(\kappa_m a) + F_\ell\kappa_\ell J_1(\kappa_\ell a) = 0, \tag{3.78}$$

$$\sum_{m=0}^{\infty} A_m\kappa_m s_m^2 J_1(\kappa_m a) - F_\ell\kappa_\ell s_\ell^2 J_1(\kappa_\ell a) = 0. \tag{3.79}$$

These conditions give the values of ψ as

$$\begin{aligned}
\psi_{m0}^{(\mathrm{a})} &= s_m^2\kappa_m J_1(\kappa_m a)/(s_m^2-\beta^2), & \psi_0^{(\mathrm{f})} &= s_\ell^2\kappa_\ell J_1(\kappa_\ell a)/(s_\ell^2-\beta^2),\\
\psi_{m1}^{(\mathrm{a})} &= \kappa_m J_1(\kappa_m a), & \psi_1^{(\mathrm{f})} &= \kappa_\ell J_1(\kappa_\ell a),\\
\psi_{m2}^{(\mathrm{a})} &= s_m^2\kappa_m J_1(\kappa_m a), & \psi_2^{(\mathrm{f})} &= s_\ell^2\kappa_\ell J_1(\kappa_\ell a).
\end{aligned} \tag{3.80}$$

The edge conditions are applied by multiplying (3.65) by $\psi_{mn}^{(\mathrm{a})}$, and on summing over m it is found that

$$\begin{aligned}
&\sum_{m=0}^{\infty} F_\ell\delta_{m\ell}\psi_{mn}^{(\mathrm{a})} + \sum_{m=0}^{\infty} \frac{\kappa_m J_1(\kappa_m a)\psi_{mn}^{(\mathrm{a})}}{s_m C_m(s_m^2-\beta^2)}E_0 + \sum_{m=0}^{\infty} \frac{(2-\kappa_m^2)\kappa_m J_1(\kappa_m a)\psi_{mn}^{(\mathrm{a})}}{s_m C_m}E_1\\
&- \sum_{m=0}^{\infty} \frac{\kappa_m J_1(\kappa_m a)\psi_{mn}^{(\mathrm{a})}}{s_m C_m}E_2 = -F_\ell\psi_n^{(\mathrm{f})}, \quad \text{for } n = 0,1,2,
\end{aligned} \tag{3.81}$$

where constants $E_0 - E_2$ are found by truncating and solving (3.81). The amplitudes of the reflected field are then found by using the found constants in (3.65) and truncating the sums.

The edges which connect the shell to the rigid disc are considered to be pin-jointed.

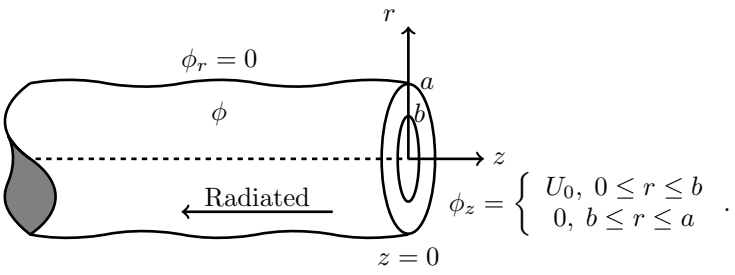

Figure 3.8: Physical configuration of the semi-infinite shell problem with a forcing piston.

Again, both with a fluid-borne forcing mode and a structure-borne forcing mode, the output energy is totally reflected.

3.5 Acoustic response due to a plane piston

The purpose of this section is to find the energy radiation by an oscillating plane piston into a semi-infinite shell (see Figure 3.8). The shell is located in the region $z \le 0,\ 0 \le r \le a$ and is closed by a rigid annular disc with a plane piston of radius $r = b$ in its centre. The annular disc is located in the region $z = 0,\ b \le r \le a$ and the plane piston is located at $z = 0,\ 0 \le r \le b$. The direction of forcing for the plane piston is in the negative z direction.

The sound source in this system is the piston which is assumed to have symmetrical axial velocity distribution $u = u(r)$. The velocity potential for this system comprises the waves radiated by the sound source

$$\phi(r, z) = \sum_{n=0}^{\infty} A_n J_0(\kappa_n r) e^{-is_n z}, \tag{3.82}$$

where A_n is the amplitude of the nth radiated wave, s_n is the wavenumber and $\kappa_n = (1 - s_n^2)^{1/2}$. The longitudinal and radial displacements (3.13) and (3.14) for the velocity potential are as follows:

$$u(z) = -\frac{\nu}{a} \sum_{n=0}^{\infty} \frac{A_n s_n \kappa_n J_1(\kappa_n a)}{s_n^2 - \beta^2} e^{-is_\ell z},\ z < 0, \tag{3.83}$$

$$w(z) = -i \sum_{n=0}^{\infty} A_n \kappa_n J_1(\kappa_n a) e^{-is_n z},\ z < 0. \tag{3.84}$$

The piston is assumed to have a symmetrical axial velocity distribution $u = u(r)$, with

$$u(r) = \begin{cases} U_0, & 0 \le r \le b \\ 0, & b \le r \le a \end{cases}, \tag{3.85}$$

where U_0 is a constant.

The normal component of velocity is matched with the velocity distribution of the piston. That is at $z = 0$

$$\frac{\partial \phi}{\partial z}(r, 0) = u(r),\ 0 \leq r \leq a. \tag{3.86}$$

The velocity potential in (3.82) is substituted into (3.86) to give

$$-i \sum_{n=0}^{\infty} A_n s_n J_0(\kappa_n r) = u(r),\ 0 \leq r \leq a. \tag{3.87}$$

On multiplying (3.87) by $\alpha J_0(\kappa_m r) r/a$ and integrating with respect to $r,\ 0 \leq r \leq a$, it is found that

$$-\frac{i\alpha}{a} \sum_{n=0}^{\infty} A_n s_n \int_0^a J_0(\kappa_n r) J_0(\kappa_m r) r \ \mathrm{d}r = \frac{\alpha}{a} \int_0^a u(r) J_0(\kappa_m r) r \ \mathrm{d}r. \tag{3.88}$$

The orthogonality relation in (3.35) is used to evaluate the integral on the left-hand side and (3.85) is considered so the integral on the right-hand side can be evaluated. It follows that

$$A_m = \frac{\kappa_m J_1(\kappa_m a)}{(s_m^2 - \beta^2) s_m C_m} E_0 + \frac{(2 - \kappa_m^2) \kappa_m J_1(\kappa_m a)}{s_m C_m} E_1 - \frac{\kappa_m J_1(\kappa_m a)}{s_m C_m} E_2 + \frac{i\alpha U_0 b J_1(\kappa_m b)}{a \kappa_m s_m C_m}, \tag{3.89}$$

where

$$E_0 = \tau \nu^2 \beta^2 \left\{ \sum_{n=0}^{\infty} \frac{A_n \kappa_n s_n J_1(\kappa_n a)}{s_n^2 - \beta^2} \right\}, \tag{3.90}$$

$$E_1 = \sum_{n=0}^{\infty} A_n \kappa_n s_n J_1(\kappa_n a), \tag{3.91}$$

$$E_2 = \sum_{n=0}^{\infty} A_n \kappa_n^3 s_n J_1(\kappa_n a). \tag{3.92}$$

The formula for impedance is the same as that given for the rigid piston system in (2.57), which is

$$Z = \frac{2i}{b^2 U_0} \int_0^b \phi(r, 0) r \ \mathrm{d}r. \tag{3.93}$$

The velocity potential in (2.43) is substituted into (3.93), with $U_0 = 1$, to express the impedance in terms of the radiated amplitude

$$Z = \frac{2i}{b^2} \sum_{n=0}^{\infty} A_n \int_0^b J_0(\kappa_n r) r \ \mathrm{d}r, \tag{3.94}$$

which reduces to

$$Z = \frac{2i}{b^2} \sum_{n=0}^{\infty} \frac{A_n b J_1(\kappa_n b)}{\kappa_n}. \tag{3.95}$$

The amplitude of the radiated waves in (3.89) are substituted into the above impedance equation, with $U_0 = 1$, to express the impedance as

$$Z = \frac{2i}{b} \sum_{n=0}^{\infty} \left\{ \frac{J_1(\kappa_n a) J_1(\kappa_n b)}{(s_n^2 - \beta^2) s_n C_n} E_0 + \frac{(2 - \kappa_n^2) J_1(\kappa_n a) J_1(\kappa_n b)}{s_n C_n} E_1 - \frac{J_1(\kappa_n a) J_1(\kappa_n b)}{s_n C_n} E_2 \right.$$
$$\left. + \frac{i\alpha b J_1^2(\kappa_n b)}{a \kappa_n^2 s_n C_n} \right\}. \tag{3.96}$$

The same method of edge condition application used in the previous section can be used here, but with the form of the edge conditions as

$$\sum_{m=0}^{\infty} A_m \psi_{mn}^{(\mathrm{a})} = 0, \text{ for } n = 0, 1, 2, \tag{3.97}$$

The edge conditions are applied by multiplying (3.89) by $\psi_{mn}^{(\mathrm{a})}$, and on summing over m it is found that

$$\sum_{m=0}^{\infty} \frac{\kappa_m J_1(\kappa_m a) \psi_{mn}^{(\mathrm{a})}}{(s_m^2 - \beta^2) s_m C_m} E_0 + \sum_{m=0}^{\infty} \frac{(2 - \kappa_m^2) \kappa_m J_1(\kappa_m a) \psi_{mn}^{(\mathrm{a})}}{s_m C_m} E_1 - \sum_{m=0}^{\infty} \frac{\kappa_m J_1(\kappa_m a) \psi_{mn}^{(\mathrm{a})}}{s_m C_m} E_2$$
$$+ \frac{i\alpha b}{a} \sum_{m=0}^{\infty} \frac{J_1(\kappa_m b) \psi_{mn}^{(\mathrm{a})}}{\kappa_m s_m C_m} \quad \text{for } n = 0, 1, 2. \tag{3.98}$$

The constants $E_0 - E_2$ are thus found by truncating and solving (3.98). These constants are then used in (3.89) and (3.96) which are truncated to find the radiated amplitudes and the radiated impedance. The radiated energy is given in (3.69) and the impedance are plotted against frequency. The energy and impedance are calculated in Matlab with the code presented in Appendix F and the plots from this are shown below. This has been done using 100 modes to calculate the amplitudes of the propagating waves.

3.5.1 Clamped edge

The displacements in (3.83) and (3.84) are used to find the values of ψ for a clamped edge as

$$\begin{aligned} \psi_{m0}^{(\mathrm{a})} &= s_m \kappa_m J_1(\kappa_m a)/(s_m^2 - \beta^2), \\ \psi_{m1}^{(\mathrm{a})} &= \kappa_m J_1(\kappa_m a), \\ \psi_{m2}^{(\mathrm{a})} &= s_m \kappa_m J_1(\kappa_m a). \end{aligned} \tag{3.99}$$

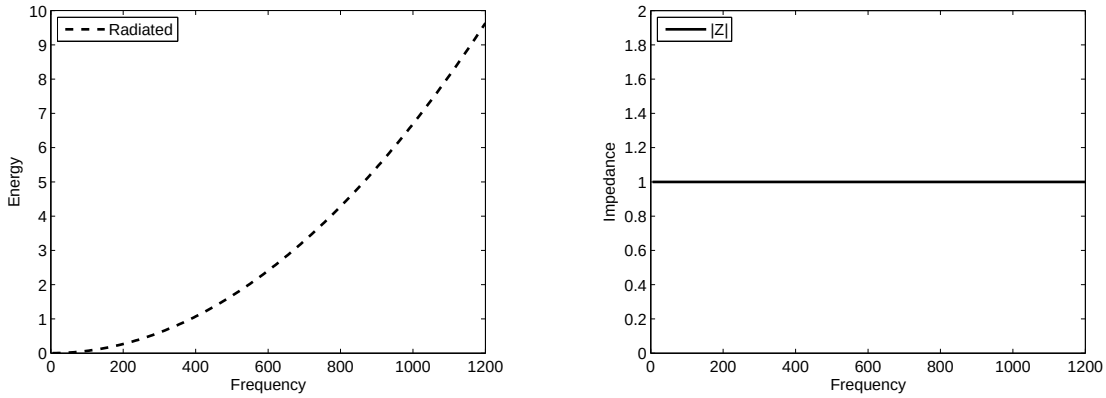

a) b)

Figure 3.9: At the closed end of a semi-infinite shell forced by a piston with a clamped edge, $\bar{a} = 0.2$m and $\bar{b} = 0.2$m: a) Radiated energy, b) Radiation impedance.

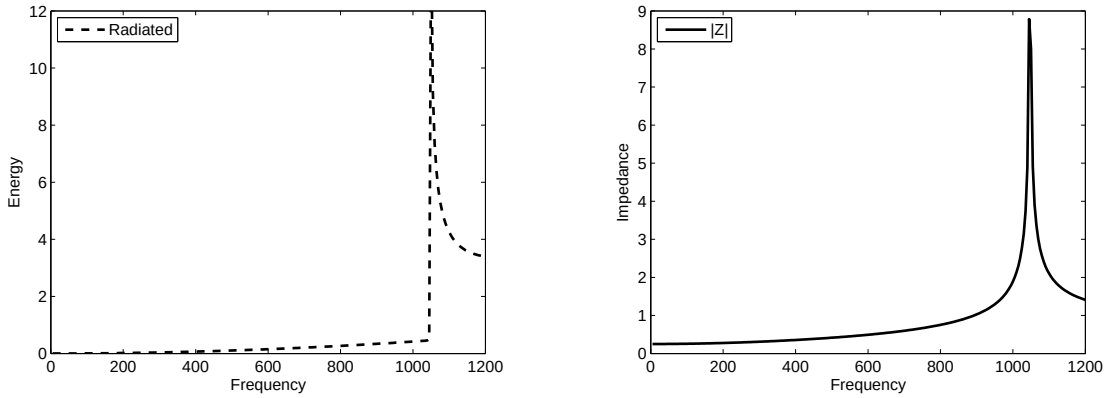

a) b)

Figure 3.10: At the closed end of a semi-infinite shell forced by a piston with a clamped edge, $\bar{a} = 0.2$m and $\bar{b} = 0.1$m: a) Radiated energy, b) Radiation impedance.

The above values of ψ are used in (3.98) in order to find the values of $E_0 - E2$. The radius of the shell is $\bar{a} = 0.2$m throughout where the first cut-on is at 1048Hz (the second cut-on occurs outside the considered frequency range).

The simplest case of a plane piston plane being equal to the radius of the shell is considered first, where $\bar{a} = \bar{b} = 0.2$m. The resulting radiated energy and radiation impedance are shown in Figure 3.9. It can be seen that these results are identical to those obtained from the rigid equivalent problem in Figure 2.2.

The radius of the piston is now reduce so that it is equal to half the radius of the shell, that is $\bar{b} = 0.1$m. The resulting radiated energy and impedance are shown in Figure 3.10. It is seen that the radiated energy in the shell increase abruptly at the first cut-on at 1048Hz, this is also reflected in the impedance.

In the last configuration the radius of the piston is assumed to be significantly smaller

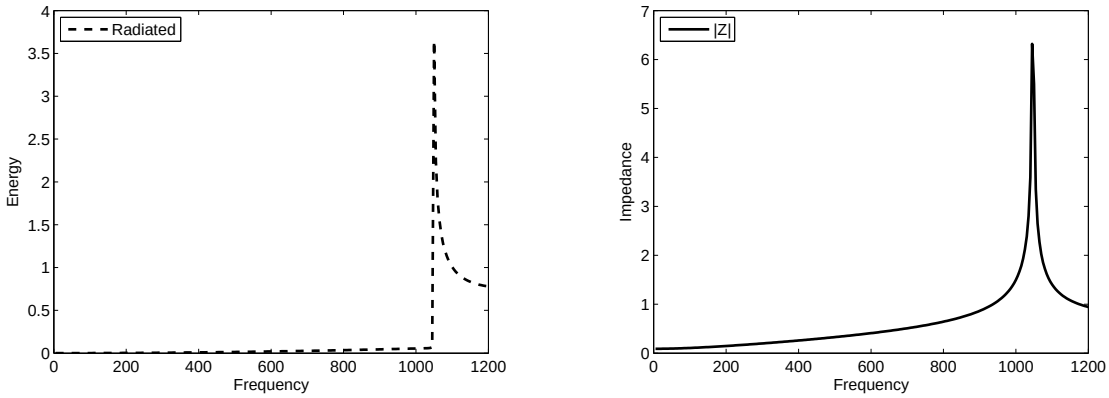

a) b)

Figure 3.11: At the closed end of a semi-infinite shell forced by a piston with a clamped edge, $\bar{a} = 0.2$m and $\bar{b} = 0.06$m: a) Radiated energy, b) Radiation impedance.

than the radius of the shell with a piston radius of $\bar{b} = 0.06$m. The resulting radiated energy and impedance are shown in Figure 3.11. Again the cut-ons in the shell cause the radiated energy and thus impedance to suddenly spike up and drop down.

3.5.2 Pin-jointed edge

The displacements in (3.83) and (3.84) are used to find the values of ψ for a pin-jointed edge as

$$\begin{aligned}
\psi_{m0}^{(\mathrm{a})} &= s_m^2 \kappa_m J_1(\kappa_m a)/(s_m^2 - \beta^2), \\
\psi_{m1}^{(\mathrm{a})} &= \kappa_m J_1(\kappa_m a), \\
\psi_{m2}^{(\mathrm{a})} &= s_m^2 \kappa_m J_1(\kappa_m a).
\end{aligned} \tag{3.100}$$

The above values of ψ are used in (3.98) in order to find the values of $E_0 - E2$. The radius of the shell is $\bar{a} = 0.2$m throughout where the first cut-on is at 1048Hz (the second cut-on occurs outside the considered frequency range).

Those configurations that were considered in the previous subsection with clamped edges were considered for pin-jointed edges also. It was found that the results obtained using pin-jointed edges were identical to those obtained from the clamped edge equivalent problems.

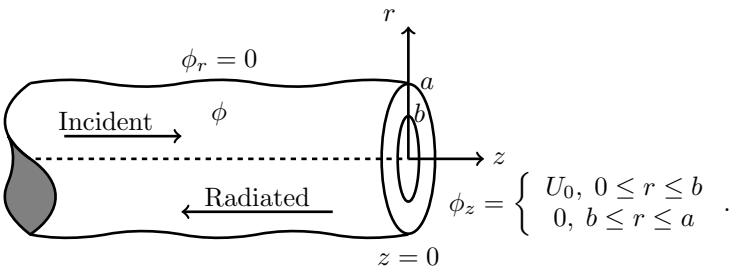

Figure 3.12: Physical configuration of the semi-infinite shell forced by a piston and a wave.

3.6 Acoustic response due to a plane piston and forcing wave

The purpose of this section is to find the energy radiation by an oscillating plane piston and a forcing wave into a semi-infinite shell. The system setup is the same as considered in Section 3.5, but with the inclusion of a forcing wave incident towards the piston (see Figure 3.12).

The velocity potential now includes the forcing wave as well as those wave radiate by the place piston, this gives

$$\phi_1(r,z) = F_\ell J_0(\kappa_\ell r)e^{is_\ell z} + \sum_{n=0}^{\infty} A_n J_0(\kappa_n r)e^{-is_n z}, 0 \le r \le a,\ z \le 0, \tag{3.101}$$

where ℓ indicates the chosen fundamental mode to force with ($\ell = 0$ or $\ell = 1$), F_ℓ is the amplitude of the forcing wave given by (3.60), A_n is the amplitude of the nth radiated wave, s_n is the nth wavenumber and $\kappa_n^2 = (1 - s_n^2)^{1/2}$. The piston is assumed to have a symmetrical axial velocity distribution $u = u(r)$, with

$$u(r) = \begin{cases} U_0, & 0 \le r \le b \\ 0, & b \le r \le a \end{cases}, \tag{3.102}$$

where U_0 is a constant.

The normal component of velocity is matched with the velocity distribution of the piston at the closed end. That is, at $z = 0$

$$is_\ell F_\ell J_0(\kappa_\ell r) - i\sum_{n=}^{\infty} A_n s_n J_0(\kappa_n r) = u(r),\ 0 \le r \le a. \tag{3.103}$$

On multiplying (3.103) by $\alpha J_0(\kappa_m r)r/a$, integrating with respect to $r,\ 0 \le r \le a$, and

on using the generalised orthogonality relation in (3.35), it is found that

$$A_m = F_\ell \delta_{\ell m} + \frac{\kappa_m J_1(\kappa_m a)}{(s_m^2 - \beta^2) s_m C_m} E_0 + \frac{(2-\kappa_m^2)\kappa_m J_1(\kappa_m a)}{s_m C_m} E_1 - \frac{\kappa_m J_1(\kappa_m a)}{s_m C_m} E_2 + \frac{i\alpha b J_1(\kappa_m b)}{a \kappa_m s_m C_m}, \tag{3.104}$$

where

$$E_0 = \tau \nu^2 \beta^2 \left\{ \sum_{n=0}^{\infty} \frac{A_n \kappa_n s_n J_1(\kappa_n a)}{s_n^2 - \beta^2} - \frac{F_\ell \kappa_\ell s_\ell J_1(\kappa_\ell a)}{s_\ell^2 - \beta^2} \right\}, \tag{3.105}$$

$$E_1 = \sum_{n=0}^{\infty} A_n \kappa_n s_n J_1(\kappa_n a) - F_\ell \kappa_\ell s_\ell J_1(\kappa_\ell a), \tag{3.106}$$

$$E_2 = \sum_{n=0}^{\infty} A_n \kappa_n^3 s_n J_1(\kappa_n a) - F_\ell \kappa_\ell^3 s_\ell J_1(\kappa_\ell a). \tag{3.107}$$

The velocity potential in (3.101) is substituted into (3.93), with $U_0 = 1$, to find the radiation impedance in terms of the radiated amplitude as

$$Z = \frac{2i}{b^2} \left\{ \frac{F_\ell b J_1(\kappa_\ell b)}{\kappa_\ell} + \sum_{n=0}^{\infty} \frac{A_n b J_1(\kappa_n b)}{\kappa_n} \right\}. \tag{3.108}$$

The amplitude for the radiated waves in (3.104) is substituted into the above equation to give

$$Z = \frac{2i F_\ell J_1(\kappa_\ell b)}{b \kappa_\ell} + \frac{2i}{b} \sum_{n=0}^{\infty} \left\{ \frac{J_1(\kappa_n a) J_1(\kappa_n b)}{(s_n^2 - \beta^2) s_n C_n} E_0 + \frac{(2-\kappa_n^2) J_1(\kappa_n a) J_1(\kappa_n b)}{s_n C_n} E_1 - \frac{J_1(\kappa_n a) J_1(\kappa_n b)}{s_n C_n} E_2 + \frac{i\alpha b J_1^2(\kappa_n b)}{a \kappa_n^2 s_n C_n} \right\}. \tag{3.109}$$

The results are created in Matlab with the code presented in Appendix F. This has been done using 100 modes to calculate the amplitudes of the propagating waves. The edge conditions for a clamped edge are as given in (3.70)-(3.72) and the edge conditions for a pin-jointed edge are as given in (3.77)-(3.79). These edge conditions are applied by multiplying (3.104) by $\psi_{mn}^{(\mathrm{a})}$, and on summing over m it is found that

$$\sum_{m=0}^{\infty} F_\ell \delta_{\ell m} \psi_{mn}^{(\mathrm{a})} + \sum_{m=0}^{\infty} \frac{\kappa_m J_1(\kappa_m a) \psi_{mn}^{(\mathrm{a})}}{(s_m^2 - \beta^2) s_m C_m} E_0 + \sum_{m=0}^{\infty} \frac{(2-\kappa_m^2)\kappa_m J_1(\kappa_m a) \psi_{mn}^{(\mathrm{a})}}{s_m C_m} E_1 - \sum_{m=0}^{\infty} \frac{\kappa_m J_1(\kappa_m a)}{s_m C_m} E_2 = \frac{i\alpha b}{a} \sum_{m=0}^{\infty} \frac{J_1(\kappa_m b) \psi_{mn}^{(\mathrm{a})}}{\kappa_m s_m C_m} - F_\ell \psi_n^{(\mathrm{f})}, \quad \text{for } n = 0, 1, 2, \tag{3.110}$$

where $\psi_{mn}^{(\mathrm{a})}$ and $\psi_n^{(\mathrm{f})}$ are as given in (3.76) for a clamped edge and as given in (3.80) for

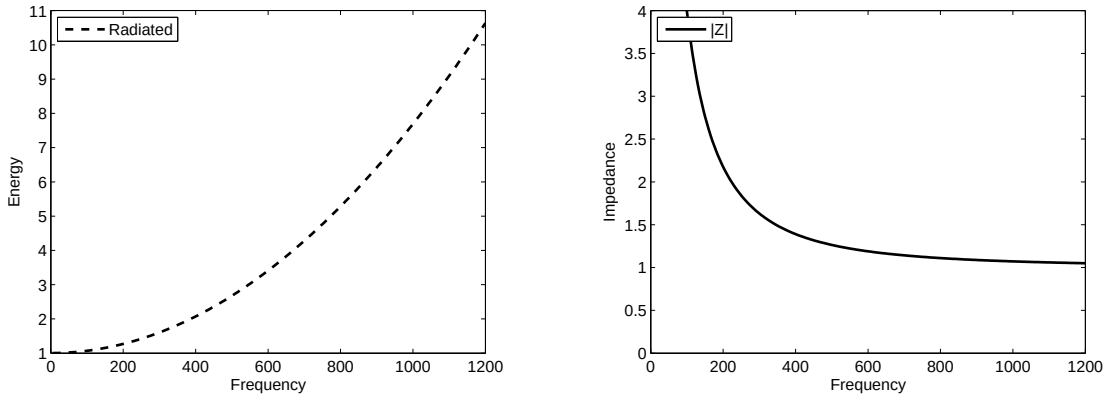

a) b)

Figure 3.13: At the closed end of a semi-infinite shell forced by a piston and a wave with a clamped edge, $\bar{a} = 0.2$m, $\bar{b} = 0.2$m and $\ell = 0$: a) Radiated energy, b) Radiation impedance.

a pin-jointed edge. The constants $E_0 - E_2$ are found by truncating and solving (3.110). These constants are then used in (3.104) which is truncated to give the amplitudes of the reflected field.

3.6.1 Clamped edge

The displacements in (3.83) and (3.84) are used to find the values of ψ for a clamped edge as

$$\begin{aligned} \psi_{m0}^{(\mathrm{a})} &= s_m \kappa_m J_1(\kappa_m a)/(s_m^2 - \beta^2), \\ \psi_{m1}^{(\mathrm{a})} &= \kappa_m J_1(\kappa_m a), \\ \psi_{m2}^{(\mathrm{a})} &= s_m \kappa_m J_1(\kappa_m a). \end{aligned} \tag{3.111}$$

The above values of ψ are used in (3.104) in order to find the values of $E_0 - E2$. The radius of the shell is $\bar{a} = 0.2$m throughout where the first cut-on is at 1048Hz (the second cut-on occurs outside the considered frequency range).

The first considered configuration assumes the radius of the plane piston to be equal to that of the shell, where $\bar{a} = \bar{b} = 0.2$m. The resulting radiated energy and radiation impedance with fluid-borne forcing ($\ell = 0$) are shown in Figure 3.13 and for structure-borne forcing ($\ell = 1$) in Figure 3.14. It is seen that the cut-on has no effect on the radiated energy or impedance.

The next configuration considers the radius of the shell to be $\bar{a} = 0.2$m with the radius of the plane piston equal to half the radius of the shell as $\bar{b} = 0.1$m. The resulting radiated energy and impedance with fluid-borne forcing ($\ell = 0$) are shown in Figure 3.15 and for structure-borne forcing ($\ell = 1$) in Figure 3.16.

The final configuration considers the radius of the shell to be $\bar{a} = 0.2$m with the

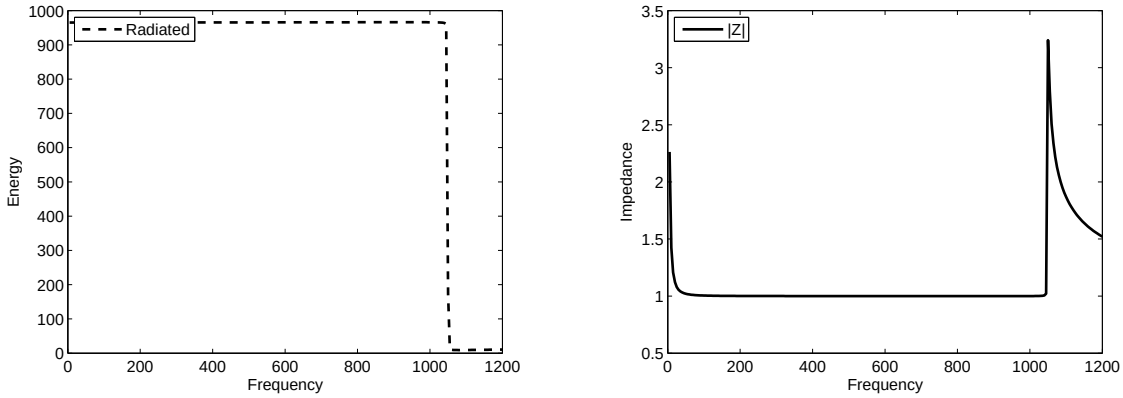

a) b)

Figure 3.14: At the closed end of a semi-infinite shell forced by a piston and a wave with a clamped edge, $\bar{a} = 0.2$m, $\bar{b} = 0.2$m and $\ell = 1$: a) Radiated energy, b) Radiation impedance.

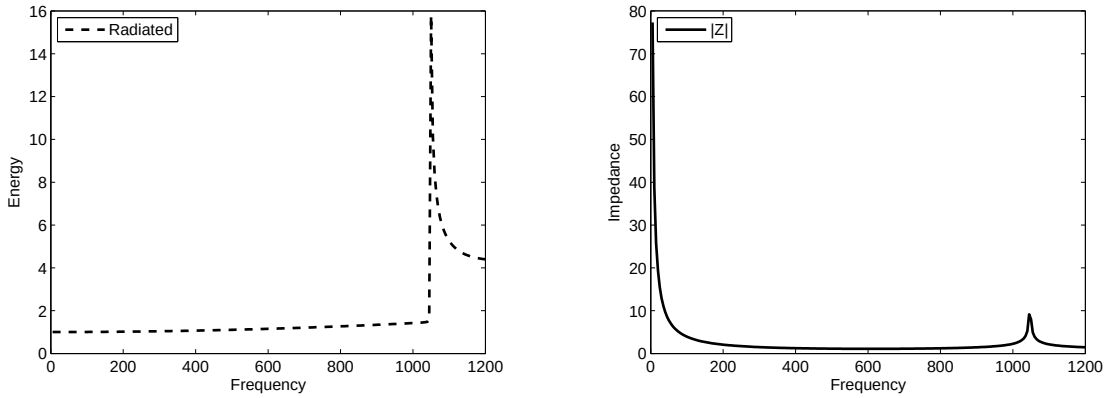

a) b)

Figure 3.15: At the closed end of a semi-infinite shell forced by a piston and a wave with a clamped edge, $\bar{a} = 0.2$m, $\bar{b} = 0.1$m and $\ell = 0$: a) Radiated energy, b) Radiation impedance.

radius of the plane piston significantly smaller with $\bar{b} = 0.06$m. The resulting radiated energy and impedance with fluid-borne forcing ($\ell = 0$) are shown in Figure 3.17 and for structure-borne forcing ($\ell = 1$) in Figure 3.18.

3.6.2 Pin-jointed edge

The values of ψ for a pin-jointed edge are

$$\begin{aligned}
\psi_{m0}^{(\mathrm{a})} &= s_m^2 \kappa_m J_1(\kappa_m a)/(s_m^2 - \beta^2), \\
\psi_{m1}^{(\mathrm{a})} &= \kappa_m J_1(\kappa_m a), \\
\psi_{m2}^{(\mathrm{a})} &= s_m^2 \kappa_m J_1(\kappa_m a).
\end{aligned} \tag{3.112}$$

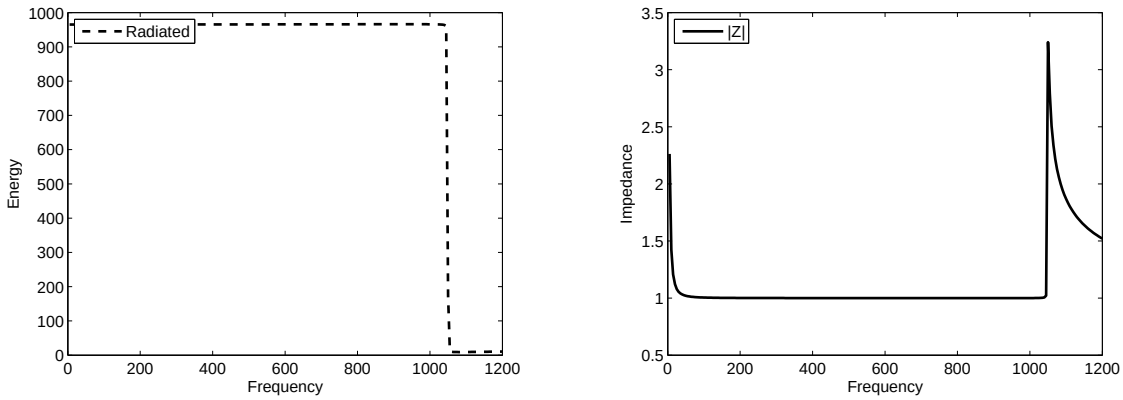

a) b)

Figure 3.16: At the closed end of a semi-infinite shell forced by a piston and a wave with a clamped edge, $\bar{a} = 0.2$m, $\bar{b} = 0.1$m and $\ell = 1$: a) Radiated energy, b) Radiation impedance.

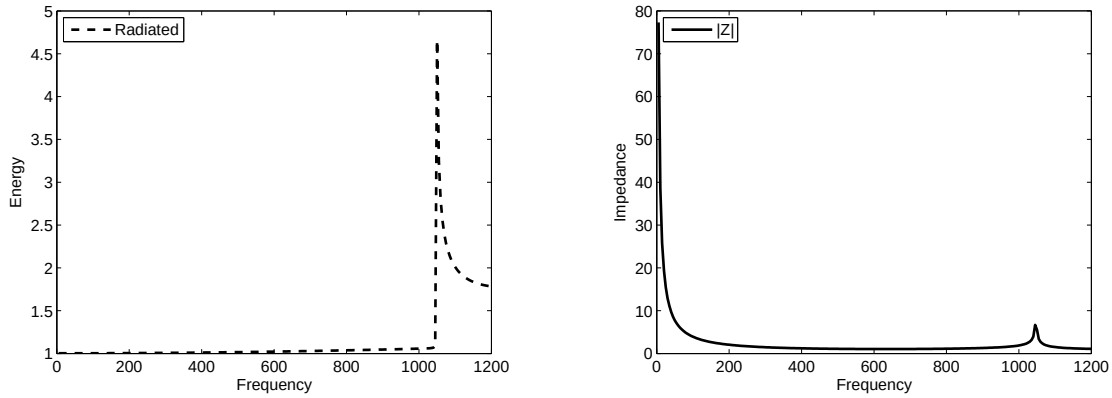

a) b)

Figure 3.17: At the closed end of a semi-infinite shell forced by a piston and a wave with a clamped edge, $\bar{a} = 0.2$m, $\bar{b} = 0.06$m and $\ell = 0$: a) Radiated energy, b) Radiation impedance.

The above values of ψ are used in (3.104) in order to find the values of $E_0 - E2$. The radius of the shell is $\bar{a} = 0.2$m throughout where the first cut-on is at 1048Hz (the second cut-on occurs outside the considered frequency range).

Those configurations that were considered in the previous subsection with clamped edges were considered for pin-jointed edges also. It was found that the results obtained using pin-jointed edges were identical to those obtained from the clamped edge equivalent problems.

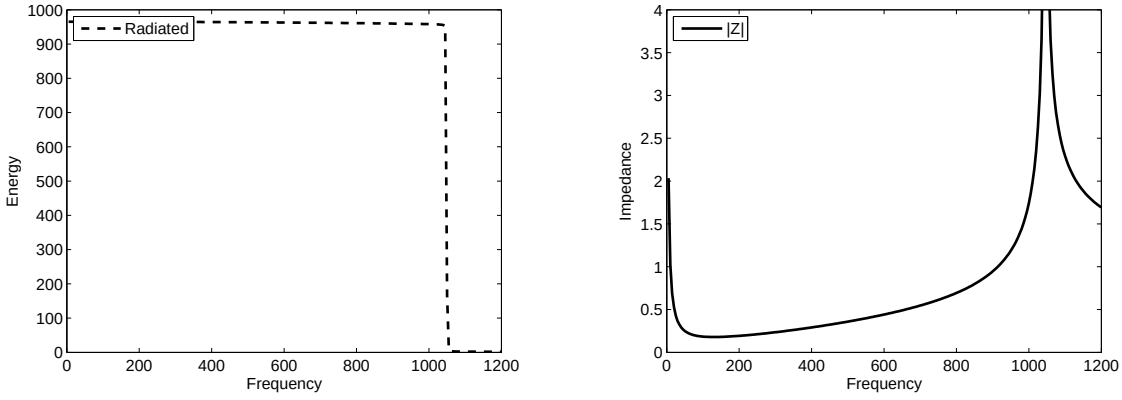

a) b)

Figure 3.18: At the closed end of a semi-infinite shell forced by a piston and a wave with a clamped edge, $\bar{a} = 0.2$m, $\bar{b} = 0.06$m and $\ell = 1$: a) Radiated energy, b) Radiation impedance.

Chapter 4

Energy radiated due to a change of radius in shells subject to axisymmetric motion

This chapter focuses on acoustic propagation in thin circular cylindrical shells with flexible walls. The purpose of each problem is to find the reflected and transmitted energy which scatters at an abrupt change of radius due to a forcing wave. The generalised orthogonality relation derived in Chapter three is used with the mode-matching method to find the resulting amplitudes. The generalised orthogonality relation is new to the research area and therefore so is the method and results that follow. The results produced in this chapter are compared with those obtained from equivalent problems in Chapter two. Three problems are presented in this chapter: Energy radiated due to a forcing wave at an abrupt increase in radius, energy leaving a rigid expansion chamber situated between two shells and energy leaving a flexible expansion chamber situated between two shells.

4.1 Energy radiated due to a forcing wave at an abrupt increase in radius

The aim of this section is to determine the energy reflected and transmitted due to a forcing wave incident toward an abrupt increase in radius. The system comprises two semi-infinite shells, the left-hand shell occupies $0 \leq r \leq a,\ z \leq 0$ and the right-hand shell occupies $0 \leq r \leq b,\ z \geq 0$, where $a \leq b$ (see Figure 4.1). It is closed by a rigid annular disc occupying $a \leq r \leq b,\ z = 0$. Forcing is by a wave propagating in the positive z direction towards the abrupt increase in radius. The velocity potential for the left-hand

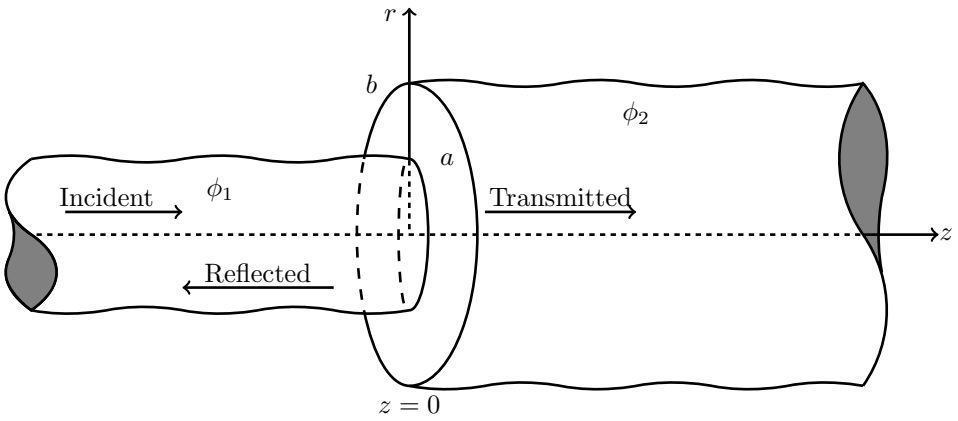

Figure 4.1: Physical configuration of the abrupt increase in radius problem.

shell ϕ_1 comprises the incident wave and the reflected sound field

$$\phi_1(r,z) = F_\ell J_0(\kappa_\ell r)e^{is_\ell z} + \sum_{n=0}^{\infty} A_n J_0(\kappa_n r)e^{-is_n z},\ 0 \le r \le a,\ z \le 0, \tag{4.1}$$

where ℓ indicates the chosen fundamental mode to force with ($\ell = 0$ or $\ell = 1$), F_ℓ is the amplitude of the forcing wave given in (3.60), A_n is the amplitude of the nth reflected wave, $s_n,\ n = 0, 1, 2, \ldots$ are the wavenumbers for the left-hand shell and $\kappa_n = (1 - s_n^2)^{1/2}$. The eigenfunction expansion forms of the longitudinal and radial displacements given in (3.13) and (3.14) are

$$\begin{aligned} u_1(z) &= \frac{\nu F_\ell s_\ell \kappa_\ell J_1(\kappa_\ell a)}{a(s_\ell^2 - \beta^2)} e^{is_\ell z} - \frac{\nu}{a}\sum_{n=0}^{\infty} \frac{A_n s_n \kappa_n J_1(\kappa_n a)}{s_n^2 - \beta^2} e^{-is_n z},\ z \le 0, \\ w_1(z) &= -F_\ell \kappa_\ell J_1(\kappa_\ell a)e^{is_\ell z} - \sum_{n=0}^{\infty} A_n \kappa_n J_1(\kappa_n a)e^{-is_n z},\ z \le 0, \end{aligned} \tag{4.2}$$

where again $\ell = 0$ and $\ell = 1$ and F_ℓ is thus known. The velocity potential for the right-hand shell is comprised of the transmitted sound field, that is

$$\phi_2(r,z) = \sum_{n=0}^{\infty} B_n J_0(\gamma_n r)e^{i\eta_n z},\ 0 \le r \le b,\ z \ge 0, \tag{4.3}$$

where B_n is the amplitude of the nth transmitted wave, $\eta_n,\ n = 0, 1, 2, \ldots$ are the wavenumbers for the right-hand shell and $\gamma_n = (1 - \eta_n^2)^{1/2}$. For the right-hand section,

the longitudinal and radial displacements are given by

$$u_2(z) = \frac{\nu}{b}\sum_{n=0}^{\infty}\frac{B_n\eta_n\gamma_n J_1(\gamma_n b)}{\eta_n^2-\beta^2}e^{i\eta_n z},\ z\geq 0,$$
$$w_2(z) = -\sum_{n=0}^{\infty}B_n\gamma_n J_1(\gamma_n b)e^{i\eta_n z},\ z\geq 0. \tag{4.4}$$

The problem is solved by matching the fluid pressure and the normal component of velocity at the interface. At the matching interface, the pressure and normal component of velocity are continuous in the fluid, while the latter vanishes on the rigid annulus. That is at $z=0$

$$\phi_1(r,0) = \phi_2(r,0),\ 0\leq r\leq a, \tag{4.5}$$
$$\frac{\partial\phi_2}{\partial z}(r,0) = \begin{cases}\frac{\partial\phi_1}{\partial z}(r,0), & 0\leq r\leq a\\ 0, & a\leq r\leq b\end{cases}. \tag{4.6}$$

On substituting (4.1) and (4.3) into (4.5), it is found that

$$F_\ell J_0(\kappa_\ell r) + \sum_{n=0}^{\infty}A_n J_0(\kappa_n r) = \sum_{n=0}^{\infty}B_n J_0(\gamma_n r),\ \ 0\leq r\leq a. \tag{4.7}$$

On multiplying (4.7) by $\alpha J_0(\kappa_m r)r/a$ and integrating with respect to $r, 0\leq r\leq a$, it is found that

$$\frac{\alpha F_\ell}{a}\int_0^a J_0(\kappa_\ell r)J_0(\kappa_m r)r\ \mathrm{d}r + \frac{\alpha}{a}\sum_{n=0}^{\infty}A_n\int_0^a J_0(\kappa_n r)J_0(\kappa_m r)r\ \mathrm{d}r$$
$$= \frac{\alpha}{a}\sum_{n=0}^{\infty}B_n\int_0^a J_0(\gamma_n r)J_0(\kappa_m r)r\ \mathrm{d}r. \tag{4.8}$$

The integrals on the left-hand side are evaluated using the generalised orthogonality relation in (3.35). It follows that

$$A_m = -F_\ell\delta_{\ell m} + \frac{\kappa_m J_1(\kappa_m a)}{(s_m^2-\beta^2)C_m}E_0 + \frac{(2-\kappa_m^2)\kappa_m J_1(\kappa_m a)}{C_m}E_1 - \frac{\kappa_m J_1(\kappa_m a)}{C_m}E_2$$
$$+\frac{\alpha}{a}\sum_{n=0}^{\infty}\frac{B_n R_{mn}}{C_m}, \tag{4.9}$$

where

$$E_0 = \tau_1 \nu^2 \beta^2 \left\{ \sum_{n=0}^{\infty} \frac{A_n \kappa_n J_1(\kappa_n a)}{s_n^2 - \beta^2} + \frac{F_\ell \kappa_\ell J_1(\kappa_\ell a)}{s_\ell^2 - \beta^2} \right\}, \tag{4.10}$$

$$E_1 = \sum_{n=0}^{\infty} A_n \kappa_n J_1(\kappa_n a) + F_\ell \kappa_\ell J_1(\kappa_\ell a), \tag{4.11}$$

$$E_2 = \sum_{n=0}^{\infty} A_n \kappa_n^3 J_1(\kappa_n a) + F_\ell \kappa_\ell^3 J_1(\kappa_\ell a), \tag{4.12}$$

and

$$R_{mn} = \int_0^a J_0(\kappa_m r) J_0(\gamma_n r) r \, \mathrm{d}r. \tag{4.13}$$

For $\kappa_m \neq \gamma_n$, R_{mn} simplifies to

$$R_{mn} = \frac{a \left\{ \kappa_m J_0(\gamma_n a) J_1(\kappa_n a) - \gamma_m J_0(\kappa_m a) J_1(\gamma_m a) \right\}}{\kappa_m^2 - \gamma_n^2}, \tag{4.14}$$

and for $\kappa_m = \gamma_n$, R_{mm} simplifies to

$$R_{mm} = \frac{a^2 \left\{ J_0^2(\kappa_m a) + J_1^2(\kappa_m a) \right\}}{2}. \tag{4.15}$$

A similar expression to (4.9) can be obtained for $B_n,\ n = 0, 1, 2, \ldots$ by multiplying (4.6) by $\alpha J_0(\gamma_m r) r / b$. The left-hand side is integrated with respect to $r,\ 0 \leq r \leq b$ and the right-hand side is integrated with respect to $r,\ 0 \leq r \leq a$. The generalised orthogonality relation in (3.36) is used to evaluate those integrals on the right-hand side to give

$$B_m = \frac{\gamma_m J_1(\gamma_m b)}{(\eta_m^2 - \beta^2)\eta_m D_m} E_3 + \frac{(2 - \gamma_m^2)\gamma_m J_1(\gamma_m b)}{\eta_m D_m} E_4 - \frac{\gamma_m J_1(\gamma_m b)}{\eta_m D_m} E_5 + \frac{\alpha F_\ell s_\ell R_{\ell m}}{b \eta_m D_m}$$
$$- \frac{\alpha}{b} \sum_{n=0}^{\infty} \frac{A_n s_n R_{nm}}{\eta_m D_m}, \tag{4.16}$$

where

$$E_3 = \tau_2 \nu^2 \beta^2 \sum_{n=0}^{\infty} \frac{B_n \eta_n \gamma_n J_1(\gamma_n b)}{\eta_n^2 - \beta^2}, \tag{4.17}$$

$$E_4 = \sum_{n=0}^{\infty} B_n \eta_n \gamma_n J_1(\gamma_n b), \tag{4.18}$$

$$E_5 = \sum_{n=0}^{\infty} B_n \eta_n \gamma_n^3 J_1(\gamma_n b), \tag{4.19}$$

and R_{nm} is as given in (4.13). The constants $E_0 - E_5$ in (4.9) and (4.16) are found by applying edge conditions which describe how the shells are connected to the rigid annulus

at the matching interface. These conditions can be written in the form

$$\sum_{m=0}^{\infty} A_m \psi_{mn}^{(\mathrm{a})} + \sum_{m=0}^{\infty} B_m \psi_{mn}^{(\mathrm{b})} + F_\ell \psi_n^{(\mathrm{f})} = 0, \quad \text{for } n = 0, 1, 2, \ldots 5, \tag{4.20}$$

where $n = 0, 1, 2$ refer to conditions applied to the left-hand shell edge and $n = 3, 4, 5$ refer to conditions applied at the right-hand shell edge. In order to apply the left-hand edge conditions (4.9) is multiplied by $\psi_{mn}^{(\mathrm{a})}$, and on summing over m it is found that

$$\begin{aligned}
&-\sum_{m=0}^{\infty} F_\ell \delta_{\ell m} \psi_{mn}^{(\mathrm{a})} + \sum_{m=0}^{\infty} \frac{\kappa_m J_1(\kappa_m a) \psi_{mn}^{(\mathrm{a})}}{(s_m^2 - \beta^2) C_m} E_0 + \sum_{m=0}^{\infty} \frac{(2 - \kappa_m^2) \kappa_m J_1(\kappa_m a) \psi_{mn}^{(\mathrm{a})}}{C_m} E_1 \\
&- \sum_{m=0}^{\infty} \frac{\kappa_m J_1(\kappa_m a) \psi_{mn}^{(\mathrm{a})}}{C_m} E_2 + \frac{\alpha}{a} \sum_{m=0}^{\infty} \sum_{n=0}^{\infty} \frac{B_n R_{mn} \psi_{mn}^{(\mathrm{a})}}{C_m} = -\sum_{m=0}^{\infty} B_m \psi_{mn}^{(\mathrm{b})} - F_\ell \psi_n^{(\mathrm{f})}, \quad n = 0, 1, 2.
\end{aligned} \tag{4.21}$$

Similarly for the right-hand edge conditions (4.16) is multiplied by $\psi_{mn}^{(\mathrm{b})}$, and on summing over m, it is found that

$$\begin{aligned}
&\sum_{m=0}^{\infty} \frac{\gamma_m J_1(\gamma_m b) \psi_{mn}^{(\mathrm{b})}}{(\eta_m^2 - \beta^2) \eta_m D_m} E_3 + \sum_{m=0}^{\infty} \frac{(2 - \gamma_m^2) \gamma_m J_1(\gamma_m b) \psi_{mn}^{(\mathrm{b})}}{\eta_m D_m} E_4 \\
&- \sum_{m=0}^{\infty} \frac{\gamma_m J_1(\gamma_m b) \psi_{mn}^{(\mathrm{b})}}{\eta_m D_m} E_5 + \sum_{m=0}^{\infty} \frac{\alpha F_\ell s_\ell R_{\ell m} \psi_{mn}^{(\mathrm{b})}}{b \eta_m D_m} - \frac{\alpha}{b} \sum_{m=0}^{\infty} \sum_{n=0}^{\infty} \frac{A_n s_n R_{nm} \psi_{mn}^{(\mathrm{b})}}{\eta_m D_m} \\
&= -\sum_{m=0}^{\infty} A_m \psi_{mn}^{(\mathrm{a})} - F_\ell \psi_n^{(\mathrm{f})}, \quad n = 3, 4, 5.
\end{aligned} \tag{4.22}$$

The expressions for $\psi_{mn}^{(\mathrm{a})}$, $\psi_{mn}^{(\mathrm{b})}$ and $\psi_n^{(\mathrm{f})}$ are found from eigenfunction expansions of the edge conditions.

4.1.1 Clamped edges

On using the displacements given in (4.4) and (4.2), the clamped edge conditions given in (3.26) lead to

$$\begin{aligned}
&\psi_{m0}^{(\mathrm{a})} = s_m \kappa_m J_1(\kappa_m a)/(s_m^2 - \beta^2), && \psi_{m0}^{(\mathrm{b})} = 0, && \psi_0^{(\mathrm{f})} = -s_\ell \kappa_\ell J_1(\kappa_\ell a)/(s_\ell^2 - \beta^2), \\
&\psi_{m1}^{(\mathrm{a})} = \kappa_m J_1(\kappa_m a), && \psi_{m1}^{(\mathrm{b})} = 0, && \psi_1^{(\mathrm{f})} = \kappa_\ell J_1(\kappa_\ell a), \\
&\psi_{m2}^{(\mathrm{a})} = s_m \kappa_m J_1(\kappa_m a), && \psi_{m2}^{(\mathrm{b})} = 0, && \psi_2^{(\mathrm{f})} = -s_\ell \kappa_\ell J_1(\kappa_\ell a) \\
&\psi_{m3}^{(\mathrm{b})} = \eta_m \gamma_m J_1(\gamma_m b)/(\eta_m^2 - \beta^2), && \psi_{m3}^{(\mathrm{a})} = 0, && \psi_3^{(\mathrm{f})} = 0, \\
&\psi_{m4}^{(\mathrm{b})} = \gamma_m J_1(\gamma_m b), && \psi_{m4}^{(\mathrm{a})} = 0, && \psi_4^{(\mathrm{f})} = 0, \\
&\psi_{m5}^{(\mathrm{b})} = \eta_m \gamma_m J_1(\gamma_m b), && \psi_{m5}^{(\mathrm{a})} = 0, && \psi_5^{(\mathrm{f})} = 0.
\end{aligned} \tag{4.23}$$

The values of $E_0 - E_5$ are found by truncating and solving equations (4.21) and (4.22) using the above values of ψ, it can be seen that $E_1 = 0$. Coupled equations are obtained by using $E_0 - E_2$ in equation (4.9) and $E_3 - E_5$ in (4.16). These equations are then truncated and solved to give the mth amplitude A_m of the reflected field and the mth amplitude B_m of the transmitted field. The energy entering the system $\mathcal{E}_{\mathrm{F}}$ is due to the wave incident in the z direction, which has unit energy. The energy leaving the system comprises the energy of the reflected field $\mathcal{E}_{\mathrm{A}}$ and the energy of the transmitted field $\mathcal{E}_{\mathrm{B}}$. The energy associated with the reflected and transmitted fields are as given in (2.41) and (2.42) which are stated below:

$$\mathcal{E}_{\mathrm{A}} = \frac{a}{\alpha}\mathrm{Real}\left[\sum_{m=0}^{M} |A_m|^2 s_m C_m\right], \tag{4.24}$$

where A_m are the amplitudes of the reflected waves and

$$\mathcal{E}_{\mathrm{B}} = \frac{b}{\alpha}\mathrm{Real}\left[\sum_{m=0}^{M} |B_m|^2 \eta_m D_m\right], \tag{4.25}$$

where B_m are the amplitudes of the transmitted waves. The results are created in Matlab with the code presented in Appendix G. The amplitudes have been formed using 100 modes, which is shown to be more than sufficient in the section that follows.

The first considered configuration assumes the radius of the two shells to be equal, where $\bar{a} = 0.2$m and $\bar{b} = 0.2$m. This forms a infinite shell which has no change in radius, however it remains clamped at $z = 0$. As stated in Section 3.1 there are two fundamental modes (s_0 being fluid-borne and s_1 being structure-borne), this gives two possible modes for the energy to propagate along in each shell. For a shell of radius $\bar{a} = 0.2$m the first cut-on mode occurs at 1048Hz (the second cut-on mode occurs outside the chosen frequency range). Thus introducing a third potential mode for the energy to propagate along. The resulting energy outputs are shown for $5 - 1200$Hz in Figure 4.2.

Figure 4.2a corresponds to the forcing wave being formed of the fluid-borne mode ($\ell = 0$). The results show that the energy is totally transmitted for the chosen frequency range. The clamped joint and the cut-on occurring at 1048Hz appear to have no effect on the energy. This is because the energy is propagating in the fluid (as $\ell = 0$ indicates a fluid-borne mode) which means it cannot be reflected by the junction. It is possible for the energy to move from the fluid into the shell (and still be transmitted), this is known as a structural mode. However, such a mode would occur at a much larger frequency (or equivalently a larger shell radius) which is outside the range considered here.

Figure 4.2b corresponds to the forcing wave being formed of the structure-borne mode ($\ell = 1$). It can be seen that the energy is totally reflected for frequencies below the cut-on 1048Hz (the first cut-on which occurs). This is because the compressional wave in the

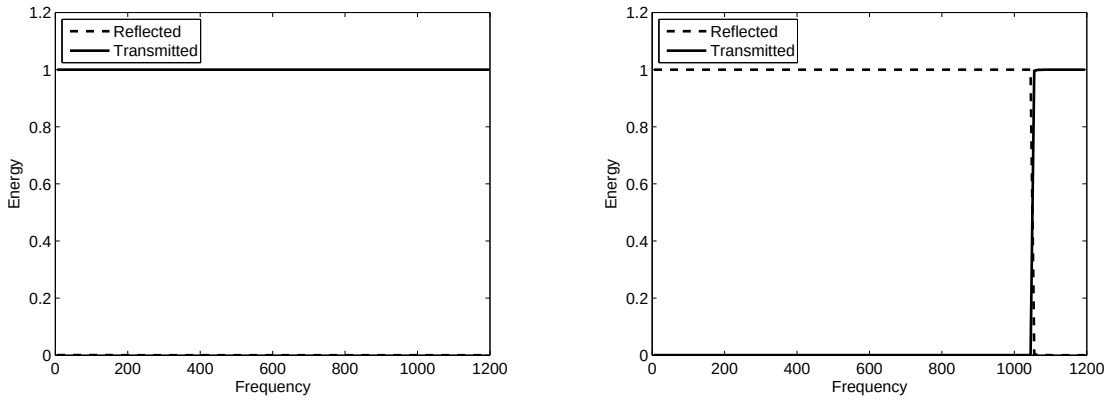

Figure 4.2: Energy output for no change in radius with clamped edges: a) $\bar{a} = 0.2$m, $\bar{b} = 0.2$m, $\ell = 0$; b) $\bar{a} = 0.2$m, $\bar{b} = 0.2$m, $\ell = 1$.

structure is unable to travel through the clamped edge and therefore is mostly reflected until the cut-on occurs. The cut-on causes a sudden inversion in the energies as it is transmitted for the remainder of the frequency range. This is because the cut-on allows for the energy to move into the fluid and be carried by this mode. This shift of energy from the shell into the fluid is a common occurrence at a cut-on and is useful for the design of HVAC systems. From this configuration, to prevent unwanted reflected noise the frequency of the forcing wave should be above 1048Hz. Similarly, to prevent unwanted reflected noise the frequency of the forcing wave should be below 1048Hz.

The energy propagating in each of the individual modes for this configuration is shown Figure 4.3, where the index indicates the direction (reflected A or transmitted B) and the mode number $(0\ , 1,\ 2)$. It is seen that the energy is initially reflected, being carried by the structure-borne mode in the left-hand shell until the cut-on occurs at 1048Hz. From this frequency onwards, the energy is transmitted, carried by the mode which cut-on at 1048Hz (essentially a fluid mode). This supports the statement about the energy being carried by the cut-on mode.

The second considered configuration assumes the radius of the right-hand shell to be larger than the left-hand shell, where $\bar{a} = 0.2$m and $\bar{b} = 0.28$m. The resulting energy outputs are shown for $5 - 1200$Hz in Figure 4.4. For a shell of radius $\bar{b} = 0.28$m the first cut-on occurs at 744Hz (the second cut-on mode occurs outside the chosen frequency range). This introduces a third mode for the energy to propagate in the right-hand shell while the third mode in the left-hand shell is introduced at 1048Hz. The resulting energy outputs are shown for $5 - 1200$Hz in Figure 4.4.

Figure 4.4a corresponds to the forcing wave being formed of the fluid-borne mode ($\ell = 0$). This result is similar to that obtained for the equivalent rigid duct in Figure 2.10a. The majority of energy is transmitted throughout the frequency range and it drops at the cut-on from the right-hand shell at 744Hz and also at the cut-on from the left-

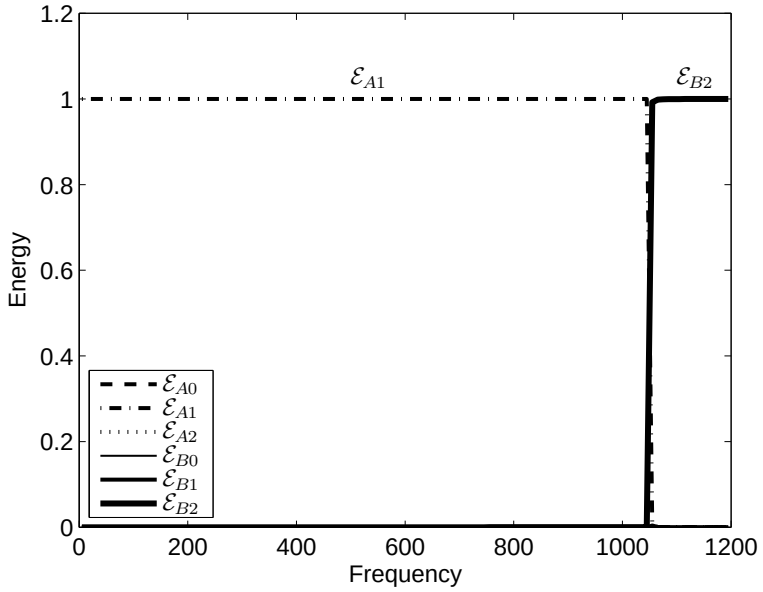

Figure 4.3: Mode energy output for no change in radius with clamped edges for $\bar{a} = 0.2$m, $\bar{b} = 0.2$m, $\ell = 1$.

hand shell at 1048Hz. From a design point of view, to minimise the amount of unwanted transmitted noise the frequency of the fluid-borne forcing wave should be near the first cut-on in the right-hand shell at 744Hz. Similarly, to minimise the amount of unwanted reflected noise the frequency of the fluid-borne forcing wave should be just before the first cut-on in the left-hand shell at 1048Hz.

Figure 4.4b corresponds to forcing using the second mode in the amplitude of the forcing wave ($\ell = 1$). It is seen that the energy is totally reflected up until the cut-on from the left-hand shell at 1048Hz. The cut-on at 744Hz from the right-hand shell has no impact on the energy. The reflected energy then continues to fall for the remainder of the chosen frequency range, thus providing an ideal frequency for minimising the amount of reflected noise from a structure-borne forcing wave. The energy propagating in each of the individual modes is shown in Figure 4.5. It can be seen that the energy is initially reflected, being carried by structure-borne mode in the left-hand shell. At the cut-on from the left-hand shell at 1048Hz the energy is no longer carried by the structure-borne mode. After 1048Hz the energy is divided between the left-hand and right-hand shells. In the left-hand shell the energy is carried by the fundamental fluid-borne mode ($\mathcal{E}_{\mathrm{A0}}$) and the mode which cut-on mode at 1048Hz ($\mathcal{E}_{\mathrm{A2}}$). In the right-hand shell the energy travels a long the fluid-borne mode ($\mathcal{E}_{\mathrm{B0}}$) and the mode which had cut-on at 744Hz ($\mathcal{E}_{\mathrm{B2}}$).

The final considered configuration assumes the radius of the left-hand shell being significantly smaller than the radius of the right-hand shell. The resulting energy outputs for a left-hand shell radius of $\bar{a} = 0.06$m and right-hand radius $\bar{b} = 0.28$m are shown for $5 - 1200$Hz in Figure 4.6. The first cut-on mode for a shell of $\bar{a} = 0.06$m occurs outside

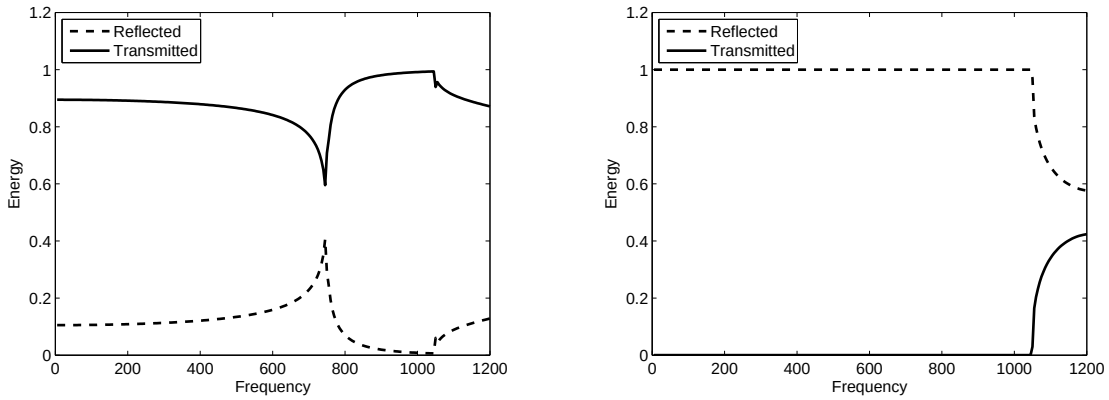

Figure 4.4: Energy output for the abrupt increase in radius with clamped edges: a) $\bar{a} = 0.2$m, $\bar{b} = 0.28$m, $\ell = 0$; b) $\bar{a} = 0.2$m, $\bar{b} = 0.28$m, $\ell = 1$.

the specified frequency range.

In Figure 4.6a the amplitude of the forcing wave comprises the fluid-borne mode ($\ell = 0$). This result is similar to that obtained with rigid ducts in Figure 2.10b. The majority of energy is reflected below the frequency for the cut-on in the right-hand shell at 748Hz. After this cut-on the energies are inverted and the transmitted energy slowly decreases for the remaining of the frequency range. This is in keeping with well known result (see for example Levine and Schwinger [2]) that the energy is totally reflected as $k\bar{a} = a \to 0$.

For the structure-borne mode in the amplitude of the forcing wave ($\ell = 1$) the system demonstrates total reflection for the whole frequency range (see Figure 4.6b). This is analogous to a slinky connected to a fixed point in that the compressional wave cannot progress through the clamped edge and so is completely reflected.

4.1.2 Pin-jointed edges

On using the displacements given in (4.2) and (4.4), the pin-jointed edge conditions given in (3.27) give

$$\begin{aligned}
&\psi_{m0}^{(\mathrm{a})} = s_m^2\kappa_m J_1(\kappa_m a)/(s_m^2-\beta^2), && \psi_{m0}^{(\mathrm{b})} = 0, && \psi_0^{(\mathrm{f})} = s_\ell^2\kappa_\ell J_1(\kappa_\ell a)/(s_\ell^2-\beta^2),\\
&\psi_{m1}^{(\mathrm{a})} = \kappa_m J_1(\kappa_m a), && \psi_{m1}^{(\mathrm{b})} = 0, && \psi_1^{(\mathrm{f})} = \kappa_\ell J_1(\kappa_\ell a),\\
&\psi_{m2}^{(\mathrm{a})} = s_m^2\kappa_m J_1(\kappa_m a), && \psi_{m2}^{(\mathrm{b})} = 0, && \psi_2^{(\mathrm{f})} = s_\ell^2\kappa_\ell J_1(\kappa_\ell a)\\
&\psi_{m3}^{(\mathrm{b})} = \eta_m^2\gamma_m J_1(\gamma_m b)/(\eta_m^2-\beta^2), && \psi_{m3}^{(\mathrm{a})} = 0, && \psi_3^{(\mathrm{f})} = 0,\\
&\psi_{m4}^{(\mathrm{b})} = \gamma_m J_1(\gamma_m b), && \psi_{m4}^{(\mathrm{a})} = 0, && \psi_4^{(\mathrm{f})} = 0,\\
&\psi_{m5}^{(\mathrm{b})} = \eta_m^2\gamma_m J_1(\gamma_m b), && \psi_{m5}^{(\mathrm{a})} = 0, && \psi_5^{(\mathrm{f})} = 0.
\end{aligned} \tag{4.26}$$

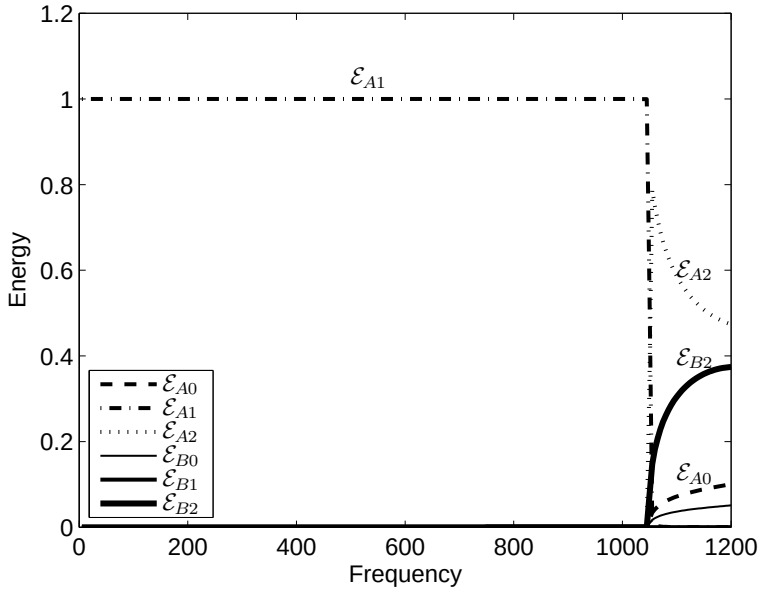

Figure 4.5: Mode energy output for the abrupt increase in radius with clamped edges $\bar{a} = 0.2$m, $\bar{b} = 0.28$m, $\ell = 1$.

The method of solving to find the amplitudes of the reflected and transmitted fields is analogous to that used for the clamped edges, but replacing values of ψ with those stated above and it is seen that $E_1 = 0$. The energy equations are given by (2.41) and (2.42), these are stated below for convenience:

$$\mathcal{E}_{\mathrm{A}} = \frac{a}{\alpha}\mathrm{Real}\left[\sum_{m=0}^{M} |A_m|^2 s_m C_m\right], \tag{4.27}$$

where A_m are the amplitudes of the reflected waves and

$$\mathcal{E}_{\mathrm{B}} = \frac{b}{\alpha}\mathrm{Real}\left[\sum_{m=0}^{M} |B_m|^2 \eta_m D_m\right], \tag{4.28}$$

where B_m are the amplitudes of the transmitted waves. The results are found in Matlab by using the code in Appendix G. This has been done using 100 modes to calculate the amplitudes of the propagating waves.

Those configurations that were considered in the previous subsection with clamped edges were considered for pin-jointed edges also. It was found that the results obtained using pin-jointed edges were identical to those obtained from the clamped edge equivalent problems.

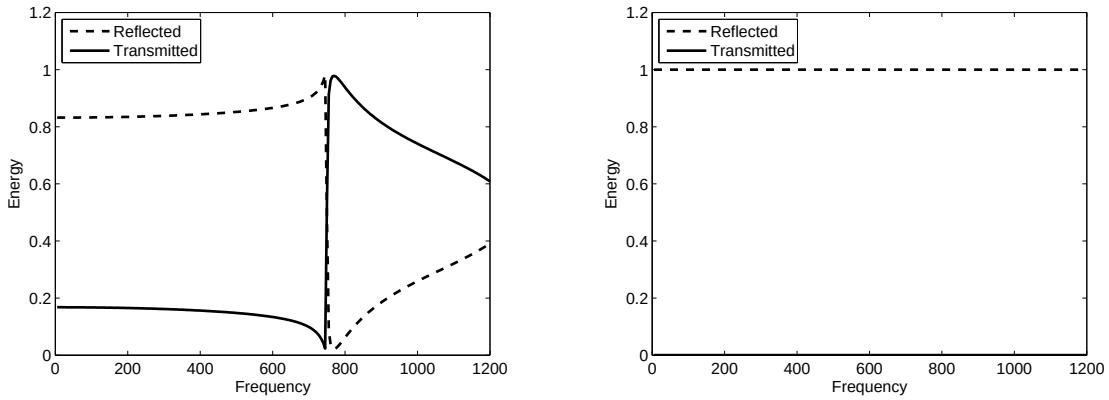

Figure 4.6: Energy output for the abrupt increase in radius with clamped edges: a) $\bar{a} = 0.06$m, $\bar{b} = 0.28$m, $\ell = 0$; b) $\bar{a} = 0.06$m, $\bar{b} = 0.28$m, $\ell = 1$.

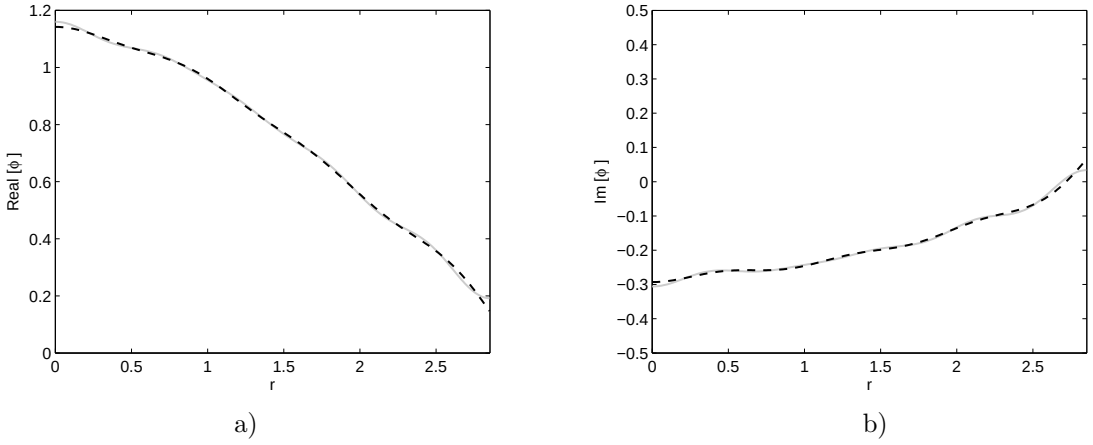

Figure 4.7: The two sides of the pressure matching condition for 10 modes with $\bar{a} = 0.2$m, $\bar{b} = 0.28$m (dashed line: left side of the condition, solid line: right side of the condition) a) Real; b) Imaginary.

4.1.3 Verification of results

It is necessary to verify the resulting amplitudes in order to ensure that the mode matching method has been correctly applied. Also this will show that a suitable number of modes have been selected. For this it is sufficient to verify one of the considered configuration, in this case the $\bar{a} = 0.2$m, $\bar{b} = 0.28$m with first mode forcing and clamped edges has been selected, which correspond to the results of Figure 4.4a. The matching condition for pressure is (4.7) which is presented against the non-dimensional radius of the shell for 10 modes at 780Hz in Figure 4.7. It is seen that with 10 modes used to formulate the amplitudes, the matching of the pressure condition drifts both in the center of the shell and towards the inner edge at $\bar{r} = a$. This in turn shows that the amplitudes have been generated with an insufficient number of modes. The number of modes used to calculate the amplitudes is now increased to 60 modes and the matching pressure

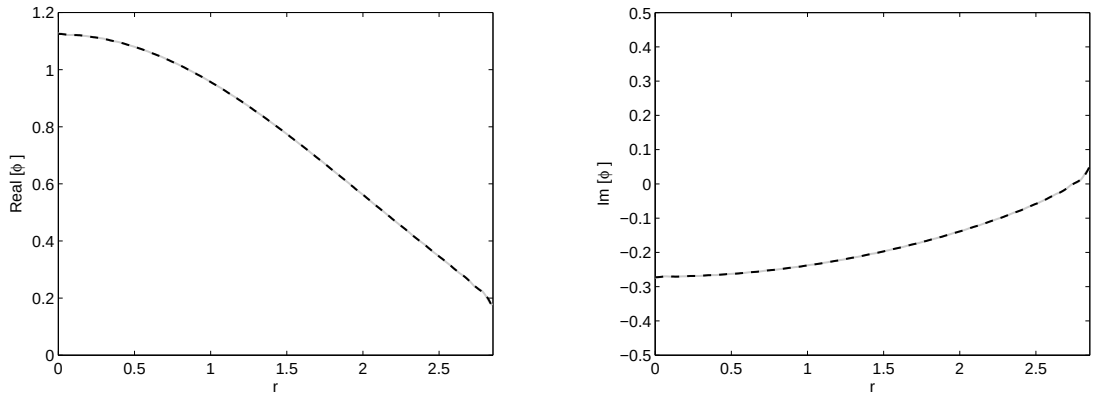

a) b)

Figure 4.8: The two sides of the pressure matching condition for 60 modes with $\bar{a} = 0.2$m, $\bar{b} = 0.28$m (dashed line: left side of the condition, solid line: right side of the condition) a) Real; b) Imaginary.

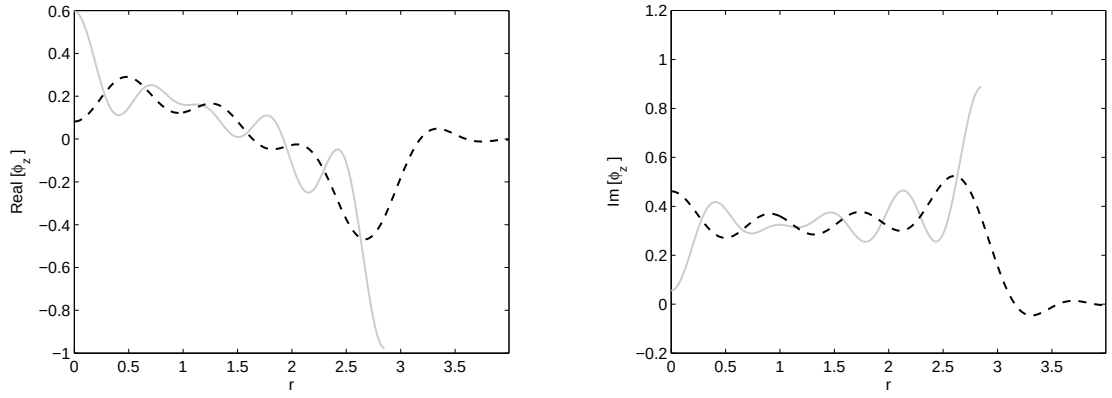

a) b)

Figure 4.9: The two sides of the velocity condition for 10 modes with $\bar{a} = 0.2$m, $\bar{b} = 0.28$m (dashed line: left side of the condition, solid line: right side of the condition) a) Real; b) Imaginary.

condition is presented against the non-dimensional radius of the shell at 780Hz in Figure 4.8. With 60 modes to form the amplitudes, the match for the pressure conditions is greatly improved as it matches for each region of the radius. This suggests that 60 modes finds suitably accurate amplitudes for fulfilling the pressure matching condition. The other matching condition to verify is the matching of the normal component of velocity, shown in Figures 4.9 and 4.10. As found in the rigid equivalent problem the piecewise nature of this condition is not suitable for the verification. A better verification would be to show matching of the velocity flux, which is given by

$$iF_0 s_0 \int_0^a J_0(\kappa_0 r) r \, \mathrm{d}r - i \sum_{n=0}^{\infty} A_n s_n \int_0^a J_0(\kappa_n r) r \, \mathrm{d}r = i \sum_{n=0}^{\infty} B_n \int_0^b J_0(\gamma_n r) r \, \mathrm{d}r. \quad (4.29)$$

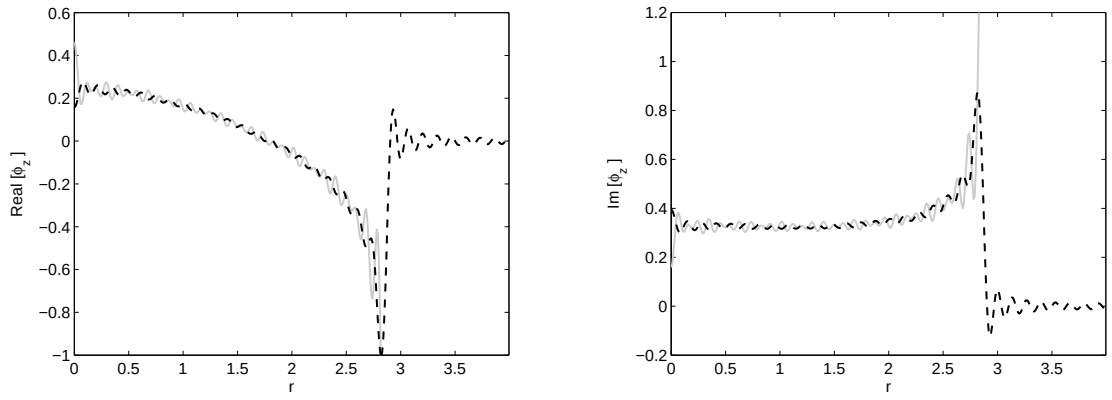

a) b)

Figure 4.10: The two sides of the velocity condition for 60 modes with $\bar{a} = 0.2$m, $\bar{b} = 0.28$m (dashed line: left side of the condition, solid line: right side of the condition) a) Real; b) Imaginary.

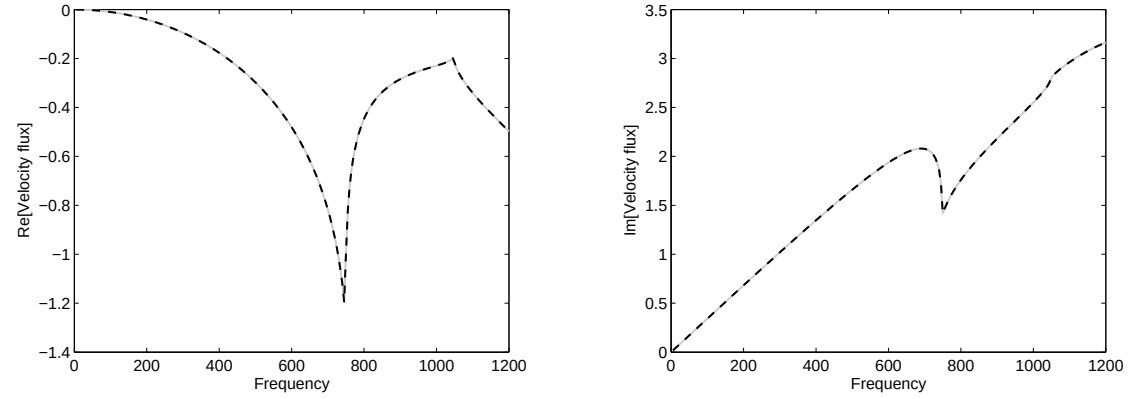

a) b)

Figure 4.11: The two sides of the velocity flux condition for 10 modes with $\bar{a} = 0.2$m, $\bar{b} = 0.28$m (dashed line: left side of the condition, solid line: right side of the condition) a) Real; b) Imaginary.

The two sides of (4.29) are found for $5 - 1200$Hz and the real and imaginary parts are presented in Figure 4.11 for 10 modes and Figure 4.12 60 modes. This shows an excellent agreement between the two sides of (4.29) when 100 modes are used to find the wave amplitudes. There is a dip in both the real and imaginary parts at 748Hz which is in keeping with the first cut-on in the larger duct. Also there is a peak in the real part (with a slight increase in the imaginary part) at 1048Hz which is due to the first cut-on in the smaller duct. The plots in this subsection show that 10 modes is more than sufficient to formulate the amplitudes with and they validate that the method has been applied correctly.

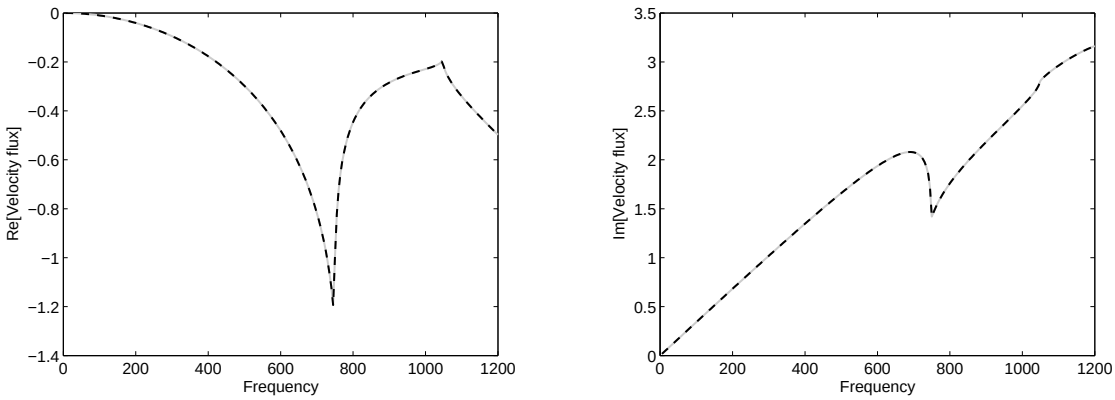

a) b)

Figure 4.12: The two sides of the velocity flux condition for 60 modes with $\bar{a} = 0.2$m, $\bar{b} = 0.28$m (dashed line: left side of the condition, solid line: right side of the condition) a) Real; b) Imaginary.

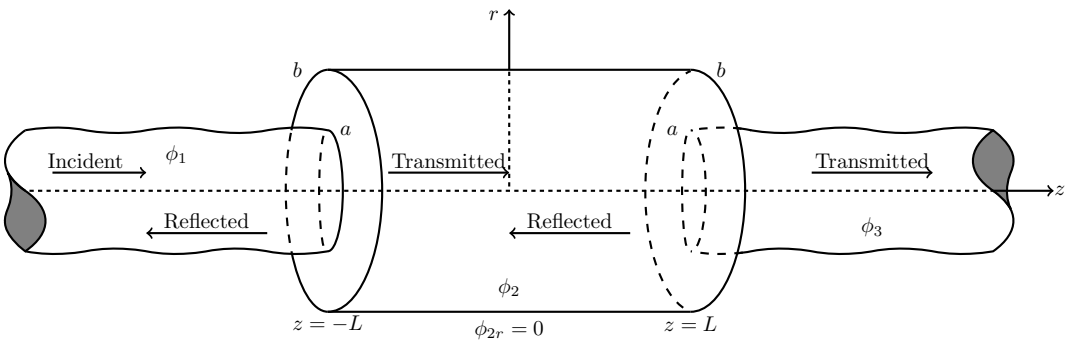

Figure 4.13: Physical configuration of the rigid expansion chamber between two shells problem.

4.2 Energy transmitted through a rigid expansion chamber situated between two shells

This section considers the energy leaving a rigid expansion chamber situated between two shells. The problem comprises two semi-infinite shells with a finite rigid-walled expansion chamber of dimensional length $2L$ between them (where $L = k\bar{L}$) as shown in Figure 4.13. The inlet shell is located in the region $0 \leq r \leq a,\ z \leq -L$, the outlet shell is located in the region $0 \leq r \leq a,\ z \geq -L$ and the expansion chamber occupies the space between them, $0 \leq r \leq b,\ -L \leq z \leq L$, thus having a length $2L$. The system is closed by rigid annular discs located at $a \leq r \leq b,\ z = \pm L$.

The velocity potential for the inlet shell ϕ_1 comprises the incident forcing wave and the field reflected at the first junctions, which is

$$\phi_1 = F_\ell J_0(\kappa_\ell r) e^{is_\ell(z+L)} + \sum_{n=0}^{\infty} A_n J_0(\kappa_n r) e^{-is_n(z+L)},\ 0 \leq r \leq a,\ z \leq -L, \tag{4.30}$$

where ℓ indicates the chosen fundamental mode to force with ($\ell = 0$ or $\ell = 1$), F_ℓ is the amplitude of the forcing wave given in (3.60), A_n is the amplitude of the nth reflected mode, s_n are the wavenumbers for a flexible shell and $\kappa_n = (1 - s_n^2)^{1/2}$. Note that the argument in the exponential is chosen such that the problem can later be reduced. The velocity potential for the rigid expansion chamber ϕ_2 is made of the waves reflected by the second junction and those which pass through the first junction. This gives the velocity potential ϕ_2 as

$$\phi_2 = \sum_{n=0}^{\infty} \left(P_n e^{-i\eta_n z} + Q_n e^{i\eta_n z} \right) J_0(\gamma_n r),\ 0 \leq r \leq b,\ -L \leq z \leq L, \tag{4.31}$$

where P_n is the amplitude of the nth reflected wave, Q_n is the amplitude of the nth transmitted wave and $\eta_n,\ n = 0, 1, 2, \ldots$ are the wavenumbers given by the roots of the

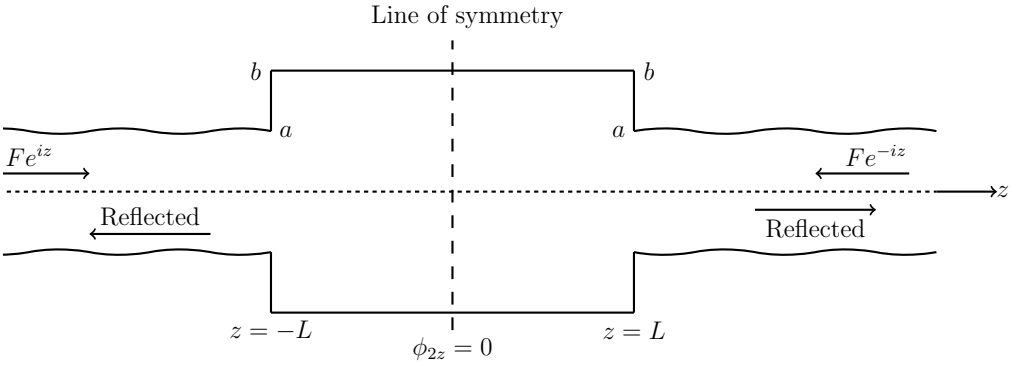

Figure 4.14: Physical configuration of the symmetric subproblem.

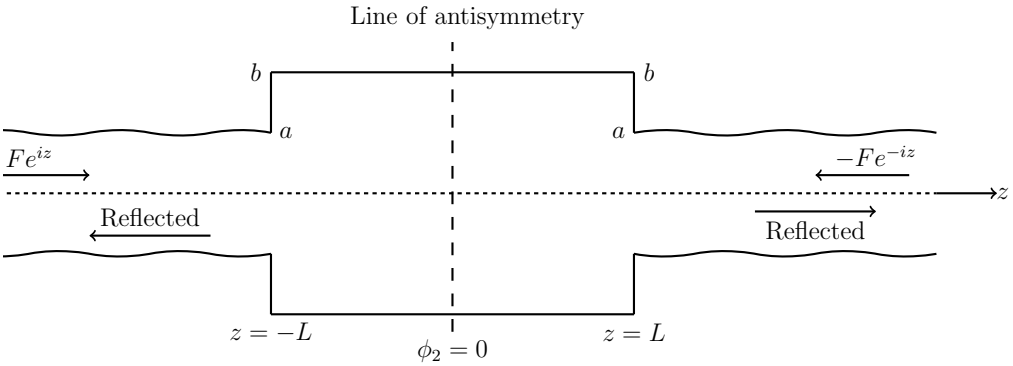

Figure 4.15: Physical configuration of the antisymmetric subproblem.

characteristic equation for a rigid duct in (2.14). The velocity potential for the outlet shell ϕ_3 is composed of those waves which are transmitted through the chamber, which is

$$\phi_3 = \sum_{n=0}^{\infty} B_n J_0(\kappa_n r) e^{is_\ell(z-L)},\ 0 \leq r \leq a,\ z \geq L, \tag{4.32}$$

where B_n is the amplitude of the nth transmitted wave. In order to find the amplitudes of the reflected and transmitted fields, the problem is broken down into symmetric and antisymmetric subproblems. This is done by introducing a second forcing wave located in the outlet shell. This forcing wave travels in the negative z direction for both problems, where for the antisymmetric system this wave has a horizontal shift of $i\pi$, which by Euler's identity results in a negative forcing amplitude.

The symmetric subproblem is so called because it has a line of symmetry down through the centre of the expansion chamber at $z = 0$ (as shown in Figure 4.14). It represents an expansion chamber with two incident waves. One located in the left section $z \leq -L$ heading towards the first junction and the second located in the right-most section $z \geq L$ heading in the negative z direction towards the second junction. Similarly, the antisymmetric problem has a line of antisymmetry through the centre expansion chamber

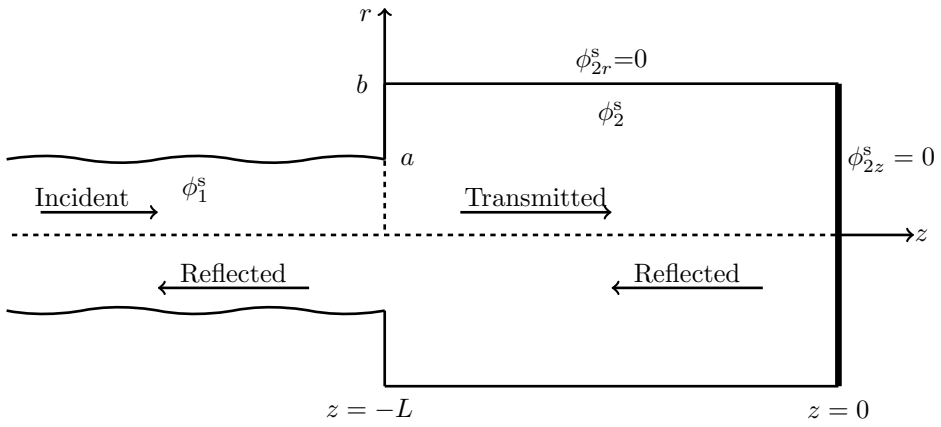

Figure 4.16: Physical configuration of the abrupt increase in radius symmetric subproblem.

at $z = 0$ (as shown in Figure 4.15). It represents an expansion chamber with two incident waves in the same locations as the symmetric subproblem, heading in the same direction , but with the incident wave in the right-most section having a negative amplitude (causing it to shift horizontally).

The line of symmetry/antisymmetric in these subproblems allows them to be reduced to a simpler system featuring an abrupt increase in radius. The coefficients of the reflected field from these systems can be used to determine the reflected and transmitted coefficients for the full problem of a rigid expansion chamber between two shells.

4.2.1 Symmetric subproblem

The symmetric nature of the symmetric subproblem enables it to be reduced to an equivalent system with an abrupt increase in radius and a rigid end plate (see Figure 4.16). The purpose of this subsection is to determine the energy radiated due to a forcing wave at an abrupt increase in radius. The system comprises a semi-infinite shell located at $0 \leq r \leq a,\ z \leq -L$ and a finite rigid duct located at $0 \leq r \leq b,\ -L \leq z \leq 0$. It is closed by a rigid annular disc occupying $a \leq r \leq b,\ z = -L$ and a rigid plate occupying $0 \leq r \leq b,\ z = 0$. Forcing is by a wave located in the left-hand shell propagating in the positive z direction towards the abrupt increase in radius.

The velocity potential for the left-hand shell ϕ^{s}_1 comprises the plane wave and the reflected field, which is

$$\phi^{\mathrm{s}}_1 = F_\ell J_0(\kappa_\ell r) e^{is_\ell(z+L)} + \sum_{n=0}^{\infty} A^{\mathrm{s}}_n J_0(\kappa_n r) e^{-is_n(z+L)},\ 0 \leq r \leq a,\ z \leq -L, \tag{4.33}$$

where the superscript denotes the symmetric subsystem, ℓ indicates the chosen fundamental mode to force with ($\ell = 0$ or $\ell = 1$), F_ℓ is the amplitude of the forcing wave given in (3.60) and $A^{\mathrm{s}}_n,\ n = 0, 1, 2, \ldots$ are the amplitudes of the reflected field for the symmetric

subsystem. The eigenfunction expansions of the longitudinal and radial displacements given in (3.13) and (3.14) are

$$u_1^{\rm s}(z) = \frac{\nu F_\ell s_\ell \kappa_\ell J_1(\kappa_\ell a) e^{is_\ell(z+L)}}{a(s_\ell^2 - \beta^2)} - \frac{\nu}{a}\sum_{n=0}^{\infty} \frac{A_n^{\rm s} s_n \kappa_n J_1(\kappa_n a)}{s_n^2 - \beta^2} e^{-is_n(z+L)},\ z \le -L, \tag{4.34}$$

$$w_1^{\rm s}(z) = -F_\ell \kappa_\ell J_1(\kappa_\ell a) e^{is_\ell(z+L)} - \sum_{n=0}^{\infty} A_n^{\rm s} \kappa_n J_1(\kappa_n a) e^{-is_n(z+L)},\ z \le -L. \tag{4.35}$$

The velocity potential for the finite section $\phi_2^{\rm s}$ comprises those waves which are transmitted through the first junction and those wave which are reflected at $z = 0$, which gives

$$\phi_2^{\rm s} = \sum_{n=0}^{\infty} \left(P_n^{\rm s} e^{-i\eta_n z} + Q_n^{\rm s} e^{i\eta_n z}\right) J_0(\gamma_n r),\ 0 \le r \le b,\ z \ge -L. \tag{4.36}$$

The velocity potential $\phi_2^{\rm s}$ can be simplified by considering the property of the end plate. The condition at the plate is $\phi_{2z}^{\rm s} = 0$, which is only satisfied when $P_n^{\rm s} = Q_n^{\rm s}$, therefore

$$\phi_2^{\rm s} = 2\sum_{n=0}^{\infty} P_n^{\rm s} \cos(\eta_n L) J_0(\gamma_n r),\ 0 \le r \le b,\ -L \le z \le 0. \tag{4.37}$$

The amplitudes are found by matching the fluid pressure and the normal component of velocity at the abrupt increase in radius. The fluid pressure and normal component of velocity are constant in the fluid, while the latter vanishes on the rigid annular disc. That is at $z = -L$

$$\phi_1^{\rm s}(r,-L) = \phi_2^{\rm s}(r,-L),\ 0 \le r \le a, \tag{4.38}$$

$$\frac{\partial \phi_2^{\rm s}}{\partial z}(r,-L) = \begin{cases} \frac{\partial \phi_1^{\rm s}}{\partial z}(r,-L), & 0 \le r \le a \\ 0, & a \le r \le b \end{cases}. \tag{4.39}$$

The first equation is found by multiplying (4.76) through by $J_0(\gamma_m b)r$ and integrating with respect to $r,\ 0 \le r \le b$ to give

$$\int_0^b \frac{\partial \phi_2^{\rm s}}{\partial z} J_0(\gamma_m r) r\ {\rm d}r = \int_0^a \frac{\partial \phi_1^{\rm s}}{\partial z} J_0(\gamma_m r) r\ {\rm d}r,\ \text{at } z = -L. \tag{4.40}$$

The above equation is expressed in eigenfunction form by substituting in the velocity potentials from (4.33) and (4.37) which leads to

$$2\sum_{n=0}^{\infty} P_n^{\rm s} \sin(\eta_n L)\eta_n \int_0^b J_0(\gamma_n r) J_0(\gamma_n r) r\ {\rm d}r = iF_\ell s_\ell R_{\ell m} - i\sum_{n=0}^{\infty} A_n^{\rm s} s_n R_{nm}, \tag{4.41}$$

where R_{nm} is as given in (4.13). The rigid wall orthogonality relation in (2.27) is now

applied to the integral on the left side of the equation to give

$$2\sum_{n=0}^{\infty} P_n^{\mathrm{s}} \sin(\eta_n L)\eta_n \delta_{nm} D_n = iF_\ell s_\ell R_{\ell m} - i\sum_{n=0}^{\infty} A_n^{\mathrm{s}} s_n R_{nm}, \tag{4.42}$$

where D_n is as given in (2.28). It follows that

$$P_m^{\mathrm{s}} = \frac{iF_\ell s_\ell R_{\ell m}}{2\eta_m \sin(\eta_m L) D_m} - \frac{i}{2}\sum_{n=0}^{\infty} \frac{A_n^{\mathrm{s}} s_n R_{nm}}{\eta_m \sin(\eta_m L) D_m}. \tag{4.43}$$

The velocity potentials in (4.33) and (4.37) are substituted into (4.38) to obtain the pressure condition in its eigenfunction form

$$F_\ell J_0(\kappa_\ell r) + \sum_{n=0}^{\infty} A_n^{\mathrm{s}} J_0(\kappa_n r) = 2\sum_{n=0}^{\infty} P_n^{\mathrm{s}} \cos(\eta_n L) J_0(\gamma_n r). \tag{4.44}$$

On multiplying (4.44) by $\alpha J_0(\kappa_m r) r/a$ and integrating with respect to r, $0 \le r \le a$ it is found that

$$\begin{aligned} &\frac{\alpha F_\ell}{a}\int_0^a J_0(\kappa_\ell r) J_0(\kappa_m r) r \,\mathrm{d}r + \frac{\alpha}{a}\sum_{n=0}^{\infty} A_n^{\mathrm{s}} \int_0^a J_0(\kappa_n r) J_0(\kappa_m r) r \,\mathrm{d}r \\ &= \frac{2\alpha}{a}\sum_{n=0}^{\infty} P_n^{\mathrm{s}} \cos(\eta_n L) R_{mn}, \end{aligned} \tag{4.45}$$

where R_{mn} is as given in (4.13) and C_n is as given in (3.34). The generalised orthogonality relation in (3.35) is now applied to both integrals on the left side of the equation to give

$$\begin{aligned} &F_\ell\left[\delta_{m\ell} C_\ell - \left\{\frac{\tau_1 \nu^2 \beta^2}{(s_\ell^2 - \beta^2)(s_m^2 - \beta^2)} + 2 - \kappa_m^2 - \kappa_\ell^2\right\}\kappa_\ell J_1(\kappa_\ell a)\kappa_m J_1(\kappa_m a)\right] \\ &+ \sum_{n=0}^{\infty} A_n^{\mathrm{s}}\left[\delta_{mn} C_n - \left\{\frac{\tau_1 \nu^2 \beta^2}{(s_n^2 - \beta^2)(s_m^2 - \beta^2)} + 2 - \kappa_m^2 - \kappa_n^2\right\}\kappa_\ell J_1(\kappa_n a)\kappa_m J_1(\kappa_m a)\right] \\ &= \frac{2\alpha}{a}\sum_{n=0}^{\infty} P_n^{\mathrm{s}} \cos(\eta_n L) R_{mn}. \end{aligned} \tag{4.46}$$

It follows that

$$\begin{aligned} A_m^{\mathrm{s}} &= -F_\ell \delta_{m\ell} + \frac{\tau_1 \nu^2 \beta^2 \kappa_m J_1(\kappa_m a)}{(s_m^2 - \beta^2) C_m} E_0 + \frac{(2 - \kappa_m^2)\kappa_m J_1(\kappa_m a)}{C_m} E_1 - \frac{\kappa_m J_1(\kappa_m a)}{C_m} E_2 \\ &+ \frac{2\alpha}{a}\sum_{n=0}^{\infty} \frac{P_n^{\mathrm{s}} \cos(\eta_n L) R_{mn}}{C_m}, \end{aligned} \tag{4.47}$$

where

$$E_0 = \sum_{n=0}^{\infty} \frac{A_n^{\mathrm{s}} \kappa_n J_1(\kappa_n a)}{s_n^2 - \beta^2} + \frac{F_\ell \kappa_\ell J_1(\kappa_\ell a)}{s_\ell^2 - \beta^2}, \tag{4.48}$$

$$E_1 = \sum_{n=0}^{\infty} A_n^{\mathrm{s}} \kappa_n J_1(\kappa_n a) + F_\ell \kappa_\ell J_1(\kappa_\ell a), \tag{4.49}$$

$$E_2 = \sum_{n=0}^{\infty} A_n^{\mathrm{s}} \kappa_n^3 J_1(\kappa_n a) + F_\ell \kappa_\ell^3 J_1(\kappa_\ell a), \tag{4.50}$$

and R_{mn} is as given in (4.13). The constants $E_0 - E_2$ in (4.47) are found by applying conditions which describe the shell edge at the matching interface. These conditions can be written in the form

$$\sum_{m=0}^{\infty} A_m \psi_{mn}^{(\mathrm{a})} + \sum_{m=0}^{\infty} P_m \psi_{mn}^{(p)} + F_\ell \psi_n^{(\mathrm{f})} = 0, \text{ for } n = 0, 1, 2, \tag{4.51}$$

In order to apply these conditions (4.47) is multiplied by $\psi_{mn}^{(\mathrm{a})}$, and on summing over m it is found that

$$\begin{aligned} &- \sum_{m=0}^{\infty} F_\ell \delta_{\ell m} \psi_{mn}^{(\mathrm{a})} + \sum_{m=0}^{\infty} \frac{\tau_1 \nu^2 \beta^2 \kappa_m J_1(\kappa_m a) \psi_{mn}^{(\mathrm{a})}}{(s_m^2 - \beta^2) C_m} E_0 + \sum_{m=0}^{\infty} \frac{(2 - \kappa_m^2) \kappa_m J_1(\kappa_m a)}{C_m} E_1 \\ &- \sum_{m=0}^{\infty} \frac{\kappa_m J_1(\kappa_m a) \psi_{mn}^{(\mathrm{a})}}{C_m} E_2 + \sum_{m=0}^{\infty} \frac{2\alpha}{a} \sum_{n=0}^{\infty} \frac{P_n^{\mathrm{s}} \cos(\eta_n L) R_{mn} \psi_{mn}^{(\mathrm{a})}}{C_m} = - \sum_{m=0}^{\infty} P_m \psi_{mn}^{(\mathrm{p})} \\ &- F_\ell \psi_n^{(\mathrm{f})}, \ n = 0, 1, 2. \end{aligned} \tag{4.52}$$

The expressions for $\psi_{mn}^{(\mathrm{a})}$, $\psi_{mn}^{(\mathrm{p})}$ and $\psi_n^{(\mathrm{f})}$ are found from eigenfunction expansions of the edge conditions. For a clamped edge these are as defined in (4.23) and it is immediately seen that $E_1 = 0$. For a pin-jointed edge these values of ψ are as defined in (4.26) and again it is seen that $E_1 = 0$. The remaining constant values E_0 and E_2 for both the clamped and the pin-jointed edge conditions are found by solving the coupled equations generated by (4.52). With all constants found, the coupled equations (4.43) and (4.47) can be solved to find the amplitudes of the reflected waves for the symmetric problem (note that the amplitudes of the transmitted waves for the symmetric subproblem are not required).

4.2.2 Antisymmetric subproblem

The nature of the antisymmetric subproblem enables it to be reduced to an equivalent system with an abrupt increase in radius and an acoustically soft end plate (see Figure 4.17). The purpose of this subsection is to determine the energy radiated due to a forcing wave at the abrupt increase in radius. The system comprises a semi-infinite shell located

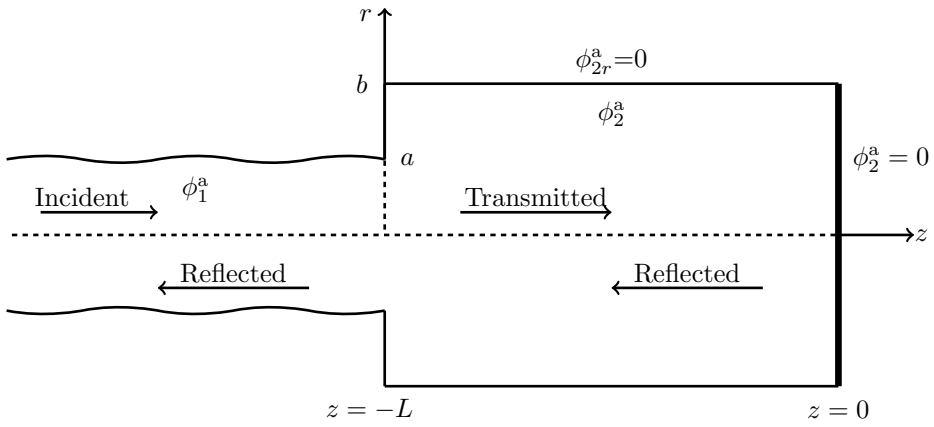

Figure 4.17: Physical configuration of the abrupt increase in radius antisymmetric subproblem.

at $0 \leq r \leq a,\ z \leq -L$ and a finite rigid duct located at $0 \leq r \leq b,\ -L \leq z \leq 0$. It is closed by a rigid annular disc occupying $a \leq r \leq b,\ z = -L$ and an acoustically soft end plate occupying $0 \leq r \leq b,\ z = 0$. Forcing is by a wave located in the left-hand shell propagating in the positive z direction towards the abrupt increase in radius.

The velocity potential for the left-hand shell ϕ^{a}_1 comprises the incident forcing wave and the reflected field

$$\phi^{\mathrm{a}}_1 = F_\ell J_0(\kappa_\ell r) e^{is_\ell(z+L)} + \sum_{n=0}^{\infty} A^{\mathrm{a}}_n J_0(\kappa_n r) e^{-is_n(z+L)},\ 0 \leq r \leq a,\ z \leq -L, \tag{4.53}$$

where the superscript denotes the antisymmetric subsystem,where ℓ indicates the chosen fundamental mode to force with ($\ell = 0$ or $\ell = 1$), F_ℓ is the amplitude of the forcing wave given in (3.60) and A^{a}_n is the amplitudes of nth reflected wave for the antisymmetric subsystem. The eigenfunction expansions of the longitudinal and radial displacements given in (3.13) and (3.14) are

$$u^{\mathrm{a}}_1(z) = \frac{\nu F_\ell s_\ell \kappa_\ell J_1(\kappa_\ell a) e^{is_\ell(z+L)}}{a(s^2_\ell - \beta^2)} - \frac{\nu}{a} \sum_{n=0}^{\infty} \frac{A^{\mathrm{a}}_n s_n \kappa_n J_1(\kappa_n a)}{s^2_n - \beta^2} e^{-is_n(z+L)},\ z \leq -L, \tag{4.54}$$

$$w^{\mathrm{a}}_1(z) = -F_\ell \kappa_\ell J_1(\kappa_\ell a) e^{is_\ell(z+L)} - \sum_{n=0}^{\infty} A^{\mathrm{a}}_n \kappa_n J_1(\kappa_n a) e^{-is_n(z+L)},\ z \leq -L. \tag{4.55}$$

The velocity potential for finite section is analogous to that of the symmetric problem but with $\cos(\cdot)$ replaced by $\sin(\cdot)$

$$\phi^{\mathrm{a}}_2 = 2 \sum_{n=0}^{\infty} P^{\mathrm{a}}_n \sin(\eta_n z) J_0(\gamma_n r),\ 0 \leq r \leq b,\ -L \leq z \leq 0. \tag{4.56}$$

Note that this satisfies the acoustically soft wall condition $\phi^{\mathrm{a}}_2 = 0$ at $z = 0$. The method of solving is analogous to that of the symmetric subproblem and thus matching the normal

component of velocity gives

$$P_m^{\mathrm{a}} = \frac{iF_\ell s_\ell R_{\ell m}}{2b\eta_m \cos(\eta_m L) D_m} - \frac{i}{2b}\sum_{n=0}^{\infty} \frac{A_n^{\mathrm{a}} s_n R_{nm}}{\eta_m \cos(\eta_m L) D_m}, \tag{4.57}$$

where D_m is as given in (3.37). Likewise, matching the pressure gives the second coupled equation as

$$\begin{aligned} A_m^{\mathrm{a}} = &-F_\ell \delta_{\ell m} + \frac{\tau_1 \nu^2 \beta^2 \kappa_m J_1(\kappa_m a)}{(s_m^2 - \beta^2) C_m} E_0 + \frac{(2-\kappa_m^2)\kappa_m J_1(\kappa_m a)}{C_m} E_1 \\ &- \frac{\kappa_m J_1(\kappa_m a)}{C_m} E_2 + \frac{2\alpha}{a}\sum_{n=0}^{\infty} \frac{P_n^{\mathrm{a}} \sin(\eta_n L) R_{mn}}{C_m}, \end{aligned} \tag{4.58}$$

where

$$E_0 = \sum_{n=0}^{\infty} \frac{A_n^{\mathrm{a}} \kappa_n J_1(\kappa_n a)}{s_n^2 - \beta^2} + \frac{F_\ell \kappa_\ell J_1(\kappa_\ell a)}{s_\ell^2 - \beta^2}, \tag{4.59}$$

$$E_1 = \sum_{n=0}^{\infty} A_n^{\mathrm{a}} \kappa_n J_1(\kappa_n a) + F_\ell \kappa_\ell J_1(\kappa_\ell a), \tag{4.60}$$

$$E_2 = \sum_{n=0}^{\infty} A_n^{\mathrm{a}} \kappa_n^3 J_1(\kappa_n a) + F_\ell \kappa_\ell^3 J_1(\kappa_\ell a), \tag{4.61}$$

and R_{mn} is as given in (4.13). The constants $E_0 - E_2$ of (4.58) are found by applying edge conditions which describe the shell edge at the matching interface. The conditions can be written in the form given in (4.51). In order to apply these conditions (4.58) is multiplied by $\psi_{mn}^{(\mathrm{a})}$, and on summing over m it is found that

$$\begin{aligned} &-\sum_{m=0}^{\infty} F_\ell \delta_{\ell m} \psi_{mn}^{(\mathrm{a})} + \sum_{m=0}^{\infty} \frac{\tau_1 \nu^2 \beta^2 \kappa_m J_1(\kappa_m a) \psi_{mn}^{(\mathrm{a})}}{(s_m^2 - \beta^2) C_m} E_0 + \sum_{m=0}^{\infty} \frac{(2-\kappa_m^2)\kappa_m J_1(\kappa_m a)}{C_m} E_1 \\ &- \sum_{m=0}^{\infty} \frac{\kappa_m J_1(\kappa_m a) \psi_{mn}^{(\mathrm{a})}}{C_m} E_2 + \sum_{m=0}^{\infty} \frac{2\alpha}{a} \sum_{n=0}^{\infty} \frac{P_n^{\mathrm{a}} \sin(\eta_n L) R_{mn} \psi_{mn}^{(\mathrm{a})}}{C_m} = -\sum_{m=0}^{\infty} P_m \psi_{mn}^{(\mathrm{p})} \\ &- F_\ell \psi_n^{(\mathrm{f})}, \ n = 0, 1, 2. \end{aligned} \tag{4.62}$$

The expressions for $\psi_{mn}^{(\mathrm{a})}$, $\psi_{mn}^{(\mathrm{p})}$ and $\psi_n^{(\mathrm{f})}$ are found from eigenfunction expansions of the edge conditions. For a clamped edge these are as defined in (4.23) and it is immediately seen that $E_1 = 0$. For a pin-jointed edge these values of ψ are as defined in (4.26) and again it is seen that $E_1 = 0$. The remaining constant values E_0 and E_2 for both the clamped and the pin-jointed edge conditions are found by solving the coupled equations created by (4.62). With all constants found, the coupled equations (4.57) and (4.58) can be solved to find the amplitudes of the reflected waves for the symmetric problem (note that the amplitudes of the transmitted waves for the antisymmetric subproblem are not

required).

The reflected and transmitted amplitudes for the whole expansion chamber system are found by using the amplitudes of the reflected field in the symmetric and antisymmetric subsystems. That is:

$$A_m = \frac{A_m^{\mathrm{s}} + A_m^{\mathrm{a}}}{2},\ B_m = \frac{A_m^{\mathrm{s}} - A_m^{\mathrm{a}}}{2}, \tag{4.63}$$

where A_m^{s} are the reflected amplitudes from the symmetric subsystem, A_m^{a} are the reflected amplitudes from the antisymmetric subsystem, A_m are the reflected amplitudes for the expansion chamber system and B_m are the transmitted amplitudes for the expansion chamber system. The results are created in Matlab with the code presented in Appendix H. This has been done using 100 modes to calculate the amplitudes of the propagating waves. Note that this code is not perfect as the root finder does not give an accurate value for one of the identified roots in the 300Hz to 600Hz range. As a result, the energy plots presented in this chapter may show some noise in this range.

4.2.3 Clamped edge

The introduction of an expansion chamber causes the energies to oscillate over frequency. This is due to the trigonometric factors $\cos(\eta_n L)$ and $\sin(\eta_n L)$ present in the symmetric and antisymmetric amplitudes respectively. As stated in Section 3.1 the first fundamental mode $s_0 \approx 1$. From this it is assumed that when the fluid-borne mode is used, the reflected energy will drop when $k\bar{L} = n\pi,\ n = 0, 1, 2, \ldots$ (as P_m corresponds to the mth amplitude of waves reflected inside the expansion chamber). This is when $f = cn/(4\bar{L}),\ n = 0, 1, 2, \ldots$ (as $k = f2\pi/c$). For plots which consider $\bar{L} = 0.25$m with a fluid-borne mode in the amplitude ($\ell = 0$), the reflected energy is expected to drop at 0Hz, 343.5Hz, 687Hz and 1030.5Hz (that is as long as it is traveling along this mode). Likewise, for $\bar{L} = 0.5$m the reflected energy is expected to drop at 0Hz, 171.75Hz, 343.5Hz, 515.25Hz, 687Hz, 858.75Hz and 1030.5Hz.

The first configuration considers the radii of the inlet and outlet shells to be equal to the radius of the rigid expansion chamber. This reduces the system to a rigid duct clamped between two flexible shells. The radii of the inlet and outlets shells is $\bar{a} = 0.2$m and the radius of the rigid shell is $\bar{b} = 0.2$m. The energies exiting the rigid duct (by being reflected at the first junction or transmitted at the second) for $5 - 1200$Hz are shown in Figure 4.18. For a duct of radius $\bar{b} = 0.2$m the first cut-on occurs at 1041Hz whereas for a shell of radius $\bar{a} = 0.2$m the first cut-on occurs at 1048Hz.

Figure 4.18a considers the amplitude of the forcing mode to use the fluid-borne mode ($\ell = 0$). It is seen that the energy is totally transmitted throughout the considered frequency range. This shows that the clamped edges have no impacts on the energy travelling in the fluid.

The structure-borne mode ($\ell = 1$) is used in the amplitude of the forcing wave to

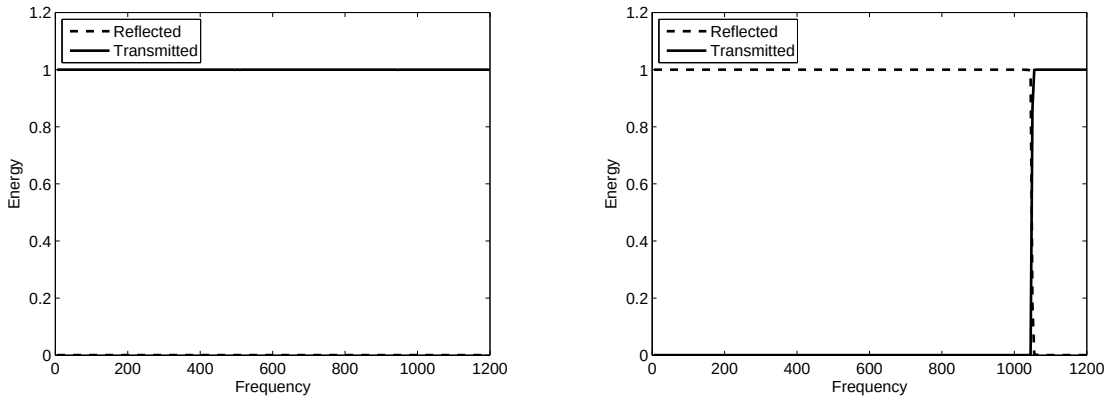

Figure 4.18: Energy output for a rigid section between two shells with clamped edges: a) $\bar{a} = 0.2$m, $\bar{b} = 0.2$m, $\bar{L} = 0.25$m, $\ell = 0$; b) $\bar{a} = 0.2$m, $\bar{b} = 0.2$m, $\bar{L} = 0.25$m, $\ell = 1$.

generate Figure 4.18b. the energy was totally reflected for frequencies below the first real cut-on at 1048Hz. After the second cut-on at 1048Hz the transmitted energy takes over and the energy is totally transmitted for the remainder of the considered frequency range. This result is similar to that obtained by the no change of configuration considered in Figure 4.2b.

The next configuration considers the radii of the inlet and outlet shells to be smaller than the radius of the expansion chamber. The radii of the inlet and outlet shells are kept at $\bar{a} = 0.2$m, while the radius of the expansion chamber is increased to $\bar{b} = 0.28$m with a length of $2\bar{L} = 0.5$m. The energies exiting the rigid duct (by being reflected at the first junction or transmitted at the second) for $5 - 1200$Hz are shown in Figure 4.19. For a rigid duct of radius $\bar{b} = 0.28$m the first cut-on occurs at 744Hz and all over cut-ons occur outside the considered frequency range.

The amplitude of the forcing wave is considered to comprise the fluid-borne mode ($\ell = 0$) in Figure 4.19a. The results show that the majority of energy is transmitted up until the cut-on from the expansion chamber at 744Hz. The reflected energy in this region drops at 343.5Hz and 687Hz which is as expected due to the trigonometric terms appearing in the amplitude equations. After the first cut-on the transmitted energy suddenly drops at 760Hz, before recovering as the dominant energy. It later falls again at 845Hz where is carries less than 10% of the total energy up until the cut-on from the inlet and outlet chambers at 1048Hz

The same configuration is considered but with the structure-borne mode in the amplitude of the forcing wave ($\ell = 1$). Figure 4.19b shows that the energy in this configuration is totally reflected up until the cut-on from the inlet and outlet shells at 1048Hz. After this frequency the reflected energy steadily drops until it is outside the considered frequency range. This result is similar to the result shown in Figure 4.4, except here the drop in reflected energy is not as smooth.

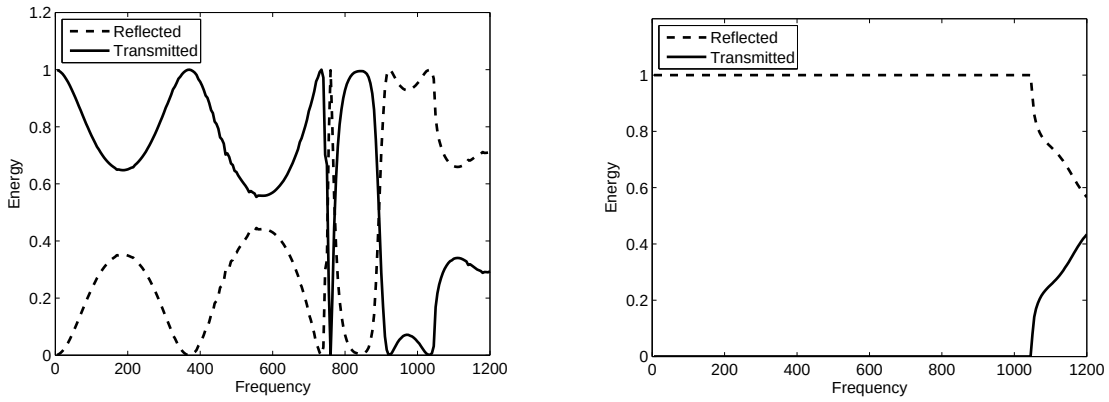

Figure 4.19: Energy output for the rigid expansion chamber between two shells with clamped edges: a) $\bar{a} = 0.2$m, $\bar{b} = 0.28$m, $\bar{L} = 0.25$m, $\ell = 0$; b) $\bar{a} = 0.2$m, $\bar{b} = 0.28$m, $\bar{L} = 0.25$m, $\ell = 1$.

The next system considers the length of the expansion chamber to be increased to $2\bar{L} = 1$m. The radius of the outer shells is kept at $\bar{a} = 0.2$m and the radius of the expansion chamber is kept at $\bar{b} = 0.28$m. The reflected and transmitted energy exiting the expansion chamber is shown in Figure 4.20.

With fluid-borne forcing (see Figure 4.20a) it is seen that the oscillations of the two energies are more frequent with the longer chamber. These are expected to occur at 0Hz 171.75Hz, 343.5Hz, 515.25Hz, 687Hz, 858.75Hz and 1030.5Hz (provided the energy is travelling along the fluid-borne mode), due to the trigonometric functions occurring in the expression for the amplitudes. After the first cut-on from the expansion chamber at 744Hz the transmitted energy suddenly drops at 760Hz and again at 900Hz. There is a slight drop in transmitted energy at 1048Hz where the cut-on from the inlet and outlet shells occurs. The transmitted drops again, with its lowest point at 1170Hz where it then increases for the remainder of the frequency range. Note that the noise mentioned at the end of the previous subsection is more evident in this plot.

The amplitude of the forcing wave is considered to comprise the structure-borne mode (see Figure 4.20b). The energy is seen to be totally reflected up until the second cut-on at 1041Hz. After the second cut-on the reflected energy drops until it reaches 1170Hz, where it then recovers. Again this result is vaguely similar to the result shown in Figure 4.4, except here the drop in reflected energy is not as smooth and there is a peak at 1170Hz.

The next configuration considers the radii of the inlet and outlet shells to be significantly smaller than the radius of the expansion chamber. The radii of the inlet and outlets shell is reduced to $\bar{a} = 0.06$m, while the expansion chamber is kept at $\bar{b} = 0.28$m and its length is changed back to $2\bar{L} = 0.5$m. The resulting energies are presented in 4.21 for $5 - 1200$Hz. For a shell of radius $\bar{a} = 0.06$m the cut-ons do not occur in the frequency range considered.

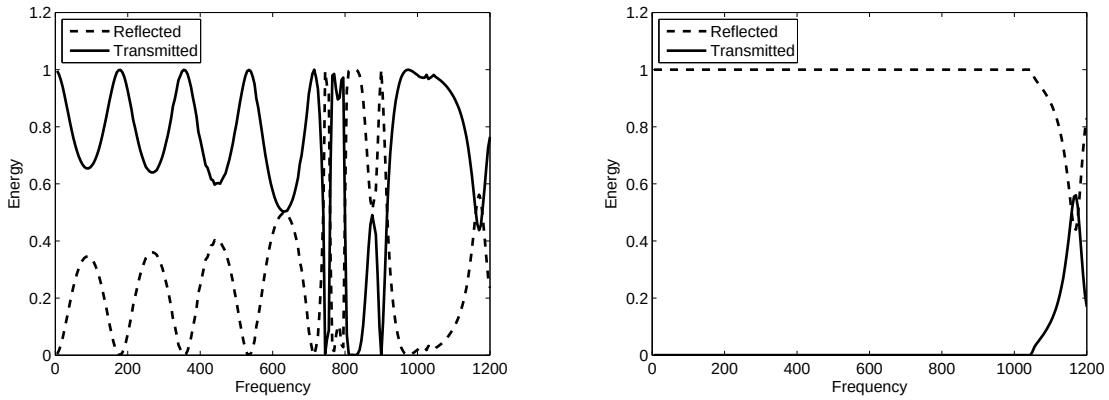

a) b)

Figure 4.20: Energy output for the rigid expansion chamber between two shells with clamped edges a) $\bar{a} = 0.2$m, $\bar{b} = 0.28$m, $\bar{L} = 0.5$m, $\ell = 0$; b) $\bar{a} = 0.2$m, $\bar{b} = 0.28$m, $\bar{L} = 0.5$m, $\ell = 1$.

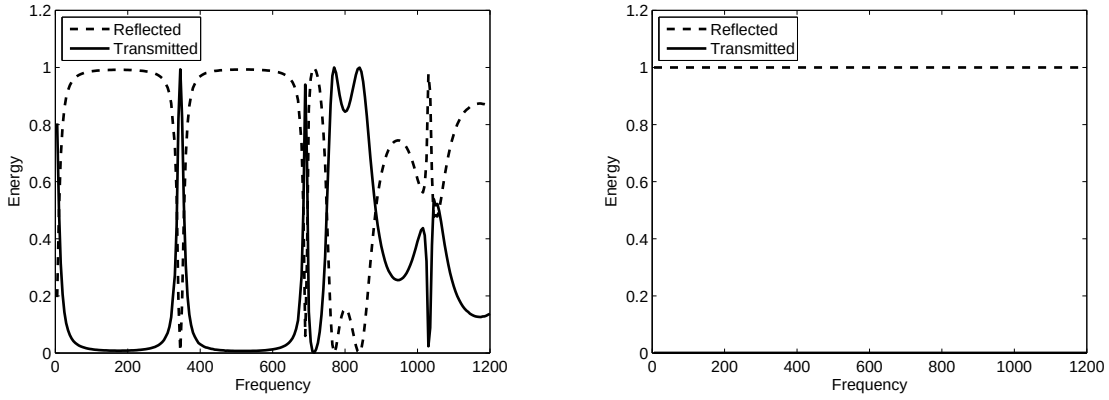

a) b)

Figure 4.21: Energy output for the rigid expansion chamber between two shells with clamped edges: a) $\bar{a} = 0.06$m, $\bar{b} = 0.28$m, $\bar{L} = 0.25$m, $\ell = 0$; b) $\bar{a} = 0.06$m, $\bar{b} = 0.28$m, $\bar{L} = 0.25$m, $\ell = 1$.

Figure 4.21a shows the results of with the fluid-borne mode in the forcing wave amplitude ($\ell = 0$). The reflected energy is dominant below the first cut-on from the expansion chamber at 744Hz apart from where it drops suddenly at 0Hz, 343.5Hz and 687Hz. These drops are due to the trigonometric term present in both the reflected and transmitted amplitudes. After the first cut-on the reflected energy drops and the transmitted energy takes over, until 838Hz where the reflected energy then takes over for the remainder of the considered frequencies. The reflected energy spikes at 1030.5Hz, which coincides with $f = 3c$.

The amplitude of the forcing wave is considered to have a structure-borne mode ($\ell = 1$) is Figure 4.21b. It is seen that the energy is totally reflected for all of the considered frequency range. This result matches the result obtained in the equivalent increase in radius problem in Figure (4.6b).

The length of the expansion chamber is now increased to $2\bar{L} = 1$m, the radius of the inlet and outlet shells is kept at $\bar{a} = 0.2$m and the radius of the expansion chamber is

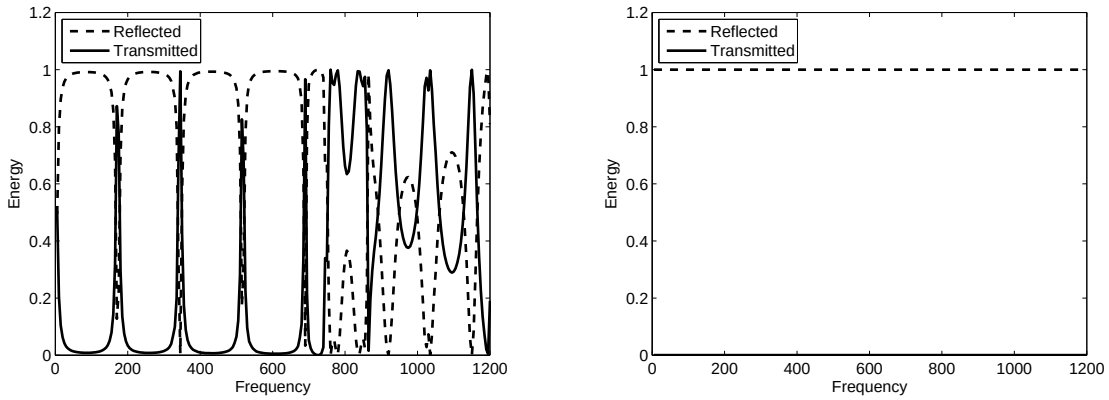

a) b)

Figure 4.22: Energy output for the rigid expansion chamber between two shells with clamped edges: a) $\bar{a} = 0.06$m, $\bar{b} = 0.28$m, $\bar{L} = 0.5$m, $\ell = 0$; b) $\bar{a} = 0.06$m, $\bar{b} = 0.28$m, $\bar{L} = 0.5$m, $\ell = 1$.

kept at $\bar{b} = 0.28$m. The reflected and transmitted energy exiting the expansion chamber is shown in Figure 4.22.

With the fluid-borne mode in the forcing amplitude (see Figure 4.22a) the majority of energy is reflected below the first cut-on at 748Hz apart from when $f = cn/2$, for $n = 0, 1, 2, \ldots$. After this frequency the energy is transmitted, with a spike of reflected energy at 864Hz. The reflected energy drops at 1030.5Hz, which coincides with $f = 3c$ and at 1149Hz.

With the structure-borne mode used in the amplitude of the forcing wave (see Figure 4.22b) the energy is totally reflected for the considered range of frequencies. This result matches the result obtained in the equivalent increase in radius problem in Figure 4.6b.

4.2.4 Pin-jointed edge

Results were obtained for systems analogous to those considered in Figure 4.18 to Figure 4.22, but with a pin-jointed edge connecting the left shell to the annular disc. It was found that the results obtained using pin-jointed edges were identical to those obtained from the clamped edge equivalent problems.

4.3 Energy transmitted through a flexible expansion chamber situated between two shells

This section considers the energy leaving a flexible expansion chamber situated between two shells. The system comprises two semi-infinite shells with a finite chamber of dimensional length $2L$ between them (where $L = k\bar{L}$). The inlet shell is located in the region $0 \leq r \leq a,\ z \leq -L$, the outlet shell is located in the region $0 \leq r \leq a,\ z \geq L$ and the expansion chamber occupies the space between them, $-L \leq z \leq L,\ 0 \leq r \leq b$,

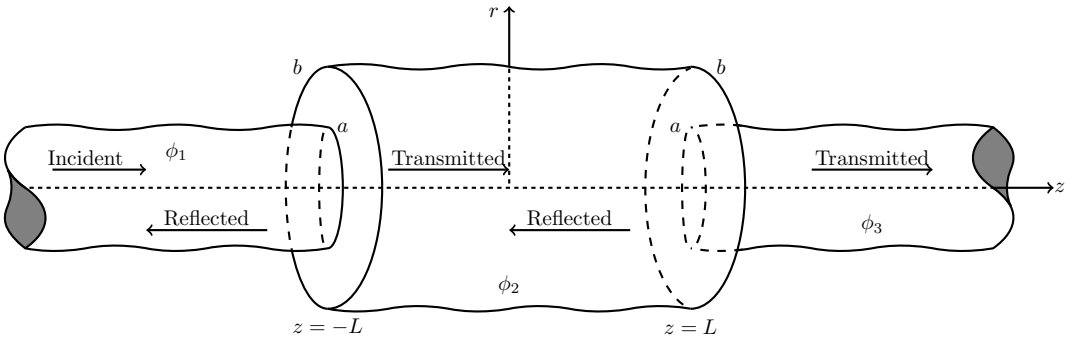

Figure 4.23: Physical configuration of the expansion chamber between two shells system.

thus the chamber has a length $2L$. The system is closed by rigid annular discs located at $a \leq r \leq b,\ z = \pm L$.

The velocity potential for the inlet shell ϕ_1 comprises the plane wave and the field reflected at the first junction, which leads to

$$\phi_1 = F_\ell J_0(\kappa_\ell r) e^{is_\ell(z+L)} + \sum_{n=0}^{\infty} A_n J_0(\kappa_n r) e^{-is_n(z+L)},\ 0 \leq r \leq a,\ z \leq -L, \tag{4.64}$$

where ℓ indicates the chosen fundamental mode to force with ($\ell = 0$ or $\ell = 1$), F_ℓ is the amplitude of the forcing wave given in (3.60), A_n is the amplitude of the nth reflected mode, s_n are the wavenumbers and $\kappa_n = (1 - s_n^2)^{1/2}$. The velocity potential for the expansion chamber consists of the waves reflected by the second junction and those which pass through the first junction. This gives the velocity potential ϕ_2 as

$$\phi_2 = \sum_{n=0}^{\infty} \left(P_n e^{-i\eta_n z} + Q_n e^{i\eta_n z} \right) J_0(\gamma_m r),\ 0 \leq r \leq b,\ -L \leq z \leq L, \tag{4.65}$$

where P_n is the amplitude of the nth reflected sound wave and Q_n is the amplitude of the nth transmitted sound wave. The velocity potential for the right shell is composed of those waves which are transmitted through the chamber, which is

$$\phi_3 = \sum_{n=0}^{\infty} B_n J_0(\kappa_n r) e^{is_n(z-L)},\ 0 \leq r \leq a,\ z \geq L, \tag{4.66}$$

where B_n is the amplitude of the nth transmitted wave.

This system can be broken down into two subproblems: the symmetric expansion chamber and the antisymmetric expansions chamber. These are created by introducing a forcing wave in the right-hand shell propagating in the negative z direction. For the antisymmetric subproblem this forcing wave has a horizontal shift of $i\pi$, which by Euler's identity results in a negative wave amplitude.

The symmetric subproblem problem is so called because it has a line of symmetry

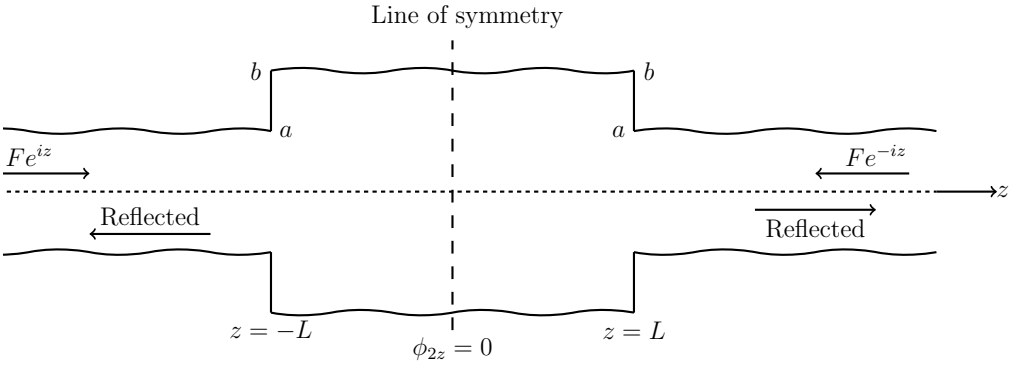

Figure 4.24: Physical configuration of the symmetric subproblem.

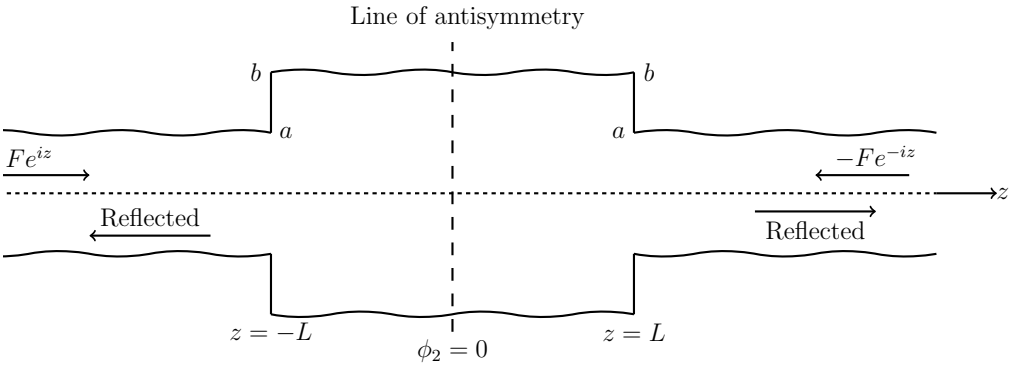

Figure 4.25: Physical configuration of the antisymmetric subproblem.

down through the centre of the expansion chamber at $z = 0$ (as shown in Figure 4.24). It represents an expansion chamber with two incident waves. One located in the left section $z \leq -L$ heading towards the first junction and the second located in the right-most section $z \geq L$ heading in the negative z direction towards the second junction. Similarly, the antisymmetric problem has a line of antisymmetry through the centre expansion chamber at $z = 0$ (as shown in Figure 4.25). It represents an expansion chamber with two incident waves in the same location, heading in the same direction, but the incident wave in the right-most section has a negative amplitude (causing it to shift horizontally).

These subproblems are simpler to solve as they have a line of symmetric/antisymmetry allowing them to be reduced to a change of radius system. The coefficients found for the reflected field in both of these subproblems can then be used to find the coefficients of the reflected and transmitted fields for the overall chamber problem.

4.3.1 Symmetric subproblem

The symmetric nature of the symmetric subproblem enables it to be reduced to an equivalent system with an abrupt increase in radius and a rigid end plate (see Figure 4.26). The purpose of this subsection is to determine the energy radiated due to a forcing

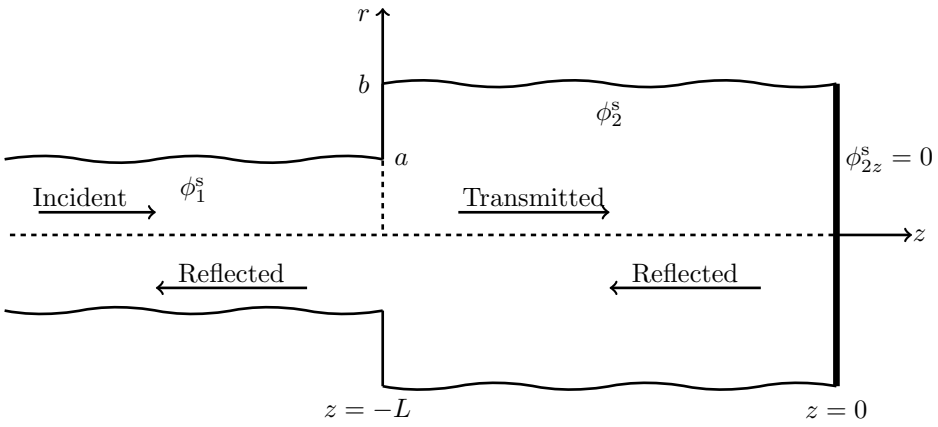

Figure 4.26: Physical configuration of the reduced symmetric subproblem.

wave at the abrupt increase in radius. The system comprises two semi-infinite shells, the left-hand shell occupies $0 \leq r \leq a,\ z \leq -L$ and the right-hand shell occupies $0 \leq r \leq b,\ -L \leq z \leq 0$. It is closed by a rigid annular disc occupying $a \leq r \leq b,\ z = -L$ and a rigid plate occupying $0 \leq r \leq b,\ z = 0$. Forcing is by a wave located in the left-hand shell propagating in the positive z direction towards the abrupt increase in radius.

The velocity potential for the left-hand shell contains the incident wave and the reflected field. This gives

$$\phi_1^{\rm s} = F_\ell J_0(\kappa_\ell r) e^{is_\ell(z+L)} + \sum_{n=0}^{\infty} A_n^{\rm s} J_0(\kappa_n r) e^{is_n(z+L)},\ 0 \leq r \leq a,\ z \leq -L, \tag{4.67}$$

where the superscript indicates that this is the symmetric subsystem, ℓ indicates the chosen fundamental mode to force with ($\ell = 0$ or $\ell = 1$), F_ℓ is the amplitude of the forcing wave given in (3.60) and $A_n^{\rm s}$ is the amplitude of the nth reflected wave. The longitudinal and radial displacements in the left-hand shell are

$$u_1^{\rm s}(z) = \frac{\nu F_\ell s_\ell \kappa_\ell J_1(\kappa_\ell a)}{a(s_\ell^2 - \beta^2)} e^{is_\ell(z+L)} - \frac{\nu}{a} \sum_{n=0}^{\infty} \frac{A_n^{\rm s} s_n \kappa_n J_1(\kappa_n a)}{s_n^2 - \beta^2} e^{-is_n(z+L)},\ z \leq -L, \tag{4.68}$$

$$w_1^{\rm s}(z) = -F_\ell \kappa_\ell J_1(\kappa_\ell a) e^{is_\ell(z+L)} - \sum_{n=0}^{\infty} A_n^{\rm s} \kappa_n J_1(\kappa_n a) e^{-is_n(z+L)},\ z \leq -L. \tag{4.69}$$

The velocity potential $\phi_2^{\rm s}$ for the finite section comprises those waves transmitted through the junction and those reflected from the plate at $z = 0$, which gives

$$\phi_2^{\rm s} = \sum_{n=0}^{\infty} \left(P_n^{\rm s} e^{-i\eta_n z} + Q_n^{\rm s} e^{i\eta_n z} \right) J_0(\gamma_n r),\ 0 \leq r \leq b,\ -L \leq z \leq 0, \tag{4.70}$$

where $P_n^{\rm s}$ are the amplitudes for the reflected waves and $Q_n^{\rm s}$ are the amplitudes for the transmitted waves. The velocity potential $\phi_2^{\rm s}$ can be simplified by considering the property

of the plate. The condition at the plate is $\phi^{\mathrm{s}}_{2z} = 0$, which leads to

$$\frac{\phi^{\mathrm{s}}_2}{\partial z} = i\sum_{n=0}^{\infty}\left(-P^{\mathrm{s}}_n + Q^{\mathrm{s}}_n\right)\eta_n J_0(\gamma_n r) = 0,\ 0 \le r \le b,\ -L \le z \le 0. \tag{4.71}$$

From this condition it is seen that it is only satisfied when $P_n = Q_n$ therefore the velocity potential ϕ^{s}_2 can be simplified to

$$\phi^{\mathrm{s}}_2 = 2\sum_{n=0}^{\infty} P^{\mathrm{s}}_n \cos(\eta_n z) J_0(\gamma_n r),\ 0 \le r \le b,\ -L \le z \le 0. \tag{4.72}$$

For the right-hand section, the longitudinal and radial displacements are given by

$$u^{\mathrm{s}}_2(z) = \frac{2\nu}{b}\sum_{n=0}^{\infty}\frac{P^{\mathrm{s}}_n \sin(\eta_n z)\eta_n\gamma_n J_1(\gamma_n b)}{\eta_n^2 - \beta^2},\ -L \le z \le 0, \tag{4.73}$$

$$w^{\mathrm{s}}_2(z) = 2\sum_{n=0}^{\infty} P^{\mathrm{s}}_n \cos(\eta_n z)\gamma_n J_1(\gamma_n b),\ -L \le z \le 0. \tag{4.74}$$

The pressure and the normal component of velocity are constant in the fluid, while the latter vanishes on the rigid annular disc. That is at $z = -L$

$$\phi^{\mathrm{s}}_1(r,-L) = \phi^{\mathrm{s}}_2(r,-L),\ 0 \le r \le a, \tag{4.75}$$

$$\frac{\partial\phi_2}{\partial z}(r,-L) = \begin{cases} \frac{\partial\phi_1}{\partial z}(r,-L), & 0 \le r \le a \\ 0, & a \le r \le b \end{cases}. \tag{4.76}$$

The velocity potentials ϕ^{s}_1 and ϕ^{s}_2 are substituted into (4.75) to obtain the pressure condition in its eigenfunction form

$$F_\ell J_0(\kappa_\ell r) + \sum_{n=0}^{\infty} A^{\mathrm{s}}_n J_0(\kappa_n r) = 2\sum_{n=0}^{\infty} P^{\mathrm{s}}_n \cos(\eta_n L) J_0(\gamma_n r),\ 0 \le r \le a. \tag{4.77}$$

The above expression is multiplied by $\alpha J_0(\kappa_m r) r/a$ and integrated with respect to $r,\ 0 \le r \le a$ to give

$$\begin{aligned}&\frac{\alpha F_\ell}{a}\int_0^a J_0(\kappa_\ell r) J_0(\kappa_m r) r\ \mathrm{d}r + \frac{\alpha}{a}\sum_{n=0}^{\infty} A^{\mathrm{s}}_n \int_0^a J_0(\kappa_n r) J_0(\kappa_m r) r\ \mathrm{d}r \\ &= \frac{2\alpha}{a}\sum_{n=0}^{\infty} P^{\mathrm{s}}_n \cos(\eta_n L) R_{mn},\end{aligned} \tag{4.78}$$

where R_{mn} is as given in (4.13) and C_n is as given in (3.34). The generalised orthogonality

relation in (3.35) is now applied to both integrals on the left side of the equation to give

$$F_\ell\left[\delta_{m\ell}C_\ell - \left\{\frac{\tau_1\nu^2\beta^2}{(s_\ell^2-\beta^2)(s_m^2-\beta^2)} + 2 - \kappa_m^2 - \kappa_\ell^2\right\}\kappa_\ell J_1(\kappa_\ell a)\kappa_m J_1(\kappa_m a)\right]$$
$$+\sum_{n=0}^{\infty} A_n^{\mathrm{s}}\left[\delta_{mn}C_n - \left\{\frac{\tau_1\nu^2\beta^2}{(s_n^2-\beta^2)(s_m^2-\beta^2)} + 2 - \kappa_m^2 - \kappa_n^2\right\}\kappa_\ell J_1(\kappa_n a)\kappa_m J_1(\kappa_m a)\right]$$
$$= \frac{2\alpha}{a}\sum_{n=0}^{\infty} P_n^{\mathrm{s}}\cos(\eta_n L)R_{mn}. \tag{4.79}$$

It follows that

$$A_m^{\mathrm{s}} = -F_\ell\delta_{m\ell} + \frac{\tau_1\nu^2\beta^2\kappa_m J_1(\kappa_m a)}{(s_m^2-\beta^2)C_m}E_0 + \frac{(2-\kappa_m^2)\kappa_m J_1(\kappa_m a)}{C_m}E_1 - \frac{\kappa_m J_1(\kappa_m a)}{C_m}E_2$$
$$+\frac{2\alpha}{a}\sum_{n=0}^{\infty}\frac{P_n^{\mathrm{s}}\cos(\eta_n L)R_{mn}}{C_m}, \tag{4.80}$$

where

$$E_0 = \sum_{n=0}^{\infty}\frac{A_n^{\mathrm{s}}\kappa_n J_1(\kappa_n a)}{s_n^2-\beta^2} + \frac{F_\ell\kappa_\ell J_1(\kappa_\ell a)}{s_\ell^2-\beta^2}, \tag{4.81}$$

$$E_1 = \sum_{n=0}^{\infty} A_n^{\mathrm{s}}\kappa_n J_1(\kappa_n a) + F_\ell\kappa_\ell J_1(\kappa_\ell a), \tag{4.82}$$

$$E_2 = \sum_{n=0}^{\infty} A_n^{\mathrm{s}}\kappa_n^3 J_1(\kappa_n a) + F_\ell\kappa_\ell^3 J_1(\kappa_\ell a), \tag{4.83}$$

and R_{mn} is as given in (4.13). A second equation is found by multiplying (4.76) through by $\alpha J_0(\gamma_m b)r/b$ and integrating with respect to r, $0 \le r \le b$ to give

$$\frac{\alpha}{b}\int_0^b \frac{\partial\phi_2^{\mathrm{s}}}{\partial z}J_0(\gamma_m r)r\,\mathrm{d}r = \frac{\alpha}{b}\int_0^a \frac{\partial\phi_1^{\mathrm{s}}}{\partial z}J_0(\gamma_m r)r\,\mathrm{d}r, \text{ at } z=-L. \tag{4.84}$$

The above equation in eigenfunction form is then

$$\frac{2\alpha}{b}\sum_{n=0}^{\infty} P_n^{\mathrm{s}}\sin(\eta_n L)\eta_n\int_0^b J_0(\gamma_n r)J_0(\gamma_n r)r\,\mathrm{d}r = \frac{i\alpha F_\ell s_\ell R_{\ell m}}{b} - \frac{i\alpha}{b}\sum_{n=0}^{\infty} A_n^{\mathrm{s}}s_n R_{nm}, \tag{4.85}$$

where R_{nm} is as given in (4.13). The generalised orthogonality relation in (3.36) is now applied to the integral on the left side of the equation to give

$$2\sum_{n=0}^{\infty} P_n^{\mathrm{s}}\sin(\eta_n L)\eta_n\left[\delta_{nm}D_n - \left\{\frac{\tau_2\nu^2\beta^2}{(\eta_n^2-\beta^2)(\eta_n^2-\beta^2)} + 2 - \gamma_m^2 - \gamma_n^2\right\}\gamma_n J_1(\gamma_n b)\gamma_m J_1(\gamma_m b)\right]$$
$$= \frac{i\alpha F_\ell s_\ell R_{\ell m}}{b} - \frac{i\alpha}{b}\sum_{n=0}^{\infty} A_n^{\mathrm{s}}s_n R_{nm}, \tag{4.86}$$

where D_n is as given in (3.37). It follows that

$$P_m^{\mathrm{s}} = \frac{\tau_2\nu^2\beta^2\gamma_m J_1(\gamma_m b)}{(\eta_m^2-\beta^2)\sin(\eta_m L)\eta_m D_m}E_3 + \frac{(2-\gamma_m^2)\gamma_m J_1(\gamma_m b)}{\sin(\eta_m L)\eta_m D_m}E_4 - \frac{\gamma_m J_1(\gamma_m b)}{\sin(\eta_m L)\eta_m D_m}E_5$$
$$+ \frac{i\alpha F_\ell s_\ell R_{\ell m}}{2b\sin(\eta_m L)\eta_m D_m} - \frac{i\alpha}{2b}\sum_{n=0}^{\infty}\frac{A_n^{\mathrm{s}} s_n R_{nm}}{\sin(\eta_m L)\eta_m D_m}, \tag{4.87}$$

where

$$E_3 = \sum_{n=0}^{\infty}\frac{P_n^{\mathrm{s}}\sin(\eta_n L)\eta_n J_1(\gamma_n b)}{\eta_n^2-\beta^2}, \tag{4.88}$$

$$E_4 = \sum_{n=0}^{\infty}P_n^{\mathrm{s}}\sin(\eta_n L)\eta_n\gamma_n J_1(\gamma_n b), \tag{4.89}$$

$$E_5 = \sum_{n=0}^{\infty}P_n^{\mathrm{s}}\sin(\eta_n L)\gamma_n^3 J_1(\gamma_n b). \tag{4.90}$$

The constants $E_0 - E_2$ are found by applying edge conditions which describe the left-hand shell edge at the matching interface and $E_3 - E_5$ are found by applying edge conditions which describe the right-hand shell edge at the matching interface. In order to apply the left-hand edge conditions (4.80) is multiplied by $\psi_{mn}^{(\mathrm{a})}$, and on summing over m it is found that

$$-\sum_{m=0}^{\infty}F_\ell\delta_{\ell m}\psi_{mn}^{(\mathrm{a})} + \sum_{m=0}^{\infty}\frac{\tau_1\nu^2\beta^2\kappa_m J_1(\kappa_m a)\psi_{mn}^{(\mathrm{a})}}{(s_m^2-\beta^2)C_m}E_0 + \sum_{m=0}^{\infty}\frac{(2-\kappa_m^2)\kappa_m J_1(\kappa_m a)}{C_m}E_1$$
$$-\sum_{m=0}^{\infty}\frac{\kappa_m J_1(\kappa_m a)\psi_{mn}^{(\mathrm{a})}}{C_m}E_2 + \frac{2\alpha}{a}\sum_{m=0}^{\infty}\sum_{n=0}^{\infty}\frac{P_n^{\mathrm{s}}\cos(\eta_n L)R_{mn}\psi_{mn}^{(\mathrm{a})}}{C_m} = -\sum_{m=0}^{\infty}P_m\psi_{mn}^{(\mathrm{p})}$$
$$-F_\ell\psi_n^{(\mathrm{f})},\ n=0,1,2. \tag{4.91}$$

Similarly for the right-hand edge conditions (4.87) is multiplied by ψ_{mn}^{p}, and on summing over m, it is found that

$$\sum_{m=0}^{\infty}\frac{\tau_2\nu^2\beta^2\gamma_m J_1(\gamma_m b)\psi_{mn}^{(\mathrm{p})}}{(\eta_m^2-\beta^2)\sin(\eta_m L)\eta_m D_m}E_3 + \sum_{m=0}^{\infty}\frac{(2-\gamma_m^2)\gamma_m J_1(\gamma_m b)\psi_{mn}^{(\mathrm{p})}}{\sin(\eta_m L)\eta_m D_m}E_4$$
$$-\sum_{m=0}^{\infty}\frac{\gamma_m J_1(\gamma_m b)\psi_{mn}^{(\mathrm{p})}}{\sin(\eta_m L)\eta_m D_m}E_5 + \frac{i\alpha}{2b}\sum_{m=0}^{\infty}\frac{F_\ell s_\ell R_{\ell m}\psi_{mn}^{(\mathrm{p})}}{\sin(\eta_m L)\eta_m D_m} - \frac{i\alpha}{2b}\sum_{m=0}^{\infty}\sum_{n=0}^{\infty}\frac{A_n^{\mathrm{s}} s_n R_{nm}\psi_{mn}^{(\mathrm{p})}}{\sin(\eta_m L)\eta_m D_m}$$
$$= -\sum_{m=0}^{\infty}A_m^{\mathrm{s}}\psi_{mn}^{(\mathrm{a})} - F_\ell\psi_n^{(\mathrm{f})},\ n=3,4,5. \tag{4.92}$$

For clamped edges the values of ψ in (4.91) and (4.92) are substituted with those in (4.23). It is found from the equation resulting from (4.91) that $E_1 = 0$ and the remaining coupled equations are solved to find E_0 and E_2. Likewise, the triadic equations resulting

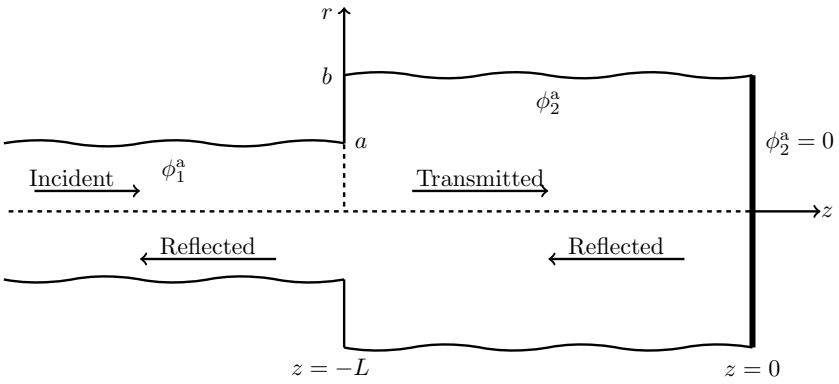

Figure 4.27: Physical configuration of the reduced antisymmetric subproblem.

from (4.92) are solved to find $E_3 - E_5$. With these constants, equations (4.80) and (4.87) can be truncated and solved to find the mth amplitude A_m^{s} of the reflected field and the mth amplitude B_m^{s} of the transmitted field.

For pin-jointed edges the values of ψ (4.91) and (4.92) are substituted with those in (4.26). It is found from the equation resulting from (4.91) that $E_1 = 0$ and the remaining coupled equations are solved to find E_0 and E_2. Likewise, the triadic equations resulting from (4.92) are solved to find $E_3 - E_5$. With these constants, equations (4.80) and (4.87) can be truncated and solved to find the mth amplitude A_m^{s} of the reflected field and the mth amplitude B_m^{s} of the transmitted field.

4.3.2 Antisymmetric subproblem

The symmetric nature of the symmetric subproblem enables it to be reduced to an equivalent system with an abrupt increase in radius and an acoustically soft end plate (see Figure 4.17). The purpose of this subsection is to determine the energy radiated due to a forcing wave at an abrupt increase in radius. The system comprises two semi-infinite shells, the left-hand shell occupies $0 \leq r \leq a,\ z \leq -L$ and the right-hand rigid duct occupies $0 \leq r \leq b,\ -L \leq z \leq 0$. It is closed by a rigid annular disc occupying $a \leq r \leq b,\ z = -L$ and an acoustically soft end plate occupying $0 \leq r \leq b,\ z = 0$. Forcing is by a wave located in the left-hand shell propagating in the positive z direction towards the abrupt increase in radius.

The velocity potential for the left-hand shell is

$$\phi_1^{\mathrm{a}} = F_\ell J_0(\kappa_\ell r) e^{is_\ell(z+L)} + \sum_{n=0}^{\infty} A_n^{\mathrm{a}} J_0(\kappa_n r) e^{-is_n(z+L)},\ 0 \leq r \leq a,\ z \leq -L, \tag{4.93}$$

where the superscript denotes the antisymmetric subsystem, ℓ indicates the chosen fundamental mode to force with ($\ell = 0$ or $\ell = 1$), F_ℓ is the amplitude of the forcing wave given in (3.60) and A_n^{a} is the amplitude of the nth reflected wave for the symmetric sub-

system. The velocity potential for the finite section is analogous to that of the symmetric problem but with $\cos(\eta_n z)$ replaced by $\sin(\eta_n z)$:

$$\phi_2^{\mathrm{a}} = 2\sum_{n=0}^{\infty} P_n^{\mathrm{a}} \sin(\eta_n z) J_0(\gamma_n r),\ 0 \le r \le b,\ -L \le z \le 0. \tag{4.94}$$

Note that this satisfies the acoustically soft wall condition $\phi_2^{\mathrm{a}} = 0$ at $z = 0$. In terms of the velocity potential ϕ_2^{a} the displacements for the right section are

$$u_2^{\mathrm{a}}(z) = -\frac{2\nu}{b}\sum_{n=0}^{\infty} \frac{P_n^{\mathrm{a}} \cos(\eta_n z)\eta_n \gamma_n J_1(\gamma_n b)}{\eta_n^2 - \beta^2},\ -L \le z \le 0, \tag{4.95}$$

$$w_2^{\mathrm{a}}(z) = -2\sum_{n=0}^{\infty} P_n^{\mathrm{a}} \sin(\eta_n z)\gamma_n J_1(\gamma_n b),\ -L \le z \le 0. \tag{4.96}$$

The steps for solving this problem are analogous to those of the symmetric problem. Following these steps for the pressure condition gives the equation for the amplitude of the reflected wave as

$$\begin{aligned} A_m^{\mathrm{a}} = {} & -F_\ell \delta_{m\ell} + \frac{\tau_1 \nu^2 \beta^2 \kappa_m J_1(\kappa_m a)}{(s_m^2 - \beta^2)C_m} E_0 + \frac{(2 - \kappa_m^2)\kappa_m J_1(\kappa_m a)}{C_m} E_1 \\ & - \frac{\kappa_m J_1(\kappa_m a)}{C_m} E_2 - \frac{2\alpha}{a}\sum_{n=0}^{\infty} \frac{P_n^{\mathrm{a}} \sin(\eta_n L) R_{mn}}{C_m}. \end{aligned} \tag{4.97}$$

$$E_0 = \sum_{n=0}^{\infty} \frac{A_n^{\mathrm{a}} \kappa_n J_1(\kappa_n a)}{s_n^2 - \beta^2} + \frac{F_\ell \kappa_\ell J_1(\kappa_\ell a)}{s_\ell^2 - \beta^2}, \tag{4.98}$$

$$E_1 = \sum_{n=0}^{\infty} A_n^{\mathrm{a}} \kappa_n J_1(\kappa_n a) + F_\ell \kappa_\ell J_1(\kappa_\ell a), \tag{4.99}$$

$$E_2 = \sum_{n=0}^{\infty} A_n^{\mathrm{a}} \kappa_n^3 J_1(\kappa_n a) + F_\ell \kappa_\ell^3 J_1(\kappa_\ell a), \tag{4.100}$$

Likewise, for the normal component of velocity condition, it is found that

$$\begin{aligned} P_m^{\mathrm{a}} = {} & \frac{\tau_2 \nu^2 \beta^2 \gamma_m J_1(\gamma_m b)}{(\eta_m^2 - \beta^2)\cos(\eta_m L)\eta_m D_m} \sum_{n=0}^{\infty} \frac{P_n^{\mathrm{a}} \cos(\eta_n L)\eta_n \gamma_n J_1(\gamma_n b)}{\eta_n^2 - \beta^2} \\ & + \frac{(2 - \gamma_m^2)\gamma_m J_1(\gamma_m b)}{\cos(\eta_m L)\eta_m D_m} \sum_{n=0}^{\infty} P_n^{\mathrm{a}} \cos(\eta_n L)\eta_n \gamma_n J_1(\gamma_n b) \\ & - \frac{\gamma_m J_1(\gamma_m b)}{\cos(\eta_m L)\eta_m D_m} \sum_{n=0}^{\infty} P_n^{\mathrm{a}} \cos(\eta_n L)\eta_n \gamma_n^3 J_1(\gamma_n b) + \frac{i\alpha F_\ell s_\ell R_{\ell m}}{2b\cos(\eta_m L)\eta_m D_m} \\ & - \frac{i\alpha}{2b}\sum_{n=0}^{\infty} \frac{A_n^{\mathrm{a}} s_n R_{nm}}{\cos(\eta_m L)\eta_m D_m}, \end{aligned} \tag{4.101}$$

which reduces to

$$P_m^{\mathrm{a}} = \frac{\tau_2\nu^2\beta^2\gamma_m J_1(\gamma_m b)}{(\eta_m^2-\beta^2)\cos(\eta_m L)\eta_m D_m}E_3 + \frac{(2-\gamma_m^2)\gamma_m J_1(\gamma_m b)}{\cos(\eta_m L)\eta_m D_m}E_4 - \frac{\gamma_m J_1(\gamma_m b)}{\cos(\eta_m L)\eta_m D_m}E_5$$
$$+ \frac{i\alpha F_\ell s_\ell R_{\ell m}}{2b\cos(\eta_m L)\eta_m D_m} - \frac{i\alpha}{2b}\sum_{n=0}^{\infty}\frac{A_n^{\mathrm{a}} s_n R_{nm}}{\cos(\eta_m L)\eta_m D_m}, \tag{4.102}$$

where

$$E_3 = \sum_{n=0}^{\infty}\frac{P_n^{\mathrm{a}}\sin(\eta_n L)\eta_n J_1(\gamma_n b)}{\eta_n^2-\beta^2}, \tag{4.103}$$

$$E_4 = \sum_{n=0}^{\infty} P_n^{\mathrm{a}}\sin(\eta_n L)\eta_n\gamma_n J_1(\gamma_n b), \tag{4.104}$$

$$E_5 = \sum_{n=0}^{\infty} P_n^{\mathrm{a}}\sin(\eta_n L)\gamma_n^3 J_1(\gamma_n b). \tag{4.105}$$

The constants $E_0 - E_2$ are found by applying edge conditions which describe the left-hand shell edge at the matching interface and $E_3 - E_5$ are found by applying edge conditions which describe the right-hand shell edge at the matching interface. In order to apply the left-hand edge conditions (4.97) is multiplied by $\psi_{mn}^{(\mathrm{a})}$, and on summing over m it is found that

$$-\sum_{m=0}^{\infty}F_\ell\delta_{\ell m}\psi_{mn}^{(\mathrm{a})} + \sum_{m=0}^{\infty}\frac{\tau_1\nu^2\beta^2\kappa_m J_1(\kappa_m a)\psi_{mn}^{(\mathrm{a})}}{(s_m^2-\beta^2)C_m}E_0 + \sum_{m=0}^{\infty}\frac{(2-\kappa_m^2)\kappa_m J_1(\kappa_m a)}{C_m}E_1$$
$$-\sum_{m=0}^{\infty}\frac{\kappa_m J_1(\kappa_m a)\psi_{mn}^{(\mathrm{a})}}{C_m}E_2 + \frac{2\alpha}{a}\sum_{m=0}^{\infty}\sum_{n=0}^{\infty}\frac{P_n^{\mathrm{s}}\sin(\eta_n L)R_{mn}\psi_{mn}^{(\mathrm{a})}}{C_m} = -\sum_{m=0}^{\infty}P_m\psi_{mn}^{(\mathrm{p})}$$
$$-F_\ell\psi_n^{(\mathrm{f})},\ n=0,1,2. \tag{4.106}$$

Similarly for the right-hand edge conditions (4.102) is multiplied by ψ_{mn}^{p}, and on summing over m, it is found that

$$\sum_{m=0}^{\infty}\frac{\tau_2\nu^2\beta^2\gamma_m J_1(\gamma_m b)\psi_{mn}^{(\mathrm{p})}}{(\eta_m^2-\beta^2)\cos(\eta_m L)\eta_m D_m}E_3 + \sum_{m=0}^{\infty}\frac{(2-\gamma_m^2)\gamma_m J_1(\gamma_m b)\psi_{mn}^{(\mathrm{p})}}{\cos(\eta_m L)\eta_m D_m}E_4$$
$$-\sum_{m=0}^{\infty}\frac{\gamma_m J_1(\gamma_m b)\psi_{mn}^{(\mathrm{p})}}{\cos(\eta_m L)\eta_m D_m}E_5 + \frac{i\alpha}{2b}\sum_{m=0}^{\infty}\frac{F_\ell s_\ell R_{\ell m}\psi_{mn}^{(\mathrm{p})}}{\cos(\eta_m L)\eta_m D_m} - \frac{i\alpha}{2b}\sum_{m=0}^{\infty}\sum_{n=0}^{\infty}\frac{A_n^{\mathrm{s}} s_n R_{nm}\psi_{mn}^{(\mathrm{p})}}{\cos(\eta_m L)\eta_m D_m}$$
$$= -\sum_{m=0}^{\infty}A_m^{\mathrm{s}}\psi_{mn}^{(\mathrm{a})} - F_\ell\psi_n^{(\mathrm{f})},\ n=3,4,5. \tag{4.107}$$

For clamped edges the values of ψ in (4.106) and (4.107) are substituted with those in (4.23). It is found from the equation resulting from (4.106) that $E_1 = 0$ and the remaining coupled equations are solved to find E_0 and E_2. Likewise, the triadic equations resulting

from (4.107) are solved to find $E_3 - E_5$. With these constants, equations (4.97) and (4.102) can be truncated and solved to find the mth amplitude A_m^{a} of the reflected field and the mth amplitude B_m^{a} of the transmitted field.

For pin-jointed edges the values of ψ (4.106) and (4.107) are substituted with those in (4.26). It is found from the equation resulting from (4.106) that $E_1 = 0$ and the remaining coupled equations are solved to find E_0 and E_2. Likewise, the triadic equations resulting from (4.107) are solved to find $E_3 - E_5$. With these constants, equations (4.97) and (4.102) can be truncated and solved to find the mth amplitude A_m^{a} of the reflected field and the mth amplitude B_m^{a} of the transmitted field. The results are created in Matlab with the code presented in Appendix I. This has been done using 100 modes to calculate the amplitudes of the propagating waves.

4.3.3 Clamped edges

The expansion chamber causes the energies to oscillate over frequency. This is due to the trigonometric factors present in the reflected and transmitted amplitudes. It is assumed that when a fluid-borne mode is used, the reflected energy will drop at the same frequencies stated in Section 4.2.3.

The first results consider the radii of the inlet and outlet shells to be equal to the radius of the centre shell. This reduces the problem to a finite shell clamped between two semi-infinite shells. The radii of the inlet and outlet shells are $\bar{a} = 0.2$m, the radius of the centre shell is $\bar{b} = 0.2$m with a length of $2\bar{L} = 0.5$m. The resulting reflected and transmitted energies are shown in Figure 4.28 for a frequency range $5 - 1200$Hz.

Figure 4.28a considers the amplitude of the forcing mode to use the fluid-borne mode ($\ell = 0$). It is seen that the energy is totally transmitted throughout the considered frequency range. This shows that the clamped edges have no impacts on the energy travelling in the fluid.

The structure-borne mode ($\ell = 1$) is used in the amplitude of the forcing wave to generate Figure 4.28b. the energy was totally reflected for frequencies below the first real cut-on at 1048Hz. After the second cut-on at 1048Hz the transmitted energy takes over and the energy is totally transmitted for the remainder of the considered frequency range. This result is similar to that obtained by the no change of radius configuration considered in Figure 4.18b and by extension Figure 4.2b.

Figure 4.29 shows the output energies for the expansion chamber problem with the outer radii $\bar{a} = 0.2$m, the expansion chamber radius $\bar{b} = 0.28$m and length $2\bar{L} = 0.5$m. Plot a) shows the energy with fluid-borne mode used in the amplitude of the forcing wave ($\ell = 0$). Below the cut-on from the expansion chamber at 748Hz, the vast majority of the energy is transmitted with very little being reflected. The transmitted energy has a sudden drop at the first cut-on from the expansion chamber section at 748Hz after which

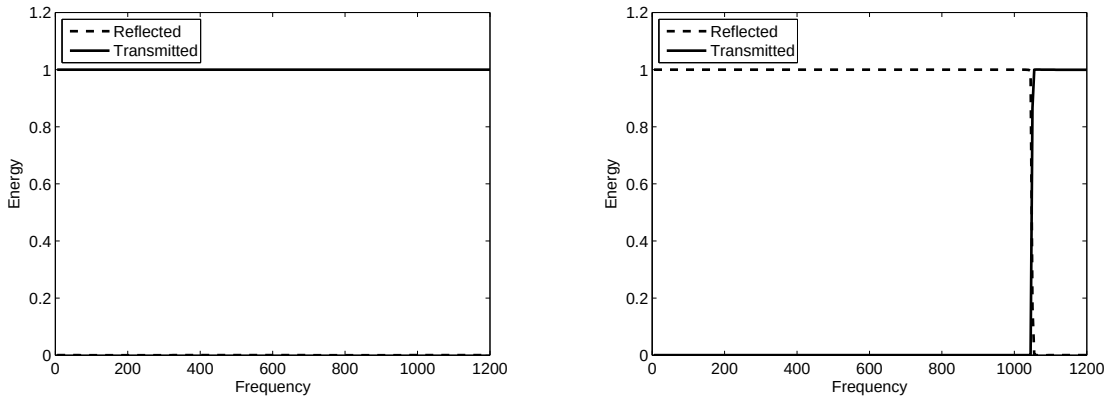

a) b)

Figure 4.28: Energy output for a flexible section between two shells with clamped edges: a) $\bar{a} = 0.2$m, $\bar{b} = 0.2$m, $\bar{L} = 0.25$m, $\ell = 0$; b) $\bar{a} = 0.2$m, $\bar{b} = 0.2$m, $\bar{L} = 0.25$m, $\ell = 1$.

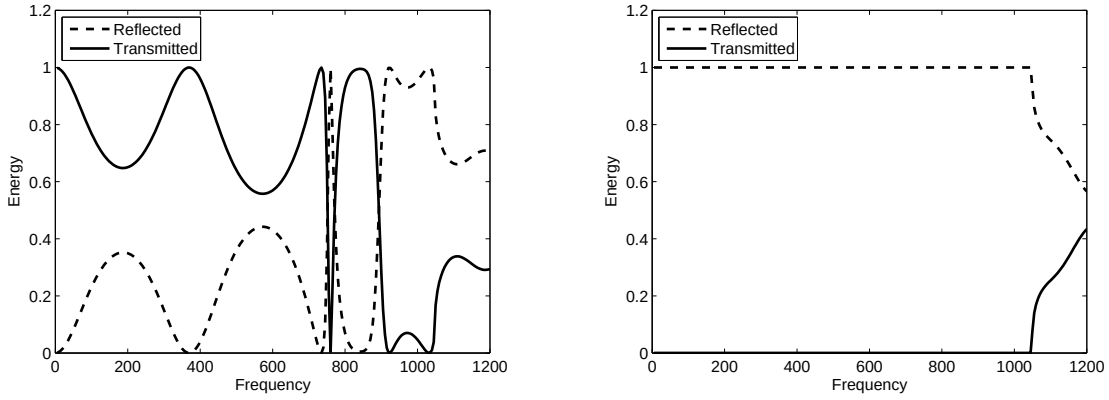

a) b)

Figure 4.29: Energy output for a finite flexible shell between two semi-infinite shells with clamped edges: a) $\bar{a} = 0.2$m, $\bar{b} = 0.28$m, $\bar{L} = 0.25$m, $\ell = 0$; b) $\bar{a} = 0.2$m, $\bar{b} = 0.28$m, $\bar{L} = 0.25$m, $\ell = 1$.

it quickly recovers. The transmitted drops again at 860Hz where it carries less than 10% of the total energy for the remainder of the frequency range considered.

Plot b) shows forcing with a structure-borne mode used in the amplitude of the forcing wave ($\ell = 1$). This plot shows that the energy is totally reflected for all frequencies below the cut-on from the outer sections at 1048Hz. After this frequency the reflected energy quickly drops. On comparing Figure 4.29 with Figure 4.4, it is clear that the two graphs are qualitatively similar and that the finite length of radius broadens the range of the near total reflection at the first cut-on.

The next system considers the length of the expansion chamber to be increased to $2\bar{L} = 1$m. The radius of the outer shells is kept at $\bar{a} = 0.2$m and the radius of the expansion chamber is kept at $\bar{b} = 0.28$m. The reflected and transmitted energy exiting the expansion chamber is shown in Figure 4.30.

With fluid-borne forcing (see Figure 4.30a) it is seen that the oscillations of the two

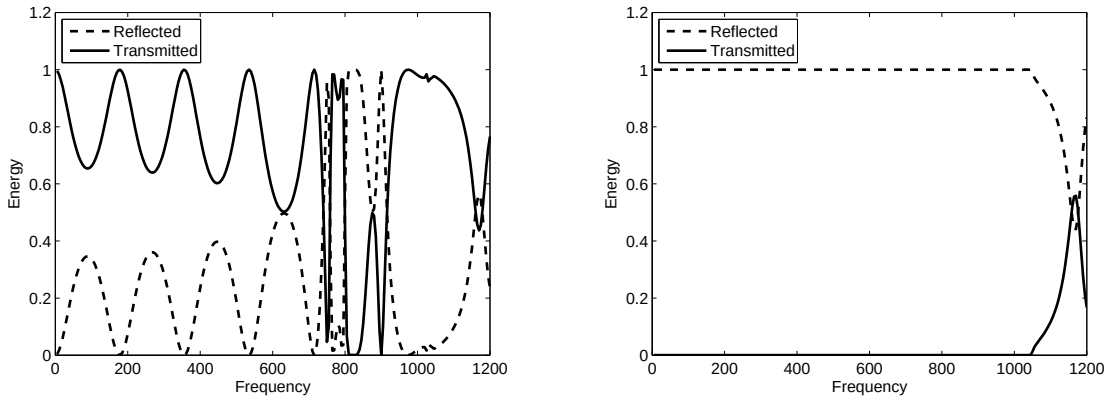

Figure 4.30: Energy output for the flexible expansion chamber between two shells with clamped edges: a) $\bar{a} = 0.2$m, $\bar{b} = 0.28$m, $\bar{L} = 0.5$m, $\ell = 0$; b) $\bar{a} = 0.2$m, $\bar{b} = 0.28$m, $\bar{L} = 0.5$m, $\ell = 1$.

energies are more frequent with the longer chamber. These are expected to occur at 0Hz 171.75Hz, 343.5Hz, 515.25Hz, 687Hz, 858.75Hz and 1030.5Hz (provided the energy is travelling along the fluid-borne mode), due to the trigonometric functions occurring in the expression for the amplitudes. After the first cut-on from the expansion chamber at 744Hz the transmitted energy suddenly drops at 760Hz and again at 900Hz. There is a slight drop in transmitted energy at 1048Hz where the cut-on from the inlet and outlet shells occurs. The transmitted drops again, with its lowest point at 1170Hz where it then increases for the remainder of the frequency range.

The amplitude of the forcing wave is considered to comprise the structure-borne mode (see Figure 4.30b). The energy is seen to be totally reflected up until the second cut-on at 1048Hz. After the second cut-on the reflected energy drops until it reaches 1170Hz, where it then recovers. This result is similar to the result shown in 4.20b and by extension vaguely similar to Figure 4.4, except here the drop in reflected energy is not as smooth and there is a peak at 1170Hz.

In the next configuration the radii of the inlet and outlet shells is considered to be significantly smaller than the radius of the expansion chamber. The radii of the inlet and outlets shell is reduced to $\bar{a} = 0.06$m, while the expansion chamber is kept at $\bar{b} = 0.28$m and its length is changed back to $2\bar{L} = 0.5$m. The resulting energies are presented in 4.31 for $5 - 1200$Hz. For a shell of radius $\bar{a} = 0.06$m the cut-ons do not occur in the frequency range considered.

Figure 4.31a shows the results of with the fluid-borne mode in the forcing wave amplitude ($\ell = 0$). The reflected energy is dominant below the first cut-on from the expansion chamber at 748Hz apart from where it drops suddenly at 0Hz, 343.5Hz and 687Hz. These drops are due to the trigonometric term present in both the reflected and transmitted amplitudes. After the first cut-on the reflected energy drops and the transmitted energy

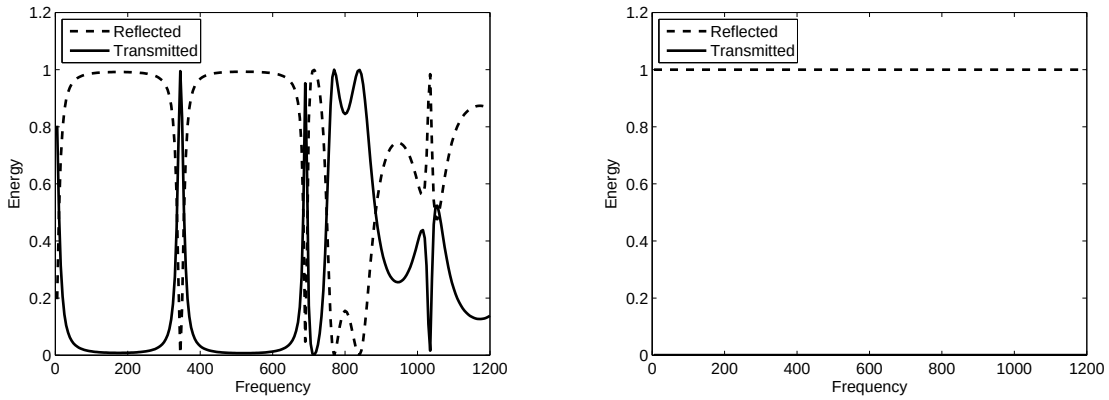

Figure 4.31: Energy output for the flexible expansion chamber between two shells with clamped edges: a) $\bar{a} = 0.06$m, $\bar{b} = 0.28$m, $\bar{L} = 0.25$m, $\ell = 0$; b) $\bar{a} = 0.06$m, $\bar{b} = 0.28$m, $\bar{L} = 0.25$m, $\ell = 1$.

takes over, until 838Hz where the reflected energy then takes over for the remainder of the considered frequencies. The reflected energy spikes at 1030.5Hz, which coincides with $f = 3c$.

The amplitude of the forcing wave is considered to have a structure-borne mode ($\ell = 1$) is Figure 4.31b. It is seen that the energy is totally reflected for all of the considered frequency range. This result matches the result obtained in the equivalent increase in radius problem in Figure 4.21 and by extension Figure 4.6b.

The final plots again considers the greatly reduced radii of the inlet and outlet shells, but this time with the length of the expansion chamber increased to $2\bar{L} = 1$m. The reflected and transmitted energy exiting the expansion chamber is shown in Figure 4.32.

With the fluid-borne mode in the forcing amplitude (see Figure 4.32a) the majority of energy is reflected below the first cut-on at 748Hz apart from when $f = cn/2$, for $n = 0, 1, 2, \ldots$. After this frequency the energy is transmitted, with a spike of reflected energy at 864Hz. The reflected energy drops at 1030.5Hz, which coincides with $f = 3c$ and at 1149Hz.

With the structure-borne mode used in the amplitude of the forcing wave (see Figure 4.32b) the energy is totally reflected for the considered range of frequencies. This result matches the result obtained in the equivalent increase in radius problem in Figure 4.22 and by extension Figure 4.6b.

4.3.4 Pin-jointed edges

Results were obtained for systems analogous to those considered in (Figures 4.28-4.32), but with a pin-jointed edge connecting the left shell to the annular disc. It was found that the results obtained using pin-jointed edges were identical to those obtained from the clamped edge equivalent problems.

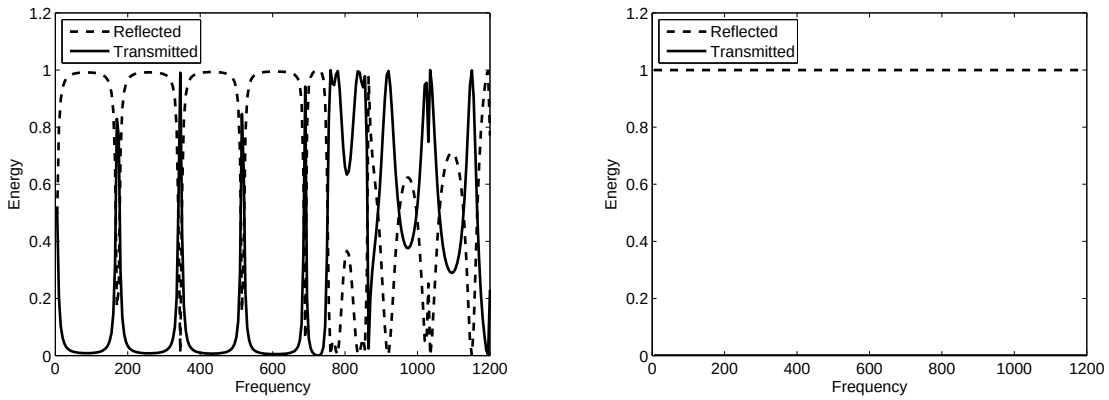

Figure 4.32: Energy output for the flexible expansion chamber between two shells with clamped edges: a) $\bar{a} = 0.06$m, $\bar{b} = 0.28$m, $\bar{L} = 0.5$m, $\ell = 0$; b) $\bar{a} = 0.06$m, $\bar{b} = 0.28$m, $\bar{L} = 0.5$m, $\ell = 1$.

Chapter 5

Energy radiated in shells subject to non-axisymmetric motion

The work in this chapter focuses on propagation in thin, circular, cylindrical shells with flexible walls and non-axisymmetric motion. The dispersion relation is derived from the wave equation and the Donnell-Mushtari equations of motion for a flexible shell. A generalised orthogonality relation for the eigenfunctions corresponding to a flexible shell with non-axisymmetric motion is derived from the dispersion relation and used with the mode matching method to find the amplitudes for some prototype problems. The generalised orthogonality relation in this chapter is new to the research area and is specific to flexible shells based on the Donnell-Mushtari equations of motion. Where possible, the results produced in this chapter are compared with those obtained from equivalent problems in Chapter two, three and four. Two problems are presented in this chapter: Energy reflected due to a rigid plate and energy radiated due to an abrupt increase in radius.

5.1 Governing equations

A thin, flexible-walled cylindrical shell described in cylindrical polar co-ordinates $(\bar{r}, \bar{\theta}, \bar{z})$ is considered. The interior region of the shell contains a compressible fluid of sound speed c and density ρ whilst the exterior region is in-vacuo. A harmonic time factor, $e^{-i\omega t}$, is assumed throughout where t is time and $\omega = ck$, with k being the fluid wavenumber.

The internal fluid is governed by Helmholtz equation, which in its non-dimensional form is

$$\left\{ \frac{\partial^2}{\partial r^2} + \frac{1}{r}\frac{\partial}{\partial r} + \frac{1}{r^2}\frac{\partial^2}{\partial \theta^2} + \frac{\partial^2}{\partial z^2} + 1 \right\} \phi = 0, \tag{5.1}$$

where ϕ is the fluid velocity potential. The method of separation of variables is used to find the velocity potential, which is dependant on r, θ and z and thus the velocity

potential assumes the form:

$$\phi = R(r)\Theta(\theta)Z(z). \tag{5.2}$$

This form of ϕ is substituted into (5.1) and is multiplied by $r^2/(R\Theta Z)$ to give the separated equation

$$\left(\frac{r^2}{R}\frac{\mathrm{d}^2R}{\mathrm{d}r^2} + \frac{r}{R}\frac{\mathrm{d}R}{\mathrm{d}r}\right) + \frac{1}{\Theta}\frac{\mathrm{d}^2\Theta}{\mathrm{d}\theta^2} + \frac{r^2}{Z}\frac{\mathrm{d}^2Z}{\mathrm{d}z^2} + r^2 = 0. \tag{5.3}$$

The terms in (5.3) involving Θ must have a negative separation constant as the solution should be periodic in θ, which leads to

$$\frac{1}{\Theta}\frac{\mathrm{d}^2\Theta}{\mathrm{d}\theta^2} = -m^2, \tag{5.4}$$

where m is the separation constant. This has solution

$$\Theta(\theta) = C\cos(m\theta) + D\sin(m\theta), \tag{5.5}$$

where C and D are arbitrary constants. These constants are selected as $C = 1$ and $D = 0$, such that the modes are symmetric in θ, which gives the solution

$$\Theta(\theta) = \cos(m\theta). \tag{5.6}$$

Note by selecting $C = 0$ and $D = 1$ antisymmetric modes could instead be considered. The differential equation in (5.3) is divided by r^2 and the separation constant is introduced, to give

$$\left(\frac{1}{R}\frac{\mathrm{d}^2R}{\mathrm{d}r^2} + \frac{1}{rR}\frac{\mathrm{d}R}{\mathrm{d}r}\right) + 1 - m^2 = -\frac{1}{Z}\frac{\mathrm{d}^2Z}{\mathrm{d}z^2} = s^2 \tag{5.7}$$

where s is the separation constant for the differential equation involving $Z(z)$. Thus

$$\frac{1}{Z}\frac{\mathrm{d}^2Z}{\mathrm{d}z^2} = -s^2, \tag{5.8}$$

which has the solution

$$Z(z) = Ee^{isz} + Fe^{-isz}, \tag{5.9}$$

where E and F are constants. These constants are selected as $E = 1$ and $F = 0$, such that the velocity potential comprises only waves travelling in the positive z direction.

Equation (5.3) is multiplied though by R and can now be written as

$$R'' + \frac{1}{r}R' + \left(1 - s^2 - \frac{m^2}{r^2}\right)R = 0. \tag{5.10}$$

Let $x = \kappa r$, then

$$\frac{\mathrm{d}^2R''}{\mathrm{d}x^2} + \frac{1}{x}\frac{\mathrm{d}R'}{\mathrm{d}x} + \left(\kappa^2 - \frac{m^2}{x^2}\right)R = 0, \tag{5.11}$$

where $\kappa^2 = (1-s^2)^{1/2}$. The above expression is recognised as Bessel's differential equation of order m found in Abramowitz and Stegun [41] which is known to have a solution of the form

$$R = AJ_{\pm m}(x) + BY_m(x), \tag{5.12}$$

where $J_{\pm m}(\cdot)$ and $Y_m(\cdot)$ are Bessel functions of the first and second kind and A, B are constants. These is a singularity in $Y_m(x)$ as $x \to 0$, therefore B is selected as zero and A now denotes the wave amplitude. Also as only non-axisymmetric motion is considered $m \geq 1$. It follows that a single mode of the velocity potential is given by

$$\phi_{mp} = A_{mp} J_m(\kappa_{mp} r)\cos(m\theta)e^{is_{mp}z}, \tag{5.13}$$

where A_{mp} is the amplitude and $\kappa_{mp}^2 = (1 - s_{mp}^2)^{1/2}$. For this chapter eigensystems for flexible shells subject to non-axisymmetric motion are considered with $m \geq 1$. However, the prototype problems will be solved for $m = 1$ (this motion is illustrated in Figure 3.1).

For a shell of thickness h, radius $\bar{a}$ and density ρ_s, the non-dimensional equations of motion are given (3.8)-(3.10) which are stated below for convenience:

$$\frac{\partial^2 u}{\partial z^2} + \frac{1-\nu}{2a^2}\frac{\partial^2 u}{\partial \theta^2} + \frac{1+\nu}{2a}\frac{\partial^2 v}{\partial z \partial \theta} + \frac{i\nu}{a}\frac{\partial^2 \phi}{\partial r \partial z} + \beta^2 u = 0, \quad \text{at } r = a, \tag{5.14}$$

$$\frac{1+\nu}{2a}\frac{\partial^2 u}{\partial z \partial \theta} + \frac{1-\nu}{2}\frac{\partial^2 v}{\partial z^2} + \frac{1}{a^2}\frac{\partial^2 v}{\partial \theta^2} + \frac{i}{a^2}\frac{\partial^2 \phi}{\partial r \partial \theta} + \beta^2 v = 0, \quad \text{at } r = a, \tag{5.15}$$

$$\begin{aligned} &-i\nu a\frac{\partial u}{\partial z} - i\frac{\partial v}{\partial \theta} + \frac{\partial \phi}{\partial r} + \frac{1}{\tau_1}\frac{\partial^5 \phi}{\partial r \partial z^4} + \frac{2}{\tau_1 a^2}\frac{\partial^5 \phi}{\partial r \partial z^2 \partial \theta^2} + \frac{1}{\tau_1 a^4}\frac{\partial^5 \phi}{\partial r \partial \theta^4} - a^2\beta^2\frac{\partial \phi}{\partial r} \\ &- \frac{a^2\beta^2\rho}{\rho_s h k}\phi = 0, \quad \text{at } r = a, \end{aligned} \tag{5.16}$$

where $\beta = \omega/(c_s k)$ and $\tau_1 = 12/(k^2 h^2 a^2)$. From (5.14) and (5.15) it is seen that expressions for the longitudinal and circumferential displacement must take the form

$$u_m(r, \theta, z) = U_m \cos(m\theta)e^{isz}, \tag{5.17}$$

$$v_m(r, \theta, z) = V_m \sin(m\theta)e^{isz}, \tag{5.18}$$

where U_m and V_m are the respective longitudinal and circumferential displacement amplitudes of Bessel order m. These are substituted with (5.13) into (5.14) to give the coupled equation

$$\left\{\beta^2 - s^2 - \frac{m^2(1-\nu)}{2a^2}\right\}U_m + \frac{ims(1+\nu)}{2a}V_m = \frac{\nu s}{a}\kappa J_m'(\kappa a). \tag{5.19}$$

A second equation is found by substituting the forms of displacement and velocity po-

tential into (5.15):

$$-\frac{ims(1+\nu)}{2a}U_m + \left\{\beta^2 - \frac{s^2(1-\nu)}{2} - \frac{m^2}{a^2}\right\}V_m = \frac{im}{a^2}\kappa J'_m(\kappa a). \tag{5.20}$$

These coupled equations are to be solved in order to find the displacement amplitudes, these are expressed in matrix form as

$$\begin{bmatrix} \frac{m^2(1-\nu)}{2} - a^2\beta^2 + a^2s^2 & -\frac{iam(1+\nu)s}{2} \\ -iam(1+\nu)s & 2a^2\beta^2 - 2m^2 - a^2(1-\nu)s^2 \end{bmatrix} \begin{bmatrix} U_m \\ V_m \end{bmatrix} = \begin{bmatrix} -a\nu s \\ 2im \end{bmatrix} \kappa J'_n(\kappa a). \tag{5.21}$$

It follows that

$$\begin{bmatrix} U_m \\ V_m \end{bmatrix} = \frac{\kappa J'_m(\kappa a)}{Q_m(s)} \begin{bmatrix} 2a^2\beta^2 - 2m^2 - a^2(1-\nu)s^2 & \frac{iam(1+\nu)s}{2} \\ iam(1+\nu)s & \frac{m^2(1-\nu)}{2} - a^2\beta^2 + a^2s^2 \end{bmatrix} \begin{bmatrix} -a\nu s \\ 2im \end{bmatrix}, \tag{5.22}$$

where $Q_m(s)$ is the determinant given by

$$Q_m(s) = \left\{\frac{m^2(1-\nu)}{2} - a^2\beta^2 + a^2s^2\right\}\left\{2a^2\beta^2 - 2m^2 - a^2(1-\nu)s^2\right\} + \frac{a^2m^2(1+\nu)^2s^2}{2}. \tag{5.23}$$

The expression for the longitudinal displacement is thus

$$u_m = a\left[\left\{m^2(\nu-1) - 2a^2\beta^2\nu\right\}s + a^2(\nu-\nu^2)s^3\right]\frac{\kappa J'_m(\kappa a)}{Q_m(s)}\cos(m\theta)e^{isz}. \tag{5.24}$$

Similarly, the expression for the circumferential displacement is

$$v_m = i\left[m^3(1-\nu) - 2a^2\beta^2m + a^2\left\{2m - m(\nu+\nu^2)\right\}s^2\right]\frac{\kappa J'_m(\kappa a)}{Q_m(s)}\sin(m\theta)e^{isz}. \tag{5.25}$$

The expressions for displacement (5.24) and (5.25) are used in the third equation of motion (5.16) to obtain the characteristic equation

$$K_m(s) = (a\nu sU_m - imV_m)\tau_1 + \left\{s^4 + \frac{2m^2s^2}{a^2} - \mu_m^4\right\}\kappa J'_m(\kappa a) - \alpha J_m(\kappa a) = 0, \tag{5.26}$$

where $\tau_1 = 12/(k^2h^2a^2)$, $\mu_m^4 = (a^2\beta^2 - 1)\tau_1 - m^4/a^4$ and $\alpha = 12\beta^2\rho/(h^3k^3\rho_s)$. The roots s_{mp} of the characteristic equation define the wavenumbers of the waves propagating within the shell. These are ordered sequentially with the largest real root first, then by increasing imaginary part. The numerical results presented herein are obtained using 100 modes with $m = 1$. The shells are taken to be aluminium, of thickness $h = 0.002$ m and of density $\rho_s = 2700$ kg m^{-3}. In addition, the values of Young's modulus and Poisson's ratio are taken to be $E = 7.2 \times 10^{10}$ Nm^{-2} and $\nu = 0.34$; whilst $c = 343.5$ms^{-1} and

$\rho = 1.2$ kg m^{-3} respectively. The roots of the characteristic equation are found in Matlab with the code presented in Appendix J.

5.1.1 The generalised orthogonality relation

The characteristic function (5.26) can be expressed in the following form

$$K_m(s) = P_m(s)\kappa J'_m(\kappa a) - \alpha Q_m(s) J_m(\kappa a), \tag{5.27}$$

where the functions $P_m(s)$ and $Q_m(s)$ are the characteristic polynomials

$$P_m(s) = P_8^{(a)} s^8 + P_6^{(a)} s^6 + P_4^{(a)} s^4 + P_2^{(a)} s^2 + P_0^{(a)}, \tag{5.28}$$

with

$$P_8^{(a)} = a^4(\nu - 1), \tag{5.29}$$
$$P_6^{(a)} = a^2\left\{a^2\beta^2(3-\nu) + 4m^2(\nu-1)\right\}, \tag{5.30}$$
$$P_4^{(a)} = 5m^4(\nu-1) + 3a^2\beta^2m^2(3-\nu) + a^4\left\{(1-\nu)\mu_m^4 - \tau(\nu^3-\nu^2) - 2\beta^4\right\}, \tag{5.31}$$
$$P_2^{(a)} = a^4\beta^2\tau\left\{a^2\beta^2(\nu-3) - 2\nu^2 - \nu + 3\right\} - 2a^2m^2\beta^2\left\{2\beta^2 + a^2\tau(\nu-1)\right\} - 3m^4\beta^2(\nu-3) + 4m^6(\nu-1)/a^2, \tag{5.32}$$
$$P_0^{(a)} = \left\{2a^2\beta^2 + m^2(\nu-1)\right\}\left\{m^2(-\mu_m^4 - \tau_1) + a^2\beta^2\mu_m^4\right\}. \tag{5.33}$$

and

$$Q_m(s_n) = Q_4^{(a)} s^4 + Q_2^{(a)} s^2 + Q_0^{(a)}, \tag{5.34}$$

with

$$Q_4^{(a)} = a^4(\nu-1), \tag{5.35}$$
$$Q_2^{(a)} = a^2\left\{a^2\beta^2(3-\nu) + 2m^2(\nu-1)\right\}, \tag{5.36}$$
$$Q_0^{(a)} = (m^2 - a^2\beta^2)\left\{2a^2\beta^2 + m^2(\nu-1)\right\}. \tag{5.37}$$

Clearly there is an infinite set of roots to $K_m(s) = 0$ for each integer value of m as indicated in (5.13). However it is convenient to use s_p rather than s_{mp} in the remainder of this section and. Let $s_p,\ p = 0, 1, 2, \ldots$ and $s_q,\ q = 0, 1, 2, \ldots$ be the roots of the characteristic function, then the following relation must hold

$$K_m(s_p)Q_m(s_q)\kappa_n J'_m(\kappa_q a) - K_m(s_q)Q_m(s_p)\kappa_n J'_m(\kappa_p a) = 0, \tag{5.38}$$

where $P_m(s)$ is given in (5.28) and $Q_m(s)$ is given in (5.34). The characteristic function $K_m(s)$ in (5.26) is substituted into (5.38) to give

$$\begin{aligned}&\{P_m(s_p)Q_m(s_q) - P_m(s_q)Q_m(s_p)\}\,\kappa_p J'_m(\kappa_p a)\kappa_q J'_m(\kappa_q a)\\&+ Q_m(s_p)Q_m(s_q)\frac{\alpha}{a}\left[\{J_m(\kappa_p r)\kappa_q J'_m(\kappa_q r) - J_m(\kappa_q r)\kappa_p J'_m(\kappa_p r)\}\,r\right]_{r=0}^{a} = 0.\end{aligned} \tag{5.39}$$

The term in square brackets is differentiated and expressed in integral form and on collecting like terms

$$\begin{aligned}&(s_q^2 - s_p^2)Q_m(s_p)Q_m(s_q)\frac{\alpha}{a}\int_0^a \Big[J_m(\kappa_q r)\left\{\kappa_p^2 J''_m(\kappa_p r)r + \kappa_p J'_m(\kappa_p r)\right\}\\&- J_m(\kappa_p r)\left\{\kappa_q^2 J''_m(\kappa_q r)r + \kappa_q J'_m(\kappa_q r)\right\}\Big]\,\mathrm{d}r\\&= -\{P_m(s_p)Q_m(s_q) - P_m(s_q)Q_m(s_p)\}\,\kappa_p J'_m(\kappa_p a)\kappa_q J'_m(\kappa_q a).\end{aligned} \tag{5.40}$$

It follows from Bessel's equation that

$$\begin{aligned}&(s_q^2 - s_p^2)Q_m(s_p)Q_m(s_q)\frac{\alpha}{a}\int_0^a J_m(\kappa_p r)J_m(\kappa_q r)r\,\mathrm{d}r\\&= -\{P_m(s_p)Q_m(s_q) - P_m(s_q)Q_m(s_p)\}\,\kappa_p J'_m(\kappa_p a)\kappa_q J'_m(\kappa_q a).\end{aligned} \tag{5.41}$$

Hence

$$\begin{aligned}&\frac{\alpha}{a}\int_0^a J_m(\kappa_p r)J_m(\kappa_q r)r\,\mathrm{d}r\\&+ \frac{K_m(s_q)Q_m(s_p)\kappa_p J'_m n(\kappa_p a)}{(s_q^2 - s_n p^2)Q_m(s_p)Q_m(s_q)} - \frac{K_m(s_p)Q_m(s_q)\kappa_q J'_m(\kappa_n q a)}{(s_q^2 - s_p^2)Q_m(s_p)Q_m(s_q)}\\&= -\frac{\{P_m(s_p)Q_m(s_q) - P_m(s_q)Q_m(s_p)\}\,\kappa_p J'_m(\kappa_p a)\kappa_q J'_m(\kappa_q a)}{(s_q^2 - s_p^2)Q_m(s_p)Q_m(s_q)}.\end{aligned} \tag{5.42}$$

The non-zero constant C_{mp} is given by,

$$C_{mp} = \frac{\kappa_p J'_m(\kappa_p a)}{Q_m(s_p)}\lim_{s\to s_p}\frac{K_m(s_n) - K_m(s)}{s^2 - s_p^2}. \tag{5.43}$$

The nature of the above equation allows for l'Hôpital's rule to be applied,

$$C_{mp} = \frac{K'_m(s_p)\kappa_p J'_m(\kappa_p a)}{2s_p Q_m(s_p)}. \tag{5.44}$$

The generalised orthogonality relation is thus,

$$\frac{\alpha}{a}\int_0^a J_m(\kappa_p r)J_m(\kappa_q r)r\mathrm{d}r = \delta_{pq}C_{mp} - \frac{G_m(s_p, s_q)\kappa_p J'_m(\kappa_p a)\kappa_q J'_m(\kappa_q a)}{Q_m(s_p)Q_m(s_q)}, \tag{5.45}$$

where δ is the Kronecker delta and

$$G_m(s_p,s_q) = P_8^{(a)}Q_m(s_p)s_q^6 + \left\{P_8^{(a)}Q_m(s_p)s_p^2 + P_6^{(a)}Q_m(s_p)\right\}s_q^4 + \left\{P_8^{(a)}Q_2^{(a)}s_p^6 + \left(P_8^{(a)}Q_0^{(a)} + P_6^{(a)}Q_2^{(a)}\right)s_p^4 + \left(P_6^{(a)}Q_0^{(a)} + P_4^{(a)}Q_2^{(a)} - P_2^{(a)}Q_4^{(a)}\right)s_p^2 + P_4^{(a)}Q_0^{(a)} - P_0^{(a)}Q_4^{(a)}\right\}s_q^2 + P_8^{(a)}Q_0^{(a)}s_n^6 + P_6^{(a)}Q_0^{(a)}s_p^4 + \left(P_4^{(a)}Q_0^{(a)} - P_0^{(a)}Q_4^{(a)}\right)s_p^2 + P_2^{(a)}Q_0^{(a)} - P_0^{(a)}Q_2^{(a)}. \tag{5.46}$$

That is

$$G_m(s_p,s_q) = G_m^{(6)}s_q^6 + G_m^{(4)}s_q^4 + G_m^{(3)}s_q^2 + G_m^{(0)}, \tag{5.47}$$

where

$$G_m^{(6)} = P_8^{(a)}Q_m(s_p), \tag{5.48}$$

$$G_m^{(4)} = P_8^{(a)}Q_m(s_p)s_p^2 + P_6^{(a)}Q_m(s_p), \tag{5.49}$$

$$G_m^{(2)} = P_8^{(a)}Q_2^{(a)}s_p^6 + \left(P_8^{(a)}Q_0^{(a)} + P_6^{(a)}Q_2^{(a)}\right)s_p^4 + \left(P_6^{(a)}Q_0^{(a)} + P_4^{(a)}Q_2^{(a)} - P_2^{(a)}Q_4^{(a)}\right)s_p^2 + P_4^{(a)}Q_0^{(a)} - P_0^{(a)}Q_4^{(a)}, \tag{5.50}$$

$$G_m^{(0)} = P_8^{(a)}Q_0^{(a)}s_n^6 + P_6^{(a)}Q_0^{(a)}s_p^4 + \left(P_4^{(a)}Q_0^{(a)} - P_0^{(a)}Q_4^{(a)}\right)s_p^2 + P_2^{(a)}Q_0^{(a)} - P_0^{(a)}Q_2^{(a)}. \tag{5.51}$$

Similarly, for a shell of radius b, the equivalent generalised orthogonality relation is

$$\frac{\alpha}{b}\int_0^b J_m(\gamma_p r)J_m(\gamma_q r)r\mathrm{d}r = \delta_{pq}D_p - \frac{G_m(\eta_p,\eta_q)\gamma_p J_m'(\gamma_p b)\gamma_q J_m'(\gamma_q b)}{Q_m(\eta_p)Q_m(\eta_q)}, \tag{5.52}$$

where $P_n^{(\mathrm{a})}$ and $Q_n^{(\mathrm{a})}$ are replaced by $P_n^{(\mathrm{b})}$ and $Q_n^{(\mathrm{b})}$, $\tau_2 = 12/(k^2h^2b^2)$, η_q are the equivalent wavenumbers, $\gamma_q = (1-\eta_q^2)^{1/2}$ and

$$D_{mp} = \frac{K_m'(\eta_p)\gamma_p J_m'(\gamma_p b)}{2\eta_p Q_m(\eta_p)}. \tag{5.53}$$

The non-zero constant C_{mp} (or equivalently D_{mp}) is a useful parameter arising in various identities which involve the characteristic equation.

5.1.2 Properties of the eigensystem

Analogous to the axisymmetric case, a number of identities can be developed to demonstrate that the eigenfunctions are linearly dependent. It is shown in Lawrie [46] that the number of such identities depends on the order of the boundary conditions. This number is the same as the number of edge conditions required (or alternatively half the order of the characteristic equation). In this case there are four such identities and these are

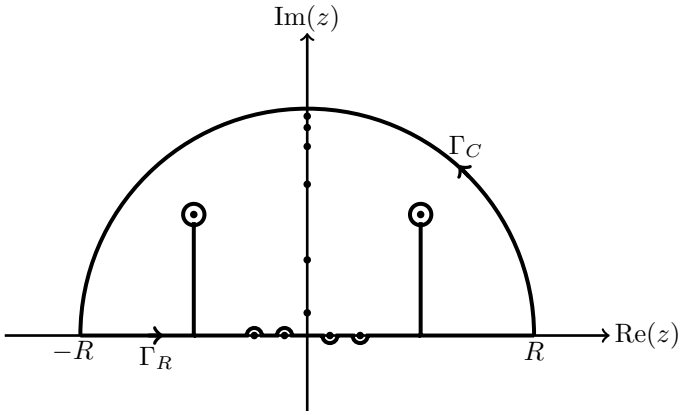

Figure 5.1: The path of integration used for Cauchy's residue theorem.

given by $I_1(r),\ I_2(r),\ I_3(r)$ and $I_4(r)$. These identities are constructed by considering contour integrals with odd integrands. On applying Cauchy's residue theorem an identity is obtained. The first identity is created considering the following integral

$$I_1(r) = \frac{1}{2\pi i}\int_{-\infty}^{\infty} \frac{2sQ_m(s)J_m(\kappa r)}{K_m(s)}\,\mathrm{d}s,\ \ 0 \le r \le a, \tag{5.54}$$

where the path of integration is indented above any poles on the negative real axis and below any poles on the positive real axis as shown in Figure 5.1. Note the p on s_p and κ_p is dropped for the workings for the first identity. The integrand of $I_1(r)$ is an odd function, which means it evaluates to 0. Contour integration can be used to express the integral as a sum of residues and thus obtain an identity. Cauchy's residue theorem gives

$$I_1(r) + \frac{1}{2\pi i}\int_{-\infty}^{\infty} \frac{2sQ_m(s)J_m(\kappa r)}{K_m(s)}\,\mathrm{d}s = \sum_{p=0}^{\infty} \varrho_{mp},\ 0 \le r \le a, \tag{5.55}$$

where ϱ_{mp} are the residues at $s = s_{mp}$. That is

$$\varrho_{mp} = \lim_{s\to s_{mp}} \frac{(s-s_{mp})2sQ_m(s)J_m(\kappa r)}{K_m(s)} = \frac{2sQ_m(s_{mp})J_m(\kappa_{mp} r)}{K_m'(s_{mp})},\ 0 \le r \le a, \tag{5.56}$$

where l'Hôpital's rule has been applied. Note that as $|s| \to \infty$ the integrand can be approximated by

$$\frac{2sQ_m(s)J_m(\kappa r)}{K_m(s)} \approx \frac{2J_m(isr)}{is^4 J_{m+1}(isa)}. \tag{5.57}$$

Hence, as $R \to \infty$

$$\int_{\Gamma_c} \frac{2sQ_m(s)J_m(\kappa r)}{K_m(s)}\,\mathrm{d}s \to 0,\ 0 \le r \le a. \tag{5.58}$$

This integral can be evaluated by use of contour integration, firstly the path of integration is deformed to a half circle in the upper half plane (denoted Γ_R) with radius R

$$I_1(r) = \frac{1}{2\pi i} \oint_{\Gamma_R} \frac{2sQ_m(s)J_m(\kappa r)}{K_m(s)} \, \mathrm{d}s, \quad 0 \leq r \leq a. \tag{5.59}$$

The half circle Γ_R can be separated into two separate contours, the arc in the upper half plane in the anti-clockwise sense (denoted C_{R^+}) and the interval $[-R, R]$. This allows for the integral to be considered as

$$I_1(r) = \frac{1}{2\pi i} \left\{ \int_{C_{R^+}} \frac{2sQ_m(s)J_m(\kappa r)}{K_m(s)} \, \mathrm{d}s + \int_{-R}^{R} \frac{2sQ_a(s)J_m(\kappa r)}{K_m(s)} \, \mathrm{d}s \right\}, \quad 0 \leq r \leq a. \tag{5.60}$$

Considering the radius R tending to infinite allows for the use of Cauchy's Residue Theorem. The contribution due to C_{R^+} tends to 0 as $R \to \infty$, this is due to the denominator having larger magnitude than the numerator. For the remaining integral, the integrand is analytic, except for an infinite family of poles when $L(s_p, a) = 0$. These poles are given when $s = s_{np}$, therefore the integral becomes the infinite sum of residues

$$I_1(r) = \sum_{p=0}^{\infty} \mathrm{Res} \left\{ \frac{2sQ_m(s)J_m(\kappa r)}{K_m(s,a)}, s_{mp} \right\} = \sum_{p=0}^{\infty} \lim_{s \to s_{mp}} \frac{(s - s_{mp})2sQ_m(s)J_m(\kappa r)}{K_m(s)}. \tag{5.61}$$

As the both the numerator and denominator of the limit tend to zero, l'Hôpital's rule can be applied in order to obtain the first identity as

$$I_1(r) = \sum_{p=0}^{\infty} \frac{2s_{mp}Q_m(s_{mp})J_m(\kappa_{mp} r)}{K'_m(s_{mp})} = \sum_{p=0}^{\infty} \frac{\kappa_{mp} J'_m(\kappa_{mp} a) J_m(\kappa_{mp} r)}{C_{mp}} = 0, \quad 0 \leq r \leq a. \tag{5.62}$$

Further identities can be found in the same way by considering the integrals,

$$I_2(r) = \frac{1}{2\pi i} \int_{-\infty}^{\infty} \frac{2sJ_m(\kappa r)}{K_m(s)} \, \mathrm{d}s, \quad 0 \leq r \leq a, \tag{5.63}$$

$$I_3(r) = \frac{1}{2\pi i} \int_{-\infty}^{\infty} \frac{2s\kappa^2 J_m(\kappa r)}{K_m(s)} \, \mathrm{d}s, \quad 0 \leq r \leq a, \tag{5.64}$$

$$I_4(r) = \frac{1}{2\pi i} \int_{-\infty}^{\infty} \frac{2s\kappa^4 J_m(\kappa r)}{K_m(s)} \, \mathrm{d}s, \quad 0 \leq r \leq a. \tag{5.65}$$

The integrand in these cases are odd functions, therefore they evaluate to zero. The second, third and fourth identities are obtained as,

$$I_2(r) = \sum_{p=0}^{\infty} \frac{2s_{mp}J_m(\kappa_{mp} r)}{K'_m(s_{mp})} = \sum_{p=0}^{\infty} \frac{\kappa_{mp} J'_m(\kappa_{mp} a) J_m(\kappa_{mp} r)}{Q_m(s_{mp}) C_{mp}} = 0, \quad 0 \leq r \leq a, \tag{5.66}$$

$$I_3(r) = \sum_{p=0}^{\infty} \frac{2s_{mp}\kappa_{mp}^2 J_m(\kappa_{mp} r)}{K'_m(s_{mp})} = \sum_{p=0}^{\infty} \frac{\kappa_{mp}^3 J'_m(\kappa_{mp} a) J_m(\kappa_{mp} r)}{Q_m(s_{mp}) C_{mp}} = 0, \quad 0 \leq r \leq a, \tag{5.67}$$

$$I_4(r) = \sum_{p=0}^{\infty} \frac{2s_{mp}\kappa_{mp}^4 J_m(\kappa_{mp} r)}{K'_m(s_{mp})} = \sum_{p=0}^{\infty} \frac{\kappa_{mp}^5 J'_m(\kappa_{mp} a) J_m(\kappa_{mp} r)}{Q_m(s_{mp}) C_{mp}} = 0, \quad 0 \leq r \leq a. \tag{5.68}$$

Further identities can be found by considering the integrals

$$I_5 = \frac{1}{2\pi i} \int_{-\infty}^{\infty} \frac{2sQ_m(s)\kappa J'_m(\kappa a)}{K_m(s)} \, \mathrm{d}s, \tag{5.69}$$

$$I_6 = \frac{1}{2\pi i} \int_{-\infty}^{\infty} \frac{2s^3 Q_m(s)\kappa J'_m(\kappa a)}{K_m(s)} \, \mathrm{d}s. \tag{5.70}$$

The above integrals were chosen such that the integrand is odd, therefore ensuring that they evaluate to zero. It follows that the identity given by I_5 is,

$$I_5 = \sum_{p=0}^{\infty} \frac{2s_{mp} Q_m(s_{mp}) \kappa_{mp} J'_m(\kappa_{mp} a)}{K'_m(s_{mp})} = \sum_{p=0}^{\infty} \frac{\left\{\kappa_{mp} J'_m(\kappa_{mp} a)\right\}^2}{C_{mp}} = 0. \tag{5.71}$$

For integral I_6 it is seen that as $R \to \infty$ the contribution from C_{R^+} is non zero. In order to find this contribution the integrand is approximated for evaluation:

$$\frac{2s^3 Q_m(s)\kappa J'_m(\kappa a)}{K_m(s)} \approx \frac{2s^7 a^4 (\nu - 1)\kappa J'_m(\kappa a)}{s^8 a^4 (\nu - 1)\kappa J'_m(\kappa a)} = \frac{2}{s}. \tag{5.72}$$

With the parameterisations $s = Re^{i\theta}$ and $ds/d\theta = iRe^{i\theta}$, the integral over the arc is

$$\frac{1}{2\pi i} \int_{C_{R^+}} \frac{2s^3 Q_m(s)\kappa J'_m(\kappa a)}{K_m(s)} \, \mathrm{d}s \approx \frac{1}{2\pi i} \int_0^{\pi} 2i \, \mathrm{d}\theta = 1. \tag{5.73}$$

Cauchy's residue theorem is used to evaluate the integral over the straight line $[-R, R]$ to give an infinite sum of residues

$$\frac{1}{2\pi i} \int_{-R}^{R} \frac{2sQ_m(s)\kappa^3 J'_m(\kappa a)}{K_m(s)} \, \mathrm{d}s = \sum_{p=0}^{\infty} \frac{s_{mp}^2 \left\{\kappa_{mp} J'_m(\kappa_{mp} a)\right\}^2}{C_{mp}}. \tag{5.74}$$

The identity obtained from I_6 is thus

$$\sum_{p=0}^{\infty} \frac{\kappa_{mp}^2 \left\{\kappa_{mp} J'_m(\kappa_{mp} a)\right\}^2}{C_{mp}} = -1. \tag{5.75}$$

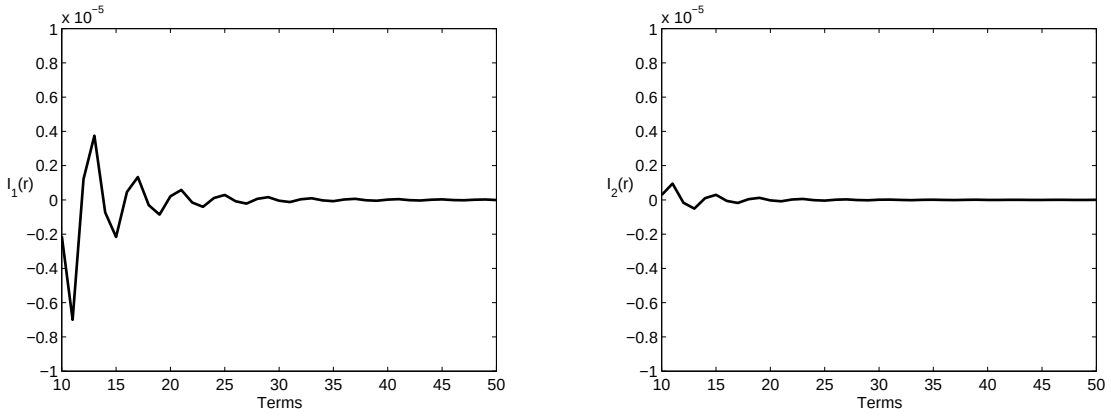

a) b)

Figure 5.2: Identities one and four.

A final identity can be obtained by multiplying the characteristic equation through by $\kappa_{mp}^3 J'_m(\kappa_{mp}a)/\{P_m(s_{mp})C_{mp}\}$ and summing to give

$$\alpha \sum_{p=0}^{\infty} \frac{Q_m(s_{mp})\kappa_{mp}^3 J'_m(\kappa_{mp}a)J_m(\kappa_{mp}a)}{P_m(s_{mp})C_{mp}} = -1. \tag{5.76}$$

The roots of the characteristic equation (5.26) from a shell of radius $\bar{a} = 0.2$m at 500Hz were used to plot the value of each identity against the number of considered modes. The number of considered modes increases from 10 to 50, which is representative of the radius of the circle in which roots are sought. The results of identities 1 and 3 (shown in Figure 5.2) show that these identities are satisfied to 5 decimal places from 10 modes and continue to converge to zero. The results of identities 2, 3, 4, 5, 6, 7 and 8 are all zero to at least 6 decimal places when 10 modes are considered.

5.2 Energy reflected by a rigid end plate

The aim of this section is to find the energy reflected by a rigid end plate in a semi-infinite shell. The system comprises a semi-infinite shell located in the region $0 \leq r \leq a, z \leq 0$ and is closed by a rigid end plate occupying $0 \leq r \leq a,\ z = 0$ (see Figure 5.3). Forcing is by a wave located in the shell propagating in the positive z direction towards the end plate. The velocity potential in the region $z \leq 0,\ 0 \leq r \leq a$ is

$$\phi(r,\theta,z) = F_{1\ell}J_1(\kappa_{1\ell}r)\cos(\theta)e^{is_{1\ell}z} + \sum_{n=0}^{\infty}\sum_{q=0}^{\infty} A_{nq}J_n(\kappa_{nq}r)\cos(n\theta)e^{-is_{nq}z},\ 0 \leq r \leq a, \tag{5.77}$$

where ℓ indicates the chosen mode to force with ($\ell = 0$ or $\ell = 1$), $F_{1\ell}$ is the amplitude of the forcing wave, A_{nq} is the amplitude of the qth reflected mode, s_{1q} are the wavenumbers

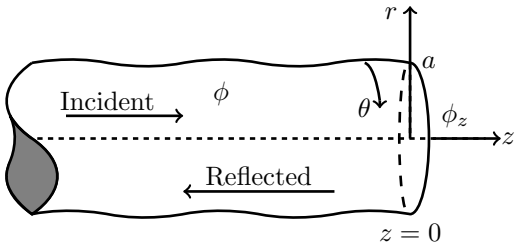

Figure 5.3: Physical configuration of the semi-infinite shell with a rigid end plate.

and $\kappa_{1q} = (1 - s_{1q}^2)^{1/2}$. There is only one real mode s_{10} at low frequencies which occur for $m = 1$, for this mode s_{10} is close to 1. A second mode cuts on later in the frequency range and shall be used in the amplitude of the forcing wave where possible. The amplitude of the forcing wave is chosen such that the incident energy is unity and is formed by using (2.36). It follows that

$$F_{1\ell} = \{1/(s_{1\ell} C_{1\ell})\}^{1/2}. \tag{5.78}$$

At the rigid wall, the normal component of velocity is zero, which gives the condition

$$\frac{\partial \phi}{\partial z} = 0, \quad \text{at } z = 0,\ 0 \le r \le a. \tag{5.79}$$

The velocity potential (5.77) is substituted into the above condition to give

$$F_{1\ell} s_{1\ell} J_1(\kappa_{1\ell} r) \cos(\theta) - \sum_{n=0}^{\infty} \sum_{q=0}^{\infty} A_{nq} s_{nq} J_n(\kappa_{nq} r) \cos(n\theta) = 0,\ 0 \le r \le a. \tag{5.80}$$

The above equation is multiplied through by $\cos(m\theta)$ and integrated with respect to $\theta,\ 0 \le \theta \le 2\pi$, to give

$$F_{1\ell} s_{1\ell} J_1(\kappa_{1\ell} r) \int_0^{2\pi} \cos(\theta)\cos(m\theta)\ \mathrm{d}\theta - \sum_{n=0}^{\infty} \sum_{q=0}^{\infty} A_{nq} s_{nq} J_n(\kappa_{nq} r) \int_0^{2\pi} \cos(n\theta)\cos(m\theta)\ \mathrm{d}\theta$$
$$= 0. \tag{5.81}$$

The orthogonality property of $\cos(\cdot)$ can be used to reduce the above equation. From Brown and Churchill [47] this is given as

$$\frac{1}{\pi} \int_0^{2\pi} \cos(n\theta)\cos(m\theta)\ \mathrm{d}\theta = \delta_{nm}, \tag{5.82}$$

where δ_{nm} is the Kroneckor delta. It follows from (5.81) that

$$F_{1\ell} s_{1\ell} J_1(\kappa_{1\ell} r) \delta_{1\ell} = \sum_{q=0}^{\infty} A_{mq} s_{mq} J_m(\kappa_{mq} r). \tag{5.83}$$

For this equation to be satisfied, either $m = 1$ or

$$\sum_{q=0}^{\infty} A_{mq} s_{mq} J_m(\kappa_{mq} r) = 0. \tag{5.84}$$

There are four ways in which (5.83) can be satisfied and these solutions come from the identities which demonstrate linear dependence of the eigenfunctions. From (5.62), (5.66)-(5.68) it is implied that the following can hold true

$$A_{mq} s_{mq} = \frac{\kappa_{mq} J'_m(\kappa_{mq} a)}{C_{mq}}, \tag{5.85}$$

$$A_{mq} s_{mq} = \frac{\kappa_{mq} J'_m(\kappa_{mq} a)}{Q_m(s_{mq}) C_{mq}}, \tag{5.86}$$

$$A_{mq} s_{mq} = \frac{\kappa_{mq}^3 J'_m(\kappa_{mq} a)}{Q_m(s_{mq}) C_{mq}}, \tag{5.87}$$

$$A_{mq} s_{mq} = \frac{\kappa_{mq}^5 J'_m(\kappa_{mq} a)}{Q_m(s_{mq}) C_{mq}}. \tag{5.88}$$

Hence this could potentially introduce four eigensolutions $T_j,\ j = 0, 1, 2, 3$ to the velocity potential defined as.

$$T_0(r, \theta, z) = \sum_{m=0}^{\infty} \sum_{q=0}^{\infty} \frac{\kappa_{mq} J'_m(\kappa_{mq} a)}{C_{mq} s_{mq}} J_m(\kappa_{mq} r) \cos(m\theta) e^{-i s_{mq} z}, \tag{5.89}$$

$$T_1(r, \theta, z) = \sum_{m=0}^{\infty} \sum_{q=0}^{\infty} \frac{\kappa_{mq} J'_m(\kappa_{mq} a)}{Q_m(s_{mq}) C_{mq} s_{mq}} J_m(\kappa_{mq} r) \cos(m\theta) e^{-i s_{mq} z}, \tag{5.90}$$

$$T_2(r, \theta, z) = \sum_{m=0}^{\infty} \sum_{q=0}^{\infty} \frac{\kappa_{mq}^3 J'_m(\kappa_{mq} a)}{Q_m(s_{mq}) C_{mq} s_{mq}} J_m(\kappa_{mq} r) \cos(m\theta) e^{-i s_{mq} z}, \tag{5.91}$$

$$T_3(r, \theta, z) = \sum_{m=0}^{\infty} \sum_{q=0}^{\infty} \frac{\kappa_{mq}^5 J'_m(\kappa_{mq} a)}{Q_m(s_{mq}) C_{mq} s_{mq}} J_m(\kappa_{mq} r) \cos(m\theta) e^{-i s_{mq} z}. \tag{5.92}$$

It follows that

$$\phi(r, \theta, z) = F_{1\ell} J_1(\kappa_{1\ell} r) \cos(\theta) e^{i s_{1\ell} z} + \sum_{q=0}^{\infty} A_{1q} J_1(\kappa_{1q} r) \cos(m\theta) e^{-i s_{1q} z} + B T_0(r, \theta, z)$$
$$+ C T_1(r, \theta, z) + D T_2(r, \theta, z) + E T_3(r, \theta, z), \tag{5.93}$$

where each $T_j(r, \theta, z),\ j = 0, 1, 2, 3$, satisfies the end plate condition and $B,\ C,\ D,\ E$ are constants. Henceforth it is assumed that $B = C = D = E = 0$.

The velocity potential (5.77) is substituted into the normal component of velocity

matching condition to give

$$F_{1\ell}s_{1\ell}J_1(\kappa_{1\ell}r)\cos(\theta) - \sum_{q=0}^{\infty} A_{1q}s_{1q}J_1(\kappa_{1q}r)\cos(\theta) = 0,\ 0 \le r \le a. \tag{5.94}$$

The above equation is multiplied through by $\alpha J_1(\kappa_{1p}r)r/a$ and integrated to give

$$F_{1\ell}s_{1\ell}\frac{\alpha}{a}\int_0^a J_1(\kappa_{1\ell}r)J_1(\kappa_{1p}r)r\ \mathrm{d}r - \sum_{q=0}^{\infty} A_{1q}s_{1q}\frac{\alpha}{a}\int_0^a J_1(\kappa_{1q}r)J_1(\kappa_{1p}r)r\ \mathrm{d}r = 0. \tag{5.95}$$

The generalised orthogonality relation in (5.45) is used to reduce this equation to

$$\begin{aligned} A_{1p} = {} & F_{1\ell}\delta_{\ell p} + \frac{G_1^{(6)}(s_{1p})\kappa_{1p}J_1'(\kappa_{1p}a)}{s_{1p}C_{1p}Q_1(s_{1p})}E_0 + \frac{G_1^{(4)}(s_{1p})\kappa_{1p}J_1'(\kappa_{1p}a)}{s_{1p}C_{1p}Q_1(s_{1p})}E_1 \\ & + \frac{G_1^{(2)}(s_{1p})\kappa_{1p}J_1'(\kappa_{1p}a)}{s_{1p}C_{1p}Q_1(s_{1p})}E_2 + \frac{G_1^{(0)}(s_{1p})\kappa_{1p}J_1'(\kappa_{1p}a)}{s_{1p}C_{1p}Q_1(s_{1p})}E_3. \end{aligned} \tag{5.96}$$

The method of edge condition application is generalised by recognising that the edge conditions take the form:

$$\sum_{p=0}^{\infty} A_{1p}\psi_{pn}^{(\mathrm{a})} + F_{1\ell}\psi_n^{(\mathrm{f})},\ n = 0, 1, 2, 3, \tag{5.97}$$

The edge conditions are applied by multiplying (5.96) by $\psi_{pn}^{(\mathrm{a})}$ (which is defined in (5.99) and (5.101)), and on summing over p it is found that

$$\begin{aligned} & \sum_{p=0}^{\infty} F_{1\ell}\delta_{\ell p}\psi_{pn}^{(\mathrm{a})} + \sum_{p=0}^{\infty} \frac{G_1^{(6)}(s_{1p})\kappa_{1p}J_1'(\kappa_{1p}a)\psi_{pn}^{(\mathrm{a})}}{s_{1p}C_{1p}Q_1(s_{1p})}E_0 + \sum_{p=0}^{\infty} \frac{G_1^{(4)}(s_{1p})\kappa_{1p}J_1'(\kappa_{1p}a)\psi_{pn}^{(\mathrm{a})}}{s_{1p}C_{1p}Q_1(s_{1p})}E_1 \\ & + \sum_{p=0}^{\infty} \frac{G_1^{(2)}(s_{1p})\kappa_{1p}J_1'(\kappa_{1p}a)\psi_{pn}^{(\mathrm{a})}}{s_{1p}C_{1p}Q_1(s_{1p})}E_2 + \sum_{p=0}^{\infty} \frac{G_1^{(0)}(s_{1p})\kappa_{1p}J_1'(\kappa_{1p}a)\psi_{pn}^{(\mathrm{a})}}{s_{1p}C_{1p}Q_1(s_{1p})}E_3 = -F_{1\ell}\psi_n^{(\mathrm{f})}. \end{aligned} \tag{5.98}$$

The results presented for this problem were created in Matlab with the code presented in Appendix K. This has been done using 100 modes to calculate the amplitudes of the propagating waves.

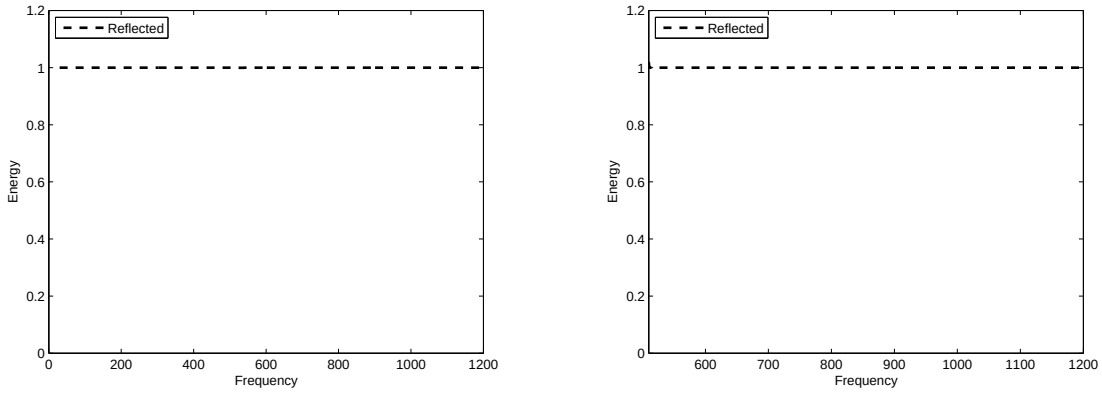

a) b)

Figure 5.4: Energy radiated due to a forcing wave at a rigid plate in a semi-finite shell with a clamped edge, $\bar{a} = 0.2$m: a) first mode forcing $\ell = 0$; b) second mode forcing $\ell = 1$.

5.2.1 Clamped edge

With clamped edge conditions the values of ψ in (5.96) are:

$$\begin{aligned}
\psi_{p0}^{(\mathrm{a})} &= U(s_{1p})\kappa_{1p}J_1'(\kappa_{1p}a), & \psi_0^{(\mathrm{f})} &= -U(s_{1\ell})\kappa_{1\ell}J_1'(\kappa_{1\ell}a),\\
\psi_{p1}^{(\mathrm{a})} &= V(s_{1p})\kappa_{1p}J_1'(\kappa_{1p}a), & \psi_1^{(\mathrm{f})} &= V(s_{1\ell})\kappa_{1\ell}J_1'(\kappa_{1\ell}a),\\
\psi_{p2}^{(\mathrm{a})} &= \kappa_{1p}J_1'(\kappa_{1p}a), & \psi_2^{(\mathrm{f})} &= -\kappa_{1\ell}J_1'(\kappa_{1\ell}a),\\
\psi_{p3}^{(\mathrm{a})} &= s_{1p}\kappa_{1p}J_1'(\kappa_{1p}a), & \psi_3^{(\mathrm{f})} &= -s_{1\ell}\kappa_{1\ell}J_1'(\kappa_{1\ell}a),
\end{aligned} \tag{5.99}$$

The values of $E_0 - E_3$ are found by truncating equations (5.98) using the above values of ψ. These values can then be used in (5.96) which is truncated to give the pth amplitude of the reflected wave. The energy associated with the reflected field is given in (2.41) which is stated below:

$$\mathcal{E}_{\mathrm{A}} = \frac{a}{\alpha}\mathrm{Real}\left[\sum_{p=0}^{P}|A_{1p}|^2 s_{1p}C_{1p}\right], \tag{5.100}$$

where A_{1p} are the amplitudes of the reflected waves.

Figure 5.4 shows the energy output for shell of radius $\bar{a} = 0.2$m clamped to the rigid plate for $5 - 1200$Hz.

Figure 5.4a assumes forcing with the first-mode in the amplitude and Figure 5.4b assumes forcing with the second-mode. The results for both plots show that the energy is totally transmitted for the entire considered frequency range.

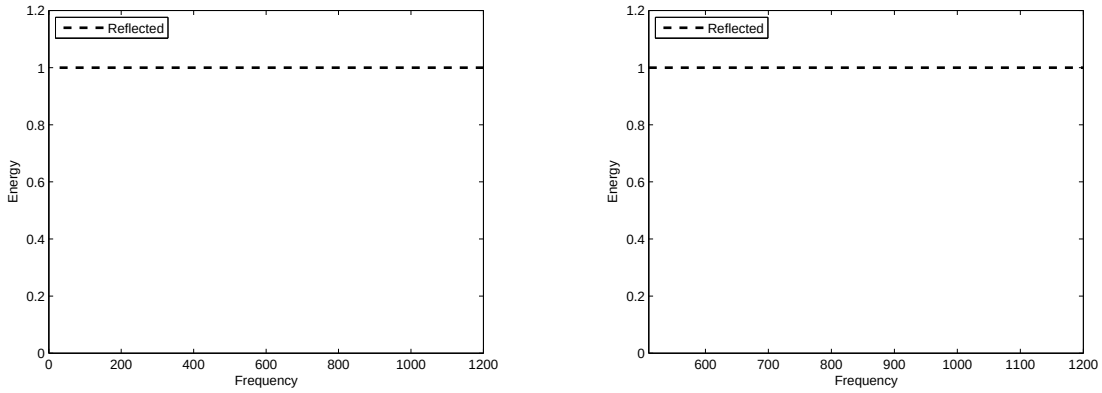

a) b)

Figure 5.5: Energy radiated due to a forcing wave at a rigid plate in a semi-finite shell with a pin-jointed edge, $\bar{a} = 0.2$m: a) first mode forcing $\ell = 0$; b) second mode forcing $\ell = 1$.

5.2.2 Pin-jointed edge

With pin-jointed edge conditions the values of ψ in (5.96) are:

$$\begin{aligned}
\psi_{p0}^{(\mathrm{a})} &= U(s_{1p})s_{1p}\kappa_{1p}J_1'(\kappa_{1p}a)), & \psi_0^{(\mathrm{f})} &= U(s_{1\ell})s_{1\ell}\kappa_{1\ell}J_1'(\kappa_{1\ell}a),\\
\psi_{p1}^{(\mathrm{a})} &= V(s_{1p})\kappa_{1p}J_1'(\kappa_{1p}a), & \psi_1^{(\mathrm{f})} &= V(s_{1\ell})\kappa_{1\ell}J_1'(\kappa_{1\ell}a),\\
\psi_{p2}^{(\mathrm{a})} &= \kappa_{1p}J_1'(\kappa_{1p}a), & \psi_2^{(\mathrm{f})} &= -\kappa_{1\ell}J_1'(\kappa_{1\ell}a),\\
\psi_{p3}^{(\mathrm{a})} &= s_{1p}^2\kappa_{1p}J_1'(\kappa_{1p}a), & \psi_3^{(\mathrm{f})} &= -s_{1\ell}^2\kappa_{1\ell}J_1'(\kappa_{1\ell}a). \qquad (5.101)
\end{aligned}$$

Figure 5.5 shows the energy output for shell of radius $\bar{a} = 0.2$m pin-jointed to the rigid plate for $5 - 1200$Hz.

Figure 5.5a assumes forcing with the first-mode in the amplitude and Figure 5.5b assumes forcing with the second-mode. Both plots show that the energy is totally transmitted for the chosen frequency range.

5.3 Energy radiated due to a forcing wave at an abrupt increase in radius

The purpose of this section is to find the energy reflected and transmitted due to an incident wave at an abrupt increase in radius. The system comprises two semi-infinite shells, the left-hand shell occupies $0 \le r \le a,\ z \le 0$ and the right-hand shell occupies $0 \le r \le b,\ z \ge 0$, where $a \le b$ (see Figure 5.6). The waveguide is closed by a rigid annular disc occupying $a \le r \le b,\ z = 0$. Forcing is introduced by a wave propagating in the positive z direction towards the abrupt increase in radius. Only the $m = 1$ case of non-axisymmetric motion will be considered in this problem. The velocity potential ϕ_1

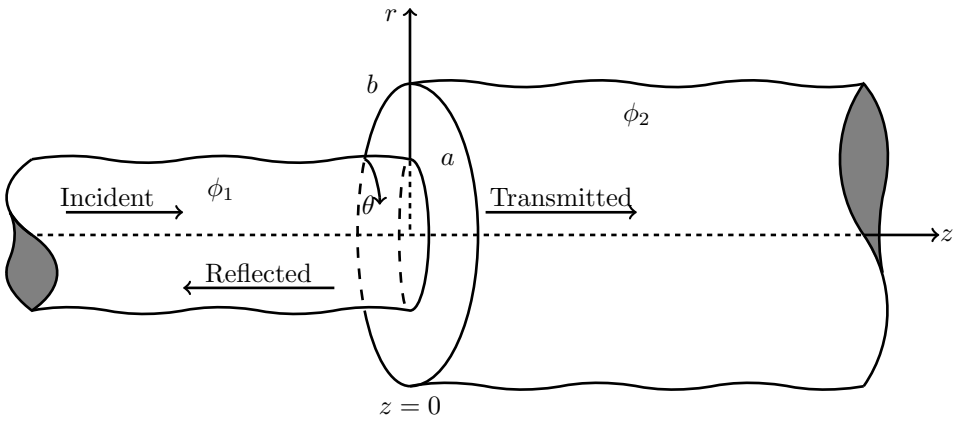

Figure 5.6: Physical configuration of the abrupt increase in radius problem.

in the region $z \leq 0,\ 0 \leq r \leq a$ comprises the forcing wave and the wave reflected at the junction, which is

$$\phi_1(r,\theta,z) = F_{1\ell}J_1(\kappa_{1\ell}r)\cos(\theta)e^{is_{1\ell}z} + \sum_{q=0}^{\infty} A_{1q}J_1(\kappa_{1q}r)\cos(\theta)e^{-is_{1q}z},\ 0 \leq r \leq a,\ z \leq 0, \tag{5.102}$$

where ℓ indicates the chosen mode to force with ($\ell = 0$ for the initial real mode or $\ell = 1$ for the first cut-on mode in the left-hand shell), $F_{1\ell}$ is the amplitude of the forcing wave given in (5.78), A_{1q} is the amplitude of the qth reflected mode, s_{1q} are the wavenumbers and $\kappa_{1q} = (1 - s_{1q}^2)^{1/2}$. The longitudinal, circumferential and radial shell displacements in eigenfunction form for the left-hand shell are found by substituting the velocity potential (5.102) into (5.24), (5.25) and using $w = i\phi_r$. It follows that

$$\begin{aligned}
u_1(\theta,z) &= U(s_{1\ell})F_{1\ell}J_1(\kappa_{1\ell}a)\cos(\theta)e^{is_{1\ell}z} - \sum_{q=0}^{\infty} U(s_{1q})A_{1q}J_1(\kappa_{1q}a)\cos(\theta)e^{-is_{1q}z},\\
v_1(\theta,z) &= V(s_{1\ell})F_{1\ell}J_1(\kappa_{1\ell}a)\sin(\theta)e^{is_{1\ell}z} + \sum_{q=0}^{\infty} V(s_{1q})A_{1q}J_1(\kappa_{1q}a)\sin(\theta)e^{-is_{1q}z},\\
w_1(\theta,z) &= -F_{1\ell}\kappa_{1\ell}J_1(\kappa_{1\ell}a)\cos(\theta)e^{is_{1\ell}z} - \sum_{q=0}^{\infty} A_{1q}\kappa_{1q}J_1(\kappa_{1q}a)\cos(\theta)e^{-is_{1q}z}.
\end{aligned} \tag{5.103}$$

The velocity potential in the region $z \geq 0,\ 0 \leq r \leq b$ contains those waves which are transmitted through the junction, that is

$$\phi_2(r,\theta,z) = \sum_{q=0}^{\infty} B_{1q}J_1(\gamma_{1q}r)\cos(\theta)e^{i\eta_{1q}z},\ 0 \leq r \leq b,\ z \geq 0, \tag{5.104}$$

where B_{1q} is the amplitude of the qth transmitted mode, η_{1q} are the roots of the dispersion function in the right-hand shell and $\gamma_{1q} = (1 - \eta_{1q}^2)^{1/2}$. The longitudinal, circumferential

and radial shell displacements in eigenfunction form for the left-hand shell are found by substituting the velocity potential (5.104) into (5.24), (5.25) and using $w = i\phi_r$. It follows that

$$\begin{aligned} u_2(\theta, z) &= \sum_{q=0}^{\infty} U(\eta_{1q}) B_{1q} J_1(\gamma_{1q} b) \cos(\theta) e^{i\eta_{1q} z}, \\ v_2(\theta, z) &= \sum_{q=0}^{\infty} V(\eta_{1q}) B_{1q} J_1(\gamma_{1q} b) \sin(\theta) e^{i\eta_{1q} z}, \\ w_2(\theta, z) &= \sum_{q=0}^{\infty} B_{1q} \gamma_{1q} J_1(\gamma_{1q} b) \cos(\theta) e^{i\eta_{1q} z}. \end{aligned} \tag{5.105}$$

In the region $z = 0,\ 0 \leq r \leq a$ the pressure is continuous, this leads to the expression

$$\phi_1(r, \theta, z) = \phi_2(r, \theta, z),\ z = 0,\ 0 \leq r \leq a. \tag{5.106}$$

The velocity potentials (5.102) and (5.104) are substituted into the above equation to give

$$F_{1\ell} J_1(\kappa_{1\ell} r) + \sum_{q=0}^{\infty} A_{1q} J_1(\kappa_{1q} r) = \sum_{q=0}^{\infty} B_{1q} J_1(\gamma_{1q} r),\ 0 \leq r \leq a. \tag{5.107}$$

The above equation is multiplied through by $\alpha J_1(\kappa_{1p} r)/a$ and integrated with respect to $r,\ 0 \leq r \leq a$, to find

$$\frac{\alpha F_{1\ell}}{a} \int_0^a J_1(\kappa_{1p} r) J_1(\kappa_{1\ell} r) r \mathrm{d}r + \frac{\alpha}{a} \sum_{q=0}^{\infty} A_{1q} \int_0^a J_1(\kappa_{1p} r) J_1(\kappa_{1q} r) r \mathrm{d}r = \sum_{q=0}^{\infty} \frac{\alpha B_{1q} R_{pq}}{a}, \tag{5.108}$$

where

$$R_{pq} = \int_0^a J_1(\kappa_{1p} r) J_1(\gamma_{1q} r) r \mathrm{d}r. \tag{5.109}$$

The generalised orthogonality relation in (5.45) is used to reduce the integrals on the left-hand side of (5.108) and on rearranging, the first coupled equation is found as

$$\begin{aligned} A_{1p} = &-F_{1\ell}\delta_{\ell p} + \frac{G_1^{(6)}(s_{1p}) J_1'(\kappa_{1p} a)}{C_{1p} Q_1(s_{1p})} E_0 + \frac{G_1^{(4)}(s_{1p}) J_1'(\kappa_{1p} a)}{C_{1p} Q_1(s_{1p})} E_1 + \frac{G_1^{(2)}(s_{1p}) J_1'(\kappa_{1p} a)}{C_{1p} Q_1(s_{1p})} E_2 \\ &+ \frac{G_1^{(0)}(s_{1p}) J_1'(\kappa_{1p} a)}{C_{1p} Q_1(s_{1p})} E_3 + \sum_{q=0}^{\infty} \frac{\alpha B_{1q} R_{pq}}{a C_{1p}}, \end{aligned} \tag{5.110}$$

where $G_1^{(n)}(s_{1p}),\ n = 0, 2, 4, 6$ are the corresponding coefficients for the nth degree of $G_1(s_{1p}, \cdot)$ given in (5.51) and $E_0 - E_3$ are constants which are determined by applying the edge conditions that describe how the left-hand shell connects to the annular disc.

The normal component of velocity should be continuous in the region $z = 0,\ 0 \leq r \leq a$

and zero on the annular disc in the region $z = 0,\ a \leq r \leq b$, which leads to

$$\frac{\partial \phi_2}{\partial z}(r,0) = \begin{cases} \frac{\partial \phi_1}{\partial z}(r,0), & z = 0,\ 0 \leq r \leq a \\ 0, & z = 0,\ a \leq r \leq b \end{cases}. \tag{5.111}$$

The velocity potentials (5.102) and (5.104) are substituted into the above equation to give

$$\sum_{q=0}^{\infty} B_{1q}\eta_{1q}J_1(\gamma_{1q}r) = F_{1\ell}s_{1\ell}J_1(\kappa_{1\ell}r) - \sum_{q=0}^{\infty} A_{1q}s_{1q}J_1(\kappa_{1q}r),\ 0 \leq r \leq a. \tag{5.112}$$

The above expression is multiplied through by $\alpha J_1(\gamma_{1p}r)r/b$ and integrated with respect to $r,\ 0 \leq r \leq b$ to find

$$\sum_{q=0}^{\infty} B_{1q}\eta_{1q}\frac{\alpha}{b}\int_0^b J_1(\gamma_{1p}r)J_1(\gamma_{1q}r)r\mathrm{d}r = \frac{\alpha F_{1\ell}s_{1\ell}R_{\ell p}}{b} - \sum_{q=0}^{\infty}\frac{\alpha A_{1q}s_{1q}R_{qp}}{b}. \tag{5.113}$$

The orthogonality relation in (5.52) is used to find the left-hand side of the expression in (5.113) and after rearranging, the second coupled equation is found as

$$\begin{aligned} B_{1p} = {} & \frac{G_1^{(6)}(\eta_{1p})J_1'(\gamma_{1p}b)}{\eta_{1p}D_{1p}Q_1(\eta_{1p})}E_4 + \frac{G_1^{(4)}(\eta_{1p})J_1'(\gamma_{1p}b)}{\eta_{1p}D_{1p}Q_1(\eta_{1p})}E_5 + \frac{G_1^{(2)}(\eta_{1p})J_1'(\gamma_{1p}b)}{\eta_{1p}D_{1p}Q_1(\eta_{1p})}E_6 \\ & + \frac{G_1^{(0)}(\eta_{1p})J_1'(\gamma_{1p}b)}{\eta_{1p}D_{1p}Q_1(\eta_{1p})}E_7 + \frac{\alpha F_{1\ell}s_{1\ell}R_{\ell p}}{b\eta_{1p}D_{1p}} - \sum_{q=0}^{\infty}\frac{A_{1q}s_{1q}R_{qp}}{b\eta_{1p}D_{1p}}, \end{aligned} \tag{5.114}$$

where $G_1^{(n)}(\eta_{1p}),\ n = 0, 2, 4, 6$ are the corresponding coefficients for the nth degree of $G_1(\eta_{1p}, \cdot)$ given in (5.51) and $E_4 - E_7$ are constants which are determined by applying the edge conditions that describe how the right section of the shell connects to the annular disc.

The constants $E_0 - E_7$ in equations (5.110) and (5.114) are found by applying edge conditions which describe how the shells are connected to the rigid annulus at the matching interface. These conditions can be written in the form

$$\sum_{p=0}^{\infty} A_{1p}\psi_{pn}^{(\mathrm{a})} + \sum_{p=0}^{\infty} B_{1p}\psi_{pn}^{(b)} + F_{1\ell}\psi_n^{(\mathrm{f})} = 0,\ \text{for } n = 0, 1, 2, \ldots, 7, \tag{5.115}$$

where $n = 0, 1, 2, 3$ refer to conditions applied to the left-hand shell edge and $n = 4, 5, 6, 7$ refer to conditions applied at the right-hand shell edge. To apply the left-hand conditions,

(5.110) is multiplied by $\psi_{pn}^{(\mathrm{a})}$, and on summing over p it is found that

$$
\begin{aligned}
&-\sum_{p=0}^{\infty} F_{1\ell}\delta_{\ell p}\psi_{pn}^{(\mathrm{a})} + \sum_{p=0}^{\infty} \frac{G_1^{(6)}(s_{1p})J_1'(\kappa_{1p}a)\psi_{pn}^{(\mathrm{a})}}{C_{1p}Q_1(s_{1p})}E_0 + \frac{G_1^{(4)}(s_{1p})J_1'(\kappa_{1p}a)\psi_{pn}^{(\mathrm{a})}}{C_{1p}Q_1(s_{1p})}E_1 \\
&+\sum_{p=0}^{\infty} \frac{G_1^{(2)}(s_{1p})J_1'(\kappa_{1p}a)\psi_{pn}^{(\mathrm{a})}}{C_{1p}Q_1(s_{1p})}E_2 + \sum_{p=0}^{\infty} \frac{G_1^{(0)}(s_{1p})J_1'(\kappa_{1p}a)\psi_{pn}^{(\mathrm{a})}}{C_{1p}Q_1(s_{1p})}E_3 \\
&+\sum_{p=0}^{\infty}\sum_{q=0}^{\infty} \frac{\alpha B_{1q}R_{pq}\psi_{pn}^{(\mathrm{a})}}{aC_{1p}} = -\sum_{p=0}^{\infty} B_{1p}\psi_{pn}^{(b)} - F_{1\ell}\psi_n^{(\mathrm{f})},\ n=0,1,2,3. \qquad (5.116)
\end{aligned}
$$

Similarly for the right-hand edge conditions (5.114) is multiplied by $\psi_{pn}^{(\mathrm{b})}$, and on summing over p it is found that

$$
\begin{aligned}
&\sum_{p=0}^{\infty} \frac{G_1^{(6)}(\eta_{1p})J_1'(\gamma_{1p}b)\psi_{pn}^{(\mathrm{b})}}{\eta_{1p}D_{1p}Q_1(\eta_{1p})}E_4 + \sum_{p=0}^{\infty} \frac{G_1^{(4)}(\eta_{1p})J_1'(\gamma_{1p}b)\psi_{pn}^{(\mathrm{b})}}{\eta_{1p}D_{1p}Q_1(\eta_{1p})}E_5 + \sum_{p=0}^{\infty} \frac{G_1^{(2)}(\eta_{1p})J_1'(\gamma_{1p}b)\psi_{pn}^{(\mathrm{b})}}{\eta_{1p}D_{1p}Q_1(\eta_{1p})}E_6 \\
&+\sum_{p=0}^{\infty} \frac{G_1^{(0)}(\eta_{1p})J_1'(\gamma_{1p}b)\psi_{pn}^{(\mathrm{b})}}{\eta_{1p}D_{1p}Q_1(\eta_{1p})}E_7 + \sum_{p=0}^{\infty} \frac{\alpha F_{1\ell}s_{1\ell}R_{\ell p}\psi_{pn}^{(\mathrm{b})}}{b\eta_{1p}D_{1p}} - \sum_{p=0}^{\infty}\sum_{q=0}^{\infty} \frac{A_{1q}s_{1q}R_{qp}\psi_{pn}^{(\mathrm{b})}}{b\eta_{1p}D_{1p}} \\
&= -\sum_{p=0}^{\infty} A_{1p}\psi_{pn}^{(\mathrm{a})} - F_{1\ell}\psi_n^{(\mathrm{f})},\ n=4,5,6,7. \qquad (5.117)
\end{aligned}
$$

The expressions for $\psi_{pn}^{(\mathrm{a})}$, $\psi_{pn}^{(\mathrm{b})}$ and $\psi_p^{(\mathrm{f})}$ are found from eigenfunction expansions of the edge conditions for clamped edges these are as given in (5.118) and for pin-jointed edges these are as given in (5.121). The results presented for this problem are created in Matlab with the code presented in Appendix L. This has been done using 100 modes to calculate the amplitudes of the propagating waves. This is shown to be more than sufficient in the verification subsection that follows.

5.3.1 Clamped edges

On using the displacements given in (5.103) and (5.105), the clamped edge conditions given (3.26) lead to

$$\begin{aligned}
&\psi_{p0}^{(\mathrm{a})} = U(s_{1p})\kappa_{1p}J_1'(\kappa_{1p}a), && \psi_{p0}^{(\mathrm{b})} = 0, && \psi_0^{(\mathrm{f})} = -U(s_{1\ell})\kappa_{1\ell}J_1'(\kappa_{1\ell}a),\\
&\psi_{p1}^{(\mathrm{a})} = V(s_{1p})\kappa_{1p}J_1'(\kappa_{1p}a), && \psi_{p1}^{(\mathrm{b})} = 0, && \psi_1^{(\mathrm{f})} = V(s_{1\ell})\kappa_{1\ell}J_1'(\kappa_{1\ell}a),\\
&\psi_{p2}^{(\mathrm{a})} = \kappa_{1p}J_1'(\kappa_{1p}a), && \psi_{p2}^{(\mathrm{b})} = 0, && \psi_2^{(\mathrm{f})} = -\kappa_{1\ell}J_1'(\kappa_{1\ell}a),\\
&\psi_{p3}^{(\mathrm{a})} = s_{1p}\kappa_{1p}J_1'(\kappa_{1p}a), && \psi_{p3}^{(\mathrm{b})} = 0, && \psi_3^{(\mathrm{f})} = -s_{1\ell}\kappa_{1\ell}J_1'(\kappa_{1\ell}a),\\
&\psi_{p4}^{(\mathrm{b})} = U(\eta_{1p})\gamma_{1p}J_1'(\gamma_{1p}b), && \psi_{p4}^{(\mathrm{a})} = 0, && \psi_4^{(\mathrm{f})} = 0,\\
&\psi_{p5}^{(\mathrm{b})} = V(\eta_{1p})\gamma_{1p}J_1'(\gamma_{1p}b), && \psi_{p5}^{(\mathrm{a})} = 0, && \psi_5^{(\mathrm{f})} = 0,\\
&\psi_{p6}^{(\mathrm{b})} = \gamma_{1p}J_1'(\gamma_{1p}b), && \psi_{p6}^{(\mathrm{a})} = 0, && \psi_6^{(\mathrm{f})} = 0,\\
&\psi_{p7}^{(\mathrm{b})} = \eta_{1p}\gamma_{1p}J_1'(\gamma_{1p}b), && \psi_{p7}^{(\mathrm{a})} = 0, && \psi_7^{(\mathrm{f})} = 0.
\end{aligned} \tag{5.118}$$

The values of $E_0 - E_7$ are found by truncating and solving equations (5.116) and (5.117) using the above values of ψ. Coupled equations are obtained by using $E_0 - E_3$ in equation (5.110) and $E_4 - E_7$ in equation (5.114). These equations are then truncated and solved to give the pth amplitude A_p of the reflected field and the pth amplitude B_p of the transmitted field. The energy entering the system $\mathcal{E}_{\mathrm{F}}$ is due to the wave incident in the z direction, which has unit energy. The energy leaving the system comprises the energy of the reflected field $\mathcal{E}_{\mathrm{A}}$ and the energy of the transmitted field $\mathcal{E}_{\mathrm{B}}$. The energy associated with the reflected and transmitted fields are as given in (2.41) and (2.42) which are stated below:

$$\mathcal{E}_{\mathrm{A}} = \frac{a}{\alpha}\mathrm{Real}\left[\sum_{p=0}^{P}|A_{1p}|^2 s_{1p}C_{1p}\right], \tag{5.119}$$

where A_{1p} are the amplitudes of the reflected waves and

$$\mathcal{E}_{\mathrm{B}} = \frac{b}{\alpha}\mathrm{Real}\left[\sum_{m=0}^{P}|B_{1p}|^2 \eta_{1p}D_{1p}\right], \tag{5.120}$$

where B_{1p} are the amplitudes of the transmitted waves.

The first configuration considers the radius of the left-hand shell to be equal to that of the right-hand shell. The energy radiated at the edge, with no change of radius, ie. for $\bar{a} = 0.2$m and $\bar{b} = 0.2$m is shown in Figure 5.7. For a shell of radius $\bar{a} = 0.2$m the first cut-on occurs at 508Hz and further cut-ons occur outside the considered frequency range. When forcing with the second-mode, the resulting energy will be considered from 508Hz as evanescent modes do not carry energy before they cut-on.

Figure 5.7a shows the energy radiated when the first mode is used in the forcing waved ($\ell = 0$). Below the first cut-on the energy is totally reflected. After which the energies

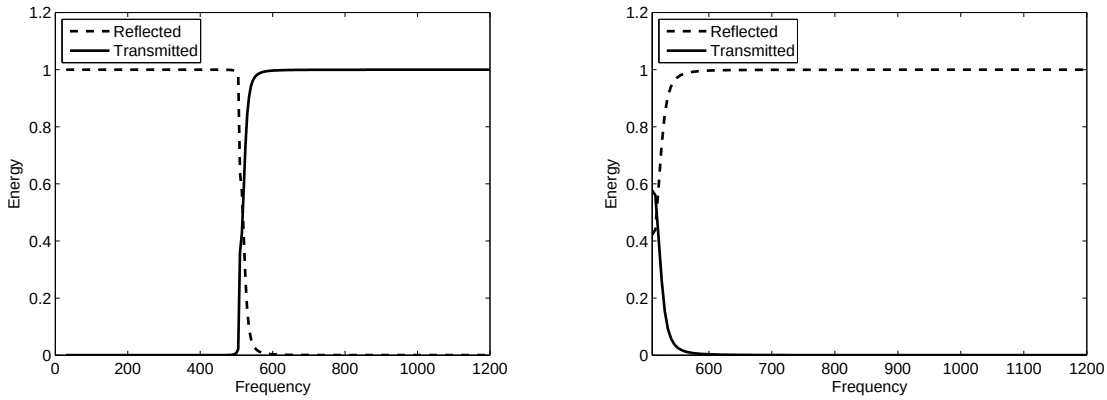

Figure 5.7: Energy output for no change in radius with clamped edges $m = 1$: a) $\bar{a} = 0.2$m, $\bar{b} = 0.2$m, $\ell = 0$; b) $\bar{a} = 0.2$m, $\bar{b} = 0.2$m, $\ell = 1$.

are inverted and the energy is totally reflected for remaining frequencies.

The energy radiated when forcing with the second mode ($\ell = 1$) in the amplitude of the forcing wave is shown in Figure 5.7b. The reflected energy increases from 40% until total reflection is achieved at 630Hz and it continues to be totally reflected for the remaining frequency range.

The next configuration considers the radius of the right-hand shell to be increased. The left-hand shell is kept at $\bar{a} = 0.2$m while the right-hand shell is increased to $\bar{b} = 0.28$m. The energy radiated at the abrupt increase in radius is shown in Figure 5.8. For a shell of radius $\bar{b} = 0.28$m the cut-ons in the frequency range occur at 365Hz and 1043Hz.

The first mode is used in the amplitude of the forcing wave ($\ell = 0$) and the energy radiated at the abrupt increase in radius is shown in Figure 5.8a. The energy is total reflected below the first cut-on from the larger shell at 365Hz. After the cut-on, the reflected energy slowly falls away until reaching the cut-on from the smaller shell at 508Hz. The reflected energy then drops suddenly and hovers around 30% before suddenly increasing at the frequency for the second cut-on from the larger shell at 1043Hz. The reflected energy finally drops away for the remainder of the frequency range.

The energy radiated at the abrupt increase in radius when the second mode is used in the forcing wave ($\ell = 1$) is shown in Figure 5.8b. The results are only valid after the mode has cut-on at 508Hz. The reflected energy begins by dipping and increasing until total reflected energy is achieved at 630Hz. The energy continues to be totally reflected for the remaining frequency range.

The final configuration considers the radius of the left-hand shell to be significantly smaller than the radius of the right-hand shell. The radius of the left-hand shell is reduced to $\bar{a} = 0.06$m while the radius of the right-hand shell is maintained at $\bar{b} = 0.28$m. The energy radiated at the abrupt increase in radius is shown in Figure (5.9) where the first mode is used in the amplitude of the forcing wave ($\ell = 0$). It is seen that the energy is

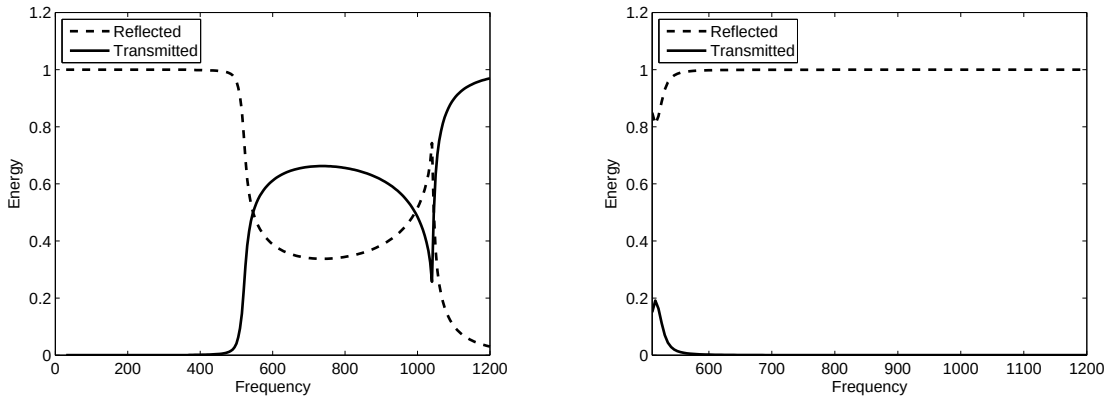

a) b)

Figure 5.8: Energy output for the abrupt increase in radius with clamped edges $m = 1$: a) $\bar{a} = 0.2$m, $\bar{b} = 0.28$m, $\ell = 0$; b) $\bar{a} = 0.2$m, $\bar{b} = 0.28$m, $\ell = 1$.

completely reflected for the entire frequency range and is unaffected by the cut-ons from the larger shell at 365Hz and 1043Hz. This is in keeping with the result that the energy is totally reflected as $k\bar{a} = a \to 0$.

The amplitude of the forcing wave comprising the first cut-on mode ($\ell = 1$) does not exist in the considered frequency range and so results using this mode are not possible.

5.3.2 Pin-jointed edges

On using the displacements given in (5.103) and (5.105), the clamped edge conditions given (3.27) lead to

$$\begin{aligned}
&\psi_{p0}^{(\mathrm{a})} = U(s_{1p})s_{1p}\kappa_{1p}J_1'(\kappa_{1p}a), && \psi_{p0}^{(\mathrm{b})} = 0, && \psi_0^{(\mathrm{f})} = U(s_{1\ell})s_{1\ell}\kappa_{1\ell}J_1'(\kappa_{1\ell}a),\\
&\psi_{p1}^{(\mathrm{a})} = V(s_{1p})\kappa_{1p}J_1'(\kappa_{1p}a), && \psi_{p1}^{(\mathrm{b})} = 0, && \psi_1^{(\mathrm{f})} = V(s_{1\ell})\kappa_{1\ell}J_1'(\kappa_{1\ell}a),\\
&\psi_{p2}^{(\mathrm{a})} = \kappa_{1p}J_1'(\kappa_{1p}a), && \psi_{p2}^{(\mathrm{b})} = 0, && \psi_2^{(\mathrm{f})} = -\kappa_{1\ell}J_1'(\kappa_{1\ell}a),\\
&\psi_{p3}^{(\mathrm{a})} = s_{1p}^2\kappa_{1p}J_1'(\kappa_{1p}a), && \psi_{p3}^{(\mathrm{b})} = 0, && \psi_3^{(\mathrm{f})} = -s_{1\ell}^2\kappa_{1\ell}J_1'(\kappa_{1\ell}a),\\
&\psi_{p4}^{(\mathrm{b})} = U(\eta_{1p})\gamma_{1p}J_1'(\gamma_{1p}b), && \psi_{p4}^{(\mathrm{a})} = 0, && \psi_4^{(\mathrm{f})} = 0,\\
&\psi_{p5}^{(\mathrm{b})} = V(\eta_{1p})\gamma_{1p}J_1'(\gamma_{1p}b), && \psi_{p5}^{(\mathrm{a})} = 0, && \psi_5^{(\mathrm{f})} = 0,\\
&\psi_{p6}^{(\mathrm{b})} = \gamma_{1p}J_1'(\gamma_{1p}b), && \psi_{p6}^{(\mathrm{a})} = 0, && \psi_6^{(\mathrm{f})} = 0,\\
&\psi_{p7}^{(\mathrm{b})} = \eta_{1p}^2\gamma_{1p}J_1'(\gamma_{1p}b), && \psi_{p7}^{(\mathrm{a})} = 0, && \psi_7^{(\mathrm{f})} = 0.
\end{aligned} \tag{5.121}$$

The method of solving to find the amplitudes of the reflected and transmitted fields is analogous to that used for the clamped edges, but replacing values of ψ with those stated above. The energy equations are then as given by (2.41) and (2.42), these are stated below for convenience:

$$\mathcal{E}_{\mathrm{A}} = \frac{a}{\alpha}\mathrm{Real}\left[\sum_{p=0}^{P}|A_{1p}|^2 s_{1p}C_{1p}\right], \tag{5.122}$$

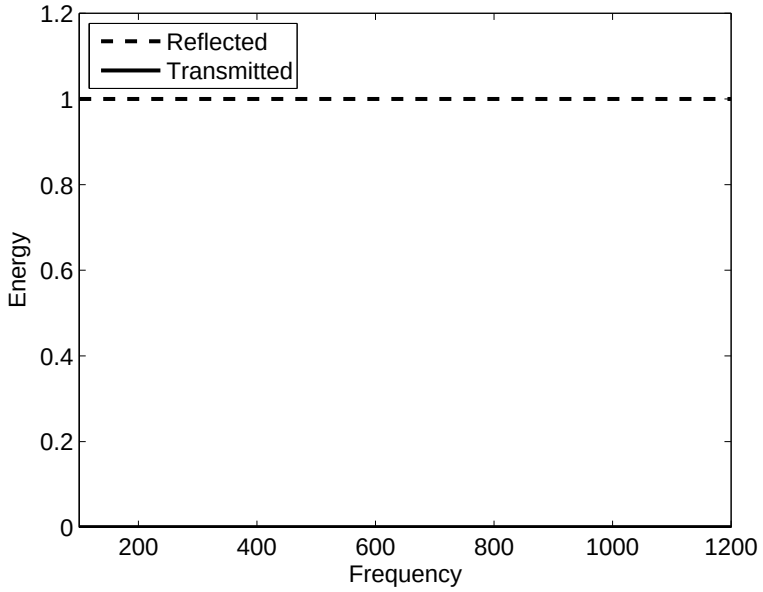

Figure 5.9: Energy output for the abrupt increase in radius with clamped edges $m = 1$, $\bar{a} = 0.06$m, $\bar{b} = 0.28$m, $\ell = 0$.

where A_{1p} are the amplitudes of the reflected waves and

$$\mathcal{E}_{\mathrm{B}} = \frac{b}{\alpha}\mathrm{Real}\left[\sum_{p=0}^{P}|B_{1p}|^2\eta_{1p}D_{1p}\right], \tag{5.123}$$

where B_{1p} are the amplitudes of the transmitted waves.

The first configuration considers the radius of the left-hand shell to be equal to that of the right-hand shell. The energy radiated at the no change of radius for $\bar{a} = 0.2$m and $\bar{b} = 0.2$m is shown in Figure 5.10. For a shell of radius $\bar{a} = 0.2$m the first cut-on occurs at 508Hz and further cut-ons occur outside the considered frequency range. When forcing with the second-mode, the resulting energy will be considered from 508Hz.

Figure 5.10a shows the energy radiated when the first mode is used in the forcing waved ($\ell = 0$). Below the first cut-on the energy is totally reflected. After which there is an inversion of the energies it is totally reflected for remaining frequencies.

The energy radiated when forcing with the second mode in the amplitude of the forcing wave is shown in Figure 5.10b. The reflected energy increases from 40% until total reflection is achieved at 630Hz and it continues to be totally reflected for the remaining frequency range.

The next configuration considers the radius of the right-hand shell to be increased. The left-hand shell is maintained at $\bar{a} = 0.2$m while the right-hand shell is increased to $\bar{b} = 0.28$m. The energy radiated at the abrupt increase in radius is shown in Figure 5.11. For a shell of radius $\bar{b} = 0.28$m the cut-ons in the frequency range occur at 365Hz and 1043Hz.

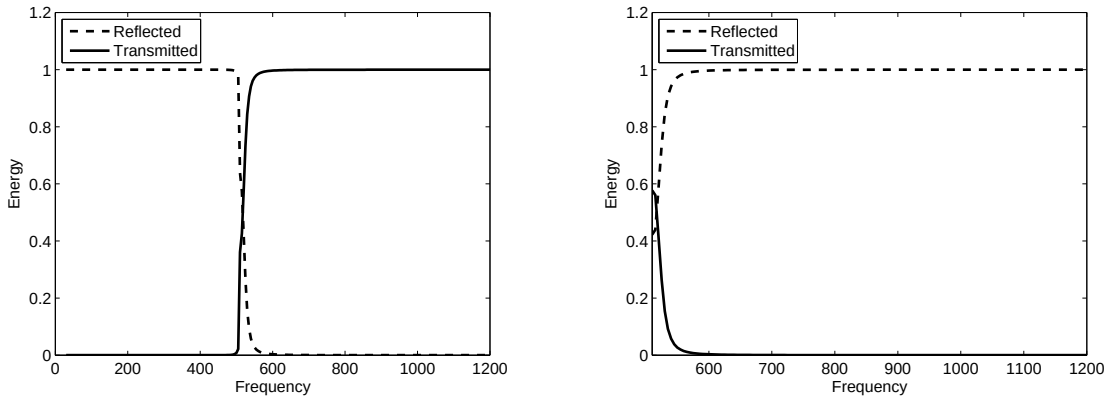

Figure 5.10: Energy output for no change in radius with pin-jointed edges $m = 1$: a) $\bar{a} = 0.2$m, $\bar{b} = 0.2$m, $\ell = 0$; b) $\bar{a} = 0.2$m, $\bar{b} = 0.2$m, $\ell = 1$.

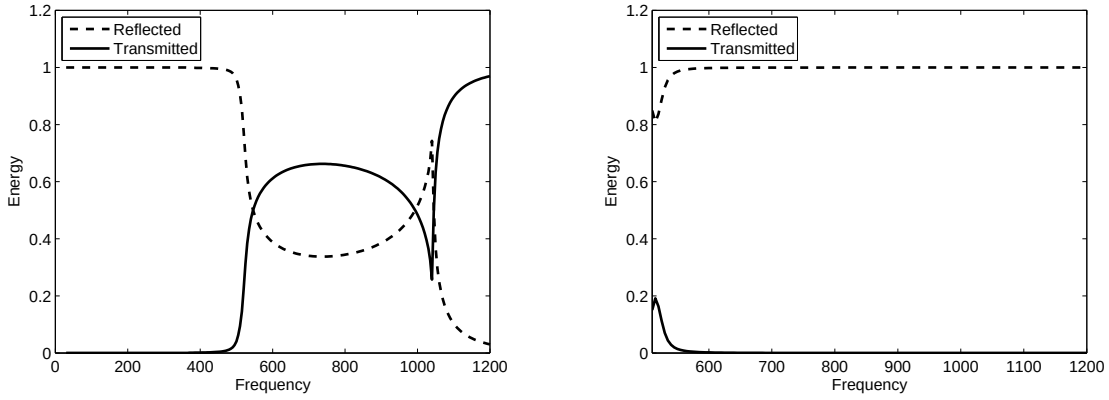

Figure 5.11: Energy output for the abrupt increase in radius with pin-jointed edges $m = 1$: a) $\bar{a} = 0.2$m, $\bar{b} = 0.28$m, $\ell = 0$; b) $\bar{a} = 0.2$m, $\bar{b} = 0.28$m, $\ell = 1$.

The first mode is used in the amplitude of the forcing wave ($\ell = 0$) and the energy radiated at the abrupt increase in radius is shown in Figure 5.11a. The energy is total reflected below the first cut-on from the larger shell at 365Hz. After this cut-on, the reflected energy slowly falls away until the cut-on frequency from the smaller shell at 508Hz is reached. The reflected energy then drops suddenly and hovers around 30% before suddenly increasing at the frequency for the second cut-on from the larger shell at 1043Hz. The reflected energy finally drops away for the remainder of the frequency range.

The energy radiated at the abrupt increase in radius when the second mode is used in the forcing wave ($\ell = 1$) is shown in Figure 5.11b. The results are only valid after the mode has cut-on at 508Hz. The reflected energy begins by dipping and increasing until total reflected energy is achieved at 630Hz. The energy continues to be totally reflected for the remaining frequency range.

The final configuration considers the radius of the left-hand shell to be significantly

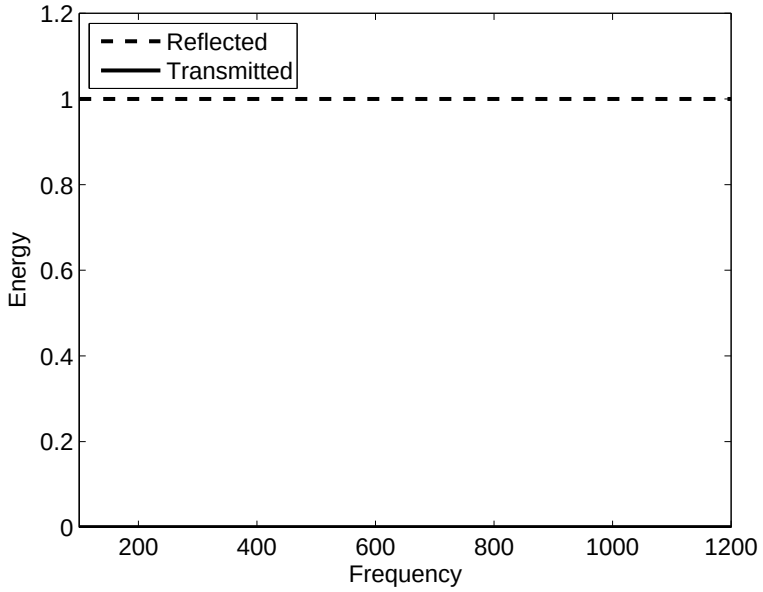

Figure 5.12: Energy output for the abrupt increase in radius with pin-jointed edges $m = 1$, $\bar{a} = 0.06$m, $\bar{b} = 0.28$m, $\ell = 0$.

smaller than the radius of the right-hand shell. The radius of the left-hand shell is reduced to $\bar{a} = 0.06$m while the radius of the right-hand shell is maintained at $\bar{b} = 0.28$m. The energy radiated at the abrupt increase in radius is shown in Figure (5.12) where the first mode is used in the amplitude of the forcing wave ($\ell = 0$). It is seen that the energy is completely reflected for the entire frequency range and is unaffected by the cut-ons from the larger shell at 365Hz and 1043Hz.

5.3.3 Verification of results

It is necessary to check the matching conditions are satisfied, this will ensure that the results are correct and that the amplitudes have been formed with a sufficient amount of modes. This will be done for the configuration which has $\bar{a} = 0.2$m, $\bar{b} = 0.28$m with first mode forcing and clamped edges, which correspond to the results of Figure 5.8a. The matching condition for pressure is (5.112) which is presented for $q = 1$ against the non-dimensional radius of the shell for 10 modes at 780Hz in Figure 5.13. It is seen that although the real part of the pressure shows a good agreement between the two sides, it does not match well at the edge of the shell. Also the imaginary part of the pressure condition shows a poor agreement between the two sides. This shows that 10 modes does not find sufficiently accurate amplitudes, therefore additional modes must be considered. The matching condition for pressure is now presented for 60 modes at 780Hz against the non-dimensional radius of the shell in Figure 5.14. With 60 it is seen that there is an excellent match between the two sides of the pressure condition for both real and imaginary parts. It is left to check that the matching condition for the normal

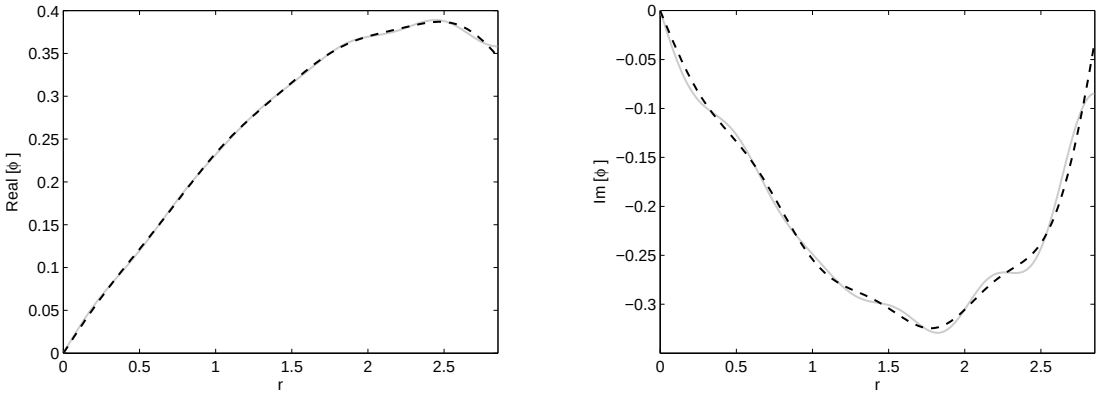

a) b)

Figure 5.13: The two sides of the pressure matching condition for 10 modes with $\bar{a} = 0.2$m, $\bar{b} = 0.28$m (dashed line: left side of the condition, solid line: right side of the condition) a) Real; b) Imaginary.

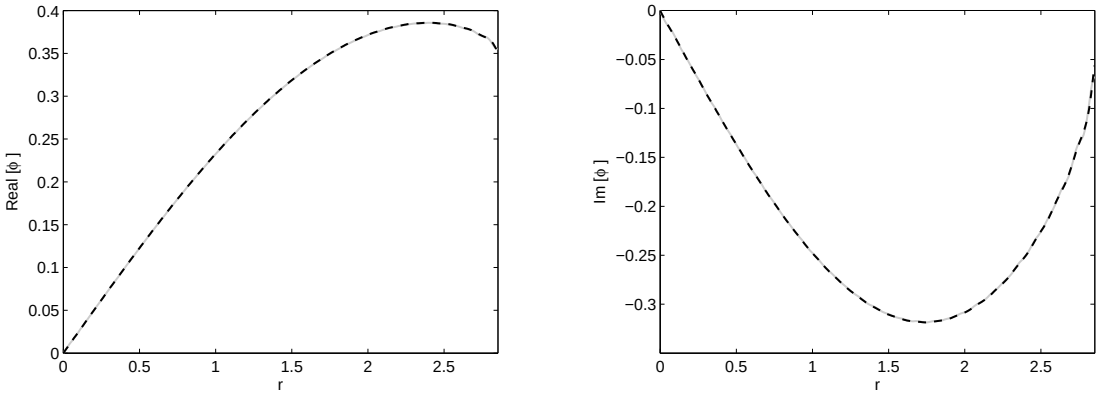

a) b)

Figure 5.14: The two sides of the pressure matching condition for 60 modes with $\bar{a} = 0.2$m, $\bar{b} = 0.28$m (dashed line: left side of the condition, solid line: right side of the condition) a) Real; b) Imaginary.

component of velocity is satisfied. Again this is done for 10 modes at 780Hz and the results for the real and imaginary parts are presented in Figure 5.15. These results show a poor match between the two sides of the matching condition and that 10 modes to form the amplitudes is not sufficient. The number of modes is increased to 60 and the results of the two sides of the matching condition are shown in Figure 5.16. There is a better agreement between the two sides of the matching condition when 60 modes are used to formulate the amplitudes, however it still not that great. This is because of a singularity that occurs due to the piecewise definition of the normal component of velocity condition i.e. it is continuous in the fluid, but zero of the rigid annular disc. The velocity flux should be considered as the integration smooths out this singularity. The matching condition

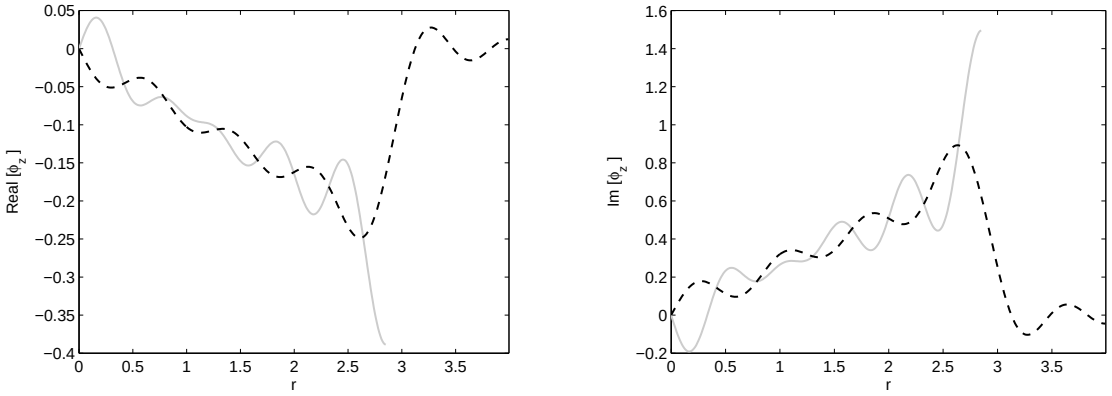

a) b)

Figure 5.15: The two sides of the normal component of velocity matching condition for 10 modes with $\bar{a} = 0.2$m, $\bar{b} = 0.28$m (dashed line: left side of the condition, solid line: right side of the condition) a) Real; b) Imaginary.

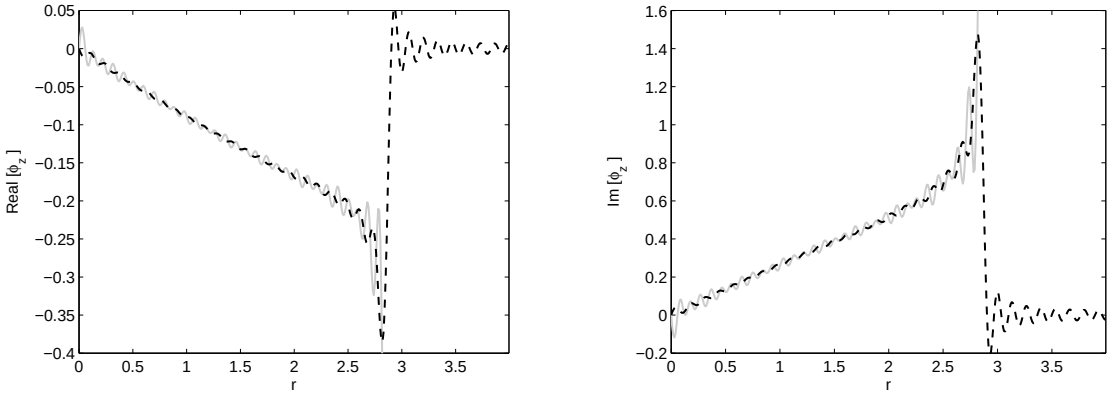

a) b)

Figure 5.16: The two sides of the normal component of velocity matching condition for 60 modes with $\bar{a} = 0.2$m, $\bar{b} = 0.28$m (dashed line: left side of the condition, solid line: right side of the condition) a) Real; b) Imaginary.

for the velocity flux is

$$\frac{ia^2 F_{1\ell} s_{1\ell} J_2(\kappa_{1\ell} a)}{\kappa_{1\ell}} - ia^2 \sum_{q=0}^{\infty} \frac{A_{1q} s_{1q} J_2(\kappa_{1q} a)}{\kappa_{1q}} = ib^2 \sum_{q=0}^{\infty} \frac{B_{1q} \eta_{1q} J_2(\gamma_{1q} b)}{\gamma_{1q}}. \tag{5.124}$$

The two sides of the above equation are presented in Figure 5.17 for 10 modes and in Figure 5.18 for 60 modes. This shows an excellent agreement between the two sides of the equation and it verifies that after smoothing at the singularity the normal component of velocity matching condition is satisfied.

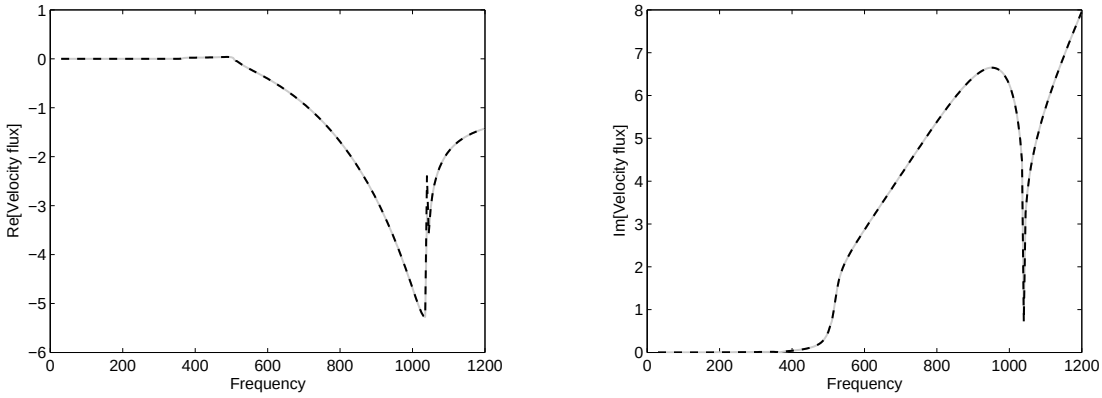

a) b)

Figure 5.17: The two sides of the velocity flux matching condition for 100 modes with $\bar{a} = 0.2$m, $\bar{b} = 0.28$m (dashed line: left side of the condition, solid line: right side of the condition) a) Real; b) Imaginary.

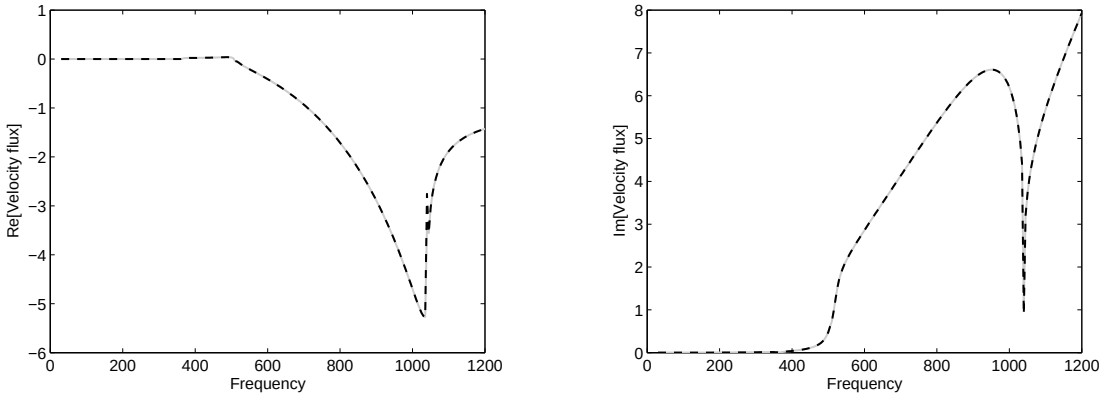

a) b)

Figure 5.18: The two sides of the velocity flux matching condition for 60 modes with $\bar{a} = 0.2$m, $\bar{b} = 0.28$m (dashed line: left side of the condition, solid line: right side of the condition) a) Real; b) Imaginary.

Chapter 6

Conclusions

The research in this thesis finds and analyses the energy radiated due to a piston or wave at the junction of rigid and flexible circular, cylindrical problems. These were solved with the mode matching method combined with a suitable orthogonality relation/ generalised orthogonality relation.

The research in Chapter two used the wave equation to formulate the dispersion relation for a rigid duct. This provided the wavenumbers for the velocity potential and was used to provide a method for deriving the orthogonality relation. This methodology and orthogonality relations is already available in the literature and serves as a foundation for research on flexible shell walls. The definition of power was used to derive expressions for the reflected and transmitted energy and to determine the amplitude of the forcing wave (as unit energy input was assumed). Problems involving a piston sound source and/or an incident wave were investigated and solved to find the radiated energy. The work of Ingard [3] was used to derive an expression for the radiated impedance and to verify the results of one of the considered duct configurations. The results showed that the cut-ons caused the resulting energy and impedance to spike, which is due to the excitation of the evanescent modes by the piston. However for a piston of radius equal to the radius of the duct, the cut-ons had no effect as it is not able to excite further modes. Two problems involving an abrupt change of radius were also considered: an abrupt increase in radius and an expansion chamber situated between two ducts of the same radius. The problem with the abrupt increase in radius was solved by matching the pressure and normal component of velocity at the junction. It was found that with no change in radius, the energy behaved as if it was in a duct of infinite length. When an increase in radius was present it was found that the scattered energy was effected by the cut-ons present in the ducts. When the radius of left-shell was significantly smaller than the right, the energy supported the known result (see for example Levine and Schwinger [2]) that the energy is totally reflect as $k\bar{a} \to 0$. The problem with the expansion chamber between two ducts was broken into two simpler problems featuring a single increase in radius: that is a symmetric and an antisymmetric subproblem. The results showed that

the presence of an expansion chamber causes the energy to oscillate over frequency. This is likely due to the waves bouncing off the internal annular discs present in the chamber. The dips in the oscillations for the reflected power could be determined provided the energy was carried by the fluid-borne mode as $s_0 = 1$. Lastly, a transfer matrix method was applied to the expansion chamber problem using only the first mode of the velocity potentials. The result of this method provided a good estimation of the energies and assisted in verifying the results obtained from the mode matching method.

In Chapter three the Donnell-Mushtari equations of motion were used to derive the dispersion relation for waves propagating within a flexible cylindrical shell. This was used to obtain the wavenumbers of the velocity potential and to derive a suitable generalised orthogonality relation using the method of Chapter two. This generalised orthogonality relation is new to the research area and therefore the mode matching method (being based on the generalised orthogonality relation) used is a novel approach to the problems. Difficulties occurred due to the increasingly oscillatory nature of the dispersion relations; the wavenumbers became increasingly harder to find for high frequencies (especially for the smaller shell radius). Hence the results for the flexible shell were presented up to 1200Hz as beyond this frequency the searching range provided to the Newton-Raphson method must be specified with increasing accuracy. The resulting generalised orthogonality relation was found to comparable to that of rigid duct, but with additional terms. These terms come from the equations of motion and therefore relate to felxible nature of the shell. Analysis into the properties of the eigenfunctions was done by formulating identities which demonstrated the linear dependance. It was found using the work in Lawrie [44] that three such identities existed. These were derived using Cauchy's Residue theorem with an additional four identities and all were numerically demonstrated to be satisfied. Semi-infinite problems forced by a piston and/or wave were considered with both a clamped and pin-jointed edge. The results showed that the energies obtained from pin-jointed edges were the same as those obtained with clamped edges. All plots concerning fluid-borne forcing were found to be similar to the equivalent rigid problem results. This may be due to the choice of material and waveguide values, however these were selected so that there is a balance between a flexible shell that could be used in HVAC ducting. The semi infinite problem with the rigid end plate served to verify the method as in this case the energy could only be reflected. The results of this particular problem serve no practical purpose as the result is commonly known is the research area.

In Chapter four, problems which incorporated a change of radius were considered. These allowed for the generalised orthogonality relation to be used to simplify the equations of matched pressure and normal component of velocity. Again it was found that the results obtained with clamped edges were identical to those obtained with a pin-jointed edge. The results from the abrupt increase in radius problem and expansion chamber problems when forced with the s_0 mode were seen to be similar to those found in the

equivalent rigid problems in Chapter two. A fundamental s_1 mode does not exist in a rigid duct (as the walls are rigid), hence comparisons using this mode could only be made between the axisymmetric increase in radius and expansion chamber problems. The energy carried by individual modes when forcing with s_1 mode was investigated and it was seen that at the cut-on for the larger shell the transmitted energy was carried by the cut-on mode. The results shown in this chapter could be useful towards the design of HVAC ducting as the cut-ons are useful for tuning the frequencies of in-bound fluid and structure borne waves to minimising or maximising the reflected or transmitted energy.

In Chapter five the Donnell-Mushtari equations of motion were used to derive the dispersion relation for waves propagating within a flexible cylindrical shell subject to non-axisymmetric motion. This was used to obtain the wavenumbers of the velocity potential and to derive a suitable generalised orthogonality relation. This generalised orthogonality relation is new to the research area and therefore the mode matching method which was used is a novel approach to the problems. The research in Chapter five presented some interesting results in the form of eigensolutions which could be generated for non-axisymmetric motions. Such solutions were found by comparing the eigenmode form of the matching condition with those identities which demonstrate the linear dependance of the eigenfunctions. There is scope for future work here to understand the significance of such solutions. Limitations were seen in Chapter five due to there being one real mode occurring for low frequencies. The cut-on mode was used where possible, but it was not possible for those frequencies for which a propagating wave had not been cut-on. The results of the abrupt increase of radius problem with non-axisymmetric motion could not be compared to those obtained from equivalent rigid and axisymmetric results as the forcing mode was too different.

The results shown demonstrate that cut-on frequencies would be of key importance for industrial applications. The results of the rigid problems serve as a good estimate for the flexible wall problems, but they are limited to the use of s_0 mode forcing. The results of the flexible-walled problems for the relevant motion would be more accurate as they consider energy being carried in the structure. The generalised orthogonality relations presented are a useful tool for evaluating integrals which occur through the application of the mode matching method. These generalised orthogonality relations could also be used in other solving methods which relate to the motion of flexible walled cylindrical shells (based on the Donnell-Mustari equations of motion).

6.1 Recommendations for future work

Presented in this Chapter are two problems which build on the research presented in this thesis and are recommended for future work. The first problem considers the abrupt increase in radius in Chapter four, but replaces the rigid annular disc with a membrane.

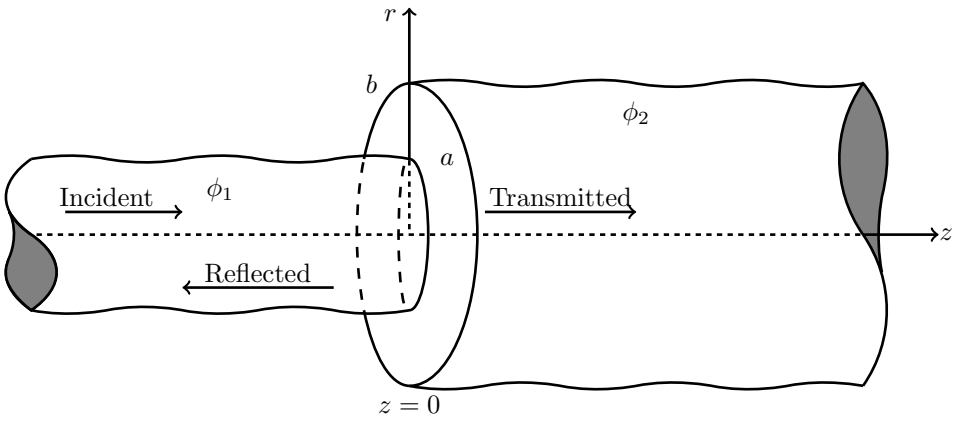

Figure 6.1: Physical configuration of the abrupt increase in radius problem with an annular membrane.

This changes the matching condition at the junction and uses the Galerkin method to match the normal component of velocity to the membrane. This same replacement can also be applied to the expansion chamber problems present in Chapter four. The method for this problem is outlined below. The second problem builds on the non-axisymmetric research presented in Chapter five, by considering expansion chamber situated between two shells of the same radius. The solution method should follow in the same way as that used to solve the rigid expansion chamber problem in Chapter two and the two expansion chamber problems presented in Chapter four.

The analysis of the eigensolutions which arise in Section 5.2 are also left for future work. These eigensolutions demonstrate that for non-axisymmetric motion of order $m = 1$ the solution is potentially coupled to all other orders. Further work is required to understand if and when these eigensolutions are required.

6.1.1 Abrupt increase in radius closed by an annular membrane

The aim here is to determine the energy transmitted due to a forcing wave at an abrupt increase of radius. The problem comprises two semi-infinite shells: the left-hand shell occupies $0 \leq r \leq a,\ z \leq 0$ and the right-hand duct occupies $0 \leq r \leq b,\ z \leq 0$, where $a \leq b$ as shown in Figure 6.1. The problem is closed by an annular membrane in the region $a \leq r \leq b,\ z = 0$. Forcing is by a wave propagating in the positive z direction towards the abrupt increase in radius. The velocity potential ϕ_1 for the left-hand shell is

$$\phi_1(r,z) = F_\ell J_0(\kappa_\ell r)e^{is_\ell z} + \sum_{n=0}^{\infty} A_n J_0(\kappa_n r)e^{-is_n z},\ \ z < 0,\ 0 \leq r \leq a, \tag{6.1}$$

where F is the amplitude of the forcing wave, A_n is the amplitude of the nth reflected wave, s_n are the wavenumbers found using the characteristic equation in Chapter four

and $\kappa_n = (1 - s_n^2)^{1/2}$. The velocity potential for the right-hand shell ϕ_2 is

$$\phi_2(r,z) = \sum_{n=0}^{\infty} B_n J_0(\gamma_n r) e^{i\eta_n z}, \quad z > 0,\ 0 \le r \le b, \tag{6.2}$$

where B_n is the nth amplitude of the transmitted wave, η_n are the wavenumbers found using the characteristic equation in Chapter four (with a shell of radius b) and $\gamma_n = (1 - \eta_n^2)^{1/2}$. At the junction between the two shell sections there is continuity of pressure in the fluid region which is expressed as

$$\phi_1(r,0) = \phi_2(r,0),\ 0 \le r \le a. \tag{6.3}$$

On substituting the velocity potentials (6.1) and (6.2) into the equation for continuity of pressure (6.3) and using the OR to simplify the eigenfunctions in $z < 0$, it is obtained that

$$A_m = -F_\ell \delta_{m\ell} + \frac{\kappa_m J_1(\kappa_m)}{C_m} \left\{ E_0 + \frac{E_1}{s_m^2 - \beta^2} + (\kappa_m^2 - 2) E_2 \right\} + \frac{\alpha}{a} \sum_{n=0}^{\infty} \frac{B_n R_{nm}}{C_m}, \tag{6.4}$$

where

$$R_{nm} = \int_0^a J_0(\gamma_n r) J_0(\kappa_m r) r \mathrm{d}r. \tag{6.5}$$

Constants $E_0 - E_2$ are found from the edge conditions that connect the left shell section to the annular disc. Considering clamped edge conditions, $w_1 = w_{1z} = u_1 = 0$, therefore

$$E_0 = 0, \quad E_j = \frac{1}{\Delta} \left\{ 2F_\ell \Omega_{j\ell} s_\ell \kappa_\ell J_1(\kappa_\ell a) - \frac{\alpha}{a} \sum_{m=0}^{\infty} \sum_{n=0}^{\infty} \frac{B_n \Omega_{jm} R_{mn} s_m \kappa_m J_1(\kappa_m a)}{C_m} \right\}, \quad j = 1, 2, \tag{6.6}$$

where $\Delta = S_1^2 + S_0 S_2$, $\Omega_{jm} = S_j - S_{j-1}/(\beta^2 - s_m^2)$ and

$$S_j = \sum_{n=0}^{\infty} \frac{s_m \kappa_m^2 J_1^2(\kappa_m a)}{(\beta^2 - s_m^2)^j C_m},\ j = 0, 1, 2. \tag{6.7}$$

At the junction the normal component of velocity is continuous in the fluid region and also needs to satisfy the vertical membrane condition

$$w_{rr} + \mu^4 w = \alpha \phi_2 = 0,\ z = 0,\ a \le r \le b, \tag{6.8}$$

where w is the displacement in the radial direction, $\alpha = 12\beta^2 \rho / (\rho_s h^3 k^3)$ and $\mu = c/\sqrt{T/m}$ with fluid sound speed c, tension T and mass per unit area m. Suppose that $w(r)$ may

be expressed as a Fourier series of the form:

$$w(r) = \sum_{n=1}^{\infty} G_n \sin\left(\frac{n\pi(r-a)}{b-a}\right). \tag{6.9}$$

This form automatically satisfies the conditions of zero axial displacement at the edges of the annular disc $w(a) = w(b) = 0$. On substituting the Fourier series expression for the radial displacement of the membrane (6.9) and the eigenfunction expansion (6.2) into the membrane condition (6.8), it is found that

$$\sum_{n=0}^{\infty} G_n \left\{\mu^2 - \frac{n^2\pi^2}{(b-a)^2}\right\} \sin\left(\frac{n\pi(r-a)}{b-a}\right) = \alpha \sum_{n=0}^{\infty} B_n J_0(\gamma_n r). \tag{6.10}$$

This equation can be simplified by using the integral identity given in Brown and Churchill [47] as

$$\int_a^b \sin\left(\frac{n\pi(r-a)}{b-a}\right) \sin\left(\frac{m\pi(r-a)}{b-a}\right) \mathrm{d}r \tag{6.11}$$

$$= \int_0^{b-a} \sin\left(\frac{n\pi v}{b-a}\right) \sin\left(\frac{n\pi v}{b-a}\right) = \frac{b-a}{2}\delta_{mn}. \tag{6.12}$$

The integral identity (6.11) is applied by multiplying (6.10) by $\sin(m\pi(r-a)/(b-a))$ and on integrating with respect to r, $a \le r \le b$, it is found that

$$G_m \left\{\mu^2 - \frac{m^2\pi^2}{(b-a)^2}\right\} = \frac{2\alpha}{b-a} \sum_{n=0}^{\infty} B_n P_{mn} \tag{6.13}$$

where

$$P_{mn} = \int_0^{b-a} J_0(\gamma_n r) \sin\left(\frac{m\pi(r-a)}{b-a}\right) \mathrm{d}r. \tag{6.14}$$

The expression for G_m is found as

$$G_m = \frac{2\alpha}{(b-a)\{\mu^2 - m^2\pi^2/(b-a)^2\}} \sum_{n=0}^{\infty} B_n P_{mn}. \tag{6.15}$$

The condition for the normal component of velocity is given as

$$\frac{\partial \phi_2}{\partial z}(r,0) = \begin{cases} \displaystyle\sum_{j=1}^{\infty} G_j \sin\left\{\frac{j\pi(r-a)}{b-a}\right\}, & a \le r \le b, \\ \frac{\partial \phi_1}{\partial z}(r,0), & 0 \le r \le a. \end{cases} \tag{6.16}$$

The velocity potentials (6.1) and (6.2) are substituted into (6.16), multiplied through by

$\alpha J_0(\gamma_m)r/b$ and integrated with respect to $r,\ 0 \leq r \leq a$ to yield

$$\frac{i\alpha}{b}\sum_{n=0} B_n\eta_n \int_0^b J_0(\gamma_n r)J_0(\gamma_m r)r\mathrm{d}r = \frac{\alpha}{b}\sum_{j=1}^{\infty} G_j T_{jm} + \frac{\alpha}{b}F_\ell s_\ell R_{\ell m} - \frac{i\alpha}{b}\sum_{n=0}^{\infty} A_n s_n R_{nm}, \tag{6.17}$$

where

$$T_{jm} = \int_a^b \sin\left(\frac{j\pi(r-a)}{b-a}\right) J_0(\gamma_m r)r\mathrm{d}r \ \text{ and } R_{nm} = \int_0^a J_0(\kappa_n r)J_0(\gamma_m r)r\mathrm{d}r \tag{6.18}$$

The generalised OR is applied to the left side of this equation

$$\sum_{n=0}^{\infty} B_n\eta_n \left(\delta_{mn}D_n + \left(2 - \gamma_m^2 - \gamma_n^2 - \frac{\tau_b\nu^2\beta^2}{(\eta_n^2-\beta^2)(\eta_m^2-\beta^2)}\right)\gamma_n J_1(\gamma_n b)\gamma_m J_1(\gamma_m b)\right)$$
$$= -\frac{i\alpha}{b}\sum_{j=1}^{\infty} G_j T_{jm} + \frac{\alpha}{b}F_\ell s_\ell R_{\ell m} - \frac{\alpha}{b}\sum_{n=0}^{\infty} A_n s_n R_{nm}. \tag{6.19}$$

It follows that

$$B_m = \frac{\gamma_m J_1(\gamma_m b)}{(\eta_m^2-\beta^2)\eta_m D_m}E_3 + (\gamma_m^3 - 2\gamma_m)\frac{J_1(\gamma_m b)}{\eta_m D_m}E_4 + \frac{\gamma_m J_1(\gamma_m b)}{\eta_m D_m}E_5 - \frac{i\alpha}{b}\sum_{j=1}^{\infty}\frac{G_j T_{jm}}{\eta_m D_m}$$
$$+ \frac{\alpha F_\ell s_\ell R_{\ell m}}{b\eta_m D_m} - \frac{\alpha}{b}\sum_{n=0}^{\infty}\frac{A_n s_n R_{nm}}{\eta_m D_m}. \tag{6.20}$$

where for clamped edge conditions $w_2 = w_{2z} = u_2 = 0$

$$E_3 = E_4 = 0, \ \ E_5 = \frac{\alpha}{bS_3}\sum_{m=0}^{\infty}\frac{\gamma_m J_1(\gamma_m b)}{\eta_m D_m}\left(i\sum_{j=1}^{\infty} G_j T_{jm} - F s_\ell R_{\ell m} + \sum_{n=0}^{\infty} A_n s_n R_{nm}\right), \tag{6.21}$$

where

$$S_3 = \sum_{m=0}^{\infty}\frac{\gamma_m^2 J_1^2(\gamma_m a)}{\eta_m D_m}. \tag{6.22}$$

The amplitudes for the reflected and transmitted amplitudes are thus given by truncating and solving (6.4) and (6.20).

6.1.2 Flexible expansion chamber with non-axisymmetric motion

The recommendation for further work builds on the problems presented in Chapter five, by considering the energy transmitted through a flexible chamber situated between two shells with non-axisymmetric motion. The system comprises two semi-finite shells with

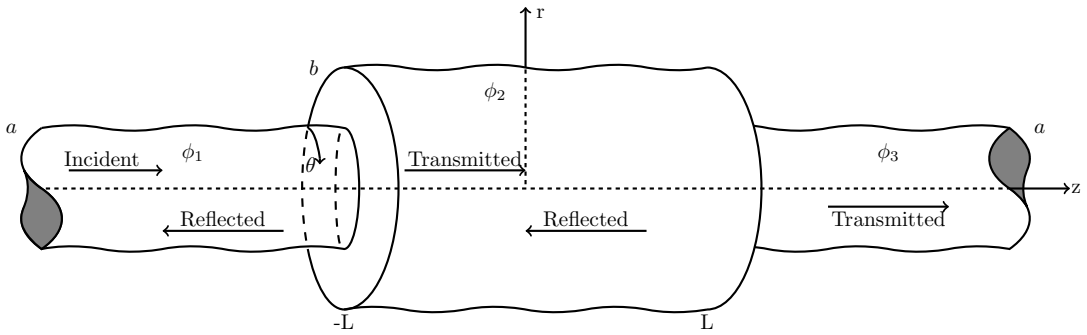

Figure 6.2: Physical configuration of the expansion chamber between two shells with non axisymmetric motion.

a flexible expansion chamber of dimensional length $2\bar{L}$ between them (where $L = k\bar{L}$). The inlet shell is located in the region $0 \leq r \leq a,\ z \leq -L$, the outlet shell is located in the region $0 \leq r \leq a,\ z \geq L$ and the expansion chamber occupies the space between them, $-L \leq z \leq L,\ 0 \leq r \leq b$, thus the chamber has a length $2L$. The system is closed by rigid annular discs located at $a \leq r \leq b,\ z = \pm L$. The velocity potential for the inlet shell ϕ_1 comprises the plane wave and the field reflected at the first junction, which leads to

$$\phi_1 = F_{1\ell} J_1(\kappa_{1\ell} r)\cos(\theta) e^{is_{1\ell}(z+L)} + \sum_{q=0}^{\infty} A_{1q} J_1(\kappa_{1q} r)\cos(\theta) e^{-is_{1q}(z+L)},\ 0 \leq r \leq a,\ z \leq -L, \tag{6.23}$$

where ℓ indicates the chosen fundamental mode to use in the forcing amplitude (with $\ell = 0$ or $\ell = 1$), $F_{1\ell}$ is the amplitude of the forcing wave, A_{1q} is the amplitude of the qth reflected wave, s_{1q} are the wavenumbers which satisfy the characteristic equation given in Chapter four (with $m = 1$) and $\kappa_{1q} = (1 - s_{1q}^2)^{1/2}$. The velocity potential ϕ_2 for the expansion chamber is given by

$$\phi_2(r, \theta, z) = \sum_{q=0}^{\infty} (P_{1q} e^{-i\eta_{1q} z} + Q_{1q} e^{i\eta_{1q} z}) J_1(\gamma_{1q} r)\cos(\theta), \tag{6.24}$$

where P_{1q} is the amplitude of the qth reflected wave, Q_{1q} is the amplitude of the qth transmitted wave and $\eta_{1q},\ q = 0, 1, 2, \ldots$ are the roots of the characteristic equation given in Chapter four (with $m = 1$ and radius b). The velocity potential ϕ_3 for the right-hand shell is given by

$$\phi_3(r, \theta, z) = \sum_{q=0}^{\infty} B_{1q} J_1(\gamma_{1q} r)\cos(\theta) e^{i\eta_{1q}(z-L)}, \tag{6.25}$$

were B_{1q} is the amplitude of the qth reflected wave.

The same method applied to the expansion chamber problems presented in Chapter two and four can be used to solve this problem. That is by noticing that it can be decomposed into two simpler problems which include a second forcing wave leaving the system. These subproblems then each reduce to an abrupt increase in radius and the solving method with the mode matching technique should be analogous to that of Section 4.3.

Appendix A

Matlab code relating to Section 2.3 and 2.4

```
function AppendixA() %Rigid pistons
clc; clear;
index=0;
for f=5:4000
% ---------- Input Variables ----------
a1=0.2; % Dimensional height a (m)
c1=0.2; % Dimensional height b (m)
Cair=343.5; % Sound speed of fluid (m/s)
terms=100; % Number of imaginary roots to seek
% ---------- Calculated Variables ----------
kno=2*pi*f/Cair; % Fluid wave number
a=a1*kno; % Nondimensional height a
c=c1*kno; % Nondimensional height b
% ------------------- sn --------------------
% Approximate root values
RGuess=0:0.01:1; IGuess=(1-(pi/a*((1:terms)+0.25)).^2).^0.5;
% Finding exact values
sn=NewtonRaphson(RGuess,IGuess,a).';
sn=sn(abs(sn)<terms*pi/a);
kappa=sqrt(1-sn.^2); Tw1=length(kappa);
% ----------------- CC -----------------
CC=FunctionHH(kappa,a);
% ---------- Solver ------------
[AA AF]=Solver(c,sn.',CC.');
PowAA=2*real(sum(abs(AA).^2.*CC.*sn)); PowAF=2*real(sum(abs(AF).^2.*CC.*sn));
FF=sqrt(1/(sn(1)*CC(1)));
ZA=-2*sum(besselj(1,kappa*c).^2./(kappa.^2.*sn.*CC));
ZF=4i*FF*besselj(1,kappa(1)*c)/(c*kappa(1))-2*sum(besselj(1,kappa*c).^2./...
    (kappa.^2.*sn.*CC));

index=index+1;
data(index,:)=[f,PowAA,PowAF,abs(ZA),abs(ZF)];
end
end

% The characteristic equation
function K=Characteristic(sn,a)
K=sqrt(1-sn.^2).*besselj(1,sqrt(1-sn.^2)*a);
end

% The Differentiated characteristic equation
function K=DCharacteristic(sn,a)
f1=@(x) Characteristic(x,a);
K=(f1(sn+1e-5)-f1(sn-1e-5))/2e-5;
```

```
end

% Newton Raphson Method
function Roots=NewtonRaphson(RGuess,IGuess,r)
warning('off','MATLAB:rankDeficientMatrix')
f1=@(x) Characteristic(x,r); df1=@(x) DCharacteristic(x,r);
xold1=RGuess; xold2=IGuess;
for i=1:20
    jac1=df1(xold1);
    sol1=xold1-f1(xold1)./jac1;
    xold1=sol1;
    jac2=df1(xold2);
    sol2=xold2-f1(xold2)./jac2;
    xold2=sol2;
end
Real=sol1;
Real=Real(abs(f1(Real))<1e-5);
Real=sort(Real(Real>0),'descend');
TempIndex=1;
TempReal(TempIndex)=Real(1);
for Index=2:length(Real)
    if abs(Real(Index)-TempReal(TempIndex))>1e-2
        TempIndex=TempIndex+1;
        TempReal(TempIndex)=Real(Index);
    end
end
Imaginary=sol2;
Imaginary=Imaginary(abs(f1(Imaginary))<1e-5);
Imaginary=sort(Imaginary(imag(Imaginary)>0),'descend');
TempIndex=1;
TempImaginary(TempIndex)=Imaginary(1);
for Index=2:length(Imaginary)
    if abs(Imaginary(Index)-TempImaginary(TempIndex))>1e-4
        TempIndex=TempIndex+1;
        TempImaginary(TempIndex)=Imaginary(Index);
    end
end
% Sort the complex roots in ascending order
[~,idx]=sort(imag(TempImaginary),'ascend');
TempImaginary=TempImaginary(idx);
Roots=[TempReal,TempImaginary];
end

function HH=FunctionHH(kappa,r)
HH=r.^2.*(besselj(0,kappa.*r).^2)/2;
end

function [AN AF]=Solver(c,sn,CC)
FF=sqrt(1/(sn(1)*CC(1)));
kappa=sqrt(1-sn.^2);
U=1;
Fdelta=zeros(1,length(sn));
for n=1:length(sn)
    Fdelta(n)=FF*kdelta(1,n);
end
AN=(1i*U*c*besselj(1,kappa*c)./(kappa.*sn.*CC)).';
AF=(Fdelta+1i*U*c*besselj(1,kappa*c)./(kappa.*sn.*CC)).';
end

%---------- Kronecker delta ----------%
function d=kdelta(n,m)
if n==m
    d=1;
else
    d=0;
end
end
```

Appendix B

Matlab code relating to Section 2.5

```
function AppendixB() % Rigid radius increase
clc; clear; index=0;
for f=780
% ---------- Input Variables ----------
a1=0.2; % Dimensional height a (m)
b1=0.28; % Dimensional height b (m)
Cair=343.5; % Sound speed of fluid (m/s)
terms=10; % Number of imaginary roots to seek
% ---------- Calculated Variables ----------
kno=2*pi*f/Cair; % Fluid wave number
a=a1*kno; % Nondimensional height a
b=b1*kno; % Nondimensional height b
% ------------------- sn -------------------
RGuess=0:0.01:1; IGuess=(1-(pi/a*((1:terms)+0.25)).^2).^0.5;
sn=NewtonRaphson(RGuess,IGuess,a).';
sn=sn(abs(sn)<terms*pi/a); kappa=sqrt(1-sn.^2); Tw1=length(kappa);
% ------------------- eta -------------------
RGuess=0:0.01:1; IGuess=(1-(pi/b*((1:terms)+0.25)).^2).^0.5;
eta=NewtonRaphson(RGuess,IGuess,b).';
eta=eta(abs(eta)<terms*pi/b); gamma=sqrt(1-eta.^2); Tw2=length(gamma)
CC=FunctionHH(kappa,a); DD=FunctionHH(gamma,b);
RR=zeros(length(kappa),length(gamma));
for n=1:length(kappa)
    for m=1:length(gamma)
        RR(n,m)=IntegralRR(kappa(n),gamma(m),a);
    end
end
% ---------- Solver -----------
F=sqrt(2)/a;
[AA BB]=Solver(sn.',eta.',F,CC.',DD.',RR);
PowA=real(sum(abs(AA).^2.*CC.*sn));
PowB=real(sum(abs(BB).^2.*DD.*eta));
index=index+1;
data(index,:)=[f,PowA,PowB];
end
end
function K=Characteristic(sn,a)
K=sqrt(1-sn.^2).*besselj(1,sqrt(1-sn.^2)*a);
end
function K=DCharacteristic(sn,a)
f1=@(x) Characteristic(x,a);
K=(f1(sn+1e-5)-f1(sn-1e-5))/2e-5;
end
function Roots=NewtonRaphson(RGuess,IGuess,r)
warning('off','MATLAB:rankDeficientMatrix')
f1=@(x) Characteristic(x,r);
df1=@(x) DCharacteristic(x,r);
```

```
xold1=RGuess; xold2=IGuess;
for i=1:20
    jac1=df1(xold1);
    sol1=xold1-f1(xold1)./jac1;
    xold1=sol1;
    jac2=df1(xold2);
    sol2=xold2-f1(xold2)./jac2;
    xold2=sol2;
end
Real=sol1;
Real=Real(abs(f1(Real))<1e-2);
Real=sort(Real(Real>0),'descend');
TempIndex=1;
TempReal(TempIndex)=Real(1);
for Index=2:length(Real)
    if abs(Real(Index)-TempReal(TempIndex))>1e-1
        TempIndex=TempIndex+1;
        TempReal(TempIndex)=Real(Index);
    end
end
Imaginary=sol2;
Imaginary=Imaginary(abs(f1(Imaginary))<1e-5);
Imaginary=sort(Imaginary(imag(Imaginary)>0),'descend');
TempIndex=1;
TempImaginary(TempIndex)=Imaginary(1);
for Index=2:length(Imaginary)
    if abs(Imaginary(Index)-TempImaginary(TempIndex))>1e-4
        TempIndex=TempIndex+1;
        TempImaginary(TempIndex)=Imaginary(Index);
    end
end
[~,idx]=sort(imag(TempImaginary),'ascend');
TempImaginary=TempImaginary(idx);
Roots=[TempReal,TempImaginary];
end
function HH=FunctionHH(kappa,r)
HH=r^2*besselj(0,r*kappa).^2/2;
end
function RR=IntegralRR(gamma,kappa,a)
if abs(real(kappa)^2-real(gamma)^2)<1e-10 && abs(imag(kappa)^2-imag(gamma)^2)<1e-10
    RR=a^2*(besselj(0,a*gamma)^2+besselj(1,a*gamma)^2)/2;
else
    RR=a*(kappa*besselj(0,a*gamma)*besselj(1,a*kappa)-...
        gamma*besselj(0,a*kappa)*besselj(1,a*gamma))/(gamma^2-kappa^2);
end
end
function [AN BM]=Solver(sn,eta,F,CC,DD,RR)
Nn=length(sn); Nm=length(eta); Fdelta=zeros(1,Nn);
for n=1:Nn
    Fdelta(n)=F*kdelta(1,n);
end
V1=zeros(Nm,1); M1=zeros(Nn,Nm); M2=zeros(Nm,Nn);
for n=1:Nn
    for m=1:Nm
        M1(n,m)=RR(n,m)/CC(n); V1(m)=F*sn(1)*RR(1,m)/eta(m)/DD(m);
        M2(m,n)=-sn(n)*RR(n,m)/eta(m)/DD(m);
    end
end
AN=(eye(Nn)-M1*M2)\(-Fdelta.'+M1*V1);
BM=(eye(Nm)-M2*M1)\(V1+M2*-Fdelta.')
end
function d=kdelta(n,m)
if n==m
    d=1;
else
    d=0;
end
end
```

Appendix C

Matlab code relating to Section 2.6

```
function AppendixC() %Rigid expansion
clc; clear;
index=0;
for f=5:1200
% ---------- Input Variables ----------
a1=0.2; % Dimensional height a (m)
b1=0.28; % Dimensional height b (m)
L1=0.5; % Half dimensional length L
Cair=343.5; % Sound speed of fluid (m/s)
Dair=1.2; % Density of fluid (kg/m^3)
terms=100; % Number of imaginary roots to seek
% ---------- Calculated Variables ----------
kno=2*pi*f/Cair; % Fluid wave number
a=a1*kno; % Nondimensional height a
b=b1*kno; % Nondimensional height b
L=L1*kno; % Nondimensional half length
% ------------------- sn -------------------
% Approximate root values
RGuess=0:0.01:1; IGuess=(1-(pi/a*((1:terms)+0.25)).^2).^0.5;
% Finding exact values
sn=NewtonRaphson(RGuess,IGuess,a).';
sn=sn(abs(sn)<terms*pi/a);
kappa=sqrt(1-sn.^2); Tw1=length(kappa);
% ------------------- eta -------------------
% Approximate root values
RGuess=0:0.01:1; IGuess=(1-(pi/b*((1:terms)+0.25)).^2).^0.5;
% Finding exact values
eta=NewtonRaphson(RGuess,IGuess,b).';
eta=eta(abs(eta)<terms*pi/b);
gamma=sqrt(1-eta.^2); Tw2=length(gamma);
% ----------------- CC & DD -----------------
CC=FunctionHH(kappa,a); DD=FunctionHH(gamma,b);
% ---------- RR Integral ----------
RR=zeros(length(kappa),length(gamma));
for n=1:length(kappa)
    for m=1:length(gamma)
        RR(n,m)=IntegralRR(kappa(n),gamma(m),a);
    end
end
% ---------- Solver ----------
F=sqrt(kno^2/(2*pi*Cair^3*Dair*CC(1)*sn(1)));
AAS=SSolver(sn.',eta.',F,CC.',DD.',RR,L);
AAA=ASolver(sn.',eta.',F,CC.',DD.',RR,L);
PowA=2*pi*Cair^3*Dair/kno^2*real(sum(abs((AAS+AAA)*0.5).^2.*CC.*sn));
PowB=2*pi*Cair^3*Dair/kno^2*real(sum(abs((AAS-AAA)*0.5).^2.*CC.*sn));
AA=F*(a^4-b^4)*sin(2*L)/...
    (2i*a^2*b^2*cos(2*L)+(a^4+b^4)*sin(2*L));
```

```
BB=2i*F*a^2*b^2/...
    (2i*a^2*b^2*cos(2*L)+(a^4+b^4)*sin(2*L));
PowAT=2*pi*Cair^3*Dair/kno^2*real(abs(AA)^2*CC(1)*sn(1));
PowBT=2*pi*Cair^3*Dair/kno^2*real(abs(BB)^2*CC(1)*sn(1));
index=index+1;
data(index,:)=[f,PowA,PowB,PowAT,PowBT];
end
end

% The characteristic equation
function K=Characteristic(sn,a)
K=sqrt(1-sn.^2).*besselj(1,sqrt(1-sn.^2)*a);
end

% The Differentiated characteristic equation
function K=DCharacteristic(sn,a)
f1=@(x) Characteristic(x,a);
K=(f1(sn+1e-5)-f1(sn-1e-5))/2e-5;
end

% Newton Raphson Method
function Roots=NewtonRaphson(RGuess,IGuess,r)
warning('off','MATLAB:rankDeficientMatrix')
f1=@(x) Characteristic(x,r); df1=@(x) DCharacteristic(x,r);
xold1=RGuess; xold2=IGuess;
for i=1:20
    jac1=df1(xold1);
    sol1=xold1-f1(xold1)./jac1;
    xold1=sol1;
    jac2=df1(xold2);
    sol2=xold2-f1(xold2)./jac2;
    xold2=sol2;
end
Real=sol1;
Real=Real(abs(f1(Real))<1e-2);
Real=sort(Real(Real>0),'descend');
TempIndex=1;
TempReal(TempIndex)=Real(1);
for Index=2:length(Real)
    if abs(Real(Index)-TempReal(TempIndex))>1e-1
        TempIndex=TempIndex+1;
        TempReal(TempIndex)=Real(Index);
    end
end
Imaginary=sol2;
Imaginary=Imaginary(abs(f1(Imaginary))<1e-5);
Imaginary=sort(Imaginary(imag(Imaginary)>0),'descend');
TempIndex=1;
TempImaginary(TempIndex)=Imaginary(1);
for Index=2:length(Imaginary)
    if abs(Imaginary(Index)-TempImaginary(TempIndex))>1e-4
        TempIndex=TempIndex+1;
        TempImaginary(TempIndex)=Imaginary(Index);
    end
end
% Sort the complex roots in ascending order
[~,idx]=sort(imag(TempImaginary),'ascend');
TempImaginary=TempImaginary(idx);
Roots=[TempReal,TempImaginary];
end

function HH=FunctionHH(kappa,r)
HH=r^2*besselj(0,r*kappa).^2/2;
end

function RR=IntegralRR(gamma,kappa,a)
if abs(real(kappa)^2-real(gamma)^2)<1e-10 && abs(imag(kappa)^2-imag(gamma)^2)<1e-10
    RR=a^2*(besselj(0,a*gamma)^2+besselj(1,a*gamma)^2)/2;
else
    RR=a*(kappa*besselj(0,a*gamma)*besselj(1,a*kappa)-...
```

```
        gamma*besselj(0,a*kappa)*besselj(1,a*gamma))/(kappa^2-gamma^2);
end
end

% --------- Symmetric Solver ----------%
function AN=SSolver(sn,eta,F,CC,DD,RR,L)
Nn=length(sn); Nm=length(eta);
Fdelta=zeros(1,Nn);
for n=1:Nn
    Fdelta(n)=F*kdelta(1,n);
end
V1=zeros(Nm,1); M1=zeros(Nn,Nm); M2=zeros(Nm,Nn);
for n=1:Nn
    for m=1:Nm
        M1(n,m)=2*RR(n,m)*cos(eta(m)*L)/CC(n);
        V1(m)=1i*F*sn(1)*RR(1,m)/2/eta(m)/DD(m)/sin(eta(m)*L);
        M2(m,n)=-1i*sn(n)*RR(n,m)/2/eta(m)/DD(m)/sin(eta(m)*L);
    end
end
AN=(eye(Nn)-M1*M2)\(-Fdelta.'+M1*V1);
end

% --------- Asymmetric Solver ----------%
function AN=ASolver(sn,eta,F,CC,DD,RR,L)
Nn=length(sn); Nm=length(eta);

Fdelta=zeros(1,Nn);
for n=1:Nn
    Fdelta(n)=F*kdelta(1,n);
end
V1=zeros(Nm,1); M1=zeros(Nn,Nm); M2=zeros(Nm,Nn);
for n=1:Nn
    for m=1:Nm
        M1(n,m)=-2*RR(n,m)*sin(eta(m)*L)/CC(n);
        V1(m)=1i*F*sn(1)*RR(1,m)/2/eta(m)/DD(m)/cos(eta(m)*L);
        M2(m,n)=-1i*sn(n)*RR(n,m)/2/eta(m)/DD(m)/cos(eta(m)*L);
    end
end
AN=(eye(Nn)-M1*M2)\(-Fdelta.'+M1*V1);
end

%---------- Kronecker delta ----------%
function d=kdelta(n,m)
if n==m
    d=1;
else
    d=0;
end
end
```

Appendix D

Matlab code relating to Section 3.1 and 3.3

```
function AppendixD() %Axi characteristic
clc; clear;
index=0;
for terms=5:50 % Number of imaginary roots to seek
% ---------- Input Variables ----------
a1=0.2; % Dimensional radius (m)
Cair=343.5; % Sound speed of fluid (m/s)
Dair=1.2; % Density of fluid (kg/m^3)
EE=7.2*10^10; % Youngs Modulus (N/m^2)
h1=0.002; % Dimensional shell thickness (m)
Dplate=2700; % Density of shell (kg/m^3)
nu=0.34; % Poisson's ratio for shell
f=500; %Frequency (Hz)
% ---------- Calculated Variables ----------
kno=2*pi*f/Cair; % Fluid wave number
a=a1*kno; % Nondimensional radius
h=h1*kno; % Nondimensional shell thickness
r=a/2; % Used for identities
cp1=sqrt(EE/(1-nu^2)/Dplate); % Sound speed of the shell
beta=Cair/cp1; omega=Cair*kno; tau=12/(h^2*a^2);
alpha=12*omega^2*Dair/(h^3*cp1^2*kno^2*Dplate);
% Starting Values
RGuess=0:0.01:1.1; IGuess=sqrt(1-(pi/a.*((0:1:terms)+5/4)).^2);
CGuess=[(-(1-a^2*beta^2)*tau)^0.25 -conj((-(1-a^2*beta^2)*tau)^0.25)];
sn=NewtonRaphson(alpha,beta,tau,nu,RGuess,IGuess,CGuess,a).';
sn=sn(abs(sn)<terms*pi/a);
Characteristic(sn,alpha,beta,tau,nu,a)
kappa=sqrt(1-sn.^2); Tw1=length(kappa);
CC=FunctionHH(alpha,beta,tau,nu,sn,kappa,a);
% Identities
I1=real(sum(kappa.*besselj(1,kappa*a).*besselj(0,kappa*r)./CC));
I2=real(sum(kappa.*besselj(1,kappa*a).*besselj(0,kappa*r)./CC./(sn.^2-beta^2)));
I3=real(sum(kappa.^3.*besselj(1,kappa*a).*besselj(0,kappa*r)./CC./(sn.^2-beta^2)));
I4=real(sum((kappa.*besselj(1,kappa*a)).^2./CC));
I5=real(sum((kappa.*besselj(1,kappa*a)).^2./CC./(sn.^2-beta^2)));
I6=real(sum(kappa.^2.*(kappa.*besselj(1,kappa*a)).^2./CC));
I7=real(sum(kappa.^4.*(kappa.*besselj(1,kappa*a)).^2./CC));
index=index+1;
data(index,:)=[terms,I1,I2,I3,I4,I5,I6,I7];
end
end

% The characteristic equation
function K=Characteristic(s,alpha,beta,tau,nu,a)
```

```
K=((-tau*nu^2*s.^2-(beta^2-s.^2).*(s.^4+(1-a^2*beta^2)*tau)).*sqrt(1-s.^2)...
    .*besselj(1,a*sqrt(1-s.^2))-(beta^2-s.^2).*alpha.*besselj(0,a*sqrt(1-s.^2)));
end

% The Differentiated characteristic equation
function K=DCharacteristic(s,alpha,beta,tau,nu,a)
f1=@(x) Characteristic(x,alpha,beta,tau,nu,a);
K=(f1(s+1e-5)-f1(s-1e-5))/2e-5;
end

% Newton Raphson Method
function Roots=NewtonRaphson(alpha,beta,tau,nu,RGuess,IGuess,CGuess,r)
warning('off','MATLAB:rankDeficientMatrix')
f1=@(x) Characteristic(x,alpha,beta,tau,nu,r);
df1=@(x) DCharacteristic(x,alpha,beta,tau,nu,r);

xold1=RGuess; xold2=IGuess; xold3=CGuess;
for i=1:10
    jac1=df1(xold1);
    sol1=xold1-f1(xold1)./jac1;
    xold1=sol1;
    jac2=df1(xold2);
    sol2=xold2-f1(xold2)./jac2;
    xold2=sol2;
    jac3=df1(xold3);
    sol3=xold3-f1(xold3)./jac3;
    xold3=sol3;
end
Real=sol1;
Real=Real(abs(f1(Real))<1e-5);
Real=sort(Real(Real>0),'descend');
TempIndex=1;
TempReal(TempIndex)=Real(1);
for Index=2:length(Real)
    if abs(Real(Index)-TempReal(TempIndex))>3e-5
        TempIndex=TempIndex+1;
        TempReal(TempIndex)=Real(Index);
    end
end
sol2=sol2((length(TempReal)-1):end);
Imaginary=sol2; Complex=sol3;
Imaginary=sort(Imaginary(imag(Imaginary)>0),'descend');
TempIndex=1;
TempIm(TempIndex)=Imaginary(1);
for Index=2:length(Imaginary)
    if abs(Imaginary(Index)-TempIm(TempIndex))>1e-5
        TempIndex=TempIndex+1;
        TempIm(TempIndex)=Imaginary(Index);
    end
end
Imaginary=[TempIm,Complex];
% Sort the complex roots in ascending order
[~,idx]=sort(imag(Imaginary),'ascend');
Imaginary=Imaginary(idx);
Roots=[TempReal,Imaginary];
end

function HH=FunctionHH(alpha,beta,tau,nu,eta,gamma,r)
f1=@(x) Characteristic(x,alpha,beta,tau,nu,r);
HH=(f1(eta+1e-5)-f1(eta-1e-5))./(2e-5).*gamma.*besselj(1,r*gamma)...
    ./(2*eta.*(eta.^2-beta^2));
end
```

Appendix E

Matlab code relating to Section 3.4

```
function AppendixE() %Semi Infinite Shell
clc; clear;
index=0;
for f=5:1200
% ---------- Input Variables ----------
a1=0.2; % Dimensional radius a (m)
Cair=343.5; % Sound speed of fluid (m/s)
Dair=1.2; % Density of fluid (kg/m^3)
EE=7.2*10^10; % Youngs Modulus (N/m^2)
h1=0.002; % Dimensional shell thickness (m)
Dplate=2700; % Density of shell (kg/m^3)
nu=0.34; % Poisson's ratio for shell
terms=100; % Number of imaginary roots to seek
ell=1; % Indicator for incident forcing mode
% ---------- Calculated Variables ----------
kno=2*pi*f/Cair; % Fluid wave number
a=a1*kno; % Nondimensional radius a
h=h1*kno; % Nondimensional shell thickness
cp1=sqrt(EE/(1-nu^2)/Dplate); % Sound speed of the shell
beta=Cair/cp1; omega=Cair*kno;
tau=12/(h^2*a^2);
alpha=12*omega^2*Dair/(h^3*cp1^2*kno^2*Dplate);
% Starting Values
RGuess=0:0.01:1.1;
IGuess=sqrt(1-(pi/a.*((0:1:terms)+5/4)).^2);
CGuess=[(-(1-a^2*beta^2)*tau)^0.25 -conj((-(1-a^2*beta^2)*tau)^0.25)];
sn=NewtonRaphson(alpha,beta,tau,nu,RGuess,IGuess,CGuess,a).';
sn=sn(abs(sn)<terms*pi/a);
kappa=sqrt(1-sn.^2); Tw1=length(kappa);
% ---------- CC ----------
CC=FunctionHH(alpha,beta,tau,nu,sn,kappa,a);
% --------- Bessel function---------
JJa=besselj(1,a*kappa);
% ---------- Solver ----------
AA=AxiSolver(beta,tau,nu,sn.',kappa.',JJa.',CC.',ell);
PowA=real(sum(abs(AA).^2.*CC.*sn));
index=index+1;
data(index,:)=[f,PowA];
end
end

% Characteristic equation
function K=Characteristic(s,alpha,beta,tau,nu,a)
K=((-tau*nu^2*s.^2-(beta^2-s.^2).*(s.^4+(1-a^2*beta^2)*tau))...
    .*sqrt(1-s.^2).*besselj(1,a*sqrt(1-s.^2))-(beta^2-s.^2)...
    .*alpha.*besselj(0,a*sqrt(1-s.^2)));
end
```

```
% The Differentiated characteristic equation
function K=DCharacteristic(s,alpha,beta,tau,nu,a)
f1=@(x) Characteristic(x,alpha,beta,tau,nu,a);
K=(f1(s+1e-5)-f1(s-1e-5))/2e-5;
end

% Newton Raphson Method
function Roots=NewtonRaphson(alpha,beta,tau,nu,RGuess,IGuess,CGuess,r)
warning('off','MATLAB:rankDeficientMatrix')
f1=@(x) Characteristic(x,alpha,beta,tau,nu,r);
df1=@(x) DCharacteristic(x,alpha,beta,tau,nu,r);
xold1=RGuess; xold2=IGuess; xold3=CGuess;
for i=1:100
    jac1=df1(xold1);
    sol1=xold1-f1(xold1)./jac1;
    xold1=sol1;
    jac2=df1(xold2);
    sol2=xold2-f1(xold2)./jac2;
    xold2=sol2;
    jac3=df1(xold3);
    sol3=xold3-f1(xold3)./jac3;
    xold3=sol3;
end
Real=sol1;
Real=Real(abs(f1(Real))<1e-5);
Real=sort(Real(Real>0),'descend');
TempIndex=1;
TempReal(TempIndex)=Real(1);
for Index=2:length(Real)
    if abs(Real(Index)-TempReal(TempIndex))>3e-5
        TempIndex=TempIndex+1;
        TempReal(TempIndex)=Real(Index);
    end
end
sol2=sol2((length(TempReal)-1):end);
Imaginary=sol2; Complex=sol3;
Imaginary=sort(Imaginary(imag(Imaginary)>0),'descend');
TempIndex=1;
TempIm(TempIndex)=Imaginary(1);
for Index=2:length(Imaginary)
    if abs(Imaginary(Index)-TempIm(TempIndex))>1e-5
        TempIndex=TempIndex+1;
        TempIm(TempIndex)=Imaginary(Index);
    end
end
Imaginary=[TempIm,Complex];
% Sort the complex roots in ascending order
[~,idx]=sort(imag(Imaginary),'ascend');
Imaginary=Imaginary(idx);
Roots=[TempReal,Imaginary];
end

function HH=FunctionHH(alpha,beta,tau,nu,eta,gamma,r)
f1=@(x) Characteristic(x,alpha,beta,tau,nu,r);
HH=(f1(eta+1e-5)-f1(eta-1e-5))./(2e-5).*gamma.*besselj(1,r*gamma)...
    ./(2*eta.*(eta.^2-beta^2));
end

function AA=AxiSolver(beta,tau,nu,sn,kappa,JJa,CC,ell)
Nn=length(sn);
F=sqrt(1/(abs(CC(ell))*sn(ell)));
%---------- The edge conditions ----------%
%---------- Sum Am E#A + E#F = 0;
%---------- Clamped ----------%
PsiA1=sn.*kappa.*JJa./(sn.^2-beta^2);
PsiF1=-sn(ell)*kappa(ell)*JJa(ell)/(sn(ell)^2-beta^2);
PsiA2=kappa.*JJa; PsiF2=kappa(ell)*JJa(ell);
PsiA3=sn.*kappa.*JJa; PsiF3=-sn(ell)*kappa(ell)*JJa(ell);
%---------- Pin Jointed ----------%
```

```
% PsiA1=kappa.*JJa; PsiF1=kappa(ell).*JJa(ell);
% PsiA2=sn.^2.*kappa.*JJa; PsiF2=sn(ell).^2.*kappa(ell).*JJa(ell);
% PsiA3=sn.^2.*kappa.*JJa./(sn.^2-beta^2);
% PsiF3=sn(ell)^2*kappa(ell)*JJa(ell)./(sn(ell).^2-beta^2);
%---------- The Summations ----------%
SA=0; SB=0; SC=0; SD=0; SE=0; SF=0; SG=0; SH=0; SI=0;
for n=1:Nn
    SA=SA+tau*nu^2*beta^2*kappa(n)*JJa(n)*PsiA1(n)...
        /(sn(n)^2-beta^2)/(sn(n)*CC(n));
    SB=SB+(2-kappa(n)^2)*kappa(n)*JJa(n)*PsiA1(n)/(sn(n)*CC(n));
    SC=SC+kappa(n)*JJa(n)*PsiA1(n)/(sn(n)*CC(n));
    SD=SD+tau*nu^2*beta^2*kappa(n)*JJa(n)*PsiA2(n)...
        /(sn(n)^2-beta^2)/(sn(n)*CC(n));
    SE=SE+(2-kappa(n)^2)*kappa(n)*JJa(n)*PsiA2(n)/(sn(n)*CC(n));
    SF=SF+kappa(n)*JJa(n)*PsiA2(n)/(sn(n)*CC(n));
    SG=SG+tau*nu^2*beta^2*kappa(n)*JJa(n)*PsiA3(n)...
        /(sn(n)^2-beta^2)/(sn(n)*CC(n));
    SH=SH+(2-kappa(n)^2)*kappa(n)*JJa(n)*PsiA3(n)/(sn(n)*CC(n));
    SI=SI+kappa(n)*JJa(n)*PsiA3(n)/(sn(n)*CC(n));
end
DA=SC*SE*SG-SB*SF*SG-SC*SD*SH+SA*SF*SH+SB*SD*SI-SA*SE*SI;
Fdelta=zeros(1,Nn); GE0a=0; GE1a=0; GE2a=0;
for n=1:Nn
    Fdelta(n)=F*kdelta(ell,n);
    GE0a=GE0a+F*kdelta(ell,n)*PsiA1(n);
    GE1a=GE1a+F*kdelta(ell,n)*PsiA2(n);
    GE2a=GE2a+F*kdelta(ell,n)*PsiA3(n);
end
E0=((SF*SH-SE*SI)*(-F*PsiF1-GE0a)+(SB*SI-SC*SH)*(-F*PsiF2-GE1a)...
    +(SC*SE-SB*SF)*(-F*PsiF3-GE2a))/DA;
E1=((SF*SG-SD*SI)*(-F*PsiF1-GE0a)+(SA*SI-SC*SG)*(-F*PsiF2-GE1a)...
    +(SC*SD-SA*SF)*(-F*PsiF3-GE2a))/-DA;
E2=((SE*SG-SD*SH)*(-F*PsiF1-GE0a)+(SA*SH-SB*SG)*(-F*PsiF2-GE1a)...
    +(SB*SD-SA*SE)*(-F*PsiF3-GE2a))/-DA;
AA=(Fdelta+tau*nu^2*beta^2*kappa.*JJa.*E0./(sn.^2-beta^2)./sn./CC...
    +(2-kappa.^2).*kappa.*JJa.*E1./sn./CC-kappa.*JJa.*E2./sn./CC).';
end

%---------- Kronecker delta ----------%
function d=kdelta(n,m)
if n==m
    d=1;
else
    d=0;
end
end
```

Appendix F

Matlab code relating to Section 3.5 and 3.6

```
function AppendixF() %Axi pistons
% clc; clear;
index=0;
for f=5:1200
% ---------- Input Variables ----------
a1=0.2; % Dimensional radius a (m)
c1=0.1; % Dimensional radius c of piston (m)
Cair=343.5; % Sound speed of fluid (m/s)
Dair=1.2; % Density of fluid (kg/m^3)
EE=7.2*10^10; % Youngs Modulus (N/m^2)
h1=0.002; % Dimensional shell thickness (m)
Dplate=2700; % Density of shell (kg/m^3)
nu=0.34; % Poisson's ratio for shell
terms=100; % Number of imaginary roots to seek
ell=1; % Indicator for incident forcing mode
% ---------- Calculated Variables ----------
kno=2*pi*f/Cair; % Fluid wave number
a=a1*kno; % Nondimensional radius a
h=h1*kno; % Nondimensional shell thickness
c=c1*kno; % Nondimensional piston radius c
cp1=sqrt(EE/(1-nu^2)/Dplate); % Sound speed of the shell
beta=Cair/cp1; omega=Cair*kno; tau=12/(h^2*a^2);
alpha=12*omega^2*Dair/(h^3*cp1^2*kno^2*Dplate);
% Starting Values
RGuess=0:0.01:1.1; IGuess=sqrt(1-(pi/a.*((0:1:terms)+5/4)).^2);
CGuess=[(-(1-a^2*beta^2)*tau)^0.25 -conj((-(1-a^2*beta^2)*tau)^0.25)];
sn=NewtonRaphson(alpha,beta,tau,nu,RGuess,IGuess,CGuess,a).';
sn=sn(abs(sn)<terms*pi/a);
kappa=sqrt(1-sn.^2); Tw1=length(kappa);
CC=FunctionHH(alpha,beta,tau,nu,sn,kappa,a);
JJa=besselj(1,a*kappa); JJc=besselj(1,c*kappa);
% ---------- Solver -----------
[AA AF]=AxiSolver(a,c,alpha,beta,tau,nu,sn.',kappa.',JJa.',JJc.',CC.',ell);
PowA=real(sum(abs(AA).^2.*CC.*sn)); PowAF=real(sum(abs(AF).^2.*CC.*sn));
ZA=-2*1i/c^2*sum(AA.*besselj(1,kappa*c)./kappa.^2);
ZF=-2*1i/c^2*sum(AA.*besselj(1,kappa*c)./kappa.^2);
index=index+1;
data(index,:)=[f,PowA,PowAF,abs(ZA),abs(ZF)];
end
end
% Characteristic equation
function K=Characteristic(s,alpha,beta,tau,nu,a)
K=((-tau*nu^2*s.^2-(beta^2-s.^2).*(s.^4+(1-a^2*beta^2)*tau))...
    .*sqrt(1-s.^2).*besselj(1,a*sqrt(1-s.^2))-(beta^2-s.^2)...
```

```
    .*alpha.*besselj(0,a*sqrt(1-s.^2)));
end
% The Differentiated characteristic equation
function K=DCharacteristic(s,alpha,beta,tau,nu,a)
f1=@(x) Characteristic(x,alpha,beta,tau,nu,a);
K=(f1(s+1e-5)-f1(s-1e-5))/2e-5;
end
% Newton Raphson Method
function Roots=NewtonRaphson(alpha,beta,tau,nu,RGuess,IGuess,CGuess,r)
warning('off','MATLAB:rankDeficientMatrix')
f1=@(x) Characteristic(x,alpha,beta,tau,nu,r);
df1=@(x) DCharacteristic(x,alpha,beta,tau,nu,r);
xold1=RGuess; xold2=IGuess; xold3=CGuess;
for i=1:100
    jac1=df1(xold1);
    sol1=xold1-f1(xold1)./jac1;
    xold1=sol1;
    jac2=df1(xold2);
    sol2=xold2-f1(xold2)./jac2;
    xold2=sol2;
    jac3=df1(xold3);
    sol3=xold3-f1(xold3)./jac3;
    xold3=sol3;
end
Real=sol1;
Real=Real(abs(f1(Real))<1e-5);
Real=sort(Real(Real>0),'descend');
TempIndex=1;
TempReal(TempIndex)=Real(1);
for Index=2:length(Real)
    if abs(Real(Index)-TempReal(TempIndex))>3e-5
        TempIndex=TempIndex+1;
        TempReal(TempIndex)=Real(Index);
    end
end
sol2=sol2((length(TempReal)-1):end);
Imaginary=sol2; Complex=sol3;
Imaginary=sort(Imaginary(imag(Imaginary)>0),'descend');
TempIndex=1;
TempIm(TempIndex)=Imaginary(1);
for Index=2:length(Imaginary)
    if abs(Imaginary(Index)-TempIm(TempIndex))>1e-5
        TempIndex=TempIndex+1;
        TempIm(TempIndex)=Imaginary(Index);
    end
end
Imaginary=[TempIm,Complex];
% Sort the complex roots in ascending order
[~,idx]=sort(imag(Imaginary),'ascend');
Imaginary=Imaginary(idx);
Roots=[TempReal,Imaginary];
end
function HH=FunctionHH(alpha,beta,tau,nu,eta,gamma,r)
f1=@(x) Characteristic(x,alpha,beta,tau,nu,r);
HH=(f1(eta+1e-5)-f1(eta-1e-5))./(2e-5).*gamma.*besselj(1,r*gamma)...
    ./(2*eta.*(eta.^2-beta^2));
end
function [AA AF]=AxiSolver(a,c,alpha,beta,tau,nu,sn,kappa,JJa,JJc,CC,ell)
Nn=length(sn); F=sqrt(1/(abs(CC(ell))*sn(ell)));
%---------- The edge conditions ----------%
%---------- Clamped ----------%
PsiA1=sn.*kappa.*JJa./(sn.^2-beta^2);
PsiF1=-sn(ell)*kappa(ell)*JJa(ell)/(sn(ell)^2-beta^2);
PsiA2=kappa.*JJa; PsiF2=kappa(ell)*JJa(ell);
PsiA3=sn.*kappa.*JJa; PsiF3=-sn(ell)*kappa(ell)*JJa(ell);
% %---------- Pin Jointed ----------%
% PsiA1=kappa.*JJa; PsiF1=kappa(ell).*JJa(ell);
% PsiA2=sn.^2.*kappa.*JJa; PsiF2=sn(ell).^2.*kappa(ell).*JJa(ell);
% PsiA3=sn.^2.*kappa.*JJa./(sn.^2-beta^2);
% PsiF3=sn(ell)^2*kappa(ell)*JJa(ell)./(sn(ell).^2-beta^2);
```

```
%---------- The Summations ----------%
SA=0; SB=0; SC=0; SD=0; SE=0; SF=0; SG=0; SH=0; SI=0;
for n=1:Nn
    SA=SA+tau*nu^2*beta^2*kappa(n)*JJa(n)*PsiA1(n)...
        /(sn(n)^2-beta^2)/(sn(n)*CC(n));
    SB=SB+(2-kappa(n)^2)*kappa(n)*JJa(n)*PsiA1(n)/(sn(n)*CC(n));
    SC=SC+kappa(n)*JJa(n)*PsiA1(n)/(sn(n)*CC(n));
    SD=SD+tau*nu^2*beta^2*kappa(n)*JJa(n)*PsiA2(n)...
        /(sn(n)^2-beta^2)/(sn(n)*CC(n));
    SE=SE+(2-kappa(n)^2)*kappa(n)*JJa(n)*PsiA2(n)/(sn(n)*CC(n));
    SF=SF+kappa(n)*JJa(n)*PsiA2(n)/(sn(n)*CC(n));
    SG=SG+tau*nu^2*beta^2*kappa(n)*JJa(n)*PsiA3(n)...
        /(sn(n)^2-beta^2)/(sn(n)*CC(n));
    SH=SH+(2-kappa(n)^2)*kappa(n)*JJa(n)*PsiA3(n)/(sn(n)*CC(n));
    SI=SI+kappa(n)*JJa(n)*PsiA3(n)/(sn(n)*CC(n));
end
DA=SC*SE*SG-SB*SF*SG-SC*SD*SH+SA*SF*SH+SB*SD*SI-SA*SE*SI;
%---------- AN with incident wave ----------%
Fdelta=zeros(1,Nn); GE0a=0; GE1a=0; GE2a=0; PE0=0; PE1=0; PE2=0;
for n=1:Nn
    Fdelta(n)=F*kdelta(ell,n); GE0a=GE0a+F*kdelta(ell,n)*PsiA1(n);
    GE1a=GE1a+F*kdelta(ell,n)*PsiA2(n); GE2a=GE2a+F*kdelta(ell,n)*PsiA3(n);
    PE0=PE0+1i*alpha*c*JJc(n)/(a*kappa(n)*sn(n)*CC(n))*PsiA1(n);
    PE1=PE1+1i*alpha*c*JJc(n)/(a*kappa(n)*sn(n)*CC(n))*PsiA2(n);
    PE2=PE2+1i*alpha*c*JJc(n)/(a*kappa(n)*sn(n)*CC(n))*PsiA3(n);
end
E0=-((SF*SH-SE*SI)*(F*PsiF1+GE0a+PE0)+(SB*SI-SC*SH)*(F*PsiF2+GE1a+PE1)...
    +(SC*SE-SB*SF)*(F*PsiF3+GE2a+PE2))/DA;
E1=-((SF*SG-SD*SI)*(F*PsiF1+GE0a+PE0)+(SA*SI-SC*SG)*(F*PsiF2+GE1a+PE1)...
    +(SC*SD-SA*SF)*(F*PsiF3+GE2a+PE2))/-DA;
E2=-((SE*SG-SD*SH)*(F*PsiF1+GE0a+PE0)+(SA*SH-SB*SG)*(F*PsiF2+GE1a+PE1)...
    +(SB*SD-SA*SE)*(F*PsiF3+GE2a+PE2))/-DA;
AF=(Fdelta+tau*nu^2*beta^2*kappa.*JJa.*E0./(sn.^2-beta^2)./sn./CC...
    +(2-kappa.^2).*kappa.*JJa.*E1./sn./CC-kappa.*JJa.*E2./sn./CC...
    +1i*alpha*c*JJc./(a*kappa.*sn.*CC)).';
%---------- AN without incident wave ----------%
F=0; Fdelta=zeros(1,Nn); GE0a=0; GE1a=0; GE2a=0; PE0=0; PE1=0; PE2=0;
for n=1:Nn
    Fdelta(n)=F*kdelta(ell,n); GE0a=GE0a+F*kdelta(ell,n)*PsiA1(n);
    GE1a=GE1a+F*kdelta(ell,n)*PsiA2(n); GE2a=GE2a+F*kdelta(ell,n)*PsiA3(n);
    PE0=PE0+1i*alpha*c*JJc(n)/(a*kappa(n)*sn(n)*CC(n))*PsiA1(n);
    PE1=PE1+1i*alpha*c*JJc(n)/(a*kappa(n)*sn(n)*CC(n))*PsiA2(n);
    PE2=PE2+1i*alpha*c*JJc(n)/(a*kappa(n)*sn(n)*CC(n))*PsiA3(n);
end
E0=-((SF*SH-SE*SI)*(F*PsiF1+GE0a+PE0)+(SB*SI-SC*SH)*(F*PsiF2+GE1a+PE1)...
    +(SC*SE-SB*SF)*(F*PsiF3+GE2a+PE2))/DA;
E1=-((SF*SG-SD*SI)*(F*PsiF1+GE0a+PE0)+(SA*SI-SC*SG)*(F*PsiF2+GE1a+PE1)...
    +(SC*SD-SA*SF)*(F*PsiF3+GE2a+PE2))/-DA;
E2=-((SE*SG-SD*SH)*(F*PsiF1+GE0a+PE0)+(SA*SH-SB*SG)*(F*PsiF2+GE1a+PE1)...
    +(SB*SD-SA*SE)*(F*PsiF3+GE2a+PE2))/-DA;
AA=(tau*nu^2*beta^2*kappa.*JJa.*E0./(sn.^2-beta^2)./sn./CC...
    +(2-kappa.^2).*kappa.*JJa.*E1./sn./CC-kappa.*JJa.*E2./sn./CC...
    +1i*alpha*c*JJc./(a*kappa.*sn.*CC)).';
end
function d=kdelta(n,m)
if n==m
    d=1;
else
    d=0;
end
end
```

Appendix G

Matlab code relating to Section 4.1

```
function AppendixG() %Axi increase radius
clc; clear;
index=0;
for f=50
% ---------- Input Variables ----------
a1=0.2; % Dimensional radius a (m)
b1=0.28; % Dimensional radius b (m)
Cair=343.5; % Sound speed of fluid (m/s)
Dair=1.2; % Density of fluid (kg/m^3)
EE=7.2*10^10; % Youngs Modulus (N/m^2)
h1=0.002; % Dimensional shell thickness (m)
Dplate=2700; % Density of shell (kg/m^3)
nu=0.34; % Poisson's ratio for shell
terms=100; % Number of imaginary roots to seek
ell=1; % Indicator for incident forcing mode
% ---------- Calculated Variables ----------
kno=2*pi*f/Cair; % Fluid wave number
a=a1*kno; % Nondimensional radius a
b=b1*kno; % Nondimensional radius b
h=h1*kno; % Nondimensional shell thickness
cp1=sqrt(EE/(1-nu^2)/Dplate);
% Sound speed of the shell
beta=Cair/cp1; omega=Cair*kno;
tau1=12/(h^2*a^2); tau2=12/(h^2*b^2);
alpha=12*omega^2*Dair/(h^3*cp1^2*kno^2*Dplate);
% Number of cut on roots
RGuess=0:0.01:1.1;
IGuess=sqrt(1-(pi/a.*((0:1:terms)+5/4)).^2);
CGuess=[(-(1-a^2*beta^2)*tau1)^0.25 -conj((-(1-a^2*beta^2)*tau1)^0.25)];
sn=NewtonRaphson(alpha,beta,tau1,nu,RGuess,IGuess,CGuess,a).';
sn=sn(abs(sn)<terms*pi/a);
kappa=sqrt(1-sn.^2); Tw1=length(kappa);
% Fundamental root values
RGuess=0:0.01:1.1;
IGuess=sqrt(1-(pi/b.*((0:1:terms)+5/4)).^2);
CGuess=[(-(1-b^2*beta^2)*tau2)^0.25 -conj((-(1-b^2*beta^2)*tau2)^0.25)];
eta=NewtonRaphson(alpha,beta,tau2,nu,RGuess,IGuess,CGuess,b).';
eta=eta(abs(eta)<terms*pi/b);
gamma=sqrt(1-eta.^2); Tw2=length(gamma);
% ---------- CC & DD ----------
CC=FunctionHH(alpha,beta,tau1,nu,sn,kappa,a);
DD=FunctionHH(alpha,beta,tau2,nu,eta,gamma,b);
% ---------- RR Integral -----------
RR=zeros(length(kappa),length(gamma));
for n=1:length(kappa)
    for m=1:length(gamma)
        RR(n,m)=IntegralRR(kappa(n),gamma(m),a);
```

```
    end
end
% --------- Bessel function---------
JJa=besselj(1,a*kappa); JJb=besselj(1,b*gamma);
% ---------- Solver -----------
[AA BB]=AxiSolver(a,b,alpha,beta,tau1,tau2,nu,sn.',eta.',JJa.',JJb.'...
    ,CC.',DD.',RR,ell);
PowA=real(sum(abs(AA).^2.*CC.*sn));
PowB=real(sum(abs(BB).^2.*DD.*eta));
index=index+1;
data(index,:)=[f,PowA,PowB];
PowA+PowB
end
end

% Characteristic equation
function K=Characteristic(s,alpha,beta,tau,nu,a)
K=((-tau*nu^2*s.^2-(beta^2-s.^2).*(s.^4+(1-a^2*beta^2)*tau))...
    .*sqrt(1-s.^2).*besselj(1,a*sqrt(1-s.^2))-(beta^2-s.^2)...
    .*alpha.*besselj(0,a*sqrt(1-s.^2)));
end

% The Differentiated characteristic equation
function K=DCharacteristic(s,alpha,beta,tau,nu,a)
f1=@(x) Characteristic(x,alpha,beta,tau,nu,a);
K=(f1(s+1e-5)-f1(s-1e-5))/2e-5;
end

% Newton Raphson Method
function Roots=NewtonRaphson(alpha,beta,tau,nu,RGuess,IGuess,CGuess,r)
warning('off','MATLAB:rankDeficientMatrix')
f1=@(x) Characteristic(x,alpha,beta,tau,nu,r);
df1=@(x) DCharacteristic(x,alpha,beta,tau,nu,r);
xold1=RGuess; xold2=IGuess; xold3=CGuess;
for i=1:10
    jac1=df1(xold1);
    sol1=xold1-f1(xold1)./jac1;
    xold1=sol1;
    jac2=df1(xold2);
    sol2=xold2-f1(xold2)./jac2;
    xold2=sol2;
    jac3=df1(xold3);
    sol3=xold3-f1(xold3)./jac3;
    xold3=sol3;
end
Real=sol1;
Real=Real(abs(f1(Real))<1e-5);
Real=sort(Real(Real>0),'descend');
TempIndex=1;
TempReal(TempIndex)=Real(1);
for Index=2:length(Real)
    if abs(Real(Index)-TempReal(TempIndex))>3e-5
        TempIndex=TempIndex+1;
        TempReal(TempIndex)=Real(Index);
    end
end
sol2=sol2((length(TempReal)-1):end);
Imaginary=sol2; Complex=sol3;
Imaginary=sort(Imaginary(imag(Imaginary)>0),'descend');
TempIndex=1;
TempIm(TempIndex)=Imaginary(1);
for Index=2:length(Imaginary)
    if abs(Imaginary(Index)-TempIm(TempIndex))>1e-5
        TempIndex=TempIndex+1;
        TempIm(TempIndex)=Imaginary(Index);
    end
end
Imaginary=[TempIm,Complex];
% Sort the complex roots in ascending order
[~,idx]=sort(imag(Imaginary),'ascend');
```

```
Imaginary=Imaginary(idx);
Roots=[TempReal,Imaginary];
end

function HH=FunctionHH(alpha,beta,tau,nu,eta,gamma,r)
f1=@(x) Characteristic(x,alpha,beta,tau,nu,r);
HH=(f1(eta+1e-5)-f1(eta-1e-5))./(2e-5).*gamma.*besselj(1,r*gamma)...
    ./(2*eta.*(eta.^2-beta^2));
end

function RR=IntegralRR(gamma,kappa,a)
if abs(kappa^2-gamma^2)<1e-5
    RR=a^2*(besselj(0,a*kappa)^2+besselj(1,a*kappa)^2)/2;
else
    RR=a*(kappa*besselj(0,a*gamma)*besselj(1,a*kappa)-...
        gamma*besselj(0,a*kappa)*besselj(1,a*gamma))/(kappa^2-gamma^2);
end
end

function [AN BM]=AxiSolver(a,b,alpha,beta,tau1,tau2,nu,sn,eta,JJa,JJb,...
    CC,DD,RR,ell)
Nn=length(sn); Nm=length(eta);
kappa=(1-sn.^2).^0.5; gamma=(1-eta.^2).^0.5;
F=sqrt(1/(abs(CC(ell))*sn(ell)));
%---------- The edge conditions ----------%
%---------- Sum Am E#A + Sum Bm E#B +E#F = 0;
%---------- Clamped ----------%
PsiA1=sn.*kappa.*JJa./(sn.^2-beta^2); PsiB1=zeros(1,Nm);
PsiF1=-sn(ell)*kappa(ell)*JJa(ell)/(sn(ell)^2-beta^2);
PsiA2=kappa.*JJa; PsiB2=zeros(1,Nm); PsiF2=kappa(ell)*JJa(ell);
PsiA3=sn.*kappa.*JJa; PsiB3=zeros(1,Nm);
PsiF3=-sn(ell)*kappa(ell)*JJa(ell);
PsiA4=zeros(1,Nn); PsiB4=eta.*gamma.*JJb./(eta.^2-beta^2); PsiF4=0;
PsiA5=zeros(1,Nn); PsiB5=eta.*gamma.*JJb; PsiF5=0;
PsiA6=zeros(1,Nn); PsiB6=gamma.*JJb; PsiF6=0;
%---------- Pin Jointed ----------%
% PsiA1=kappa.*JJa; PsiF1=kappa(ell).*JJa(ell); PsiB1=zeros(1,Nm);
% PsiA2=sn.^2.*kappa.*JJa; PsiB2=zeros(1,Nm);
% PsiF2=sn(ell).^2.*kappa(ell).*JJa(ell);
% PsiA3=sn.^2.*kappa.*JJa./(sn.^2-beta^2); PsiB3=zeros(1,Nm);
% PsiF3=sn(ell)^2*kappa(ell)*JJa(ell)./(sn(ell).^2-beta^2);
% PsiA4=zeros(1,Nn); PsiB4=gamma.*JJb./(eta.^2-beta^2); PsiF4=0;
% PsiA5=zeros(1,Nn); PsiB5=eta.^2.*gamma.*JJb; PsiF5=0;
% PsiA6=zeros(1,Nn); PsiB6=gamma.*JJb; PsiF6=0;
%---------- The Summations ----------%
SA0=0; SB0=0; SC0=0; SA1=0; SB1=0; SC1=0; SA2=0; SB2=0; SC2=0;
for n=1:Nn
    SA0=SA0+tau1*nu^2*beta^2*kappa(n)*JJa(n)*PsiA1(n)...
        /(sn(n)^2-beta^2)/CC(n);
    SB0=SB0+(2-kappa(n)^2)*kappa(n)*JJa(n)*PsiA1(n)/CC(n);
    SC0=SC0+kappa(n)*JJa(n)*PsiA1(n)/CC(n);
    SA1=SA1+tau1*nu^2*beta^2*kappa(n)*JJa(n)*PsiA2(n)...
        /(sn(n)^2-beta^2)/CC(n);
    SB1=SB1+(2-kappa(n)^2)*kappa(n)*JJa(n)*PsiA2(n)/CC(n);
    SC1=SC1+kappa(n)*JJa(n)*PsiA2(n)/CC(n);
    SA2=SA2+tau1*nu^2*beta^2*kappa(n)*JJa(n)*PsiA3(n)...
        /(sn(n)^2-beta^2)/CC(n);
    SB2=SB2+(2-kappa(n)^2)*kappa(n)*JJa(n)*PsiA3(n)/CC(n);
    SC2=SC2+kappa(n)*JJa(n)*PsiA3(n)/CC(n);
end
SD3=0; SE3=0; SF3=0; SD4=0; SE4=0; SF4=0; SD5=0; SE5=0; SF5=0;
for m=1:Nm
    SD3=SD3+tau2*nu^2*beta^2*gamma(m)*JJb(m)*PsiB4(m)...
        /(eta(m)^2-beta^2)/eta(m)/DD(m);
    SE3=SE3+(2-gamma(m)^2)*gamma(m)*JJb(m)*PsiB4(m)/eta(m)/DD(m);
    SF3=SF3+gamma(m)*JJb(m)*PsiB4(m)/eta(m)/DD(m);
    SD4=SD4+tau2*nu^2*beta^2*gamma(m)*JJb(m)*PsiB5(m)...
        /(eta(m)^2-beta^2)/eta(m)/DD(m);
    SE4=SE4+(2-gamma(m)^2)*gamma(m)*JJb(m)*PsiB5(m)/eta(m)/DD(m);
    SF4=SF4+gamma(m)*JJb(m)*PsiB5(m)/eta(m)/DD(m);
```

```
    SD5=SD5+tau2*nu^2*beta^2*gamma(m)*JJb(m)*PsiB6(m)...
        /(eta(m)^2-beta^2)/eta(m)/DD(m);
    SE5=SE5+(2-gamma(m)^2)*gamma(m)*JJb(m)*PsiB6(m)/eta(m)/DD(m);
    SF5=SF5+gamma(m)*JJb(m)*PsiB6(m)/eta(m)/DD(m);
end
DA=-SA2*SB1*SC0+SA1*SB2*SC0+SA2*SB0*SC1-SA0*SB2*SC1...
    -SA1*SB0*SC2+SA0*SB1*SC2;
DB=-SD5*SE4*SF3+SD4*SE5*SF3+SD5*SE3*SF4-SD3*SE5*SF4...
    -SD4*SE3*SF5+SD3*SE4*SF5;
Fdelta=zeros(1,Nn); GE0=zeros(1,Nn); GE1=zeros(1,Nn); GE2=zeros(1,Nn);
GE0a=0; GE1a=0; GE2a=0;
for n=1:Nn
    GE0a=GE0a+F*kdelta(ell,n)*PsiA1(n);
    GE1a=GE1a+F*kdelta(ell,n)*PsiA2(n);
    GE2a=GE2a+F*kdelta(ell,n)*PsiA3(n);
end
for n=1:Nn
    Fdelta(n)=F*kdelta(ell,n);
    GE0(n)=((SB2*SC1-SB1*SC2)*(F*PsiF1-GE0a)+(SB0*SC2-SB2*SC0)*...
        (F*PsiF2-GE1a)+(SB1*SC0-SB0*SC1)*(F*PsiF3-GE2a))/DA;
    GE1(n)=((SA2*SC1-SA1*SC2)*(F*PsiF1-GE0a)+(SA0*SC2-SA2*SC0)*...
        (F*PsiF2-GE1a)+(SA1*SC0-SA0*SC1)*(F*PsiF3-GE2a))/DA;
    GE2(n)=((SA2*SB1-SA1*SB2)*(F*PsiF1-GE0a)+(SA0*SB2-SA2*SB0)*...
        (F*PsiF2-GE1a)+(SA1*SB0-SA0*SB1)*(F*PsiF3-GE2a))/DA;
end
GE3b=0; GE4b=0; GE5b=0;
for m=1:Nm
    GE3b=GE3b+F*sn(ell)*RR(ell,m)*PsiB4(m)/(eta(m)*DD(m));
    GE4b=GE4b+F*sn(ell)*RR(ell,m)*PsiB5(m)/(eta(m)*DD(m));
    GE5b=GE5b+F*sn(ell)*RR(ell,m)*PsiB6(m)/(eta(m)*DD(m));
end
GE3=zeros(1,Nm); GE4=zeros(1,Nm); GE5=zeros(1,Nm);
for m=1:Nm
    GE3(m)=((SE5*SF4-SE4*SF5)*(GE3b+F*PsiF4)+(SE3*SF5-SE5*SF3)*...
        (GE4b+F*PsiF5)+(SE4*SF3-SE3*SF4)*(GE5b+F*PsiF6))/DB;
    GE4(m)=((SD5*SF4-SD4*SF5)*(GE3b+F*PsiF4)+(SD3*SF5-SD5*SF3)*...
        (GE4b+F*PsiF5)+(SD4*SF3-SD3*SF4)*(GE5b+F*PsiF6))/DB;
    GE5(m)=((SD5*SE4-SD4*SE5)*(GE3b+F*PsiF4)+(SD3*SE5-SD5*SE3)*...
        (GE4b+F*PsiF5)+(SD4*SE3-SD3*SE4)*(GE5b+F*PsiF6))/DB;
end
V1=(-Fdelta+tau1*nu^2*beta^2*kappa.*JJa.*GE0./(sn.^2-beta^2)...
    ./CC+(2-kappa.^2).*kappa.*JJa.*GE1./CC-kappa.*JJa.*GE2./CC).';
V2=(tau1*nu^2*beta^2*kappa.*JJa./(sn.^2-beta^2)./CC/DA).';
V3=-((2-kappa.^2).*kappa.*JJa./CC/DA).';
V4=(kappa.*JJa./CC/DA).';
V5=(F*sn(ell).*RR(ell,:)./(eta.*DD)+tau2*nu^2*beta^2*...
    gamma.*JJb.*GE3./(eta.^2-beta^2)./eta./DD+(2-gamma.^2).*...
    gamma.*JJb.*GE4./eta./DD-gamma.*JJb.*GE5./eta./DD).';
V6=(tau2*nu^2*beta^2*gamma.*JJb./(eta.^2-beta^2)./eta./DD/DB).';
V7=-((2-gamma.^2).*gamma.*JJb./eta./DD/DB).';
V8=(gamma.*JJb./eta./DD/DB).';
M1=zeros(Nn,Nm); M2=zeros(Nn,Nm); M3=zeros(Nn,Nm); M4=zeros(Nn,Nm);
M5=zeros(Nn,Nm); M6=zeros(Nn,Nm); M7=zeros(Nn,Nm);
for n=1:Nn
    for m=1:Nm
        M1(end,m)=PsiB1(m);
        M2(n,m)=alpha*RR(n,m)*PsiA1(n)/CC(n)/a;
        M3(end,m)=PsiB2(m);
        M4(n,m)=alpha*RR(n,m)*PsiA2(n)/CC(n)/a;
        M5(end,m)=PsiB3(m);
        M6(n,m)=alpha*RR(n,m)*PsiA3(n)/CC(n)/a;
        M7(n,m)=alpha*RR(n,m)/CC(n)/a;
    end
end
M8=zeros(Nm,Nn); M9=zeros(Nm,Nn); M10=zeros(Nm,Nn); M11=zeros(Nm,Nn);
M12=zeros(Nm,Nn); M13=zeros(Nm,Nn); M14=zeros(Nm,Nn);
for n=1:Nn
    for m=1:Nm
        M9(m,n)=-alpha*sn(n)*RR(n,m)*PsiB4(m)/(b*eta(m)*DD(m));
        M11(m,n)=-alpha*sn(n)*RR(n,m)*PsiB5(m)/(b*eta(m)*DD(m));
```

```
        M13(m,n)=-alpha*sn(n)*RR(n,m)*PsiB6(m)/(b*eta(m)*DD(m));
        M14(m,n)=alpha*sn(n)*RR(n,m)/(b*eta(m)*DD(m));
    end
    M8(end,n)=PsiA4(n);
    M10(end,n)=PsiA5(n);
    M12(end,n)=PsiA6(n);
end
em=ones(1,Nm); en=ones(1,Nn);
BM=(eye(Nm)-(...
    +((SE5*SF4-SE4*SF5)*V6+(SD5*SF4-SD4*SF5)*V7+(SD5*SE4-SD4*SE5)*V8)...
    *em*M8...
    +((SE5*SF4-SE4*SF5)*V6+(SD5*SF4-SD4*SF5)*V7+(SD5*SE4-SD4*SE5)*V8)...
    *em*M9...
    +((SE3*SF5-SE5*SF3)*V6+(SD3*SF5-SD5*SF3)*V7+(SD3*SE5-SD5*SE3)*V8)...
    *em*M10...
    +((SE3*SF5-SE5*SF3)*V6+(SD3*SF5-SD5*SF3)*V7+(SD3*SE5-SD5*SE3)*V8)...
    *em*M11...
    +((SE4*SF3-SE3*SF4)*V6+(SD4*SF3-SD3*SF4)*V7+(SD4*SE3-SD3*SE4)*V8)...
    *em*M12...
    +((SE4*SF3-SE3*SF4)*V6+(SD4*SF3-SD3*SF4)*V7+(SD4*SE3-SD3*SE4)*V8)...
    *em*M13-M14)*(...
    +((SB2*SC1-SB1*SC2)*V2+(SA2*SC1-SA1*SC2)*V3+(SA2*SB1-SA1*SB2)*V4)...
    *en*M1...
    +((SB2*SC1-SB1*SC2)*V2+(SA2*SC1-SA1*SC2)*V3+(SA2*SB1-SA1*SB2)*V4)...
    *en*M2...
    +((SB0*SC2-SB2*SC0)*V2+(SA0*SC2-SA2*SC0)*V3+(SA0*SB2-SA2*SB0)*V4)...
    *en*M3...
    +((SB0*SC2-SB2*SC0)*V2+(SA0*SC2-SA2*SC0)*V3+(SA0*SB2-SA2*SB0)*V4)...
    *en*M4...
    +((SB1*SC0-SB0*SC1)*V2+(SA1*SC0-SA0*SC1)*V3+(SA1*SB0-SA0*SB1)*V4)...
    *en*M5...
    +((SB1*SC0-SB0*SC1)*V2+(SA1*SC0-SA0*SC1)*V3+(SA1*SB0-SA0*SB1)*V4)...
    *en*M6+M7))\(V5+(...
    +((SE5*SF4-SE4*SF5)*V6+(SD5*SF4-SD4*SF5)*V7+(SD5*SE4-SD4*SE5)*V8)...
    *em*M8*V1...
    +((SE5*SF4-SE4*SF5)*V6+(SD5*SF4-SD4*SF5)*V7+(SD5*SE4-SD4*SE5)*V8)...
    *em*M9*V1...
    +((SE3*SF5-SE5*SF3)*V6+(SD3*SF5-SD5*SF3)*V7+(SD3*SE5-SD5*SE3)*V8)...
    *em*M10*V1...
    +((SE3*SF5-SE5*SF3)*V6+(SD3*SF5-SD5*SF3)*V7+(SD3*SE5-SD5*SE3)*V8)...
    *em*M11*V1...
    +((SE4*SF3-SE3*SF4)*V6+(SD4*SF3-SD3*SF4)*V7+(SD4*SE3-SD3*SE4)*V8)...
    *em*M12*V1...
    +((SE4*SF3-SE3*SF4)*V6+(SD4*SF3-SD3*SF4)*V7+(SD4*SE3-SD3*SE4)*V8)...
    *em*M13*V1-M14*V1));
AN=V1+...
   (((SB2*SC1-SB1*SC2)*V2+(SA2*SC1-SA1*SC2)*V3+(SA2*SB1-SA1*SB2)*V4)...
    *en*M1...
    +((SB2*SC1-SB1*SC2)*V2+(SA2*SC1-SA1*SC2)*V3+(SA2*SB1-SA1*SB2)*V4)...
    *en*M2...
    +((SB0*SC2-SB2*SC0)*V2+(SA0*SC2-SA2*SC0)*V3+(SA0*SB2-SA2*SB0)*V4)...
    *en*M3...
    +((SB0*SC2-SB2*SC0)*V2+(SA0*SC2-SA2*SC0)*V3+(SA0*SB2-SA2*SB0)*V4)...
    *en*M4...
    +((SB1*SC0-SB0*SC1)*V2+(SA1*SC0-SA0*SC1)*V3+(SA1*SB0-SA0*SB1)*V4)...
    *en*M5...
    +((SB1*SC0-SB0*SC1)*V2+(SA1*SC0-SA0*SC1)*V3+(SA1*SB0-SA0*SB1)*V4)...
    *en*M6+M7)*BM;
end

%---------- Kronecker delta ----------%
function d=kdelta(n,m)
if n==m
    d=1;
else
    d=0;
end
end
```

Appendix H

Matlab code relating to Section 4.2

```
function AppendixH()% Rigid expansion two shells
clc; clear;
index=0;
for f=5:1200
% ---------- Input Variables ----------
a1=0.2; % Dimensional radius a (m)
b1=0.28; % Dimensional radius b (m)
L1=0.5; % Half the length of expansion chamber (m)
Cair=343.5; % Sound speed of fluid (m/s)
Dair=1.2; % Density of fluid (kg/m^3)
EE=7.2*10^10; % Youngs Modulus (N/m^2)
h1=0.002; % Dimensional shell thickness (m)
Dplate=2700; % Density of shell (kg/m^3)
nu=0.34; % Poisson's ratio for shell
terms=100; % Number of imaginary roots to seek
ell=1; % Indicator for fundamental root
% ---------- Calculated Variables ----------
kno=2*pi*f/Cair; % Fluid wave number
a=a1*kno; % Nondimensional radius a
b=b1*kno; % Nondimensional radius b
L=L1*kno; % Nondimensional length
h=h1*kno; % Nondimensional shell thickness
cp1=sqrt(EE/(1-nu^2)/Dplate); % Sound speed of the shell
beta=Cair/cp1; omega=Cair*kno; tau1=12/(h^2*a^2);
alpha=12*omega^2*Dair/(h^3*cp1^2*kno^2*Dplate);
% ---------- sn ----------
RGuess=0:0.01:1.1;
IGuess=sqrt(1-(pi/a.*((0:1:terms)+5/4)).^2);
CGuess=[(-(1-a^2*beta^2)*tau1)^0.25 -conj((-(1-a^2*beta^2)*tau1)^0.25)];
sn=NewtonRaphson(alpha,beta,tau1,nu,RGuess,IGuess,CGuess,a).';
sn=sn(abs(sn)<terms*pi/a);
kappa=sqrt(1-sn.^2); Tw1=length(kappa);
% ---------- eta ----------
RealGuess=0:0.01:1;
ImaginaryGuess=(1-(pi/b*((1:terms)+0.25)).^2).^0.5;
eta=NewtonRaphsonRigid(RealGuess,ImaginaryGuess,b).';
eta=eta(abs(eta)<terms*pi/b);
gamma=sqrt(1-eta.^2); Tw2=length(gamma);
% ---------- CC & DD ----------
CC=FunctionCC(alpha,beta,tau1,nu,sn,kappa,a);
DD=FunctionDD(eta,gamma,b);
% ---------- RR Integral ----------
RR=zeros(length(kappa),length(gamma));
for n=1:length(kappa)
    for m=1:length(gamma)
        RR(n,m)=IntegralRR(kappa(n),gamma(m),a);
    end
```

```
end
% --------- Bessel function---------
JJa=besselj(1,a*kappa);
% ---------- Solver -----------
AAS=SSolver(alpha,beta,tau1,nu,a,b,eta.',sn.',CC.',DD.',JJa.',RR,ell,L);
AAA=ASolver(alpha,beta,tau1,nu,a,b,eta.',sn.',CC.',DD.',JJa.',RR,ell,L);
PowA=real(sum(abs((AAS+AAA)*0.5).^2.*CC.*sn));
PowB=real(sum(abs((AAS-AAA)*0.5).^2.*CC.*sn));
index=index+1;
data(index,:)=[f,PowA,PowB];
end
end

% Characteristic equation
function K=Characteristic(s,alpha,beta,tau,nu,a)
K=(-tau*nu^2*s.^2-(beta^2-s.^2).*(s.^4+(1-a^2*beta^2)*tau))...
    .*sqrt(1-s.^2).*besselj(1,a*sqrt(1-s.^2))-(beta^2-s.^2)...
    .*alpha.*besselj(0,a*sqrt(1-s.^2));
end

% The Differentiated characteristic equation
function K=DCharacteristic(s,alpha,beta,tau,nu,a)
f1=@(x) Characteristic(x,alpha,beta,tau,nu,a);
K=(f1(s+1e-5)-f1(s-1e-5))/2e-5;
end

% Characteristic equation for rigid
function K=RigidDispersion(sn,r)
kappa=(1-sn.^2).^0.5;
K=kappa.*besselj(1,r*kappa);
end

% The Differentiated characteristic equation for rigid
function K=RigidDDispersion(s,r)
f1=@(x) RigidDispersion(x,r);
K=(f1(s+1e-5)-f1(s-1e-5))/2e-5;
end

% Newton Raphson Method
function Roots=NewtonRaphson(alpha,beta,tau,nu,RGuess,IGuess,CGuess,r)
warning('off','MATLAB:rankDeficientMatrix')
f1=@(x) Characteristic(x,alpha,beta,tau,nu,r);
df1=@(x) DCharacteristic(x,alpha,beta,tau,nu,r);
xold1=RGuess; xold2=IGuess; xold3=CGuess;
for i=1:10
    jac1=df1(xold1);
    sol1=xold1-f1(xold1)./jac1;
    xold1=sol1;
    jac2=df1(xold2);
    sol2=xold2-f1(xold2)./jac2;
    xold2=sol2;
    jac3=df1(xold3);
    sol3=xold3-f1(xold3)./jac3;
    xold3=sol3;
end
Real=sol1;
Real=Real(abs(f1(Real))<1e-5);
Real=sort(Real(Real>0),'descend');
TempIndex=1;
TempReal(TempIndex)=Real(1);
for Index=2:length(Real)
    if abs(Real(Index)-TempReal(TempIndex))>3e-5
        TempIndex=TempIndex+1;
        TempReal(TempIndex)=Real(Index);
    end
end
sol2=sol2((length(TempReal)-1):end);
Imaginary=sol2; Complex=sol3;
Imaginary=sort(Imaginary(imag(Imaginary)>0),'descend');
TempIndex=1;
```

```
TempIm(TempIndex)=Imaginary(1);
for Index=2:length(Imaginary)
    if abs(Imaginary(Index)-TempIm(TempIndex))>1e-5
        TempIndex=TempIndex+1;
        TempIm(TempIndex)=Imaginary(Index);
    end
end
Imaginary=[TempIm,Complex];
% Sort the complex roots in ascending order
[~,idx]=sort(imag(Imaginary),'ascend');
Imaginary=Imaginary(idx);
Roots=[TempReal,Imaginary];
end

function Roots=NewtonRaphsonRigid(RGuess,IGuess,r)
warning('off','MATLAB:rankDeficientMatrix')
f1=@(x) RigidDispersion(x,r); df1=@(x) RigidDDispersion(x,r);
xold1=RGuess; xold2=IGuess;
for i=1:20
    jac1=df1(xold1);
    sol1=xold1-f1(xold1)./jac1;
    xold1=sol1;
    jac2=df1(xold2);
    sol2=xold2-f1(xold2)./jac2;
    xold2=sol2;
end
Real=sol1;
Real=Real(abs(f1(Real))<1e-2);
Real=sort(Real(Real>0),'descend');
TempIndex=1;
TempReal(TempIndex)=Real(1);
for Index=2:length(Real)
    if abs(Real(Index)-TempReal(TempIndex))>1e-1
        TempIndex=TempIndex+1;
        TempReal(TempIndex)=Real(Index);
    end
end
Imaginary=sol2;
Imaginary=Imaginary(abs(f1(Imaginary))<1e-5);
Imaginary=sort(Imaginary(imag(Imaginary)>0),'descend');
TempIndex=1;
TempImaginary(TempIndex)=Imaginary(1);
for Index=2:length(Imaginary)
    if abs(Imaginary(Index)-TempImaginary(TempIndex))>1e-4
        TempIndex=TempIndex+1;
        TempImaginary(TempIndex)=Imaginary(Index);
    end
end
% Sort the complex roots in ascending order
[~,idx]=sort(imag(TempImaginary),'ascend');
TempImaginary=TempImaginary(idx);
Roots=[TempReal,TempImaginary];
end

function CC=FunctionCC(alpha,beta,tau,nu,eta,gamma,r)
f1=@(x) Characteristic(x,alpha,beta,tau,nu,r);
CC=(f1(eta+1e-5)-f1(eta-1e-5))./(2e-5).*gamma.*besselj(1,r*gamma)...
    ./(2*eta.*(eta.^2-beta^2));
end

function DD=FunctionDD(eta,gamma,r)
f1=@(x) RigidDispersion(x,r);
DD=-(f1(eta+1e-5)-f1(eta-1e-5))./(2e-5).*besselj(0,r*gamma)./(2*eta);
end

function RR=IntegralRR(gamma,kappa,a)
if abs(kappa^2-gamma^2)<1e-5
    RR=a^2*(besselj(0,a*gamma)^2+besselj(1,a*gamma)^2)/2;
else
    RR=a*(kappa*besselj(0,a*gamma)*besselj(1,a*kappa)-...
```

```
        gamma*besselj(0,a*kappa)*besselj(1,a*gamma))/(kappa^2-gamma^2);
end
end

function [AN PM]=SSolver(alpha,beta,tau1,nu,a,b,eta,s,CC,DD,JJa,RR,ell,L)
Nn=length(s); Nm=length(eta);
kappa=(1-s.^2).^0.5; F=sqrt(1/(abs(CC(ell))*s(ell)));
%---------- The edge conditions ----------%
%---------- Clamped ----------%
E0A=s.*kappa.*JJa; E0B=zeros(1,Nm); E0F=-s(ell)*kappa(ell)*JJa(ell);
E1A=kappa.*JJa; E1B=zeros(1,Nm); E1F=kappa(ell)*JJa(ell);
E2A=s.*kappa.*JJa./(s.^2-beta^2); E2B=zeros(1,Nm);
E2F=s(ell)*kappa(ell)*JJa(ell)/(s(ell)^2-beta^2);
%---------- Pin-Jointed ----------%
% E0A=s.^2.*kappa.*JJa; E0B=zeros(1,Nm); E0F=-s(ell)^2*kappa(ell)*JJa(ell);
% E1A=kappa.*JJa; E1B=zeros(1,Nm); E1F=kappa(ell)*JJa(ell);
% E2A=s.^2.*kappa.*JJa./(s.^2-beta^2); E2B=zeros(1,Nm);
% E2F=s(ell)^2*kappa(ell)*JJa(ell)/(s(ell)^2-beta^2);
%---------- The Summations ----------%
S0=0; S1=0; S2=0; S3=0; S4=0; S5=0; S6=0; S7=0; S8=0;
for n=1:Nn
    S0=S0+tau1*nu^2*beta^2*kappa(n)*JJa(n)*E0A(n)/(s(n)^2-beta^2)/CC(n);
    S1=S1+(2-kappa(n)^2)*kappa(n)*JJa(n)*E0A(n)/CC(n);
    S2=S2+kappa(n)*JJa(n)*E0A(n)/CC(n);
    S3=S3+tau1*nu^2*beta^2*kappa(n)*JJa(n)*E1A(n)/(s(n)^2-beta^2)/CC(n);
    S4=S4+(2-kappa(n)^2)*kappa(n)*JJa(n)*E1A(n)/CC(n);
    S5=S5+kappa(n)*JJa(n)*E1A(n)/CC(n);
    S6=S6+tau1*nu^2*beta^2*kappa(n)*JJa(n)*E2A(n)/(s(n)^2-beta^2)/CC(n);
    S7=S7+(2-kappa(n)^2)*kappa(n)*JJa(n)*E2A(n)/CC(n);
    S8=S8+kappa(n)*JJa(n)*E2A(n)/CC(n);
end
DEA=-S2*S4*S6+S1*S5*S6+S2*S3*S7-S0*S5*S7-S1*S3*S8+S0*S4*S8;
Fdelta=zeros(1,Nn); GE0=zeros(1,Nn); GE1=zeros(1,Nn); GE2=zeros(1,Nn);
GE0a=0; GE1a=0; GE2a=0;
for n=1:Nn
    GE0a=GE0a+F*kdelta(ell,n)*E0A(n);
    GE1a=GE1a+F*kdelta(ell,n)*E1A(n);
    GE2a=GE2a+F*kdelta(ell,n)*E2A(n);
end
for n=1:Nn
    Fdelta(n)=F*kdelta(ell,n);
    GE0(n)=((S5*S7-S4*S8)*(F*E0F-GE0a)+(S1*S8-S2*S7)*(F*E1F-GE1a)+...
        (S2*S4-S1*S5)*(F*E2F-GE2a))/DEA;
    GE1(n)=((S5*S6-S3*S8)*(F*E0F-GE0a)+(S0*S8-S2*S6)*(F*E1F-GE1a)+...
        (S2*S3-S0*S5)*(F*E2F-GE2a))/-DEA;
    GE2(n)=((S4*S6-S3*S7)*(F*E0F-GE0a)+(S0*S7-S1*S6)*(F*E1F-GE1a)+...
        (S1*S3-S0*S4)*(F*E2F-GE2a))/-DEA;
end
VFA=(-Fdelta+tau1*nu^2*beta^2*kappa.*JJa.*GE0./(s.^2-beta^2)./CC+...
    (2-kappa.^2).*kappa.*JJa.*GE1./CC-kappa.*JJa.*GE2./CC).';
V0=(tau1*nu^2*beta^2*kappa.*JJa./(s.^2-beta^2)./CC/DEA).';
V1=((2-kappa.^2).*kappa.*JJa./CC/-DEA).';
V2=-(kappa.*JJa./CC/-DEA).';
VFP=(1i*F*s(ell).*RR(ell,:)./(2*b*eta.*DD)./sin(eta*L)).';
M0=zeros(Nn,Nm); M1=zeros(Nn,Nm); M2=zeros(Nn,Nm); M3=zeros(Nn,Nm);
M4=zeros(Nn,Nm); M5=zeros(Nn,Nm); M6=zeros(Nn,Nm);
for n=1:Nn
    for m=1:Nm
        M0(n,m)=2*alpha*RR(n,m)*cos(eta(m)*L)*E0A(n)/CC(n)/a;
        M1(n,m)=2*alpha*RR(n,m)*cos(eta(m)*L)*E1A(n)/CC(n)/a;
        M2(n,m)=2*alpha*RR(n,m)*cos(eta(m)*L)*E2A(n)/CC(n)/a;
        M3(end,m)=E0B(m);
        M4(end,m)=E1B(m);
        M5(end,m)=E2B(m);
        M6(n,m)=2*alpha*RR(n,m)*cos(eta(m)*L)/CC(n)/a;
    end
end
M13=zeros(Nm,Nn);
for n=1:Nn
    for m=1:Nm
```

```
        M13(m,n)=-1i*s(n)*RR(n,m)/(2*b*eta(m)*DD(m)*sin(eta(m)*L));
    end
end
en=ones(1,Nn);
AN=(eye(Nn)-(...
    +((S5*S7-S4*S8)*V0+(S5*S6-S3*S8)*V1+(S4*S6-S3*S7)*V2)*en*M0+...
    ((S5*S7-S4*S8)*V0+(S5*S6-S3*S8)*V1+(S4*S6-S3*S7)*V2)*en*M3...
    +((S1*S8-S2*S7)*V0+(S0*S8-S2*S6)*V1+(S0*S7-S1*S6)*V2)*en*M1+...
    ((S1*S8-S2*S7)*V0+(S0*S8-S2*S6)*V1+(S0*S7-S1*S6)*V2)*en*M4...
    +((S2*S4-S1*S5)*V0+(S2*S3-S0*S5)*V1+(S1*S3-S0*S4)*V2)*en*M2+...
    ((S2*S4-S1*S5)*V0+(S2*S3-S0*S5)*V1+(S1*S3-S0*S4)*V2)*en*M5+M6)...
    *M13)\...
    (VFA+(...
    +((S5*S7-S4*S8)*V0+(S5*S6-S3*S8)*V1+(S4*S6-S3*S7)*V2)*en*M0*VFP+...
    ((S5*S7-S4*S8)*V0+(S5*S6-S3*S8)*V1+(S4*S6-S3*S7)*V2)*en*M3*VFP...
    +((S1*S8-S2*S7)*V0+(S0*S8-S2*S6)*V1+(S0*S7-S1*S6)*V2)*en*M1*VFP+...
    ((S1*S8-S2*S7)*V0+(S0*S8-S2*S6)*V1+(S0*S7-S1*S6)*V2)*en*M4*VFP...
    +((S2*S4-S1*S5)*V0+(S2*S3-S0*S5)*V1+(S1*S3-S0*S4)*V2)*en*M2*VFP+...
    ((S2*S4-S1*S5)*V0+(S2*S3-S0*S5)*V1+(S1*S3-S0*S4)*V2)*en*M5*VFP+M6*VFP));
PM=VFP+M13*AN;
end

function [AN PM]=ASolver(alpha,beta,tau1,nu,a,b,eta,s,CC,DD,JJa,RR,ell,L)
Nn=length(s); Nm=length(eta);
kappa=(1-s.^2).^0.5; F=sqrt(1/(abs(CC(ell))*s(ell)));
%---------- The edge conditions ----------%
%---------- Clamped ----------%
E0A=s.*kappa.*JJa; E0B=zeros(1,Nm); E0F=-s(ell)*kappa(ell)*JJa(ell);
E1A=kappa.*JJa; E1B=zeros(1,Nm); E1F=kappa(ell)*JJa(ell);
E2A=s.*kappa.*JJa./(s.^2-beta^2); E2B=zeros(1,Nm);
E2F=s(ell)*kappa(ell)*JJa(ell)/(s(ell)^2-beta^2);
%---------- Pin Jointed ----------%
% E0A=gamma.*JJa; E0B=zeros(1,Nm); E0F=gamma(ell)*JJa(ell);
% E1A=eta.*gamma.*JJa; E1B=zeros(1,Nm); E1F=-eta(ell)*gamma(ell)*JJa(ell);
% E2A=eta.^2.*gamma.*JJa./(eta.^2-beta^2); E2B=zeros(1,Nm);
% E2F=eta(ell)^2*gamma(ell)*JJa(ell)/(eta(ell)^2-beta^2);
S0=0; S1=0; S2=0; S3=0; S4=0; S5=0; S6=0; S7=0; S8=0;
for n=1:Nn
    S0=S0+tau1*nu^2*beta^2*kappa(n)*JJa(n)*E0A(n)/(s(n)^2-beta^2)/CC(n);
    S1=S1+(2-kappa(n)^2)*kappa(n)*JJa(n)*E0A(n)/CC(n);
    S2=S2+kappa(n)*JJa(n)*E0A(n)/CC(n);
    S3=S3+tau1*nu^2*beta^2*kappa(n)*JJa(n)*E1A(n)/(s(n)^2-beta^2)/CC(n);
    S4=S4+(2-kappa(n)^2)*kappa(n)*JJa(n)*E1A(n)/CC(n);
    S5=S5+kappa(n)*JJa(n)*E1A(n)/CC(n);
    S6=S6+tau1*nu^2*beta^2*kappa(n)*JJa(n)*E2A(n)/(s(n)^2-beta^2)/CC(n);
    S7=S7+(2-kappa(n)^2)*kappa(n)*JJa(n)*E2A(n)/CC(n);
    S8=S8+kappa(n)*JJa(n)*E2A(n)/CC(n);
end
DEA=-S2*S4*S6+S1*S5*S6+S2*S3*S7-S0*S5*S7-S1*S3*S8+S0*S4*S8;
Fdelta=zeros(1,Nn); GE0=zeros(1,Nn); GE1=zeros(1,Nn); GE2=zeros(1,Nn);
GE0a=0; GE1a=0; GE2a=0;
for n=1:Nn
    GE0a=GE0a+F*kdelta(ell,n)*E0A(n);
    GE1a=GE1a+F*kdelta(ell,n)*E1A(n);
    GE2a=GE2a+F*kdelta(ell,n)*E2A(n);
end
for n=1:Nn
    Fdelta(n)=F*kdelta(ell,n);
    GE0(n)=((S5*S7-S4*S8)*(F*E0F-GE0a)+(S1*S8-S2*S7)*(F*E1F-GE1a)+...
        (S2*S4-S1*S5)*(F*E2F-GE2a))/DEA;
    GE1(n)=((S5*S6-S3*S8)*(F*E0F-GE0a)+(S0*S8-S2*S6)*(F*E1F-GE1a)+...
        (S2*S3-S0*S5)*(F*E2F-GE2a))/-DEA;
    GE2(n)=((S4*S6-S3*S7)*(F*E0F-GE0a)+(S0*S7-S1*S6)*(F*E1F-GE1a)+...
        (S1*S3-S0*S4)*(F*E2F-GE2a))/-DEA;
end
VFA=(-Fdelta+tau1*nu^2*beta^2*kappa.*JJa.*GE0./(s.^2-beta^2)./CC+...
    (2-kappa.^2).*kappa.*JJa.*GE1./CC-kappa.*JJa.*GE2./CC).';
V0=(tau1*nu^2*beta^2*kappa.*JJa./(s.^2-beta^2)./CC/DEA).';
V1=((2-kappa.^2).*kappa.*JJa./CC/-DEA).';
V2=-(kappa.*JJa./CC/-DEA).';
```

```
VFP=(1i*F*s(ell).*RR(ell,:)./(2*b*eta.*DD)./cos(eta*L)).';
M0=zeros(Nn,Nm); M1=zeros(Nn,Nm); M2=zeros(Nn,Nm); M3=zeros(Nn,Nm);
M4=zeros(Nn,Nm); M5=zeros(Nn,Nm); M6=zeros(Nn,Nm);
for n=1:Nn
    for m=1:Nm
        M0(n,m)=2*alpha*RR(n,m)*sin(-eta(m)*L)*E0A(n)/CC(n)/a;
        M1(n,m)=2*alpha*RR(n,m)*sin(-eta(m)*L)*E1A(n)/CC(n)/a;
        M2(n,m)=2*alpha*RR(n,m)*sin(-eta(m)*L)*E2A(n)/CC(n)/a;
        M3(end,m)=E0B(m);
        M4(end,m)=E1B(m);
        M5(end,m)=E2B(m);
        M6(n,m)=2*alpha*RR(n,m)*sin(-eta(m)*L)/CC(n)/a;
    end
end
M13=zeros(Nm,Nn);
for n=1:Nn
    for m=1:Nm
        M13(m,n)=-1i*s(n)*RR(n,m)/(2*b*eta(m)*DD(m)*cos(eta(m)*L));
    end
end
en=ones(1,Nn);
AN=(eye(Nn)-(...
    +((S5*S7-S4*S8)*V0+(S5*S6-S3*S8)*V1+(S4*S6-S3*S7)*V2)*en*M0+...
    ((S5*S7-S4*S8)*V0+(S5*S6-S3*S8)*V1+(S4*S6-S3*S7)*V2)*en*M3...
    +((S1*S8-S2*S7)*V0+(S0*S8-S2*S6)*V1+(S0*S7-S1*S6)*V2)*en*M1+...
    ((S1*S8-S2*S7)*V0+(S0*S8-S2*S6)*V1+(S0*S7-S1*S6)*V2)*en*M4...
    +((S2*S4-S1*S5)*V0+(S2*S3-S0*S5)*V1+(S1*S3-S0*S4)*V2)*en*M2+...
    ((S2*S4-S1*S5)*V0+(S2*S3-S0*S5)*V1+(S1*S3-S0*S4)*V2)*en*M5+M6)...
    *M13)\...
    (VFA+(...
    +((S5*S7-S4*S8)*V0+(S5*S6-S3*S8)*V1+(S4*S6-S3*S7)*V2)*en*M0*VFP+...
    ((S5*S7-S4*S8)*V0+(S5*S6-S3*S8)*V1+(S4*S6-S3*S7)*V2)*en*M3*VFP...
    +((S1*S8-S2*S7)*V0+(S0*S8-S2*S6)*V1+(S0*S7-S1*S6)*V2)*en*M1*VFP+...
    ((S1*S8-S2*S7)*V0+(S0*S8-S2*S6)*V1+(S0*S7-S1*S6)*V2)*en*M4*VFP...
    +((S2*S4-S1*S5)*V0+(S2*S3-S0*S5)*V1+(S1*S3-S0*S4)*V2)*en*M2*VFP+...
    ((S2*S4-S1*S5)*V0+(S2*S3-S0*S5)*V1+(S1*S3-S0*S4)*V2)*en*M5*VFP+M6*VFP));
PM=VFP+M13*AN;
end

%---------- Kronecker delta ----------%
function d=kdelta(n,m)
if n==m
    d=1;
else
    d=0;
end
end
```

Appendix I

Matlab code relating to Section 4.3

```
function AppendixI() % Flexible expansion
clc; clear;
index=0;
for f=5:1200
% ---------- Input Variables ----------
a1=0.2; % Dimensional radius a (m)
b1=0.28; % Dimensional radius b (m)
L1=0.25; % Half the length of expansion chamber (m)
Cair=343.5; % Sound speed of fluid (m/s)
Dair=1.2; % Density of fluid (kg/m^3)
EE=7.2*10^10; % Youngs Modulus (N/m^2)
h1=0.002; % Dimensional shell thickness (m)
Dplate=2700; % Density of shell (kg/m^3)
nu=0.34; % Poisson's ratio for shell
terms=100; % Number of imaginary roots to seek
ell=1; % Indicator for fundamental root
% ---------- Calculated Variables ----------
kno=2*pi*f/Cair; % Fluid wave number
a=a1*kno; % Nondimensional radius a
b=b1*kno; % Nondimensional radius b
L=L1*kno; % Nondimensional length
h=h1*kno; % Nondimensional shell thickness
cp1=sqrt(EE/(1-nu^2)/Dplate); % Sound speed of the shell
beta=Cair/cp1; omega=Cair*kno;
tau1=12/(h^2*a^2); tau2=12/(h^2*b^2);
alpha=12*omega^2*Dair/(h^3*cp1^2*kno^2*Dplate);
% Number of cut on roots
RGuess=0:0.01:1.1;
IGuess=sqrt(1-(pi/a.*((0:1:terms)+5/4)).^2);
CGuess=[(-(1-a^2*beta^2)*tau1)^0.25 -conj((-(1-a^2*beta^2)*tau1)^0.25)];
sn=NewtonRaphson(alpha,beta,tau1,nu,RGuess,IGuess,CGuess,a).';
sn=sn(abs(sn)<terms*pi/a);
kappa=sqrt(1-sn.^2); Tw1=length(kappa);
% Fundemental root values
RGuess=0:0.01:1.1;
IGuess=sqrt(1-(pi/b.*((0:1:terms)+5/4)).^2);
CGuess=[(-(1-b^2*beta^2)*tau2)^0.25 -conj((-(1-b^2*beta^2)*tau2)^0.25)];
eta=NewtonRaphson(alpha,beta,tau2,nu,RGuess,IGuess,CGuess,b).';
eta=eta(abs(eta)<terms*pi/b);
gamma=sqrt(1-eta.^2);
Tw2=length(gamma);
% ---------- CC & DD ----------
CC=FunctionHH(alpha,beta,tau1,nu,sn,kappa,a);
DD=FunctionHH(alpha,beta,tau2,nu,eta,gamma,b);
% ---------- RR Integral -----------
RR=zeros(length(kappa),length(gamma));
for n=1:length(kappa)
```

```
    for m=1:length(gamma)
        RR(n,m)=IntegralRR(kappa(n),gamma(m),a);
    end
end
% --------- Bessel function---------
JJa=besselj(1,a*kappa); JJb=besselj(1,b*gamma);
% ---------- Solver -----------
AAS=SSolver(a,b,alpha,beta,tau1,tau2,nu,sn.',eta.'...
    ,JJa.',JJb.',CC.',DD.',RR,ell,L);
AAA=ASolver(a,b,alpha,beta,tau1,tau2,nu,sn.',eta.'...
    ,JJa.',JJb.',CC.',DD.',RR,ell,L);
PowA=real(sum(abs((AAS+AAA)*0.5).^2.*CC.*sn));
PowB=real(sum(abs((AAS-AAA)*0.5).^2.*CC.*sn));
index=index+1;
data(index,:)=[f,PowA,PowB];
end
end
% Characteristic equation
function K=Characteristic(s,alpha,beta,tau,nu,a)
K=(-tau*nu^2*s.^2-(beta^2-s.^2).*(s.^4+(1-a^2*beta^2)*tau))...
    .*sqrt(1-s.^2).*besselj(1,a*sqrt(1-s.^2))-(beta^2-s.^2)...
    .*alpha.*besselj(0,a*sqrt(1-s.^2));
end

% The Differentiated characteristic equation
function K=DCharacteristic(s,alpha,beta,tau,nu,a)
f1=@(x) Characteristic(x,alpha,beta,tau,nu,a);
K=(f1(s+1e-5)-f1(s-1e-5))/2e-5;
end

% Newton Raphson Method
function Roots=NewtonRaphson(alpha,beta,tau,nu,RGuess,IGuess,CGuess,r)
warning('off','MATLAB:rankDeficientMatrix')
f1=@(x) Characteristic(x,alpha,beta,tau,nu,r);
df1=@(x) DCharacteristic(x,alpha,beta,tau,nu,r);
xold1=RGuess; xold2=IGuess; xold3=CGuess;
for i=1:100
    jac1=df1(xold1);
    sol1=xold1-f1(xold1)./jac1;
    xold1=sol1;
    jac2=df1(xold2);
    sol2=xold2-f1(xold2)./jac2;
    xold2=sol2;
    jac3=df1(xold3);
    sol3=xold3-f1(xold3)./jac3;
    xold3=sol3;
end
Real=sol1;
Real=Real(abs(f1(Real))<1e-5);
Real=sort(Real(Real>0),'descend');
TempIndex=1;
TempReal(TempIndex)=Real(1);
for Index=2:length(Real)
    if abs(Real(Index)-TempReal(TempIndex))>3e-5
        TempIndex=TempIndex+1;
        TempReal(TempIndex)=Real(Index);
    end
end
sol2=sol2((length(TempReal)-1):end);
Imaginary=sol2; Complex=sol3;
Imaginary=sort(Imaginary(imag(Imaginary)>0),'descend');
TempIndex=1;
TempIm(TempIndex)=Imaginary(1);
for Index=2:length(Imaginary)
    if abs(Imaginary(Index)-TempIm(TempIndex))>1e-5
        TempIndex=TempIndex+1;
        TempIm(TempIndex)=Imaginary(Index);
    end
end
Imaginary=[TempIm,Complex];
```

```
% Sort the complex roots in ascending order
[~,idx]=sort(imag(Imaginary),'ascend');
Imaginary=Imaginary(idx);
Roots=[TempReal,Imaginary];
end

function HH=FunctionHH(alpha,beta,tau,nu,eta,gamma,r)
f1=@(x) Characteristic(x,alpha,beta,tau,nu,r);
HH=(f1(eta+1e-5)-f1(eta-1e-5))./(2e-5).*gamma.*besselj(1,r*gamma)...
    ./(2*eta.*(eta.^2-beta^2));
end

function RR=IntegralRR(gamma,kappa,a)
if abs(kappa^2-gamma^2)<1e-5
    RR=a^2*(besselj(0,a*gamma)^2+besselj(1,a*gamma)^2)/2;
else
    RR=a*(kappa*besselj(0,a*gamma)*besselj(1,a*kappa)-...
        gamma*besselj(0,a*kappa)*besselj(1,a*gamma))/(kappa^2-gamma^2);
end
end

function AN=SSolver(a,b,alpha,beta,tau1,tau2,nu,sn,eta...
    ,JJa,JJb,CC,DD,RR,ell,L)
Nn=length(sn); Nm=length(eta);
kappa=(1-sn.^2).^0.5; gamma=(1-eta.^2).^0.5;
F=sqrt(1/(abs(CC(ell))*sn(ell)));
%---------- The edge conditions ----------%
%---------- Clamped ----------%
% PsiA1=sn.*kappa.*JJa; PsiB1=zeros(1,Nm);
% PsiF1=-sn(ell)*kappa(ell)*JJa(ell);
% PsiA2=kappa.*JJa; PsiB2=zeros(1,Nm); PsiF2=kappa(ell)*JJa(ell);
% PsiA3=sn.*kappa.*JJa./(sn.^2-beta^2); PsiB3=zeros(1,Nm);
% PsiF3=sn(ell)*kappa(ell)*JJa(ell)/(sn(ell)^2-beta^2);
% PsiA4=zeros(1,Nn); PsiB4=cos(eta*L).*eta.*gamma.*JJb./(eta.^2-beta^2);
% PsiF4=0;
% PsiA5=zeros(1,Nn); PsiB5=cos(eta*L).*gamma.*JJb; PsiF5=0;
% PsiA6=zeros(1,Nn); PsiB6=-sin(eta*L).*eta.*gamma.*JJb; PsiF6=0;
%---------- Pin-Jointed ----------%
PsiA1=sn.^2.*kappa.*JJa; PsiB1=zeros(1,Nm);
PsiF1=-sn(ell)^2*kappa(ell)*JJa(ell);
PsiA2=kappa.*JJa; PsiB2=zeros(1,Nm); PsiF2=kappa(ell)*JJa(ell);
PsiA3=sn.^2.*kappa.*JJa./(sn.^2-beta^2); PsiB3=zeros(1,Nm);
PsiF3=sn(ell)^2*kappa(ell)*JJa(ell)/(sn(ell)^2-beta^2);
PsiA4=zeros(1,Nn); PsiB4=-sin(eta*L).*eta.^2.*gamma.*JJb./(eta.^2-beta^2);
PsiF4=0;
PsiA5=zeros(1,Nn); PsiB5=-sin(eta*L).*gamma.*JJb; PsiF5=0;
PsiA6=zeros(1,Nn); PsiB6=-cos(eta*L).*eta.^2.*gamma.*JJb; PsiF6=0;
SA0=0; SB0=0; SC0=0; SA1=0; SB1=0; SC1=0; SA2=0; SB2=0; SC2=0;
for n=1:Nn
    SA0=SA0+tau1*nu^2*beta^2*kappa(n)*JJa(n)*PsiA1(n)/(sn(n)^2-beta^2)/CC(n);
    SB0=SB0+(2-kappa(n)^2)*kappa(n)*JJa(n)*PsiA1(n)/CC(n);
    SC0=SC0+kappa(n)*JJa(n)*PsiA1(n)/CC(n);
    SA1=SA1+tau1*nu^2*beta^2*kappa(n)*JJa(n)*PsiA2(n)/(sn(n)^2-beta^2)/CC(n);
    SB1=SB1+(2-kappa(n)^2)*kappa(n)*JJa(n)*PsiA2(n)/CC(n);
    SC1=SC1+kappa(n)*JJa(n)*PsiA2(n)/CC(n);
    SA2=SA2+tau1*nu^2*beta^2*kappa(n)*JJa(n)*PsiA3(n)/(sn(n)^2-beta^2)/CC(n);
    SB2=SB2+(2-kappa(n)^2)*kappa(n)*JJa(n)*PsiA3(n)/CC(n);
    SC2=SC2+kappa(n)*JJa(n)*PsiA3(n)/CC(n);
end
SD3=0; SE3=0; SF3=0; SD4=0; SE4=0; SF4=0; SD5=0; SE5=0; SF5=0;
for m=1:Nm
    SD3=SD3+tau2*nu^2*beta^2*gamma(m)*JJb(m)*PsiB4(m)...
        /(eta(m)^2-beta^2)/eta(m)/DD(m)/sin(-eta(m)*L);
    SE3=SE3+(2-gamma(m)^2)*gamma(m)*JJb(m)*PsiB4(m)...
        /eta(m)/DD(m)/sin(-eta(m)*L);
    SF3=SF3+gamma(m)*JJb(m)*PsiB4(m)/eta(m)/DD(m)/sin(-eta(m)*L);
    SD4=SD4+tau2*nu^2*beta^2*gamma(m)*JJb(m)*PsiB5(m)...
        /(eta(m)^2-beta^2)/eta(m)/DD(m)/sin(-eta(m)*L);
    SE4=SE4+(2-gamma(m)^2)*gamma(m)*JJb(m)*PsiB5(m)...
        /eta(m)/DD(m)/sin(-eta(m)*L);
```

```
    SF4=SF4+gamma(m)*JJb(m)*PsiB5(m)/eta(m)/DD(m)/sin(-eta(m)*L);
    SD5=SD5+tau2*nu^2*beta^2*gamma(m)*JJb(m)*PsiB6(m)...
        /(eta(m)^2-beta^2)/eta(m)/DD(m)/sin(-eta(m)*L);
    SE5=SE5+(2-gamma(m)^2)*gamma(m)*JJb(m)*PsiB6(m)...
        /eta(m)/DD(m)/sin(-eta(m)*L);
    SF5=SF5+gamma(m)*JJb(m)*PsiB6(m)/eta(m)/DD(m)/sin(-eta(m)*L);
end
DA=-SC0*SB1*SA2+SB0*SC1*SA2+SC0*SA1*SB2-SA0*SC1*SB2...
    -SB0*SA1*SC2+SA0*SB1*SC2;
DP=-(SF3*SE4*SD5-SE3*SF4*SD5-SF3*SD4*SE5+SE3*SD4*SF5...
    +SF4*SE5*SD3-SE4*SF5*SD3);
Fdelta=zeros(1,Nn); GE0=zeros(1,Nn); GE1=zeros(1,Nn); GE2=zeros(1,Nn);
GE0a=0; GE1a=0; GE2a=0;
for n=1:Nn
    GE0a=GE0a+F*kdelta(ell,n)*PsiA1(n);
    GE1a=GE1a+F*kdelta(ell,n)*PsiA2(n);
    GE2a=GE2a+F*kdelta(ell,n)*PsiA3(n);
end
for n=1:Nn
    Fdelta(n)=F*kdelta(ell,n);
    GE0(n)=((SC1*SB2-SB1*SC2)*(F*PsiF1-GE0a)+(SB0*SC2-SC0*SB2)...
        *(F*PsiF2-GE1a)+(SC0*SB1-SB0*SC1)*(F*PsiF3-GE2a))/DA;
    GE1(n)=((SC1*SA2-SA1*SC2)*(F*PsiF1-GE0a)+(SA0*SC2-SC0*SA2)...
        *(F*PsiF2-GE1a)+(SC0*SA1-SA0*SC1)*(F*PsiF3-GE2a))/-DA;
    GE2(n)=((SB1*SA2-SA1*SB2)*(F*PsiF1-GE0a)+(SA0*SB2-SB0*SA2)...
        *(F*PsiF2-GE1a)+(SB0*SA1-SA0*SB1)*(F*PsiF3-GE2a))/-DA;
end
GE3b=0; GE4b=0; GE5b=0;
for m=1:Nm
    GE3b=GE3b+1i*F*alpha*sn(ell)*RR(ell,m)*PsiB4(m)...
        /(2*b*sin(-eta(m)*L)*eta(m)*DD(m));
    GE4b=GE4b+1i*F*alpha*sn(ell)*RR(ell,m)*PsiB5(m)...
        /(2*b*sin(-eta(m)*L)*eta(m)*DD(m));
    GE5b=GE5b+1i*F*alpha*sn(ell)*RR(ell,m)*PsiB6(m)...
        /(2*b*sin(-eta(m)*L)*eta(m)*DD(m));
end
GE3=zeros(1,Nm); GE4=zeros(1,Nm); GE5=zeros(1,Nm);
for m=1:Nm
    GE3(m)=((SF4*SE5-SE4*SF5)*(-GE3b+F*PsiF4)+(SE3*SF5-SF3*SE5)...
        *(-GE4b+F*PsiF5)+(SF3*SE4-SE3*SF4)*(-GE5b+F*PsiF6))/DP;
    GE4(m)=((SF4*SD5-SD4*SF5)*(-GE3b+F*PsiF4)+(SF5*SD3-SF3*SD5)...
        *(-GE4b+F*PsiF5)+(SF3*SD4-SF4*SD3)*(-GE5b+F*PsiF6))/-DP;
    GE5(m)=((SE4*SD5-SD4*SE5)*(-GE3b+F*PsiF4)+(SE5*SD3-SE3*SD5)...
        *(-GE4b+F*PsiF5)+(SE3*SD4-SE4*SD3)*(-GE5b+F*PsiF6))/-DP;
end
VFA=(-Fdelta+tau1*nu^2*beta^2*kappa.*JJa.*GE0./(sn.^2-beta^2)./CC...
    +(2-kappa.^2).*kappa.*JJa.*GE1./CC-kappa.*JJa.*GE2./CC).';
V0=(tau1*nu^2*beta^2*kappa.*JJa./(sn.^2-beta^2)./CC/DA).';
V1=((2-kappa.^2).*kappa.*JJa./CC/-DA).';
V2=-(kappa.*JJa./CC/-DA).';
VFP=(-1i*F*alpha*sn(ell).*RR(ell,:)./(2*b*eta.*DD)./sin(-eta*L)...
    +tau2*nu^2*beta^2*gamma.*JJb.*GE3...
    ./(eta.^2-beta^2)./eta./DD./sin(-eta*L)...
    +(2-gamma.^2).*gamma.*JJb.*GE4./eta./DD./sin(-eta*L)...
    -gamma.*JJb.*GE5./eta./DD./sin(-eta*L)).';
V3=(tau2*nu^2*beta^2*gamma.*JJb./(eta.^2-beta^2)...
    ./eta./DD/DP./sin(-eta*L)).';
V4=((2-gamma.^2).*gamma.*JJb./eta./DD/-DP./sin(-eta*L)).';
V5=-(gamma.*JJb./eta./DD/-DP./sin(-eta*L)).';
M0=zeros(Nn,Nm); M1=zeros(Nn,Nm); M2=zeros(Nn,Nm); M3=zeros(Nn,Nm);
M4=zeros(Nn,Nm); M5=zeros(Nn,Nm); M6=zeros(Nn,Nm);
for n=1:Nn
    for m=1:Nm
        M0(n,m)=2*alpha*RR(n,m)*cos(eta(m)*L)*PsiA1(n)/CC(n)/a;
        M1(n,m)=2*alpha*RR(n,m)*cos(eta(m)*L)*PsiA2(n)/CC(n)/a;
        M2(n,m)=2*alpha*RR(n,m)*cos(eta(m)*L)*PsiA3(n)/CC(n)/a;
        M3(end,m)=PsiB1(m);
        M4(end,m)=PsiB2(m);
        M5(end,m)=PsiB3(m);
        M6(n,m)=2*alpha*RR(n,m)*cos(eta(m)*L)/CC(n)/a;
```

```
    end
end
M7=zeros(Nm,Nn); M8=zeros(Nm,Nn); M9=zeros(Nm,Nn); M10=zeros(Nm,Nn);
M11=zeros(Nm,Nn); M12=zeros(Nm,Nn); M13=zeros(Nm,Nn);
for n=1:Nn
    for m=1:Nm
        M7(m,n)=-1i*alpha*sn(n)*RR(n,m)*PsiB4(m)...
            /(2*b*eta(m)*DD(m)*sin(eta(m)*L));
        M8(m,n)=-1i*alpha*sn(n)*RR(n,m)*PsiB5(m)...
            /(2*b*eta(m)*DD(m)*sin(eta(m)*L));
        M9(m,n)=-1i*alpha*sn(n)*RR(n,m)*PsiB6(m)...
            /(2*b*eta(m)*DD(m)*sin(eta(m)*L));
        M13(m,n)=-1i*alpha*sn(n)*RR(n,m)...
            /(2*b*eta(m)*DD(m)*sin(eta(m)*L));
    end
    M10(end,n)=PsiA4(n);
    M11(end,n)=PsiA5(n);
    M12(end,n)=PsiA6(n);
end
em=ones(1,Nm); en=ones(1,Nn);
AN=(eye(Nn)-(...
    +((SC1*SB2-SB1*SC2)*V0+(SC1*SA2-SA1*SC2)*V1+(SB1*SA2-SA1*SB2)*V2)...
    *en*M0...
    +((SC1*SB2-SB1*SC2)*V0+(SC1*SA2-SA1*SC2)*V1+(SB1*SA2-SA1*SB2)*V2)...
    *en*M3...
    +((SB0*SC2-SC0*SB2)*V0+(SA0*SC2-SC0*SA2)*V1+(SA0*SB2-SB0*SA2)*V2)...
    *en*M1...
    +((SB0*SC2-SC0*SB2)*V0+(SA0*SC2-SC0*SA2)*V1+(SA0*SB2-SB0*SA2)*V2)...
    *en*M4...
    +((SC0*SB1-SB0*SC1)*V0+(SC0*SA1-SA0*SC1)*V1+(SB0*SA1-SA0*SB1)*V2)...
    *en*M2...
    +((SC0*SB1-SB0*SC1)*V0+(SC0*SA1-SA0*SC1)*V1+(SB0*SA1-SA0*SB1)*V2)...
    *en*M5+M6)...
    *(...
    +((SF4*SE5-SE4*SF5)*V3+(SF4*SD5-SD4*SF5)*V4+(SE4*SD5-SD4*SE5)*V5)...
    *em*M7+...
    ((SF4*SE5-SE4*SF5)*V3+(SF4*SD5-SD4*SF5)*V4+(SE4*SD5-SD4*SE5)*V5)...
    *em*M10...
    +((SE3*SF5-SF3*SE5)*V3+(SF5*SD3-SF3*SD5)*V4+(SE5*SD3-SE3*SD5)*V5)...
    *em*M8...
    +((SE3*SF5-SF3*SE5)*V3+(SF5*SD3-SF3*SD5)*V4+(SE5*SD3-SE3*SD5)*V5)...
    *em*M11...
    +((SF3*SE4-SE3*SF4)*V3+(SF3*SD4-SF4*SD3)*V4+(SE3*SD4-SD3*SE4)*V5)...
    *em*M9...
    +((SF3*SE4-SE3*SF4)*V3+(SF3*SD4-SF4*SD3)*V4+(SE3*SD4-SD3*SE4)*V5)...
    *em*M12+M13))\(VFA+(...
    +((SC1*SB2-SB1*SC2)*V0+(SC1*SA2-SA1*SC2)*V1+(SB1*SA2-SA1*SB2)*V2)...
    *en*M0*VFP...
    +((SC1*SB2-SB1*SC2)*V0+(SC1*SA2-SA1*SC2)*V1+(SB1*SA2-SA1*SB2)*V2)...
    *en*M3*VFP...
    +((SB0*SC2-SC0*SB2)*V0+(SA0*SC2-SC0*SA2)*V1+(SA0*SB2-SB0*SA2)*V2)...
    *en*M1*VFP...
    +((SB0*SC2-SC0*SB2)*V0+(SA0*SC2-SC0*SA2)*V1+(SA0*SB2-SB0*SA2)*V2)...
    *en*M4*VFP...
    +((SC0*SB1-SB0*SC1)*V0+(SC0*SA1-SA0*SC1)*V1+(SB0*SA1-SA0*SB1)*V2)...
    *en*M2*VFP...
    +((SC0*SB1-SB0*SC1)*V0+(SC0*SA1-SA0*SC1)*V1+(SB0*SA1-SA0*SB1)*V2)...
    *en*M5*VFP+M6*VFP));
end

function AN=ASolver(a,b,alpha,beta,tau1,tau2,nu,sn,eta...
    ,JJa,JJb,CC,DD,RR,ell,L)
Nn=length(sn); Nm=length(eta);
kappa=(1-sn.^2).^0.5; gamma=(1-eta.^2).^0.5;
F=sqrt(1/(abs(CC(ell))*sn(ell)));
%---------- The edge conditions ----------%
%---------- Clamped ----------%
PsiA1=sn.*kappa.*JJa; PsiB1=zeros(1,Nm);
PsiF1=-sn(ell)*kappa(ell)*JJa(ell);
PsiA2=kappa.*JJa; PsiB2=zeros(1,Nm); PsiF2=kappa(ell)*JJa(ell);
```

```
PsiA3=sn.*kappa.*JJa./(sn.^2-beta^2); PsiB3=zeros(1,Nm);
PsiF3=sn(ell)*kappa(ell)*JJa(ell)/(sn(ell)^2-beta^2);
PsiA4=zeros(1,Nn); PsiB4=-sin(eta*L).*eta.*gamma.*JJb./(eta.^2-beta^2);
PsiF4=0;
PsiA5=zeros(1,Nn); PsiB5=-sin(eta*L).*gamma.*JJb; PsiF5=0;
PsiA6=zeros(1,Nn); PsiB6=-cos(eta*L).*eta.*gamma.*JJb; PsiF6=0;
%---------- Pin-Jointed ----------%
% PsiA1=sn.^2.*kappa.*JJa; PsiB1=zeros(1,Nm);
% PsiF1=-sn(ell)^2*kappa(ell)*JJa(ell);
% PsiA2=kappa.*JJa; PsiB2=zeros(1,Nm); PsiF2=kappa(ell)*JJa(ell);
% PsiA3=sn.^2.*kappa.*JJa./(sn.^2-beta^2); PsiB3=zeros(1,Nm);
% PsiF3=sn(ell)^2*kappa(ell)*JJa(ell)/(sn(ell)^2-beta^2);
% PsiA4=zeros(1,Nn); PsiB4=-sin(eta*L).*eta.^2.*gamma.*JJb./(eta.^2-beta^2);
% PsiF4=0;
% PsiA5=zeros(1,Nn); PsiB5=-sin(eta*L).*gamma.*JJb; PsiF5=0;
% PsiA6=zeros(1,Nn); PsiB6=-cos(eta*L).*eta.^2.*gamma.*JJb; PsiF6=0;
SA0=0; SB0=0; SC0=0; SA1=0; SB1=0; SC1=0; SA2=0; SB2=0; SC2=0;
for n=1:Nn
    SA0=SA0+tau1*nu^2*beta^2*kappa(n)*JJa(n)*PsiA1(n)...
        /(sn(n)^2-beta^2)/CC(n);
    SB0=SB0+(2-kappa(n)^2)*kappa(n)*JJa(n)*PsiA1(n)/CC(n);
    SC0=SC0+kappa(n)*JJa(n)*PsiA1(n)/CC(n);
    SA1=SA1+tau1*nu^2*beta^2*kappa(n)*JJa(n)*PsiA2(n)...
        /(sn(n)^2-beta^2)/CC(n);
    SB1=SB1+(2-kappa(n)^2)*kappa(n)*JJa(n)*PsiA2(n)/CC(n);
    SC1=SC1+kappa(n)*JJa(n)*PsiA2(n)/CC(n);
    SA2=SA2+tau1*nu^2*beta^2*kappa(n)*JJa(n)*PsiA3(n)...
        /(sn(n)^2-beta^2)/CC(n);
    SB2=SB2+(2-kappa(n)^2)*kappa(n)*JJa(n)*PsiA3(n)/CC(n);
    SC2=SC2+kappa(n)*JJa(n)*PsiA3(n)/CC(n);
end
SD3=0; SE3=0; SF3=0; SD4=0; SE4=0; SF4=0; SD5=0; SE5=0; SF5=0;
for m=1:Nm
    SD3=SD3+tau2*nu^2*beta^2*gamma(m)*JJb(m)*PsiB4(m)...
        /(eta(m)^2-beta^2)/eta(m)/DD(m)/cos(eta(m)*L);
    SE3=SE3+(2-gamma(m)^2)*gamma(m)*JJb(m)*PsiB4(m)...
        /eta(m)/DD(m)/cos(eta(m)*L);
    SF3=SF3+gamma(m)*JJb(m)*PsiB4(m)/eta(m)/DD(m)/cos(eta(m)*L);
    SD4=SD4+tau2*nu^2*beta^2*gamma(m)*JJb(m)*PsiB5(m)...
        /(eta(m)^2-beta^2)/eta(m)/DD(m)/cos(eta(m)*L);
    SE4=SE4+(2-gamma(m)^2)*gamma(m)*JJb(m)*PsiB5(m)...
        /eta(m)/DD(m)/cos(eta(m)*L);
    SF4=SF4+gamma(m)*JJb(m)*PsiB5(m)/eta(m)/DD(m)/cos(eta(m)*L);
    SD5=SD5+tau2*nu^2*beta^2*gamma(m)*JJb(m)*PsiB6(m)...
        /(eta(m)^2-beta^2)/eta(m)/DD(m)/cos(eta(m)*L);
    SE5=SE5+(2-gamma(m)^2)*gamma(m)*JJb(m)*PsiB6(m)...
        /eta(m)/DD(m)/cos(eta(m)*L);
    SF5=SF5+gamma(m)*JJb(m)*PsiB6(m)/eta(m)/DD(m)/cos(eta(m)*L);
end
DA=-SC0*SB1*SA2+SB0*SC1*SA2+SC0*SA1*SB2-SA0*SC1*SB2...
    -SB0*SA1*SC2+SA0*SB1*SC2;
DP=-(SF3*SE4*SD5-SE3*SF4*SD5-SF3*SD4*SE5+SE3*SD4*SF5...
    +SF4*SE5*SD3-SE4*SF5*SD3);
Fdelta=zeros(1,Nn); GE0=zeros(1,Nn); GE1=zeros(1,Nn); GE2=zeros(1,Nn);
GE0a=0; GE1a=0; GE2a=0;
for n=1:Nn
    GE0a=GE0a+F*kdelta(ell,n)*PsiA1(n);
    GE1a=GE1a+F*kdelta(ell,n)*PsiA2(n);
    GE2a=GE2a+F*kdelta(ell,n)*PsiA3(n);
end
for n=1:Nn
    Fdelta(n)=F*kdelta(ell,n);
    GE0(n)=((SC1*SB2-SB1*SC2)*(F*PsiF1-GE0a)+(SB0*SC2-SC0*SB2)...
        *(F*PsiF2-GE1a)+(SC0*SB1-SB0*SC1)*(F*PsiF3-GE2a))/DA;
    GE1(n)=((SC1*SA2-SA1*SC2)*(F*PsiF1-GE0a)+(SA0*SC2-SC0*SA2)...
        *(F*PsiF2-GE1a)+(SC0*SA1-SA0*SC1)*(F*PsiF3-GE2a))/-DA;
    GE2(n)=((SB1*SA2-SA1*SB2)*(F*PsiF1-GE0a)+(SA0*SB2-SB0*SA2)...
        *(F*PsiF2-GE1a)+(SB0*SA1-SA0*SB1)*(F*PsiF3-GE2a))/-DA;
end
GE3b=0; GE4b=0; GE5b=0;
```

```
for m=1:Nm
    GE3b=GE3b+1i*F*alpha*sn(ell)*RR(ell,m)*PsiB4(m)...
        /(2*b*cos(-eta(m)*L)*eta(m)*DD(m));
    GE4b=GE4b+1i*F*alpha*sn(ell)*RR(ell,m)*PsiB5(m)...
        /(2*b*cos(-eta(m)*L)*eta(m)*DD(m));
    GE5b=GE5b+1i*F*alpha*sn(ell)*RR(ell,m)*PsiB6(m)...
        /(2*b*cos(-eta(m)*L)*eta(m)*DD(m));
end
GE3=zeros(1,Nm); GE4=zeros(1,Nm); GE5=zeros(1,Nm);
for m=1:Nm
    GE3(m)=((SF4*SE5-SE4*SF5)*(GE3b+F*PsiF4)+(SE3*SF5-SF3*SE5)...
        *(GE4b+F*PsiF5)+(SF3*SE4-SE3*SF4)*(GE5b+F*PsiF6))/DP;
    GE4(m)=((SF4*SD5-SD4*SF5)*(GE3b+F*PsiF4)+(SF5*SD3-SF3*SD5)...
        *(GE4b+F*PsiF5)+(SF3*SD4-SF4*SD3)*(GE5b+F*PsiF6))/-DP;
    GE5(m)=((SE4*SD5-SD4*SE5)*(GE3b+F*PsiF4)+(SE5*SD3-SE3*SD5)...
        *(GE4b+F*PsiF5)+(SE3*SD4-SE4*SD3)*(GE5b+F*PsiF6))/-DP;
end
VFA=(-Fdelta+tau1*nu^2*beta^2*kappa.*JJa.*GE0./(sn.^2-beta^2)./CC...
    +(2-kappa.^2).*kappa.*JJa.*GE1./CC-kappa.*JJa.*GE2./CC).';
V0=(tau1*nu^2*beta^2*kappa.*JJa./(sn.^2-beta^2)./CC/DA).';
V1=((2-kappa.^2).*kappa.*JJa./CC/-DA).';
V2=-(kappa.*JJa./CC/-DA).';
VFP=(1i*F*alpha*sn(ell).*RR(ell,:)./(2*b*eta.*DD)./cos(eta*L)...
    +tau2*nu^2*beta^2*gamma.*JJb.*GE3./(eta.^2-beta^2)...
    ./eta./DD./cos(eta*L)+(2-gamma.^2).*gamma.*JJb.*GE4...
    ./eta./DD./cos(eta*L)-gamma.*JJb.*GE5./eta./DD./cos(eta*L)).';
V3=(tau2*nu^2*beta^2*gamma.*JJb./(eta.^2-beta^2)...
    ./eta./DD/DP./cos(eta*L)).';
V4=((2-gamma.^2).*gamma.*JJb./eta./DD/-DP./cos(eta*L)).';
V5=-(gamma.*JJb./eta./DD/-DP./cos(eta*L)).';
M0=zeros(Nn,Nm); M1=zeros(Nn,Nm); M2=zeros(Nn,Nm); M3=zeros(Nn,Nm);
M4=zeros(Nn,Nm); M5=zeros(Nn,Nm); M6=zeros(Nn,Nm);
for n=1:Nn
    for m=1:Nm
        M0(n,m)=-4*alpha*RR(n,m)*sin(eta(m)*L)*PsiA1(n)/CC(n)/a;
        M1(n,m)=-4*alpha*RR(n,m)*sin(eta(m)*L)*PsiA2(n)/CC(n)/a;
        M2(n,m)=-4*alpha*RR(n,m)*sin(eta(m)*L)*PsiA3(n)/CC(n)/a;
        M3(end,m)=PsiB1(m);
        M4(end,m)=PsiB2(m);
        M5(end,m)=PsiB3(m);
        M6(n,m)=-4*alpha*RR(n,m)*sin(eta(m)*L)/CC(n)/a;
    end
end
M7=zeros(Nm,Nn); M8=zeros(Nm,Nn); M9=zeros(Nm,Nn); M10=zeros(Nm,Nn);
M11=zeros(Nm,Nn); M12=zeros(Nm,Nn); M13=zeros(Nm,Nn);
for n=1:Nn
    for m=1:Nm
        M7(m,n)=-1i*alpha*sn(n)*RR(n,m)*PsiB4(m)...
            /(4*b*eta(m)*DD(m)*cos(eta(m)*L));
        M8(m,n)=-1i*alpha*sn(n)*RR(n,m)*PsiB5(m)...
            /(4*b*eta(m)*DD(m)*cos(eta(m)*L));
        M9(m,n)=-1i*alpha*sn(n)*RR(n,m)*PsiB6(m)...
            /(4*b*eta(m)*DD(m)*cos(eta(m)*L));
        M13(m,n)=-1i*alpha*sn(n)*RR(n,m)...
            /(4*b*eta(m)*DD(m)*cos(eta(m)*L));
    end
    M10(end,n)=PsiA4(n);
    M11(end,n)=PsiA5(n);
    M12(end,n)=PsiA6(n);
end
em=ones(1,Nm); en=ones(1,Nn);
AN=(eye(Nn)-(...
    +((SC1*SB2-SB1*SC2)*V0+(SC1*SA2-SA1*SC2)*V1+(SB1*SA2-SA1*SB2)*V2)...
    *en*M0...
    +((SC1*SB2-SB1*SC2)*V0+(SC1*SA2-SA1*SC2)*V1+(SB1*SA2-SA1*SB2)*V2)...
    *en*M3...
    +((SB0*SC2-SC0*SB2)*V0+(SA0*SC2-SC0*SA2)*V1+(SA0*SB2-SB0*SA2)*V2)...
    *en*M1...
    +((SB0*SC2-SC0*SB2)*V0+(SA0*SC2-SC0*SA2)*V1+(SA0*SB2-SB0*SA2)*V2)...
    *en*M4...
```

```
    +((SC0*SB1-SB0*SC1)*V0+(SC0*SA1-SA0*SC1)*V1+(SB0*SA1-SA0*SB1)*V2)...
    *en*M2...
    +((SC0*SB1-SB0*SC1)*V0+(SC0*SA1-SA0*SC1)*V1+(SB0*SA1-SA0*SB1)*V2)...
    *en*M5+M6)...
    *(...
    +((SF4*SE5-SE4*SF5)*V3+(SF4*SD5-SD4*SF5)*V4+(SE4*SD5-SD4*SE5)*V5)...
    *em*M7...
    +((SF4*SE5-SE4*SF5)*V3+(SF4*SD5-SD4*SF5)*V4+(SE4*SD5-SD4*SE5)*V5)...
    *em*M10...
    +((SE3*SF5-SF3*SE5)*V3+(SF5*SD3-SF3*SD5)*V4+(SE5*SD3-SE3*SD5)*V5)...
    *em*M8...
    +((SE3*SF5-SF3*SE5)*V3+(SF5*SD3-SF3*SD5)*V4+(SE5*SD3-SE3*SD5)*V5)...
    *em*M11...
    +((SF3*SE4-SE3*SF4)*V3+(SF3*SD4-SF4*SD3)*V4+(SE3*SD4-SD3*SE4)*V5)...
    *em*M9...
    +((SF3*SE4-SE3*SF4)*V3+(SF3*SD4-SF4*SD3)*V4+(SE3*SD4-SD3*SE4)*V5)...
    *em*M12+M13))\(VFA+(...
    +((SC1*SB2-SB1*SC2)*V0+(SC1*SA2-SA1*SC2)*V1+(SB1*SA2-SA1*SB2)*V2)...
    *en*M0*VFP...
    +((SC1*SB2-SB1*SC2)*V0+(SC1*SA2-SA1*SC2)*V1+(SB1*SA2-SA1*SB2)*V2)...
    *en*M3*VFP...
    +((SB0*SC2-SC0*SB2)*V0+(SA0*SC2-SC0*SA2)*V1+(SA0*SB2-SB0*SA2)*V2)...
    *en*M1*VFP...
    +((SB0*SC2-SC0*SB2)*V0+(SA0*SC2-SC0*SA2)*V1+(SA0*SB2-SB0*SA2)*V2)...
    *en*M4*VFP...
    +((SC0*SB1-SB0*SC1)*V0+(SC0*SA1-SA0*SC1)*V1+(SB0*SA1-SA0*SB1)*V2)...
    *en*M2*VFP...
    +((SC0*SB1-SB0*SC1)*V0+(SC0*SA1-SA0*SC1)*V1+(SB0*SA1-SA0*SB1)*V2)...
    *en*M5*VFP+M6*VFP));
end


%---------- Kronecker delta ----------%
function d=kdelta(n,m)
if n==m
    d=1;
else
    d=0;
end
end
```

Appendix J

Matlab code relating to Section 5.1

```
function AppendixJ() % Nonaxi characteristic
clc; clear;
% ---------- Input Variables ----------
a1=0.2; % Dimensional radius (m)
Cair=343.5; % Sound speed of fluid (m/s)
Dair=1.2; % Density of fluid (kg/m^3)
EE=7.2*10^10; % Youngs Modulus (N/m^2)
h1=0.002; % Dimensional shell thickness (m)
Dplate=2700; % Density of shell (kg/m^3)
nu=0.34; % Poisson's ratio for shell
f=500; %Frequency (Hz)
terms=100; % Number of imaginary roots to seek
% ---------- Calculated Variables ----------
kno=2*pi*f/Cair; % Fluid wave number
a=a1*kno; % Nondimensional radius
h=h1*kno; % Nondimensional shell thickness
cp1=sqrt(EE/(1-nu^2)/Dplate); % Sound speed of the shell
beta=Cair/cp1; omega=Cair*kno; tau1=12/(h^2*a^2);
alpha=12*omega^2*Dair/(h^3*cp1^2*kno^2*Dplate);
% Starting Values
if a1==0.28
    RealGuess=0.1:0.01:0.98;
    ComplexGuess=(35:0.1:98)+(35:0.1:98)*1i;
    ImaginaryGuess=[(0.4:0.1:0.8)*1i (3/4+(0:1:terms))*pi*1i/a];
    if f>80
        ComplexGuess=(35:0.1:40)+(35:0.1:40)*1i;
        ImaginaryGuess=[(0.2:0.1:0.4)*1i (3/4+(0:1:terms))*pi*1i/a];
    if f>90
        ComplexGuess=(9:0.1:35)+(9:0.1:35)*1i;
        ImaginaryGuess=[(0.2:0.1:0.4)*1i (3/4+(0:1:terms))*pi*1i/a];
    if f>290
        ComplexGuess=(9:0.1:10)+(9:0.1:10)*1i;
        ImaginaryGuess=[(0.2:0.1:0.4)*1i (3/4+(0:1:terms))*pi*1i/a];
    if f>340
        ComplexGuess=(0:0.1:9)+(0:0.1:9)*1i;
        ImaginaryGuess=[(0.2:0.1:0.4)*1i (3/4+(0:1:terms))*pi*1i/a];
    if f>700
        ComplexGuess=(2:0.1:5)+(2:0.1:5)*1i;
        ImaginaryGuess=[(0.2:0.1:0.4)*1i (3/4+(0:1:terms))*pi*1i/a];
    if f>850
        ComplexGuess=(2:0.1:4)+(2:0.1:4)*1i;
        ImaginaryGuess=[(0.1:0.1:1.5)*1i (3/4+(0:1:terms))*pi*1i/a];
    if f>1030
        ComplexGuess=(0:0.1:4)+(0:0.1:4)*1i;
        ImaginaryGuess=[(0.1:0.1:1.5)*1i (3/4+(0:1:terms))*pi*1i/a];
    end
    end
```

```
    end
    end
    end
    end
    end
elseif a1==0.2
    RealGuess=0:0.01:1.1;
    ComplexGuess=(50:1:120)+(50:1:120)*1i;
    ImaginaryGuess=[(0.2:0.01:1)*1i (3/4+(1:1:terms))*pi*1i/a];
    if f>70
        ComplexGuess=(10:1:50)+(10:1:50)*1i;
        ImaginaryGuess=[(0.2:0.01:1)*1i (3/4+(0:1:terms))*pi*1i/a];
    if f>350
        ComplexGuess=(8:0.1:11)+(8:0.1:11)*1i;
        ImaginaryGuess=[(0.2:0.01:1)*1i (3/4+(0:1:terms))*pi*1i/a];
    if f>450
        ComplexGuess=(0:0.1:8)+(0:0.1:8)*1i;
        ImaginaryGuess=(3/4+(1:1:terms))*pi*1i/a;
    if f>750
        ComplexGuess=(1:0.1:5)+(1:0.1:5)*1i;
        ImaginaryGuess=[(1)*1i (3/4+(1:1:terms))*pi*1i/a];
    if f>950
        ComplexGuess=(1:0.1:5)+(1:0.1:5)*1i;
        ImaginaryGuess=[(1)*1i (3/4+(1:1:terms))*pi*1i/a];
    if f>1000
        ComplexGuess=(1:0.1:3.4)+(1:0.1:3.4)*1i;
        ImaginaryGuess=(3/4+(1:1:terms))*pi*1i/a;
    end
    end
    end
    end
    end
    end
elseif a1==0.06
    RealGuess=0:0.01:1.1;
    ComplexGuess=(50:1:70)+(50:1:70)*1i;
    ImaginaryGuess=[(0.2:0.01:1)*1i (3/4+(1:1:terms))*pi*1i/a];
    if f>150
        ComplexGuess=(18:1:50)+(18:1:50)*1i;
        ImaginaryGuess=[(0.2:0.01:1)*1i (3/4+(0:1:terms))*pi*1i/a];
    if f>350
        ComplexGuess=(12:0.1:18)+(12:0.1:18)*1i;
        ImaginaryGuess=[(0.2:0.01:1)*1i (3/4+(0:1:terms))*pi*1i/a];
    if f>650
        ComplexGuess=(1:0.1:10)+(1:0.1:10)*1i;
        ImaginaryGuess=[(1)*1i (3/4+(1:1:terms))*pi*1i/a];
    if f>1000
        ComplexGuess=(1:0.1:7)+(1:0.1:7)*1i;
        ImaginaryGuess=(3/4+(1:1:terms))*pi*1i/a;
    end
    end
    end
    end
end
sn=NewtonRaphson(alpha,beta,tau1,nu,RealGuess,ImaginaryGuess,ComplexGuess,a).';
sn=sn(abs(sn)<terms*pi/a);
kappa=sqrt(1-sn.^2-1/a^2); Tw1=length(kappa)
end

function KK=Characteristic(s,alpha,beta,tau,nu,a)
n=1;
U=a*(n^2*(nu-1)-2*a^2*beta^2*nu)*s+a^3*(nu-nu^2)*s.^3;
V=1i*(n^3*(1-nu)-2*a^2*beta^2*n+a^2*(2*n-n*(nu+nu^2))*s.^2);
QQ=(n^2*(1-nu)/2-a^2*beta^2+a^2*s.^2).*(2*a^2*beta^2-2*n^2-a^2*(1-nu)*s.^2)+...
    a^2*n^2*(1+nu)^2*s.^2/2;
PP=(a*nu*s.*U-1i*n*V)*tau+QQ.*(s.^4+2*n^2*s.^2/a^2+(1-a^2*beta^2)*tau+n^4/a^4);
KK=(PP.*sqrt(1-s.^2).*(besselj(n-1,sqrt(1-s.^2)*a)-besselj(n+1,sqrt(1-s.^2)*a))/2-...
    alpha*QQ.*besselj(n,sqrt(1-s.^2)*a));
end
```

```
% The Differentiated characteristic equation
function K=DCharacteristic(s,alpha,beta,tau,nu,a)
f1=@(x) Characteristic(x,alpha,beta,tau,nu,a);
K=(f1(s+1e-5)-f1(s-1e-5))/2e-5;
end

% Newton Raphson Method
function Roots=NewtonRaphson(alpha,beta,tau,nu,RGuess,IGuess,CGuess,r)
warning('off','MATLAB:rankDeficientMatrix')
f1=@(x) Characteristic(x,alpha,beta,tau,nu,r);
df1=@(x) DCharacteristic(x,alpha,beta,tau,nu,r);
xold1=RGuess; xold2=IGuess; xold3=CGuess;
for i=1:100
    jac1=df1(xold1);
    sol1=xold1-f1(xold1)./jac1;
    xold1=sol1;
    jac2=df1(xold2);
    sol2=xold2-f1(xold2)./jac2;
    xold2=sol2;
    jac3=df1(xold3);
    sol3=xold3-f1(xold3)./jac3;
    xold3=sol3;
end
Real=sol1;
Real=Real(abs(f1(Real))<1e-5);
Real=Real(Real<1);
Real=sort(Real(Real>0),'descend');
TempIndex=1;
TempReal(TempIndex)=Real(1);
for Index=2:length(Real)
    if abs(Real(Index)-TempReal(TempIndex))>3e-5
        TempIndex=TempIndex+1;
        TempReal(TempIndex)=Real(Index);
    end
end
sol2=sol2((length(TempReal)):end);
Imaginary=sol2;
Imaginary=sort(Imaginary(imag(Imaginary)>0),'descend');
TempIndex=1;
TempIm(TempIndex)=Imaginary(1);
for Index=2:length(Imaginary)
    if abs(Imaginary(Index)-TempIm(TempIndex))>1e-5
        TempIndex=TempIndex+1;
        TempIm(TempIndex)=Imaginary(Index);
    end
end
Complex=sol3(abs(imag(sol3))>1e-5);
Complex=sort(Complex(real(Complex)>1e-5),'descend');
TempIndex=1;
TempComplex(TempIndex)=Complex(1);
for Index=2:length(Complex)
    if abs(Complex(Index)-TempComplex(TempIndex))>1e-5
        TempIndex=TempIndex+1;
        TempComplex(TempIndex)=Complex(Index);
    end
end
TempComplex=[TempComplex -conj(TempComplex)];
Imaginary=[TempIm,TempComplex];
% Sort the complex roots in ascending order
[~,idx]=sort(imag(Imaginary),'ascend');
Imaginary=Imaginary(idx);
Roots=[TempReal,Imaginary];
end
```

Appendix K

Matlab code relating to Section 5.2

```
function AppendixK() %Nonaxi Semi infinte
clc; clear;
index=0;
for f=30:1200
% ---------- Input Variables ----------
a1=0.2; % Dimensional radius (m)
Cair=343.5; % Sound speed of fluid (m/s)
Dair=1.2; % Density of fluid (kg/m^3)
EE=7.2*10^10; % Youngs Modulus (N/m^2)
h1=0.002; % Dimensional shell thickness (m)
Dplate=2700; % Density of shell (kg/m^3)
nu=0.34; % Poisson's ratio for shell
terms=100; % Number of imaginary roots to seek
ell=1; % Indicator for incident forcing mode
n=1;
% ---------- Calculated Variables ----------
kno=2*pi*f/Cair; % Fluid wave number
a=a1*kno; % Nondimensional radius
h=h1*kno; % Nondimensional shell thickness
cp1=sqrt(EE/(1-nu^2)/Dplate); % Sound speed of the shell
beta=Cair/cp1; omega=Cair*kno; tau1=12/(h^2*a^2);
alpha=12*omega^2*Dair/(h^3*cp1^2*kno^2*Dplate);
% Starting Values
if a1==0.28
    RealGuess=0.1:0.01:0.98;
    ComplexGuess=(35:0.1:98)+(35:0.1:98)*1i;
    ImaginaryGuess=[(0.4:0.1:0.8)*1i (3/4+(0:1:terms))*pi*1i/a];
    if f>80
        ComplexGuess=(35:0.1:40)+(35:0.1:40)*1i;
        ImaginaryGuess=[(0.2:0.1:0.4)*1i (3/4+(0:1:terms))*pi*1i/a];
    if f>90
        ComplexGuess=(9:0.1:35)+(9:0.1:35)*1i;
        ImaginaryGuess=[(0.2:0.1:0.4)*1i (3/4+(0:1:terms))*pi*1i/a];
    if f>290
        ComplexGuess=(9:0.1:10)+(9:0.1:10)*1i;
        ImaginaryGuess=[(0.2:0.1:0.4)*1i (3/4+(0:1:terms))*pi*1i/a];
    if f>340
        ComplexGuess=(0:0.1:9)+(0:0.1:9)*1i;
        ImaginaryGuess=[(0.2:0.1:0.4)*1i (3/4+(0:1:terms))*pi*1i/a];
    if f>700
        ComplexGuess=(2:0.1:5)+(2:0.1:5)*1i;
        ImaginaryGuess=[(0.2:0.1:0.4)*1i (3/4+(0:1:terms))*pi*1i/a];
    if f>850
        ComplexGuess=(2:0.1:4)+(2:0.1:4)*1i;
        ImaginaryGuess=[(0.1:0.1:1.5)*1i (3/4+(0:1:terms))*pi*1i/a];
    if f>1030
        ComplexGuess=(0:0.1:4)+(0:0.1:4)*1i;
```

```
        ImaginaryGuess=[(0.1:0.1:1.5)*1i (3/4+(0:1:terms))*pi*1i/a];
    end
    end
    end
    end
    end
    end
    end
elseif a1==0.2
    RealGuess=0:0.01:1.1;
    ComplexGuess=(50:1:120)+(50:1:120)*1i;
    ImaginaryGuess=[(0.2:0.01:1)*1i (3/4+(1:1:terms))*pi*1i/a];
    if f>70
        ComplexGuess=(10:1:50)+(10:1:50)*1i;
        ImaginaryGuess=[(0.2:0.01:1)*1i (3/4+(0:1:terms))*pi*1i/a];
    if f>350
        ComplexGuess=(8:0.1:11)+(8:0.1:11)*1i;
        ImaginaryGuess=[(0.2:0.01:1)*1i (3/4+(0:1:terms))*pi*1i/a];
    if f>450
        ComplexGuess=(0:0.1:8)+(0:0.1:8)*1i;
        ImaginaryGuess=(3/4+(1:1:terms))*pi*1i/a;
    if f>750
        ComplexGuess=(1:0.1:5)+(1:0.1:5)*1i;
        ImaginaryGuess=[(1)*1i (3/4+(1:1:terms))*pi*1i/a];
    if f>950
        ComplexGuess=(1:0.1:5)+(1:0.1:5)*1i;
        ImaginaryGuess=[(1)*1i (3/4+(1:1:terms))*pi*1i/a];
    if f>1000
        ComplexGuess=(1:0.1:3.4)+(1:0.1:3.4)*1i;
        ImaginaryGuess=(3/4+(1:1:terms))*pi*1i/a;
    end
    end
    end
    end
    end
    end
elseif a1==0.06
    RealGuess=0:0.01:1.1;
    ComplexGuess=(50:1:70)+(50:1:70)*1i;
    ImaginaryGuess=[(0.2:0.01:1)*1i (3/4+(1:1:terms))*pi*1i/a];
    if f>150
        ComplexGuess=(18:1:50)+(18:1:50)*1i;
        ImaginaryGuess=[(0.2:0.01:1)*1i (3/4+(0:1:terms))*pi*1i/a];
    if f>350
        ComplexGuess=(12:0.1:18)+(12:0.1:18)*1i;
        ImaginaryGuess=[(0.2:0.01:1)*1i (3/4+(0:1:terms))*pi*1i/a];
    if f>650
        ComplexGuess=(1:0.1:10)+(1:0.1:10)*1i;
        ImaginaryGuess=[(1)*1i (3/4+(1:1:terms))*pi*1i/a];
    if f>1000
        ComplexGuess=(1:0.1:7)+(1:0.1:7)*1i;
        ImaginaryGuess=(3/4+(1:1:terms))*pi*1i/a;
    end
    end
    end
    end
end
eta=NewtonRaphson(alpha,beta,tau1,nu,RealGuess,ImaginaryGuess,ComplexGuess,a,n).';
eta=eta(abs(eta)<terms*pi/a);
gamma=sqrt(1-eta.^2-1/a^2); Tw1=length(gamma)
% ---------- CC & DD ----------
CC=FunctionHH(alpha,beta,tau1,nu,eta,gamma,a);
AP=NonAxiSolver(a,nu,alpha,beta,tau1,eta,CC,ell,n);
PowA=real(sum(abs(AP.').^2.*CC.*eta));
index=index+1;
data(index,:)=[f,PowA];
end
end

function KK=Characteristic(eta,alpha,beta,tau,nu,a)
```

```
n=1;
U=a*(n^2*(nu-1)-2*a^2*beta^2*nu)*eta+a^3*(nu-nu^2)*eta.^3;
V=1i*(n^3*(1-nu)-2*a^2*beta^2*n+a^2*(2*n-n*(nu+nu^2))*eta.^2);
QQ=(n^2*(1-nu)/2-a^2*beta^2+a^2*eta.^2).*(2*a^2*beta^2-2*n^2-...
    a^2*(1-nu)*eta.^2)+a^2*n^2*(1+nu)^2*eta.^2/2;
PP=(a*nu*eta.*U-1i*n*V)*tau+QQ.*(eta.^4+2*n^2*eta.^2/a^2+...
    (1-a^2*beta^2)*tau+n^4/a^4);
KK=(PP.*sqrt(1-eta.^2).*(besselj(n-1,sqrt(1-eta.^2)*a)-...
    besselj(n+1,sqrt(1-eta.^2)*a))/2-alpha*QQ.*besselj(n,sqrt(1-eta.^2)*a));
end

% The Differentiated characteristic equation
function K=DCharacteristic(s,alpha,beta,tau,nu,a)
f1=@(x) Characteristic(x,alpha,beta,tau,nu,a);
K=(f1(s+1e-5)-f1(s-1e-5))/2e-5;
end

% Newton Raphson Method
function Roots=NewtonRaphson(alpha,beta,tau,nu,RGuess,IGuess,CGuess,r,n)
warning('off','MATLAB:rankDeficientMatrix')
f1=@(x) Characteristic(x,alpha,beta,tau,nu,r);
df1=@(x) DCharacteristic(x,alpha,beta,tau,nu,r);
xold=[RGuess,CGuess,IGuess];
for i=1:110
    jac=df1(xold);
    sol=xold-f1(xold)./jac;
    xold=sol;
end
Real=sol(1:length(RGuess));
Complex=sol(length(RGuess)+(1:length(CGuess)));
Imaginary=sol(length(CGuess)+1:end);
Real=Real(abs(f1(Real))<1e-5);
Real=sort(Real(Real>0),'descend');
TempIndex=1;
TempReal(TempIndex)=Real(1);
for Index=2:length(Real)
    if abs(Real(Index)-TempReal(TempIndex))>2e-5
        TempIndex=TempIndex+1;
        TempReal(TempIndex)=Real(Index);
    end
end
Complex=Complex(angle(Complex)>40/360*2*pi);
Complex=Complex(angle(Complex)<88.5/360*2*pi);
Complex=sort(Complex,'descend');
TempIndex=1;
if numel(Complex)>0
TempComplex(TempIndex)=Complex(1);
TempIndex=TempIndex+1;
TempComplex(TempIndex)=-conj(TempComplex(TempIndex-1));
for Index=2:length(Complex)
    if abs(abs(Complex(Index))-abs(TempComplex(TempIndex)))>1e-2
        TempIndex=TempIndex+1;
        TempComplex(TempIndex)=Complex(Index);
        TempIndex=TempIndex+1;
        TempComplex(TempIndex)=-conj(TempComplex(TempIndex-1));
    end
end
else
    TempComplex=1e+500i;
end
Imaginary=Imaginary(imag(Imaginary)>1e-5);
Imaginary=Imaginary(abs(real(Imaginary))<1e-5);
Imaginary=sort(Imaginary,'descend');
TempIndex=1;
TempImaginary(TempIndex)=Imaginary(1);
for Index=2:length(Imaginary)
    if abs(imag(Imaginary(Index))-imag(TempImaginary(TempIndex)))>1e-5
        TempIndex=TempIndex+1;
        TempImaginary(TempIndex)=Imaginary(Index);
        if real(TempImaginary(TempIndex))>1e-5
```

```
            TempIndex=TempIndex+1;
            TempImaginary(TempIndex)=-conj(TempImaginary(TempIndex-1));
        end
    end
end
TempImaginary=[TempImaginary,TempComplex];
[~,idx]=sort(imag(TempImaginary),'ascend');
TempImaginary=TempImaginary(idx);
Roots=[TempReal,TempImaginary];
end

function HH=FunctionHH(alpha,beta,tau,nu,eta,gamma,r)
n=1;
a=r;
QQ=@(s) (n^2*(1-nu)/2-a^2*beta^2+a^2*s.^2).*(2*a^2*beta^2-2*n^2-...
    a^2*(1-nu)*s.^2)+a^2*n^2*(1+nu)^2/2*s.^2;
f1=@(x) Characteristic(x,alpha,beta,tau,nu,r);

HH=(f1(eta+1e-5)-f1(eta-1e-5))/(2e-5).*gamma.*(besselj(n-1,r*gamma)-...
    besselj(n+1,r*gamma))./(2*2*eta.*QQ(eta));
end

function [P8 P6 P4 P2 P0]=FunctionPP(beta,tau,nu,a,n)
P8=a^4*(nu-1);
P6=a^2*(a^2*beta^2*(3-nu)+4*n^2*(nu-1));
P4=(-4*n^4+6*a^2*n^2*beta^2-2*a^4*beta^4-2*n^4*(1-nu)+...
    3*a^2*n^2*beta^2*(1-nu)-n^4*(1-nu)^2+n^4*(1+nu)^2-...
    a^4*(1-a^2*beta^2)*(1-nu)*tau+a^4*nu*(nu-nu^2)*tau);
P2=a^4*beta^2*tau*(a^2*beta^2*(nu-3)-2*nu^2-nu+3)-...
    2*a^2*n^2*beta^2*(2*beta^2+a^2*tau*(nu-1))-3*n^4*beta^2*(nu-3)+4*n^6*(nu-1)/a^2;
P0=-2*a^2*n^2*beta^2*tau+2*a^2*n^2*beta^2*(1-a^2*beta^2)*tau-...
    2*a^4*beta^4*(1-a^2*beta^2)*tau+n^4*(1-nu)*tau-...
    n^4*(1-a^2*beta^2)*(1-nu)*tau+a^2*n^2*beta^2*(1-a^2*beta^2)*(1-nu)*tau+...
    (2*n^6*beta^2)/a^2-2*n^4*beta^4-(n^8*(1-nu))/a^4+(n^6*beta^2*(1-nu))/a^2;
end

function [Q4 Q2 Q0]=FunctionQQ(beta,nu,a,n)
Q4=a^4*(nu-1);
Q2=a^2*(a^2*beta^2*(3-nu)+2*n^2*(nu-1));
Q0=(n^2-a^2*beta^2)*(2*a^2*beta^2+n^2*(nu-1));
end

function AP=NonAxiSolver(a,nu,alpha,beta,tau1,eta,CC,ell,n)
Np=length(eta);
gamma=(1-eta.^2).^0.5;
FF=sqrt(alpha/(a*CC(ell)*eta(ell)));
[P8a P6a P4a P2a P0a]=FunctionPP(beta,tau1,nu,a,n);
[Q4a Q2a Q0a]=FunctionQQ(beta,nu,a,n);
s=eta;
U=a*(n^2*(nu-1)-2*a^2*beta^2*nu)*s+a^3*(nu-nu^2)*s.^3;
V=1i*(n^3*(1-nu)-2*a^2*beta^2*n+a^2*(2*n-n*(nu+nu^2))*s.^2);
QQa=(n^2*(1-nu)/2-a^2*beta^2+a^2*s.^2).*(2*a^2*beta^2-2*n^2-a^2*(1-nu)*s.^2)+...
    a^2*n^2*(1+nu)^2/2*s.^2;
G6a=P8a*(Q4a*eta.^4+Q2a*eta.^2+Q0a);
G4a=P8a*(Q4a*eta.^4+Q2a*eta.^2+Q0a).*eta.^2+P6a*(Q4a*eta.^4+Q2a*eta.^2+Q0a);
G2a=P8a*Q2a*eta.^6+(P8a*Q0a+P6a*Q2a).*eta.^4+(P6a*Q0a+P4a*Q2a-P2a*Q4a).*eta.^2+...
    P4a*Q0a-P0a*Q4a;
G0a=P8a*Q0a.*eta.^6+P6a*Q0a*eta.^4+(P4a*Q0a-P0a*Q4a)*eta.^2+P2a*Q0a-P0a*Q2a;
%---------- Clamped ----------%
U=@(s) a*(n^2*(nu-1)-2*a^2*beta^2*nu)*s+a^3*(nu-nu^2)*s.^3;
V=@(s) 1i*(n^3*(1-nu)-2*a^2*beta^2*n+a^2*(2*n-n*(nu+nu^2))*s.^2);
E0A=-U(eta).*gamma.*(besselj(n-1,gamma*a)-besselj(n+1,gamma*a))./QQa/2;
E0F=U(eta(ell)).*gamma(ell)*(besselj(n-1,gamma(ell)*a)-...
      besselj(n+1,gamma(ell)*a))/QQa(ell)/2;
E1A=V(eta).*gamma.*(besselj(n-1,gamma*a)-besselj(n+1,gamma*a))./QQa/2;
E1F=V(eta(ell))*gamma(ell)*(besselj(n-1,gamma(ell)*a)-...
besselj(n+1,gamma(ell)*a))/QQa(ell)/2;
E2A=gamma.*(besselj(n-1,gamma*a)-besselj(n+1,gamma*a))/2;
E2F=gamma(ell)*(besselj(n-1,gamma(ell)*a)-besselj(n+1,gamma(ell)*a))/2;
E3A=-eta.*gamma.*(besselj(n-1,gamma*a)-besselj(n+1,gamma*a))/2;
```

```
E3F=eta(ell)*gamma(ell)*(besselj(n-1,gamma(ell)*a)-besselj(n+1,gamma(ell)*a))/2;
%---------- Pin-Jointed ----------%
% U=@(s) a*(n^2*(nu-1)-2*a^2*beta^2*nu)*s+a^3*(nu-nu^2)*s.^3;
% V=@(s) 1i*(n^3*(1-nu)-2*a^2*beta^2*n+a^2*(2*n-n*(nu+nu^2))*s.^2);
% E0A=eta.*U(eta).*gamma.*(besselj(n-1,gamma*a)-besselj(n+1,gamma*a))./QQa/2;
% E0F=eta(ell)*U(eta(ell)).*gamma(ell)*(besselj(n-1,gamma(ell)*a)-...
%     besselj(n+1,gamma(ell)*a))/QQa(ell)/2;
% E1A=V(eta).*gamma.*(besselj(n-1,gamma*a)-besselj(n+1,gamma*a))./QQa/2;
% E1F=V(eta(ell))*gamma(ell)*(besselj(n-1,gamma(ell)*a)-...
%     besselj(n+1,gamma(ell)*a))/QQa(ell)/2;
% E2A=gamma.*(besselj(n-1,gamma*a)-besselj(n+1,gamma*a))/2;
% E2F=gamma(ell)*(besselj(n-1,gamma(ell)*a)-besselj(n+1,gamma(ell)*a))/2;
% E3A=eta.^2.*gamma.*(besselj(n-1,gamma*a)-besselj(n+1,gamma*a))/2;
% E3F=eta(ell)^2*gamma(ell)*(besselj(n-1,gamma(ell)*a)-besselj(n+1,gamma(ell)*a))/2;
%---------- The Summations ----------%
SA0=0; SA1=0; SA2=0; SA3=0; SB0=0; SB1=0; SB2=0; SB3=0;
SC0=0; SC1=0; SC2=0; SC3=0; SD0=0; SD1=0; SD2=0; SD3=0;
for p=1:Np
    SA0=SA0+G6a(p)*(besselj(n-1,gamma(p)*a)-...
        besselj(n+1,gamma(p)*a))*gamma(p)*E0A(p)/2/eta(p)/CC(p)/QQa(p);
    SA1=SA1+G6a(p)*(besselj(n-1,gamma(p)*a)-...
        besselj(n+1,gamma(p)*a))*gamma(p)*E1A(p)/2/eta(p)/CC(p)/QQa(p);
    SA2=SA2+G6a(p)*(besselj(n-1,gamma(p)*a)-...
        besselj(n+1,gamma(p)*a))*gamma(p)*E2A(p)/2/eta(p)/CC(p)/QQa(p);
    SA3=SA3+G6a(p)*(besselj(n-1,gamma(p)*a)-...
        besselj(n+1,gamma(p)*a))*gamma(p)*E3A(p)/2/eta(p)/CC(p)/QQa(p);
    SB0=SB0+G4a(p)*(besselj(n-1,gamma(p)*a)-...
        besselj(n+1,gamma(p)*a))*gamma(p)*E0A(p)/2/eta(p)/CC(p)/QQa(p);
    SB1=SB1+G4a(p)*(besselj(n-1,gamma(p)*a)-...
        besselj(n+1,gamma(p)*a))*gamma(p)*E1A(p)/2/eta(p)/CC(p)/QQa(p);
    SB2=SB2+G4a(p)*(besselj(n-1,gamma(p)*a)-...
        besselj(n+1,gamma(p)*a))*gamma(p)*E2A(p)/2/eta(p)/CC(p)/QQa(p);
    SB3=SB3+G4a(p)*(besselj(n-1,gamma(p)*a)-...
        besselj(n+1,gamma(p)*a))*gamma(p)*E3A(p)/2/eta(p)/CC(p)/QQa(p);
    SC0=SC0+G2a(p)*(besselj(n-1,gamma(p)*a)-...
        besselj(n+1,gamma(p)*a))*gamma(p)*E0A(p)/2/eta(p)/CC(p)/QQa(p);
    SC1=SC1+G2a(p)*(besselj(n-1,gamma(p)*a)-...
        besselj(n+1,gamma(p)*a))*gamma(p)*E1A(p)/2/eta(p)/CC(p)/QQa(p);
    SC2=SC2+G2a(p)*(besselj(n-1,gamma(p)*a)-...
        besselj(n+1,gamma(p)*a))*gamma(p)*E2A(p)/2/eta(p)/CC(p)/QQa(p);
    SC3=SC3+G2a(p)*(besselj(n-1,gamma(p)*a)-...
        besselj(n+1,gamma(p)*a))*gamma(p)*E3A(p)/2/eta(p)/CC(p)/QQa(p);
    SD0=SD0+G0a(p)*(besselj(n-1,gamma(p)*a)-...
        besselj(n+1,gamma(p)*a))*gamma(p)*E0A(p)/2/eta(p)/CC(p)/QQa(p);
    SD1=SD1+G0a(p)*(besselj(n-1,gamma(p)*a)-...
        besselj(n+1,gamma(p)*a))*gamma(p)*E1A(p)/2/eta(p)/CC(p)/QQa(p);
    SD2=SD2+G0a(p)*(besselj(n-1,gamma(p)*a)-...
        besselj(n+1,gamma(p)*a))*gamma(p)*E2A(p)/2/eta(p)/CC(p)/QQa(p);
    SD3=SD3+G0a(p)*(besselj(n-1,gamma(p)*a)-...
        besselj(n+1,gamma(p)*a))*gamma(p)*E3A(p)/2/eta(p)/CC(p)/QQa(p);
end
DA=(-SA3*SB2*SC1*SD0+SA2*SB3*SC1*SD0+SA3*SB1*SC2*SD0-SA1*SB3*SC2*SD0-...
    SA2*SB1*SC3*SD0+SA1*SB2*SC3*SD0+...
    SA3*SB2*SC0*SD1-SA2*SB3*SC0*SD1-SA3*SB0*SC2*SD1+SA0*SB3*SC2*SD1+...
    SA2*SB0*SC3*SD1-SA0*SB2*SC3*SD1-...
    SA3*SB1*SC0*SD2+SA1*SB3*SC0*SD2+SA3*SB0*SC1*SD2-SA0*SB3*SC1*SD2-...
    SA1*SB0*SC3*SD2+SA0*SB1*SC3*SD2+...
    SA2*SB1*SC0*SD3-SA1*SB2*SC0*SD3-SA2*SB0*SC1*SD3+SA0*SB2*SC1*SD3+...
    SA1*SB0*SC2*SD3-SA0*SB1*SC2*SD3);
Fdelta=zeros(Np,1); GE0a=0; GE1a=0; GE2a=0; GE3a=0;
for p=1:Np
    Fdelta(p)=FF*kdelta(ell,p);
    GE0a=GE0a+FF*kdelta(ell,p)*E0A(p);
    GE1a=GE1a+FF*kdelta(ell,p)*E1A(p);
    GE2a=GE2a+FF*kdelta(ell,p)*E2A(p);
    GE3a=GE3a+FF*kdelta(ell,p)*E3A(p);
end
GE0=((FF*E0F+GE0a)*(-SB3*SC2*SD1+SB2*SC3*SD1+SB3*SC1*SD2-...
    SB1*SC3*SD2-SB2*SC1*SD3+SB1*SC2*SD3)+(FF*E1F+GE1a)*(SB3*SC2*SD0-...
    SB2*SC3*SD0-SB3*SC0*SD2+SB0*SC3*SD2+SB2*SC0*SD3-SB0*SC2*SD3)+...
```

```
    (FF*E2F+GE2a)*(-SB3*SC1*SD0+SB1*SC3*SD0+SB3*SC0*SD1-SB0*SC3*SD1-...
    SB1*SC0*SD3+SB0*SC1*SD3)+(FF*E3F+GE3a)*(SB2*SC1*SD0-SB1*SC2*SD0-...
    SB2*SC0*SD1+SB0*SC2*SD1+SB1*SC0*SD2-SB0*SC1*SD2))/DA;
GE1=-((FF*E0F+GE0a)*(-SA3*SC2*SD1+SA2*SC3*SD1+SA3*SC1*SD2-SA1*SC3*SD2-...
    SA2*SC1*SD3+SA1*SC2*SD3)+(FF*E1F+GE1a)*(SA3*SC2*SD0-SA2*SC3*SD0-...
    SA3*SC0*SD2+SA0*SC3*SD2+SA2*SC0*SD3-SA0*SC2*SD3)+...
    (FF*E2F+GE2a)*(-SA3*SC1*SD0+SA1*SC3*SD0+SA3*SC0*SD1-SA0*SC3*SD1-...
    SA1*SC0*SD3+SA0*SC1*SD3)+(FF*E3F+GE3a)*(SA2*SC1*SD0-SA1*SC2*SD0-...
    SA2*SC0*SD1+SA0*SC2*SD1+SA1*SC0*SD2-SA0*SC1*SD2))/DA;
GE2=((FF*E0F+GE0a)*(-SA3*SB2*SD1+SA2*SB3*SD1+SA3*SB1*SD2-SA1*SB3*SD2-...
    SA2*SB1*SD3+SA1*SB2*SD3)+(FF*E1F+GE1a)*(SA3*SB2*SD0-SA2*SB3*SD0-...
    SA3*SB0*SD2+SA0*SB3*SD2+SA2*SB0*SD3-SA0*SB2*SD3)+...
    (FF*E2F+GE2a)*(-SA3*SB1*SD0+SA1*SB3*SD0+SA3*SB0*SD1-SA0*SB3*SD1-...
    SA1*SB0*SD3+SA0*SB1*SD3)+(FF*E3F+GE3a)*(SA2*SB1*SD0-SA1*SB2*SD0-...
    SA2*SB0*SD1+SA0*SB2*SD1+SA1*SB0*SD2-SA0*SB1*SD2))/DA;
GE3=-((FF*E0F+GE0a)*(-SA3*SB2*SC1+SA2*SB3*SC1+SA3*SB1*SC2-SA1*SB3*SC2-...
    SA2*SB1*SC3+SA1*SB2*SC3)+(FF*E1F+GE1a)*(SA3*SB2*SC0-SA2*SB3*SC0-...
    SA3*SB0*SC2+SA0*SB3*SC2+SA2*SB0*SC3-SA0*SB2*SC3)+...
    (FF*E2F+GE2a)*(-SA3*SB1*SC0+SA1*SB3*SC0+SA3*SB0*SC1-SA0*SB3*SC1-...
    SA1*SB0*SC3+SA0*SB1*SC3)+(FF*E3F+GE3a)*(SA2*SB1*SC0-SA1*SB2*SC0-...
    SA2*SB0*SC1+SA0*SB2*SC1+SA1*SB0*SC2-SA0*SB1*SC2))/DA;
AP=(Fdelta+GE0*G6a.*(besselj(n-1,gamma*a)-besselj(n+1,gamma*a)).*gamma./eta./CC./QQa/2+...
    GE1*G4a.*(besselj(n-1,gamma*a)-besselj(n+1,gamma*a)).*gamma./eta./CC./QQa/2+...
    GE2*G2a.*(besselj(n-1,gamma*a)-besselj(n+1,gamma*a)).*gamma./eta./CC./QQa/2+...
    GE3*G0a.*(besselj(n-1,gamma*a)-besselj(n+1,gamma*a)).*gamma./eta./CC./QQa/2).';
end

%---------- Kronecker delta ----------%
function d=kdelta(n,m)
if n==m
    d=1;
else
    d=0;
end
end
```

Appendix L

Matlab code relating to Section 5.3

```
function AppendixL() %Nonaxi increase radius
clc; clear;
index=0;
for f=30:1200
% ---------- Input Variables ----------
a1=0.2; % Dimensional radius (m)
b1=0.28; % Dimensional radius (m)
Cair=343.5; % Sound speed of fluid (m/s)
Dair=1.2; % Density of fluid (kg/m^3)
EE=7.2*10^10; % Youngs Modulus (N/m^2)
h1=0.002; % Dimensional shell thickness (m)
Dplate=2700; % Density of shell (kg/m^3)
nu=0.34; % Poisson's ratio for shell
terms=100; % Number of imaginary roots to seek
ell=1; n=1;
% ---------- Calculated Variables ----------
kno=2*pi*f/Cair; % Fluid wave number
a=a1*kno; % Nondimensional radius
b=b1*kno; % Nondimensional radius
h=h1*kno; % Nondimensional shell thickness
cp1=sqrt(EE/(1-nu^2)/Dplate); % Sound speed of the shell
beta=Cair/cp1; omega=Cair*kno; tau1=12/(h^2*a^2); tau2=12/(h^2*b^2);
alpha=12*omega^2*Dair/(h^3*cp1^2*kno^2*Dplate);
% ---------- Root Finder ---------
% ---------- eta ----------
if a1==0.28
    RealGuess=0.1:0.01:0.98;
    ComplexGuess=(35:0.1:98)+(35:0.1:98)*1i;
    ImaginaryGuess=[(0.4:0.1:0.8)*1i (3/4+(0:1:terms))*pi*1i/a];
    if f>80
        ComplexGuess=(35:0.1:40)+(35:0.1:40)*1i;
        ImaginaryGuess=[(0.2:0.1:0.4)*1i (3/4+(0:1:terms))*pi*1i/a];
    if f>90
        ComplexGuess=(9:0.1:35)+(9:0.1:35)*1i;
        ImaginaryGuess=[(0.2:0.1:0.4)*1i (3/4+(0:1:terms))*pi*1i/a];
    if f>290
        ComplexGuess=(9:0.1:10)+(9:0.1:10)*1i;
        ImaginaryGuess=[(0.2:0.1:0.4)*1i (3/4+(0:1:terms))*pi*1i/a];
    if f>340
        ComplexGuess=(0:0.1:9)+(0:0.1:9)*1i;
        ImaginaryGuess=[(0.2:0.1:0.4)*1i (3/4+(0:1:terms))*pi*1i/a];
    if f>700
        ComplexGuess=(2:0.1:5)+(2:0.1:5)*1i;
        ImaginaryGuess=[(0.2:0.1:0.4)*1i (3/4+(0:1:terms))*pi*1i/a];
    if f>850
        ComplexGuess=(2:0.1:4)+(2:0.1:4)*1i;
        ImaginaryGuess=[(0.1:0.1:1.5)*1i (3/4+(0:1:terms))*pi*1i/a];
```

```
    if f>1030
        ComplexGuess=(0:0.1:4)+(0:0.1:4)*1i;
        ImaginaryGuess=[(0.1:0.1:1.5)*1i (3/4+(0:1:terms))*pi*1i/a];
    end
    end
    end
    end
    end
    end
    end
elseif a1==0.2
    RealGuess=0:0.01:1.1;
    ComplexGuess=(50:1:120)+(50:1:120)*1i;
    ImaginaryGuess=[(0.2:0.01:1)*1i (3/4+(1:1:terms))*pi*1i/a];
    if f>70
        ComplexGuess=(10:1:50)+(10:1:50)*1i;
        ImaginaryGuess=[(0.2:0.01:1)*1i (3/4+(0:1:terms))*pi*1i/a];
    if f>350
        ComplexGuess=(8:0.1:11)+(8:0.1:11)*1i;
        ImaginaryGuess=[(0.2:0.01:1)*1i (3/4+(0:1:terms))*pi*1i/a];
    if f>450
        ComplexGuess=(0:0.1:8)+(0:0.1:8)*1i;
        ImaginaryGuess=(3/4+(1:1:terms))*pi*1i/a;
    if f>750
        ComplexGuess=(1:0.1:5)+(1:0.1:5)*1i;
        ImaginaryGuess=[(1)*1i (3/4+(1:1:terms))*pi*1i/a];
    if f>950
        ComplexGuess=(1:0.1:5)+(1:0.1:5)*1i;
        ImaginaryGuess=[(1)*1i (3/4+(1:1:terms))*pi*1i/a];
    if f>1000
        ComplexGuess=(1:0.1:3.4)+(1:0.1:3.4)*1i;
        ImaginaryGuess=(3/4+(1:1:terms))*pi*1i/a;
    end
    end
    end
    end
    end
    end
elseif a1==0.06
    RealGuess=0:0.01:1.1;
    ComplexGuess=(50:1:70)+(50:1:70)*1i;
    ImaginaryGuess=[(0.2:0.01:1)*1i (3/4+(1:1:terms))*pi*1i/a];
    if f>150
        ComplexGuess=(18:1:50)+(18:1:50)*1i;
        ImaginaryGuess=[(0.2:0.01:1)*1i (3/4+(0:1:terms))*pi*1i/a];
    if f>350
        ComplexGuess=(12:0.1:18)+(12:0.1:18)*1i;
        ImaginaryGuess=[(0.2:0.01:1)*1i (3/4+(0:1:terms))*pi*1i/a];
    if f>650
        ComplexGuess=(1:0.1:10)+(1:0.1:10)*1i;
        ImaginaryGuess=[(1)*1i (3/4+(1:1:terms))*pi*1i/a];
    if f>1000
        ComplexGuess=(1:0.1:7)+(1:0.1:7)*1i;
        ImaginaryGuess=(3/4+(1:1:terms))*pi*1i/a;
    end
    end
    end
    end
end
eta=NewtonRaphson(alpha,beta,tau1,nu,RealGuess,ImaginaryGuess,ComplexGuess,a).';
eta=eta(abs(eta)<terms*pi/a); gamma=sqrt(1-eta.^2-1/a^2); Tw1=length(gamma);
% ---------- sn ----------
if b1==0.28
    RealGuess=0.1:0.01:0.98;
    ComplexGuess=(35:0.1:98)+(35:0.1:98)*1i;
    ImaginaryGuess=[(0.4:0.1:0.8)*1i (3/4+(0:1:terms))*pi*1i/b];
    if f>80
        ComplexGuess=(35:0.1:40)+(35:0.1:40)*1i;
        ImaginaryGuess=[(0.2:0.1:0.4)*1i (3/4+(0:1:terms))*pi*1i/b];
    if f>90
```

```
        ComplexGuess=(9:0.1:35)+(9:0.1:35)*1i;
        ImaginaryGuess=[(0.2:0.1:0.4)*1i (3/4+(0:1:terms))*pi*1i/b];
    if f>290
        ComplexGuess=(9:0.1:10)+(9:0.1:10)*1i;
        ImaginaryGuess=[(0.2:0.1:0.4)*1i (3/4+(0:1:terms))*pi*1i/b];
    if f>340
        ComplexGuess=(0:0.1:9)+(0:0.1:9)*1i;
        ImaginaryGuess=[(0.2:0.1:0.4)*1i (3/4+(0:1:terms))*pi*1i/b];
    if f>700
        ComplexGuess=(2:0.1:5)+(2:0.1:5)*1i;
        ImaginaryGuess=[(0.2:0.1:0.4)*1i (3/4+(0:1:terms))*pi*1i/b];
    if f>850
        ComplexGuess=(2:0.1:4)+(2:0.1:4)*1i;
        ImaginaryGuess=[(0.1:0.1:1.5)*1i (3/4+(0:1:terms))*pi*1i/b];
    if f>1030
        ComplexGuess=(0:0.1:4)+(0:0.1:4)*1i;
        ImaginaryGuess=[(0.1:0.1:1.5)*1i (3/4+(0:1:terms))*pi*1i/b];
    end
    end
    end
    end
    end
    end
    end
elseif b1==0.2
    RealGuess=0:0.01:1.1;
    ComplexGuess=(50:1:120)+(50:1:120)*1i;
    ImaginaryGuess=[(0.2:0.01:1)*1i (3/4+(1:1:terms))*pi*1i/b];
    if f>70
        ComplexGuess=(10:1:50)+(10:1:50)*1i;
        ImaginaryGuess=[(0.2:0.01:1)*1i (3/4+(0:1:terms))*pi*1i/b];
    if f>350
        ComplexGuess=(8:0.1:11)+(8:0.1:11)*1i;
        ImaginaryGuess=[(0.2:0.01:1)*1i (3/4+(0:1:terms))*pi*1i/b];
    if f>450
        ComplexGuess=(0:0.1:8)+(0:0.1:8)*1i;
        ImaginaryGuess=(3/4+(1:1:terms))*pi*1i/b;
    if f>750
        ComplexGuess=(1:0.1:5)+(1:0.1:5)*1i;
        ImaginaryGuess=[(1)*1i (3/4+(1:1:terms))*pi*1i/b];
    if f>950
        ComplexGuess=(1:0.1:5)+(1:0.1:5)*1i;
        ImaginaryGuess=[(1)*1i (3/4+(1:1:terms))*pi*1i/b];
    if f>1000
        ComplexGuess=(1:0.1:3.4)+(1:0.1:3.4)*1i;
        ImaginaryGuess=(3/4+(1:1:terms))*pi*1i/b;
    end
    end
    end
    end
    end
    end
    end
elseif b1==0.06
    RealGuess=0:0.01:1.1;
    ComplexGuess=(50:1:70)+(50:1:70)*1i;
    ImaginaryGuess=[(0.2:0.01:1)*1i (3/4+(1:1:terms))*pi*1i/b];
    if f>150
        ComplexGuess=(18:1:50)+(18:1:50)*1i;
        ImaginaryGuess=[(0.2:0.01:1)*1i (3/4+(0:1:terms))*pi*1i/b];
    if f>350
        ComplexGuess=(12:0.1:18)+(12:0.1:18)*1i;
        ImaginaryGuess=[(0.2:0.01:1)*1i (3/4+(0:1:terms))*pi*1i/b];
    if f>650
        ComplexGuess=(1:0.1:10)+(1:0.1:10)*1i;
        ImaginaryGuess=[(1)*1i (3/4+(1:1:terms))*pi*1i/b];
    if f>1000
        ComplexGuess=(1:0.1:7)+(1:0.1:7)*1i;
        ImaginaryGuess=(3/4+(1:1:terms))*pi*1i/b;
    end
    end
```

```
    end
    end
end
sn=NewtonRaphson(alpha,beta,tau2,nu,RealGuess,ImaginaryGuess,ComplexGuess,b).';
sn=sn(abs(sn)<terms*pi/b); kappa=sqrt(1-sn.^2-1/b^2); Tw2=length(kappa);
% ---------- CC & DD ----------
CC=FunctionHH(alpha,beta,tau1,nu,eta,gamma,a);
DD=FunctionHH(alpha,beta,tau2,nu,sn,kappa,b);
% ---------- RR Integral -----------
RR=zeros(length(gamma),length(kappa));
for p=1:length(gamma)
    for q=1:length(kappa)
        RR(p,q)=IntegralRR(gamma(p),kappa(q),a,n);
    end
end
[AN BM]=NonAxiSolver(a,b,nu,alpha,beta,tau1,tau2,eta.',sn.',CC.',DD.',RR,n,ell);
index=index+1;
PowA=a*real(sum(abs(AN).^2.*CC.*eta))/alpha;
PowB=b*real(sum(abs(BM).^2.*DD.*sn))/alpha;
data(index,:)=[f,PowA,PowB,PowA+PowB];
end
plot(data(:,1),data(:,2),'--k','LineWidth',2);hold on;
plot(data(:,1),data(:,3),'k','LineWidth',2);hold off;
axis([0 1200 0 1.2])
xlabel('Frequency')
ylabel('Energy')
legend('Reflected','Transmitted','Location','northwest')
end
function KK=Characteristic(eta,alpha,beta,tau,nu,a)
n=1;
U=a*(n^2*(nu-1)-2*a^2*beta^2*nu)*eta+a^3*(nu-nu^2)*eta.^3;
V=1i*(n^3*(1-nu)-2*a^2*beta^2*n+a^2*(2*n-n*(nu+nu^2))*eta.^2);
QQ=(n^2*(1-nu)/2-a^2*beta^2+a^2*eta.^2).*(2*a^2*beta^2-2*n^2-...
    a^2*(1-nu)*eta.^2)+a^2*n^2*(1+nu)^2*eta.^2/2;
PP=(a*nu*eta.*U-1i*n*V)*tau+QQ.*(eta.^4+2*n^2*eta.^2/a^2+...
    (1-a^2*beta^2)*tau+n^4/a^4);
KK=(PP.*sqrt(1-eta.^2).*(besselj(n-1,sqrt(1-eta.^2)*a)-...
    besselj(n+1,sqrt(1-eta.^2)*a))/2-...
    alpha*QQ.*besselj(n,sqrt(1-eta.^2)*a));
end
% The Differentiated characteristic equation
function K=DCharacteristic(s,alpha,beta,tau,nu,a)
f1=@(x) Characteristic(x,alpha,beta,tau,nu,a);
K=(f1(s+1e-5)-f1(s-1e-5))/2e-5;
end
% Newton Raphson Method
function Roots=NewtonRaphson(alpha,beta,tau,nu,RGuess,IGuess,CGuess,r)
warning('off','MATLAB:rankDeficientMatrix')
f1=@(x) Characteristic(x,alpha,beta,tau,nu,r);
df1=@(x) DCharacteristic(x,alpha,beta,tau,nu,r);
xold1=RGuess; xold2=IGuess; xold3=CGuess;
for i=1:100
    jac1=df1(xold1); sol1=xold1-f1(xold1)./jac1; xold1=sol1;
    jac2=df1(xold2); sol2=xold2-f1(xold2)./jac2; xold2=sol2;
    jac3=df1(xold3); sol3=xold3-f1(xold3)./jac3; xold3=sol3;
end
Real=sol1;
Real=Real(abs(f1(Real))<1e-5);
Real=Real(Real<1);
Real=sort(Real(Real>0),'descend');
TempIndex=1;
TempReal(TempIndex)=Real(1);
for Index=2:length(Real)
    if abs(Real(Index)-TempReal(TempIndex))>3e-5
        TempIndex=TempIndex+1;
        TempReal(TempIndex)=Real(Index);
    end
end
sol2=sol2((length(TempReal)):end);
Imaginary=sol2;
```

```
Imaginary=sort(Imaginary(imag(Imaginary)>0),'descend');
TempIndex=1;
TempIm(TempIndex)=Imaginary(1);
for Index=2:length(Imaginary)
    if abs(Imaginary(Index)-TempIm(TempIndex))>1e-5
        TempIndex=TempIndex+1;
        TempIm(TempIndex)=Imaginary(Index);
    end
end
Complex=sol3(abs(imag(sol3))>1e-5);
Complex=sort(Complex(real(Complex)>1e-5),'descend');
TempIndex=1;
TempComplex(TempIndex)=Complex(1);
for Index=2:length(Complex)
    if abs(Complex(Index)-TempComplex(TempIndex))>1e-5
        TempIndex=TempIndex+1;
        TempComplex(TempIndex)=Complex(Index);
    end
end
TempComplex=[TempComplex -conj(TempComplex)];
Imaginary=[TempIm,TempComplex];
[~,idx]=sort(imag(Imaginary),'ascend');
Imaginary=Imaginary(idx);
Roots=[TempReal,Imaginary];
end
function HH=FunctionHH(alpha,beta,tau,nu,eta,gamma,r)
n=1; a=r;
QQ=@(s) (n^2*(1-nu)/2-a^2*beta^2+a^2*s.^2).*(2*a^2*beta^2-2*n^2-...
    a^2*(1-nu)*s.^2)+a^2*n^2*(1+nu)^2/2*s.^2;
f1=@(x) Characteristic(x,alpha,beta,tau,nu,r);
HH=(f1(eta+1e-5)-f1(eta-1e-5))/(2e-5).*gamma.*(besselj(n-1,r*gamma)-...
    besselj(n+1,r*gamma))./...
    (2*2*eta.*QQ(eta));
end
function [P8 P6 P4 P2 P0]=FunctionPP(beta,tau,nu,a,n)
P8=a^4*(nu-1);
P6=a^2*(a^2*beta^2*(3-nu)+4*n^2*(nu-1));
P4=(-4*n^4+6*a^2*n^2*beta^2-2*a^4*beta^4-2*n^4*(1-nu)+...
    3*a^2*n^2*beta^2*(1-nu)-n^4*(1-nu)^2+n^4*(1+nu)^2-...
    a^4*(1-a^2*beta^2)*(1-nu)*tau+a^4*nu*(nu-nu^2)*tau);
P2=a^4*beta^2*tau*(a^2*beta^2*(nu-3)-2*nu^2-nu+3)-...
    2*a^2*n^2*beta^2*(2*beta^2+a^2*tau*(nu-1))-3*n^4*beta^2*(nu-3)+4*n^6*(nu-1)/a^2;
P0=-2*a^2*n^2*beta^2*tau+2*a^2*n^2*beta^2*(1-a^2*beta^2)*tau-...
    2*a^4*beta^4*(1-a^2*beta^2)*tau+n^4*(1-nu)*tau-...
    n^4*(1-a^2*beta^2)*(1-nu)*tau+a^2*n^2*beta^2*(1-a^2*beta^2)*(1-nu)*tau+...
    (2*n^6*beta^2)/a^2-2*n^4*beta^4-(n^8*(1-nu))/a^4+(n^6*beta^2*(1-nu))/a^2;
end
function [Q4 Q2 Q0]=FunctionQQ(beta,nu,a,n)
Q4=a^4*(nu-1); Q2=a^2*(a^2*beta^2*(3-nu)+2*n^2*(nu-1));
Q0=(n^2-a^2*beta^2)*(2*a^2*beta^2+n^2*(nu-1));
end
function RR=IntegralRR(gamma,kappa,a,n)
if abs(kappa^2-gamma^2)<1e-10
    if abs(gamma)<1e-10
        RR=0;
    else
        RR=a*(a*gamma*besselj(n-1,gamma*a)^2-2*n*besselj(n-1,gamma*a)*...
            besselj(n,gamma*a)+a*gamma*besselj(n,gamma*a)^2)/(2*gamma);
    end
else
    RR=a*(kappa*besselj(n-1,a*kappa)*besselj(n,a*gamma)-...
        gamma*besselj(n-1,a*gamma)*besselj(n,a*kappa))/(gamma^2-kappa^2);
end
end
function [Ap Bq]=NonAxiSolver(a,b,nu,alpha,beta,tau1,tau2,eta,s,CC,DD,RR,n,ell)
Np=length(eta); Nq=length(s);
gamma=(1-eta.^2-1/a^2).^0.5; kappa=(1-s.^2-1/b^2).^0.5;
FF=sqrt(1/(CC(ell)*eta(ell)));
[P8a P6a P4a P2a P0a]=FunctionPP(beta,tau1,nu,a,n);
[Q4a Q2a Q0a]=FunctionQQ(beta,nu,a,n);
```

```
QQa=Q4a*eta.^4+Q2a*eta.^2+Q0a;
[P8b P6b P4b P2b P0b]=FunctionPP(beta,tau2,nu,b,n);
[Q4b Q2b Q0b]=FunctionQQ(beta,nu,b,n);
QQb=Q4b*s.^4+Q2b*s.^2+Q0b;
G6a=P8a*(Q4a*eta.^4+Q2a*eta.^2+Q0a);
G4a=P8a*(Q4a*eta.^4+Q2a*eta.^2+Q0a).*eta.^2+P6a*(Q4a*eta.^4+Q2a*eta.^2+Q0a);
G2a=P8a*Q2a*eta.^6+(P8a*Q0a+P6a*Q2a).*eta.^4+(P6a*Q0a+P4a*Q2a-...
    P2a*Q4a).*eta.^2+P4a*Q0a-P0a*Q4a;
G0a=P8a*Q0a.*eta.^6+P6a*Q0a*eta.^4+(P4a*Q0a-P0a*Q4a)*eta.^2+P2a*Q0a-P0a*Q2a;
G6b=P8b*(Q4b*s.^4+Q2b*s.^2+Q0b);
G4b=P8b*(Q4b*s.^4+Q2b*s.^2+Q0b).*s.^2+P6b*(Q4b*s.^4+Q2b*s.^2+Q0b);
G2b=P8b*Q2b*s.^6+(P8b*Q0b+P6b*Q2b).*s.^4+(P6b*Q0b+P4b*Q2b-P2b*Q4b).*s.^2+...
    P4b*Q0b-P0b*Q4b;
G0b=P8b*Q0b*s.^6+P6b*Q0b*s.^4+(P4b*Q0b-P0b*Q4b)*s.^2+P2b*Q0b-P0b*Q2b;
U=@(s) a*(n^2*(nu-1)-2*a^2*beta^2*nu)*s+a^3*(nu-nu^2)*s.^3;
V=@(s) 1i*(n^3*(1-nu)-2*a^2*beta^2*n+a^2*(2*n-n*(nu+nu^2))*s.^2);
%---------- The edge conditions ----------%
%---------- Clamped ----------%
E0A=-U(eta).*gamma.*(besselj(n-1,gamma*a)-besselj(n+1,gamma*a))./QQa/2;
E0B=zeros(1,Nq); E0F=U(eta(ell)).*gamma(ell)*(besselj(n-1,gamma(ell)*a)-...
    besselj(n+1,gamma(ell)*a))/QQa(ell)/2;
E4A=zeros(1,Np); E4B=U(s).*kappa.*(besselj(n-1,kappa*b)-besselj(n+1,kappa*b))./QQb/2;
E4F=0; E1A=V(eta).*gamma.*(besselj(n-1,gamma*a)-besselj(n+1,gamma*a))./QQa/2;
E1B=zeros(1,Nq); E1F=V(eta(ell))*gamma(ell)*(besselj(n-1,gamma(ell)*a)-...
    besselj(n+1,gamma(ell)*a))/QQa(ell)/2;
E5A=zeros(1,Np); E5B=V(s).*kappa.*(besselj(n-1,kappa*b)-besselj(n+1,kappa*b))./QQb/2;
E5F=0; E2A=gamma.*(besselj(n-1,gamma*a)-besselj(n+1,gamma*a))/2; E2B=zeros(1,Nq);
E2F=gamma(ell)*(besselj(n-1,gamma(ell)*a)-besselj(n+1,gamma(ell)*a))/2;
E6A=zeros(1,Np); E6B=kappa.*(besselj(n-1,kappa*b)-besselj(n+1,kappa*b))/2;
E6F=0; E3A=-eta.*gamma.*(besselj(n-1,gamma*a)-besselj(n+1,gamma*a))/2;
E3B=zeros(1,Nq); E3F=eta(ell)*gamma(ell)*(besselj(n-1,gamma(ell)*a)-...
    besselj(n+1,gamma(ell)*a))/2; E7F=0;
E7A=zeros(1,Np); E7B=s.*kappa.*(besselj(n-1,kappa*b)-besselj(n+1,kappa*b))/2;
% %---------- Pin-Jointed ----------%
% E0A=eta.*U(eta).*gamma.*(besselj(n-1,gamma*a)-besselj(n+1,gamma*a))./QQa/2;
% E0B=zeros(1,Nq); E0F=eta(ell)*U(eta(ell)).*gamma(ell)*...
%     (besselj(n-1,gamma(ell)*a)-besselj(n+1,gamma(ell)*a))/QQa(ell)/2;
% E4A=zeros(1,Np); E4B=s.*U(s).*kappa.*(besselj(n-1,kappa*b)-...
%     besselj(n+1,kappa*b))./QQb/2; E4F=0;
% E1A=V(eta).*gamma.*(besselj(n-1,gamma*a)-besselj(n+1,gamma*a))./QQa/2;
% E1B=zeros(1,Nq); E1F=V(eta(ell))*gamma(ell)*(besselj(n-1,gamma(ell)*a)-...
%     besselj(n+1,gamma(ell)*a))/QQa(ell)/2;
% E5A=zeros(1,Np); E5B=V(s).*kappa.*(besselj(n-1,kappa*b)-...
%     besselj(n+1,kappa*b))./QQb/2; E5F=0;
% E2A=gamma.*(besselj(n-1,gamma*a)-besselj(n+1,gamma*a))/2; E2B=zeros(1,Nq);
% E2F=gamma(ell)*(besselj(n-1,gamma(ell)*a)-besselj(n+1,gamma(ell)*a))/2;
% E6A=zeros(1,Np); E6B=kappa.*(besselj(n-1,kappa*b)-besselj(n+1,kappa*b))/2;
% E6F=0; E3A=eta.^2.*gamma.*(besselj(n-1,gamma*a)-besselj(n+1,gamma*a))/2;
% E3B=zeros(1,Nq); E3F=eta(ell)^2*gamma(ell)*(besselj(n-1,gamma(ell)*a)-...
%     besselj(n+1,gamma(ell)*a))/2; E7F=0;
% E7A=zeros(1,Np); E7B=s.^2.*kappa.*(besselj(n-1,kappa*b)-besselj(n+1,kappa*b))/2;
SA0=0; SA1=0; SA2=0; SA3=0; SB0=0; SB1=0; SB2=0; SB3=0;
SC0=0; SC1=0; SC2=0; SC3=0; SD0=0; SD1=0; SD2=0; SD3=0;
for p=1:Np
    SA0=SA0+G6a(p)*(besselj(n-1,gamma(p)*a)-...
        besselj(n+1,gamma(p)*a))*gamma(p)*E0A(p)/2/CC(p)/QQa(p);
    SA1=SA1+G6a(p)*(besselj(n-1,gamma(p)*a)-...
        besselj(n+1,gamma(p)*a))*gamma(p)*E1A(p)/2/CC(p)/QQa(p);
    SA2=SA2+G6a(p)*(besselj(n-1,gamma(p)*a)-...
        besselj(n+1,gamma(p)*a))*gamma(p)*E2A(p)/2/CC(p)/QQa(p);
    SA3=SA3+G6a(p)*(besselj(n-1,gamma(p)*a)-...
        besselj(n+1,gamma(p)*a))*gamma(p)*E3A(p)/2/CC(p)/QQa(p);
    SB0=SB0+G4a(p)*(besselj(n-1,gamma(p)*a)-...
        besselj(n+1,gamma(p)*a))*gamma(p)*E0A(p)/2/CC(p);
    SB1=SB1+G4a(p)*(besselj(n-1,gamma(p)*a)-...
        besselj(n+1,gamma(p)*a))*gamma(p)*E1A(p)/2/CC(p)/QQa(p);
    SB2=SB2+G4a(p)*(besselj(n-1,gamma(p)*a)-...
        besselj(n+1,gamma(p)*a))*gamma(p)*E2A(p)/2/CC(p)/QQa(p);
    SB3=SB3+G4a(p)*(besselj(n-1,gamma(p)*a)-...
        besselj(n+1,gamma(p)*a))*gamma(p)*E3A(p)/2/CC(p)/QQa(p);
```

```
    SC0=SC0+G2a(p)*(besselj(n-1,gamma(p)*a)-...
        besselj(n+1,gamma(p)*a))*gamma(p)*E0A(p)/2/CC(p)/QQa(p);
    SC1=SC1+G2a(p)*(besselj(n-1,gamma(p)*a)-...
        besselj(n+1,gamma(p)*a))*gamma(p)*E1A(p)/2/CC(p)/QQa(p);
    SC2=SC2+G2a(p)*(besselj(n-1,gamma(p)*a)-...
        besselj(n+1,gamma(p)*a))*gamma(p)*E2A(p)/2/CC(p)/QQa(p);
    SC3=SC3+G2a(p)*(besselj(n-1,gamma(p)*a)-...
        besselj(n+1,gamma(p)*a))*gamma(p)*E3A(p)/2/CC(p)/QQa(p);
    SD0=SD0+G0a(p)*(besselj(n-1,gamma(p)*a)-...
        besselj(n+1,gamma(p)*a))*gamma(p)*E0A(p)/2/CC(p)/QQa(p);
    SD1=SD1+G0a(p)*(besselj(n-1,gamma(p)*a)-...
        besselj(n+1,gamma(p)*a))*gamma(p)*E1A(p)/2/CC(p)/QQa(p);
    SD2=SD2+G0a(p)*(besselj(n-1,gamma(p)*a)-...
        besselj(n+1,gamma(p)*a))*gamma(p)*E2A(p)/2/CC(p)/QQa(p);
    SD3=SD3+G0a(p)*(besselj(n-1,gamma(p)*a)-...
        besselj(n+1,gamma(p)*a))*gamma(p)*E3A(p)/2/CC(p)/QQa(p);
end
SE4=0; SE5=0; SE6=0; SE7=0; SF4=0; SF5=0; SF6=0; SF7=0;
SG4=0; SG5=0; SG6=0; SG7=0; SH4=0; SH5=0; SH6=0; SH7=0;
for q=1:Nq
    SE4=SE4+G6b(q)*(besselj(n-1,kappa(q)*b)-...
        besselj(n+1,kappa(q)*b))*gamma(p)*E4B(q)/2/s(q)/DD(q)/QQb(q);
    SE5=SE5+G6b(q)*(besselj(n-1,kappa(q)*b)-...
        besselj(n+1,kappa(q)*b))*gamma(p)*E5B(q)/2/s(q)/DD(q)/QQb(q);
    SE6=SE6+G6b(q)*(besselj(n-1,kappa(q)*b)-...
        besselj(n+1,kappa(q)*b))*gamma(p)*E6B(q)/2/s(q)/DD(q)/QQb(q);
    SE7=SE7+G6b(q)*(besselj(n-1,kappa(q)*b)-...
        besselj(n+1,kappa(q)*b))*gamma(p)*E7B(q)/2/s(q)/DD(q)/QQb(q);
    SF4=SF4+G4b(q)*(besselj(n-1,kappa(q)*b)-...
        besselj(n+1,kappa(q)*b))*gamma(p)*E4B(q)/2/s(q)/DD(q)/QQb(q);
    SF5=SF5+G4b(q)*(besselj(n-1,kappa(q)*b)-...
        besselj(n+1,kappa(q)*b))*gamma(p)*E5B(q)/2/s(q)/DD(q)/QQb(q);
    SF6=SF6+G4b(q)*(besselj(n-1,kappa(q)*b)-...
        besselj(n+1,kappa(q)*b))*gamma(p)*E6B(q)/2/s(q)/DD(q)/QQb(q);
    SF7=SF7+G4b(q)*(besselj(n-1,kappa(q)*b)-...
        besselj(n+1,kappa(q)*b))*gamma(p)*E7B(q)/2/s(q)/DD(q)/QQb(q);
    SG4=SG4+G2b(q)*(besselj(n-1,kappa(q)*b)-...
        besselj(n+1,kappa(q)*b))*gamma(p)*E4B(q)/2/s(q)/DD(q)/QQb(q);
    SG5=SG5+G2b(q)*(besselj(n-1,kappa(q)*b)-...
        besselj(n+1,kappa(q)*b))*gamma(p)*E5B(q)/2/s(q)/DD(q)/QQb(q);
    SG6=SG6+G2b(q)*(besselj(n-1,kappa(q)*b)-...
        besselj(n+1,kappa(q)*b))*gamma(p)*E6B(q)/2/s(q)/DD(q)/QQb(q);
    SG7=SG7+G2b(q)*(besselj(n-1,kappa(q)*b)-...
        besselj(n+1,kappa(q)*b))*gamma(p)*E7B(q)/2/s(q)/DD(q)/QQb(q);
    SH4=SH4+G0b(q)*(besselj(n-1,kappa(q)*b)-...
        besselj(n+1,kappa(q)*b))*gamma(p)*E4B(q)/2/s(q)/DD(q)/QQb(q);
    SH5=SH5+G0b(q)*(besselj(n-1,kappa(q)*b)-...
        besselj(n+1,kappa(q)*b))*gamma(p)*E5B(q)/2/s(q)/DD(q)/QQb(q);
    SH6=SH6+G0b(q)*(besselj(n-1,kappa(q)*b)-...
        besselj(n+1,kappa(q)*b))*gamma(p)*E6B(q)/2/s(q)/DD(q)/QQb(q);
    SH7=SH7+G0b(q)*(besselj(n-1,kappa(q)*b)-...
        besselj(n+1,kappa(q)*b))*gamma(p)*E7B(q)/2/s(q)/DD(q)/QQb(q);
end
DA=(-SA3*SB2*SC1*SD0+SA2*SB3*SC1*SD0+SA3*SB1*SC2*SD0-SA1*SB3*SC2*SD0-...
    SA2*SB1*SC3*SD0+SA1*SB2*SC3*SD0+...
    SA3*SB2*SC0*SD1-SA2*SB3*SC0*SD1-SA3*SB0*SC2*SD1+SA0*SB3*SC2*SD1+...
    SA2*SB0*SC3*SD1-SA0*SB2*SC3*SD1-...
    SA3*SB1*SC0*SD2+SA1*SB3*SC0*SD2+SA3*SB0*SC1*SD2-SA0*SB3*SC1*SD2-...
    SA1*SB0*SC3*SD2+SA0*SB1*SC3*SD2+...
    SA2*SB1*SC0*SD3-SA1*SB2*SC0*SD3-SA2*SB0*SC1*SD3+SA0*SB2*SC1*SD3+...
    SA1*SB0*SC2*SD3-SA0*SB1*SC2*SD3);
DB=(SE7*SF6*SG5*SH4-SE6*SF7*SG5*SH4-SE7*SF5*SG6*SH4+SE5*SF7*SG6*SH4+...
    SE6*SF5*SG7*SH4-SE5*SF6*SG7*SH4-...
    SE7*SF6*SG4*SH5+SE6*SF7*SG4*SH5+SE7*SF4*SG6*SH5-SE4*SF7*SG6*SH5-...
    SE6*SF4*SG7*SH5+SE4*SF6*SG7*SH5+...
    SE7*SF5*SG4*SH6-SE5*SF7*SG4*SH6-SE7*SF4*SG5*SH6+SE4*SF7*SG5*SH6+...
    SE5*SF4*SG7*SH6-SE4*SF5*SG7*SH6-...
    SE6*SF5*SG4*SH7+SE5*SF6*SG4*SH7+SE6*SF4*SG5*SH7-SE4*SF6*SG5*SH7-...
    SE5*SF4*SG6*SH7+SE4*SF5*SG6*SH7);
Fdelta=zeros(1,Np); GE0a=0; GE1a=0; GE2a=0; GE3a=0;
```

```
for p=1:Np
    Fdelta(p)=FF*kdelta(ell,p);
    GE0a=GE0a+FF*kdelta(ell,p)*E0A(p); GE1a=GE1a+FF*kdelta(ell,p)*E1A(p);
    GE2a=GE2a+FF*kdelta(ell,p)*E2A(p); GE3a=GE3a+FF*kdelta(ell,p)*E3A(p);
end
GE0=((FF*E0F-GE0a)*(-SB3*SC2*SD1+SB2*SC3*SD1+SB3*SC1*SD2-SB1*SC3*SD2-...
    SB2*SC1*SD3+SB1*SC2*SD3)+(FF*E1F-GE1a)*(SB3*SC2*SD0-SB2*SC3*SD0-...
    SB3*SC0*SD2+SB0*SC3*SD2+SB2*SC0*SD3-SB0*SC2*SD3)+...
    (FF*E2F-GE2a)*(-SB3*SC1*SD0+SB1*SC3*SD0+SB3*SC0*SD1-SB0*SC3*SD1-...
    SB1*SC0*SD3+SB0*SC1*SD3)+(FF*E3F-GE3a)*(SB2*SC1*SD0-SB1*SC2*SD0-...
    SB2*SC0*SD1+SB0*SC2*SD1+SB1*SC0*SD2-SB0*SC1*SD2))/DA;
GE1=-((FF*E0F-GE0a)*(-SA3*SC2*SD1+SA2*SC3*SD1+SA3*SC1*SD2-SA1*SC3*SD2-...
    SA2*SC1*SD3+SA1*SC2*SD3)+(FF*E1F-GE1a)*(SA3*SC2*SD0-SA2*SC3*SD0-...
    SA3*SC0*SD2+SA0*SC3*SD2+SA2*SC0*SD3-SA0*SC2*SD3)+...
    (FF*E2F-GE2a)*(-SA3*SC1*SD0+SA1*SC3*SD0+SA3*SC0*SD1-SA0*SC3*SD1-...
    SA1*SC0*SD3+SA0*SC1*SD3)+(FF*E3F-GE3a)*(SA2*SC1*SD0-SA1*SC2*SD0-...
    SA2*SC0*SD1+SA0*SC2*SD1+SA1*SC0*SD2-SA0*SC1*SD2))/DA;
GE2=((FF*E0F-GE0a)*(-SA3*SB2*SD1+SA2*SB3*SD1+SA3*SB1*SD2-SA1*SB3*SD2-...
    SA2*SB1*SD3+SA1*SB2*SD3)+(FF*E1F-GE1a)*(SA3*SB2*SD0-SA2*SB3*SD0-...
    SA3*SB0*SD2+SA0*SB3*SD2+SA2*SB0*SD3-SA0*SB2*SD3)+...
    (FF*E2F-GE2a)*(-SA3*SB1*SD0+SA1*SB3*SD0+SA3*SB0*SD1-SA0*SB3*SD1-...
    SA1*SB0*SD3+SA0*SB1*SD3)+(FF*E3F-GE3a)*(SA2*SB1*SD0-SA1*SB2*SD0-...
    SA2*SB0*SD1+SA0*SB2*SD1+SA1*SB0*SD2-SA0*SB1*SD2))/DA;
GE3=-((FF*E0F-GE0a)*(-SA3*SB2*SC1+SA2*SB3*SC1+SA3*SB1*SC2-SA1*SB3*SC2-...
    SA2*SB1*SC3+SA1*SB2*SC3)+(FF*E1F-GE1a)*(SA3*SB2*SC0-SA2*SB3*SC0-...
    SA3*SB0*SC2+SA0*SB3*SC2+SA2*SB0*SC3-SA0*SB2*SC3)+...
    (FF*E2F-GE2a)*(-SA3*SB1*SC0+SA1*SB3*SC0+SA3*SB0*SC1-SA0*SB3*SC1-...
    SA1*SB0*SC3+SA0*SB1*SC3)+(FF*E3F-GE3a)*(SA2*SB1*SC0-SA1*SB2*SC0-...
    SA2*SB0*SC1+SA0*SB2*SC1+SA1*SB0*SC2-SA0*SB1*SC2))/DA;
GE4b=0; GE5b=0; GE6b=0; GE7b=0;
for q=1:Nq
    GE4b=GE4b+alpha*FF*eta(ell)*RR(ell,q)*E4B(q)/b/s(q)/DD(q);
    GE5b=GE5b+alpha*FF*eta(ell)*RR(ell,q)*E5B(q)/b/s(q)/DD(q);
    GE6b=GE6b+alpha*FF*eta(ell)*RR(ell,q)*E6B(q)/b/s(q)/DD(q);
    GE7b=GE7b+alpha*FF*eta(ell)*RR(ell,q)*E7B(q)/b/s(q)/DD(q);
end
GE4=((-GE4b-FF*E4F)*(-SF7*SG6*SH5+SF6*SG7*SH5+SF7*SG5*SH6-SF5*SG7*SH6-...
    SF6*SG5*SH7+SF5*SG6*SH7)+(-GE5b-FF*E5F)*(SF7*SG6*SH4-SF6*SG7*SH4-...
    SF7*SG4*SH6+SF4*SG7*SH6+SF6*SG4*SH7-SF4*SG6*SH7)+...
    (-GE6b-FF*E6F)*(-SF7*SG5*SH4+SF5*SG7*SH4+SF7*SG4*SH5-SF4*SG7*SH5-...
    SF5*SG4*SH7+SF4*SG5*SH7)+(-GE7b-FF*E7F)*(SF6*SG5*SH4-SF5*SG6*SH4-...
    SF6*SG4*SH5+SF4*SG6*SH5+SF5*SG4*SH6-SF4*SG5*SH6))/DB;
GE5=-((-GE4b-FF*E4F)*(-SE7*SG6*SH5+SE6*SG7*SH5+SE7*SG5*SH6-SE5*SG7*SH6-...
    SE6*SG5*SH7+SE5*SG6*SH7)+(-GE5b-FF*E5F)*(SE7*SG6*SH4-SE6*SG7*SH4-...
    SE7*SG4*SH6+SE4*SG7*SH6+SE6*SG4*SH7-SE4*SG6*SH7)+...
    (-GE6b-FF*E6F)*(-SE7*SG5*SH4+SE5*SG7*SH4+SE7*SG4*SH5-SE4*SG7*SH5-...
    SE5*SG4*SH7+SE4*SG5*SH7)+(-GE7b-FF*E7F)*(SE6*SG5*SH4-SE5*SG6*SH4-...
    SE6*SG4*SH5+SE4*SG6*SH5+SE5*SG4*SH6-SE4*SG5*SH6))/DB;
GE6=((-GE4b-FF*E4F)*(-SE7*SF6*SH5+SE6*SF7*SH5+SE7*SF5*SH6-SE5*SF7*SH6-...
    SE6*SF5*SH7+SE5*SF6*SH7)+(-GE5b-FF*E5F)*(SE7*SF6*SH4-SE6*SF7*SH4-...
    SE7*SF4*SH6+SE4*SF7*SH6+SE6*SF4*SH7-SE4*SF6*SH7)+...
    (-GE6b-FF*E6F)*(-SE7*SF5*SH4+SE5*SF7*SH4+SE7*SF4*SH5-SE4*SF7*SH5-...
    SE5*SF4*SH7+SE4*SF5*SH7)+(-GE7b-FF*E7F)*(SE6*SF5*SH4-SE5*SF6*SH4-...
    SE6*SF4*SH5+SE4*SF6*SH5+SE5*SF4*SH6-SE4*SF5*SH6))/DB;
GE7=-((-GE4b-FF*E4F)*(-SE7*SF6*SG5+SE6*SF7*SG5+SE7*SF5*SG6-SE5*SF7*SG6-...
    SE6*SF5*SG7+SE5*SF6*SG7)+(-GE5b-FF*E5F)*(SE7*SF6*SG4-SE6*SF7*SG4-...
    SE7*SF4*SG6+SE4*SF7*SG6+SE6*SF4*SG7-SE4*SF6*SG7)+...
    (-GE6b-FF*E6F)*(-SE7*SF5*SG4+SE5*SF7*SG4+SE7*SF4*SG5-SE4*SF7*SG5-...
    SE5*SF4*SG7+SE4*SF5*SG7)+(-GE7b-FF*E7F)*(SE6*SF5*SG4-SE5*SF6*SG4-...
    SE6*SF4*SG5+SE4*SF6*SG5+SE5*SF4*SG6-SE4*SF5*SG6))/DB;
VFA=(-Fdelta+GE0*G6a.*(besselj(n-1,gamma*a)-besselj(n+1,gamma*a)).*gamma./CC./QQa/2+...
    GE1*G4a.*(besselj(n-1,gamma*a)-besselj(n+1,gamma*a)).*gamma./CC./QQa/2+...
    GE2*G2a.*(besselj(n-1,gamma*a)-besselj(n+1,gamma*a)).*gamma./CC./QQa/2+...
    GE3*G0a.*(besselj(n-1,gamma*a)-besselj(n+1,gamma*a)).*gamma./CC./QQa/2).';
V0=(G6a.*(besselj(n-1,gamma*a)-besselj(n+1,gamma*a)).*gamma./CC./QQa/2/DA).';
V1=-(G4a.*(besselj(n-1,gamma*a)-besselj(n+1,gamma*a)).*gamma./CC./QQa/2/DA).';
V2=(G2a.*(besselj(n-1,gamma*a)-besselj(n+1,gamma*a)).*gamma./CC./QQa/2/DA).';
V3=-(G0a.*(besselj(n-1,gamma*a)-besselj(n+1,gamma*a)).*gamma./CC./QQa/2/DA).';
VFB=(alpha*FF*eta(ell).*RR(ell,:)./s./DD/b+...
    GE4*G6b.*(besselj(n-1,kappa*b)-besselj(n+1,kappa*b)).*kappa./s./DD./QQb/2+...
```

```
    GE5*G4b.*(besselj(n-1,kappa*b)-besselj(n+1,kappa*b)).*kappa./s./DD./QQb/2+...
    GE6*G2b.*(besselj(n-1,kappa*b)-besselj(n+1,kappa*b)).*kappa./s./DD./QQb/2+...
    GE7*G0b.*(besselj(n-1,kappa*b)-besselj(n+1,kappa*b)).*kappa./s./DD./QQb/2).';
V4=(G6b.*(besselj(n-1,kappa*b)-besselj(n+1,kappa*b)).*kappa./s./DD./QQb/2/DB).';
V5=-(G4b.*(besselj(n-1,kappa*b)-besselj(n+1,kappa*b)).*kappa./s./DD./QQb/2/DB).';
V6=(G2b.*(besselj(n-1,kappa*b)-besselj(n+1,kappa*b)).*kappa./s./DD./QQb/2/DB).';
V7=-(G0b.*(besselj(n-1,kappa*b)-besselj(n+1,kappa*b)).*kappa./s./DD./QQb/2/DB).';
M0=zeros(Np,Nq); M1=zeros(Np,Nq); M2=zeros(Np,Nq); M3=zeros(Np,Nq); M4=zeros(Np,Nq);
M5=zeros(Np,Nq); M6=zeros(Np,Nq); M7=zeros(Np,Nq); MFA=zeros(Np,Nq);
for p=1:Np
    for q=1:Nq
        M0(end,q)=E0B(q);
        M1(p,q)=alpha*RR(p,q)*E0A(p)/a/CC(p);
        M2(end,q)=E1B(q);
        M3(p,q)=alpha*RR(p,q)*E1A(p)/a/CC(p);
        M4(end,q)=E2B(q);
        M5(p,q)=alpha*RR(p,q)*E2A(p)/a/CC(p);
        M6(end,q)=E3B(q);
        M7(p,q)=alpha*RR(p,q)*E3A(p)/a/CC(p);
        MFA(p,q)=alpha*RR(p,q)/a/CC(p);
    end
end
M8=zeros(Nq,Np); M9=zeros(Nq,Np); M10=zeros(Nq,Np); M11=zeros(Nq,Np); M12=zeros(Nq,Np);
M13=zeros(Nq,Np); M14=zeros(Nq,Np); M15=zeros(Nq,Np); MFB=zeros(Nq,Np);
for p=1:Np
    for q=1:Nq
        M8(q,p)=-alpha*eta(p)*RR(p,q)*E4B(q)/b/s(q)/DD(q);
        M10(q,p)=-alpha*eta(p)*RR(p,q)*E5B(q)/b/s(q)/DD(q);
        M12(q,p)=-alpha*eta(p)*RR(p,q)*E6B(q)/b/s(q)/DD(q);
        M14(q,p)=-alpha*eta(p)*RR(p,q)*E7B(q)/b/s(q)/DD(q);
        MFB(q,p)=alpha*eta(p)*RR(p,q)/b/s(q)/DD(q);
    end
    M9(end,p)=E4A(p);
    M11(end,p)=E5A(p);
    M13(end,p)=E6A(p);
    M15(end,p)=E7A(p);
end
ep=ones(1,Np); eq=ones(1,Nq);
Ap=(eye(Np)-(...
    +((-SB3*SC2*SD1+SB2*SC3*SD1+SB3*SC1*SD2-SB1*SC3*SD2-SB2*SC1*SD3+...
    SB1*SC2*SD3)*V0+(-SA3*SC2*SD1+SA2*SC3*SD1+SA3*SC1*SD2-SA1*SC3*SD2-...
    SA2*SC1*SD3+SA1*SC2*SD3)*V1+(-SA3*SB2*SD1+SA2*SB3*SD1+SA3*SB1*SD2-...
    SA1*SB3*SD2-SA2*SB1*SD3+SA1*SB2*SD3)*V2+(-SA3*SB2*SC1+SA2*SB3*SC1+...
    SA3*SB1*SC2-SA1*SB3*SC2-SA2*SB1*SC3+SA1*SB2*SC3)*V3)*ep*M0...
    +((-SB3*SC2*SD1+SB2*SC3*SD1+SB3*SC1*SD2-SB1*SC3*SD2-SB2*SC1*SD3+...
    SB1*SC2*SD3)*V0+(-SA3*SC2*SD1+SA2*SC3*SD1+SA3*SC1*SD2-SA1*SC3*SD2-...
    SA2*SC1*SD3+SA1*SC2*SD3)*V1+(-SA3*SB2*SD1+SA2*SB3*SD1+SA3*SB1*SD2-...
    SA1*SB3*SD2-SA2*SB1*SD3+SA1*SB2*SD3)*V2+(-SA3*SB2*SC1+SA2*SB3*SC1+...
    SA3*SB1*SC2-SA1*SB3*SC2-SA2*SB1*SC3+SA1*SB2*SC3)*V3)*ep*M1...
    +((SB3*SC2*SD0-SB2*SC3*SD0-SB3*SC0*SD2+SB0*SC3*SD2+SB2*SC0*SD3-...
    SB0*SC2*SD3)*V0+(SA3*SC2*SD0-SA2*SC3*SD0-SA3*SC0*SD2+SA0*SC3*SD2+...
    SA2*SC0*SD3-SA0*SC2*SD3)*V1+(SA3*SB2*SD0-SA2*SB3*SD0-SA3*SB0*SD2+...
    SA0*SB3*SD2+SA2*SB0*SD3-SA0*SB2*SD3)*V2+(SA3*SB2*SC0-SA2*SB3*SC0-...
    SA3*SB0*SC2+SA0*SB3*SC2+SA2*SB0*SC3-SA0*SB2*SC3)*V3)*ep*M2...
    +((SB3*SC2*SD0-SB2*SC3*SD0-SB3*SC0*SD2+SB0*SC3*SD2+SB2*SC0*SD3-...
    SB0*SC2*SD3)*V0+(SA3*SC2*SD0-SA2*SC3*SD0-SA3*SC0*SD2+SA0*SC3*SD2+...
    SA2*SC0*SD3-SA0*SC2*SD3)*V1+(SA3*SB2*SD0-SA2*SB3*SD0-SA3*SB0*SD2+...
    SA0*SB3*SD2+SA2*SB0*SD3-SA0*SB2*SD3)*V2+(SA3*SB2*SC0-SA2*SB3*SC0-...
    SA3*SB0*SC2+SA0*SB3*SC2+SA2*SB0*SC3-SA0*SB2*SC3)*V3)*ep*M3...
    +((-SB3*SC1*SD0+SB1*SC3*SD0+SB3*SC0*SD1-SB0*SC3*SD1-SB1*SC0*SD3+...
    SB0*SC1*SD3)*V0+(-SA3*SC1*SD0+SA1*SC3*SD0+SA3*SC0*SD1-SA0*SC3*SD1-...
    SA1*SC0*SD3+SA0*SC1*SD3)*V1+(-SA3*SB1*SD0+SA1*SB3*SD0+SA3*SB0*SD1-...
    SA0*SB3*SD1-SA1*SB0*SD3+SA0*SB1*SD3)*V2+(-SA3*SB1*SC0+SA1*SB3*SC0+...
    SA3*SB0*SC1-SA0*SB3*SC1-SA1*SB0*SC3+SA0*SB1*SC3)*V3)*ep*M4...
    +((-SB3*SC1*SD0+SB1*SC3*SD0+SB3*SC0*SD1-SB0*SC3*SD1-SB1*SC0*SD3+...
    SB0*SC1*SD3)*V0+(-SA3*SC1*SD0+SA1*SC3*SD0+SA3*SC0*SD1-SA0*SC3*SD1-...
    SA1*SC0*SD3+SA0*SC1*SD3)*V1+(-SA3*SB1*SD0+SA1*SB3*SD0+SA3*SB0*SD1-...
    SA0*SB3*SD1-SA1*SB0*SD3+SA0*SB1*SD3)*V2+(-SA3*SB1*SC0+SA1*SB3*SC0+...
    SA3*SB0*SC1-SA0*SB3*SC1-SA1*SB0*SC3+SA0*SB1*SC3)*V3)*ep*M5...
    +((SB2*SC1*SD0-SB1*SC2*SD0-SB2*SC0*SD1+SB0*SC2*SD1+SB1*SC0*SD2-...
```

```
SB0*SC1*SD2)*V0+(SA2*SC1*SD0-SA1*SC2*SD0-SA2*SC0*SD1+SA0*SC2*SD1+...
SA1*SC0*SD2-SA0*SC1*SD2)*V1+(SA2*SB1*SD0-SA1*SB2*SD0-SA2*SB0*SD1+...
SA0*SB2*SD1+SA1*SB0*SD2-SA0*SB1*SD2)*V2+(SA2*SB1*SC0-SA1*SB2*SC0-...
SA2*SB0*SC1+SA0*SB2*SC1+SA1*SB0*SC2-SA0*SB1*SC2)*V3)*ep*M6...
+((SB2*SC1*SD0-SB1*SC2*SD0-SB2*SC0*SD1+SB0*SC2*SD1+SB1*SC0*SD2-...
SB0*SC1*SD2)*V0+(SA2*SC1*SD0-SA1*SC2*SD0-SA2*SC0*SD1+SA0*SC2*SD1+...
SA1*SC0*SD2-SA0*SC1*SD2)*V1+(SA2*SB1*SD0-SA1*SB2*SD0-SA2*SB0*SD1+...
SA0*SB2*SD1+SA1*SB0*SD2-SA0*SB1*SD2)*V2+(SA2*SB1*SC0-SA1*SB2*SC0-...
SA2*SB0*SC1+SA0*SB2*SC1+SA1*SB0*SC2-SA0*SB1*SC2)*V3)*ep*M7+MFA)...
*(...
+((SF7*SG6*SH5-SF6*SG7*SH5-SF7*SG5*SH6+SF5*SG7*SH6+SF6*SG5*SH7-...
SF5*SG6*SH7)*V4+(SE7*SG6*SH5-SE6*SG7*SH5-SE7*SG5*SH6+SE5*SG7*SH6+...
SE6*SG5*SH7-SE5*SG6*SH7)*V5+(SE7*SF6*SH5-SE6*SF7*SH5-SE7*SF5*SH6+...
SE5*SF7*SH6+SE6*SF5*SH7-SE5*SF6*SH7)*V6+(SE7*SF6*SG5-SE6*SF7*SG5-...
SE7*SF5*SG6+SE5*SF7*SG6+SE6*SF5*SG7-SE5*SF6*SG7)*V7)*eq*M8...
+((SF7*SG6*SH5-SF6*SG7*SH5-SF7*SG5*SH6+SF5*SG7*SH6+SF6*SG5*SH7-...
SF5*SG6*SH7)*V4+(SE7*SG6*SH5-SE6*SG7*SH5-SE7*SG5*SH6+SE5*SG7*SH6+...
SE6*SG5*SH7-SE5*SG6*SH7)*V5+(SE7*SF6*SH5-SE6*SF7*SH5-SE7*SF5*SH6+...
SE5*SF7*SH6+SE6*SF5*SH7-SE5*SF6*SH7)*V6+(SE7*SF6*SG5-SE6*SF7*SG5-...
SE7*SF5*SG6+SE5*SF7*SG6+SE6*SF5*SG7-SE5*SF6*SG7)*V7)*eq*M9...
+((-SF7*SG6*SH4+SF6*SG7*SH4+SF7*SG4*SH6-SF4*SG7*SH6-SF6*SG4*SH7+...
SF4*SG6*SH7)*V4+(-SE7*SG6*SH4+SE6*SG7*SH4+SE7*SG4*SH6-SE4*SG7*SH6-...
SE6*SG4*SH7+SE4*SG6*SH7)*V5+(-SE7*SF6*SH4+SE6*SF7*SH4+SE7*SF4*SH6-...
SE4*SF7*SH6-SE6*SF4*SH7+SE4*SF6*SH7)*V6+(-SE7*SF6*SG4+SE6*SF7*SG4+...
SE7*SF4*SG6-SE4*SF7*SG6-SE6*SF4*SG7+SE4*SF6*SG7)*V7)*eq*M10...
+((-SF7*SG6*SH4+SF6*SG7*SH4+SF7*SG4*SH6-SF4*SG7*SH6-SF6*SG4*SH7+...
SF4*SG6*SH7)*V4+(-SE7*SG6*SH4+SE6*SG7*SH4+SE7*SG4*SH6-SE4*SG7*SH6-...
SE6*SG4*SH7+SE4*SG6*SH7)*V5+(-SE7*SF6*SH4+SE6*SF7*SH4+SE7*SF4*SH6-...
SE4*SF7*SH6-SE6*SF4*SH7+SE4*SF6*SH7)*V6+(-SE7*SF6*SG4+SE6*SF7*SG4+...
SE7*SF4*SG6-SE4*SF7*SG6-SE6*SF4*SG7+SE4*SF6*SG7)*V7)*eq*M11...
+((SF7*SG5*SH4-SF5*SG7*SH4-SF7*SG4*SH5+SF4*SG7*SH5+SF5*SG4*SH7-...
SF4*SG5*SH7)*V4+(SE7*SG5*SH4-SE5*SG7*SH4-SE7*SG4*SH5+SE4*SG7*SH5+...
SE5*SG4*SH7-SE4*SG5*SH7)*V5+(SE7*SF5*SH4-SE5*SF7*SH4-SE7*SF4*SH5+...
SE4*SF7*SH5+SE5*SF4*SH7-SE4*SF5*SH7)*V6+(SE7*SF5*SG4-SE5*SF7*SG4-...
SE7*SF4*SG5+SE4*SF7*SG5+SE5*SF4*SG7-SE4*SF5*SG7)*V7)*eq*M12...
+((SF7*SG5*SH4-SF5*SG7*SH4-SF7*SG4*SH5+SF4*SG7*SH5+SF5*SG4*SH7-...
SF4*SG5*SH7)*V4+(SE7*SG5*SH4-SE5*SG7*SH4-SE7*SG4*SH5+SE4*SG7*SH5+...
SE5*SG4*SH7-SE4*SG5*SH7)*V5+(SE7*SF5*SH4-SE5*SF7*SH4-SE7*SF4*SH5+...
SE4*SF7*SH5+SE5*SF4*SH7-SE4*SF5*SH7)*V6+(SE7*SF5*SG4-SE5*SF7*SG4-...
SE7*SF4*SG5+SE4*SF7*SG5+SE5*SF4*SG7-SE4*SF5*SG7)*V7)*eq*M13...
+((-SF6*SG5*SH4+SF5*SG6*SH4+SF6*SG4*SH5-SF4*SG6*SH5-SF5*SG4*SH6+...
SF4*SG5*SH6)*V4+(-SE6*SG5*SH4+SE5*SG6*SH4+SE6*SG4*SH5-SE4*SG6*SH5-...
SE5*SG4*SH6+SE4*SG5*SH6)*V5+(-SE6*SF5*SH4+SE5*SF6*SH4+SE6*SF4*SH5-...
SE4*SF6*SH5-SE5*SF4*SH6+SE4*SF5*SH6)*V6+(-SE6*SF5*SG4+SE5*SF6*SG4+...
SE6*SF4*SG5-SE4*SF6*SG5-SE5*SF4*SG6+SE4*SF5*SG6)*V7)*eq*M14...
+((-SF6*SG5*SH4+SF5*SG6*SH4+SF6*SG4*SH5-SF4*SG6*SH5-SF5*SG4*SH6+...
SF4*SG5*SH6)*V4+(-SE6*SG5*SH4+SE5*SG6*SH4+SE6*SG4*SH5-SE4*SG6*SH5-...
SE5*SG4*SH6+SE4*SG5*SH6)*V5+(-SE6*SF5*SH4+SE5*SF6*SH4+SE6*SF4*SH5-...
SE4*SF6*SH5-SE5*SF4*SH6+SE4*SF5*SH6)*V6+(-SE6*SF5*SG4+SE5*SF6*SG4+...
SE6*SF4*SG5-SE4*SF6*SG5-SE5*SF4*SG6+SE4*SF5*SG6)*V7)*eq*M15-MFB))\...
(VFA+(...
+((-SB3*SC2*SD1+SB2*SC3*SD1+SB3*SC1*SD2-SB1*SC3*SD2-SB2*SC1*SD3+...
SB1*SC2*SD3)*V0+(-SA3*SC2*SD1+SA2*SC3*SD1+SA3*SC1*SD2-SA1*SC3*SD2-...
SA2*SC1*SD3+SA1*SC2*SD3)*V1+(-SA3*SB2*SD1+SA2*SB3*SD1+SA3*SB1*SD2-...
SA1*SB3*SD2-SA2*SB1*SD3+SA1*SB2*SD3)*V2+(-SA3*SB2*SC1+SA2*SB3*SC1+...
SA3*SB1*SC2-SA1*SB3*SC2-SA2*SB1*SC3+SA1*SB2*SC3)*V3)*ep*M0*VFB...
+((-SB3*SC2*SD1+SB2*SC3*SD1+SB3*SC1*SD2-SB1*SC3*SD2-SB2*SC1*SD3+...
SB1*SC2*SD3)*V0+(-SA3*SC2*SD1+SA2*SC3*SD1+SA3*SC1*SD2-SA1*SC3*SD2-...
SA2*SC1*SD3+SA1*SC2*SD3)*V1+(-SA3*SB2*SD1+SA2*SB3*SD1+SA3*SB1*SD2-...
SA1*SB3*SD2-SA2*SB1*SD3+SA1*SB2*SD3)*V2+(-SA3*SB2*SC1+SA2*SB3*SC1+...
SA3*SB1*SC2-SA1*SB3*SC2-SA2*SB1*SC3+SA1*SB2*SC3)*V3)*ep*M1*VFB...
+((SB3*SC2*SD0-SB2*SC3*SD0-SB3*SC0*SD2+SB0*SC3*SD2+SB2*SC0*SD3-...
SB0*SC2*SD3)*V0+(SA3*SC2*SD0-SA2*SC3*SD0-SA3*SC0*SD2+SA0*SC3*SD2+...
SA2*SC0*SD3-SA0*SC2*SD3)*V1+(SA3*SB2*SD0-SA2*SB3*SD0-SA3*SB0*SD2+...
SA0*SB3*SD2+SA2*SB0*SD3-SA0*SB2*SD3)*V2+(SA3*SB2*SC0-SA2*SB3*SC0-...
SA3*SB0*SC2+SA0*SB3*SC2+SA2*SB0*SC3-SA0*SB2*SC3)*V3)*ep*M2*VFB...
+((SB3*SC2*SD0-SB2*SC3*SD0-SB3*SC0*SD2+SB0*SC3*SD2+SB2*SC0*SD3-...
SB0*SC2*SD3)*V0+(SA3*SC2*SD0-SA2*SC3*SD0-SA3*SC0*SD2+SA0*SC3*SD2+...
SA2*SC0*SD3-SA0*SC2*SD3)*V1+(SA3*SB2*SD0-SA2*SB3*SD0-SA3*SB0*SD2+...
SA0*SB3*SD2+SA2*SB0*SD3-SA0*SB2*SD3)*V2+(SA3*SB2*SC0-SA2*SB3*SC0-...
```

```
    SA3*SB0*SC2+SA0*SB3*SC2+SA2*SB0*SC3-SA0*SB2*SC3)*V3)*ep*M3*VFB...
    +((-SB3*SC1*SD0+SB1*SC3*SD0+SB3*SC0*SD1-SB0*SC3*SD1-SB1*SC0*SD3+...
    SB0*SC1*SD3)*V0+(-SA3*SC1*SD0+SA1*SC3*SD0+SA3*SC0*SD1-SA0*SC3*SD1-...
    SA1*SC0*SD3+SA0*SC1*SD3)*V1+(-SA3*SB1*SD0+SA1*SB3*SD0+SA3*SB0*SD1-...
    SA0*SB3*SD1-SA1*SB0*SD3+SA0*SB1*SD3)*V2+(-SA3*SB1*SC0+SA1*SB3*SC0+...
    SA3*SB0*SC1-SA0*SB3*SC1-SA1*SB0*SC3+SA0*SB1*SC3)*V3)*ep*M4*VFB...
    +((-SB3*SC1*SD0+SB1*SC3*SD0+SB3*SC0*SD1-SB0*SC3*SD1-SB1*SC0*SD3+...
    SB0*SC1*SD3)*V0+(-SA3*SC1*SD0+SA1*SC3*SD0+SA3*SC0*SD1-SA0*SC3*SD1-...
    SA1*SC0*SD3+SA0*SC1*SD3)*V1+(-SA3*SB1*SD0+SA1*SB3*SD0+SA3*SB0*SD1-...
    SA0*SB3*SD1-SA1*SB0*SD3+SA0*SB1*SD3)*V2+(-SA3*SB1*SC0+SA1*SB3*SC0+...
    SA3*SB0*SC1-SA0*SB3*SC1-SA1*SB0*SC3+SA0*SB1*SC3)*V3)*ep*M5*VFB...
    +((SB2*SC1*SD0-SB1*SC2*SD0-SB2*SC0*SD1+SB0*SC2*SD1+SB1*SC0*SD2-...
    SB0*SC1*SD2)*V0+(-SA2*SC1*SD0+SA1*SC2*SD0+SA2*SC0*SD1-SA0*SC2*SD1-...
    SA1*SC0*SD2+SA0*SC1*SD2)*V1+(SA2*SB1*SD0-SA1*SB2*SD0-SA2*SB0*SD1+...
    SA0*SB2*SD1+SA1*SB0*SD2-SA0*SB1*SD2)*V2+(SA2*SB1*SC0-SA1*SB2*SC0-...
    SA2*SB0*SC1+SA0*SB2*SC1+SA1*SB0*SC2-SA0*SB1*SC2)*V3)*ep*M6*VFB...
    +((SB2*SC1*SD0-SB1*SC2*SD0-SB2*SC0*SD1+SB0*SC2*SD1+SB1*SC0*SD2-...
    SB0*SC1*SD2)*V0+(-SA2*SC1*SD0+SA1*SC2*SD0+SA2*SC0*SD1-SA0*SC2*SD1-...
    SA1*SC0*SD2+SA0*SC1*SD2)*V1+(SA2*SB1*SD0-SA1*SB2*SD0-SA2*SB0*SD1+...
    SA0*SB2*SD1+SA1*SB0*SD2-SA0*SB1*SD2)*V2+(SA2*SB1*SC0-SA1*SB2*SC0-...
    SA2*SB0*SC1+SA0*SB2*SC1+SA1*SB0*SC2-SA0*SB1*SC2)*V3)*ep*M7*VFB+MFA*VFB));
Bq=VFB+(...
    +((SF7*SG6*SH5-SF6*SG7*SH5-SF7*SG5*SH6+SF5*SG7*SH6+SF6*SG5*SH7-...
    SF5*SG6*SH7)*V4+(SE7*SG6*SH5-SE6*SG7*SH5-SE7*SG5*SH6+SE5*SG7*SH6+...
    SE6*SG5*SH7-SE5*SG6*SH7)*V5+(SE7*SF6*SH5-SE6*SF7*SH5-SE7*SF5*SH6+...
    SE5*SF7*SH6+SE6*SF5*SH7-SE5*SF6*SH7)*V6+(SE7*SF6*SG5-SE6*SF7*SG5-...
    SE7*SF5*SG6+SE5*SF7*SG6+SE6*SF5*SG7-SE5*SF6*SG7)*V7)*eq*M8...
    +((SF7*SG6*SH5-SF6*SG7*SH5-SF7*SG5*SH6+SF5*SG7*SH6+SF6*SG5*SH7-...
    SF5*SG6*SH7)*V4+(SE7*SG6*SH5-SE6*SG7*SH5-SE7*SG5*SH6+SE5*SG7*SH6+...
    SE6*SG5*SH7-SE5*SG6*SH7)*V5+(SE7*SF6*SH5-SE6*SF7*SH5-SE7*SF5*SH6+...
    SE5*SF7*SH6+SE6*SF5*SH7-SE5*SF6*SH7)*V6+(SE7*SF6*SG5-SE6*SF7*SG5-...
    SE7*SF5*SG6+SE5*SF7*SG6+SE6*SF5*SG7-SE5*SF6*SG7)*V7)*eq*M9...
    +((-SF7*SG6*SH4+SF6*SG7*SH4+SF7*SG4*SH6-SF4*SG7*SH6-SF6*SG4*SH7+...
    SF4*SG6*SH7)*V4+(-SE7*SG6*SH4+SE6*SG7*SH4+SE7*SG4*SH6-SE4*SG7*SH6-...
    SE6*SG4*SH7+SE4*SG6*SH7)*V5+(-SE7*SF6*SH4+SE6*SF7*SH4+SE7*SF4*SH6-...
    SE4*SF7*SH6-SE6*SF4*SH7+SE4*SF6*SH7)*V6+(-SE7*SF6*SG4+SE6*SF7*SG4+...
    SE7*SF4*SG6-SE4*SF7*SG6-SE6*SF4*SG7+SE4*SF6*SG7)*V7)*eq*M10...
    +((-SF7*SG6*SH4+SF6*SG7*SH4+SF7*SG4*SH6-SF4*SG7*SH6-SF6*SG4*SH7+...
    SF4*SG6*SH7)*V4+(-SE7*SG6*SH4+SE6*SG7*SH4+SE7*SG4*SH6-SE4*SG7*SH6-...
    SE6*SG4*SH7+SE4*SG6*SH7)*V5+(-SE7*SF6*SH4+SE6*SF7*SH4+SE7*SF4*SH6-...
    SE4*SF7*SH6-SE6*SF4*SH7+SE4*SF6*SH7)*V6+(-SE7*SF6*SG4+SE6*SF7*SG4+...
    SE7*SF4*SG6-SE4*SF7*SG6-SE6*SF4*SG7+SE4*SF6*SG7)*V7)*eq*M11...
    +((SF7*SG5*SH4-SF5*SG7*SH4-SF7*SG4*SH5+SF4*SG7*SH5+SF5*SG4*SH7-...
    SF4*SG5*SH7)*V4+(SE7*SG5*SH4-SE5*SG7*SH4-SE7*SG4*SH5+SE4*SG7*SH5+...
    SE5*SG4*SH7-SE4*SG5*SH7)*V5+(SE7*SF5*SH4-SE5*SF7*SH4-SE7*SF4*SH5+...
    SE4*SF7*SH5+SE5*SF4*SH7-SE4*SF5*SH7)*V6+(SE7*SF5*SG4-SE5*SF7*SG4-...
    SE7*SF4*SG5+SE4*SF7*SG5+SE5*SF4*SG7-SE4*SF5*SG7)*V7)*eq*M12...
    +((SF7*SG5*SH4-SF5*SG7*SH4-SF7*SG4*SH5+SF4*SG7*SH5+SF5*SG4*SH7-...
    SF4*SG5*SH7)*V4+(SE7*SG5*SH4-SE5*SG7*SH4-SE7*SG4*SH5+SE4*SG7*SH5+...
    SE5*SG4*SH7-SE4*SG5*SH7)*V5+(SE7*SF5*SH4-SE5*SF7*SH4-SE7*SF4*SH5+...
    SE4*SF7*SH5+SE5*SF4*SH7-SE4*SF5*SH7)*V6+(SE7*SF5*SG4-SE5*SF7*SG4-...
    SE7*SF4*SG5+SE4*SF7*SG5+SE5*SF4*SG7-SE4*SF5*SG7)*V7)*eq*M13...
    +((-SF6*SG5*SH4+SF5*SG6*SH4+SF6*SG4*SH5-SF4*SG6*SH5-SF5*SG4*SH6+...
    SF4*SG5*SH6)*V4+(-SE6*SG5*SH4+SE5*SG6*SH4+SE6*SG4*SH5-SE4*SG6*SH5-...
    SE5*SG4*SH6+SE4*SG5*SH6)*V5+(-SE6*SF5*SH4+SE5*SF6*SH4+SE6*SF4*SH5-...
    SE4*SF6*SH5-SE5*SF4*SH6+SE4*SF5*SH6)*V6+(-SE6*SF5*SG4+SE5*SF6*SG4+...
    SE6*SF4*SG5-SE4*SF6*SG5-SE5*SF4*SG6+SE4*SF5*SG6)*V7)*eq*M14...
    +((-SF6*SG5*SH4+SF5*SG6*SH4+SF6*SG4*SH5-SF4*SG6*SH5-SF5*SG4*SH6+...
    SF4*SG5*SH6)*V4+(-SE6*SG5*SH4+SE5*SG6*SH4+SE6*SG4*SH5-SE4*SG6*SH5-...
    SE5*SG4*SH6+SE4*SG5*SH6)*V5+(-SE6*SF5*SH4+SE5*SF6*SH4+SE6*SF4*SH5-...
    SE4*SF6*SH5-SE5*SF4*SH6+SE4*SF5*SH6)*V6+(-SE6*SF5*SG4+SE5*SF6*SG4+...
    SE6*SF4*SG5-SE4*SF6*SG5-SE5*SF4*SG6+SE4*SF5*SG6)*V7)*eq*M15-MFB)*Ap;
end
function d=kdelta(n,m)
if n==m
    d=1;
else
    d=0;
end
end
```

Bibliography

[1] J. W. Miles, "The analysis of plane discontinuities in cylindrical tubes. Part I", Journal of the Acoustical Society of America, **17**(3), 259-271, (1946).

[2] H. Levine and J. Schwinger, "On the radition of sound from an unflanged circular pipe", Physical Review, **73**(4), 383-406, (1948).

[3] U. Ingárd, "On the radiation of sound into a circular tube, with an application to resonators", Journal of the Acoustical Society of America, **20**(5), 665-682, (1948).

[4] F. C. Karal, "The analogous acoustical impedance for discontinuities and constrictions of circular cross section", Journal of the Acoustical Society of America, **25**(2), 327-334, (1953).

[5] A. Cummings, "Sound transmission at sudden area exapansions in circular ducts, with superimposed mean flow", Journal of Sound and Vibration, **38**, 149-155, (1975).

[6] D. Ronneberger, "Experimentelle untersuchungen zum akustischen reflexionsfaktor von unstetigen querschnittsänderungen in einem luftdurchströmten rohr", Acustica, **19**, 222-235, (1967).

[7] M. L. Munjal, "Velocity ratio-cum-transfer matrix method for the evaluation of a muffler with mean flow", Journal of Sound and Vibration, **39**(1), 105-119, (1975).

[8] K. S. Peat, "Evaluation of four-pole parameters for ducts with flow by the finite element method", Journal of Sound and Vibration, **84**(3), 389-395, (1982).

[9] M. L. Munjal and M. G. Prasad, "On plane-wave propagation in a uniform pipe in the presence of a mean flow and a temperature gradient", Journal of the Acoustical Society of America, **80**(5), 1501-1506, (1986).

[10] C. I. J. Young, "Acoustic analysis of mufflers for engine exhuast systems", Ph.D thesis School of Mechanical Engineering, Purdue University, Appendix IV, (1973).

[11] K. S. Peat, "The transfer matrix of a uniform duct with a linear temperature gradient", Journal of Sound and Vibration, **123**(1), 43-53, (1988).

[12] R. I. Sujith, "Transfer matrix of a uniform duct with an axial mean temperature gradient", Journal of the Acoustical Society of America, **100**(4), 2540-2542, (1996).

[13] A. M. Cargill, "Low frequency acoustic radiation from a jet pipe -a second order theory", Journal of Sound and Vibration, **83**(3), 339-354, (1982).

[14] R. M. Munt, "The interaction of sound with a subsonic jet issuing from a semi-infinite cylindrical pipe", Journal of Fluid Mechanics, **83**, 609-640, (1977).

[15] J. Ih and B. Lee, "Analysis of higher-order mode effects in the circular expansion chamber with mean flow", Journal of the Acoustical Society of America, **77**(4), 1377-1388, (1985).

[16] S. Yi and B. Lee, "Three-dimensional acoustic analysis of a circular expansion chamber with side inlet and end outlet", Journal of the Acoustical Society of America, **81**(5), 1279-1287, (1987).

[17] K. S. Peat, "The acoustical impedance at discontinuities of ducts in the presence of a mean flow", Journal of Sound and Vibration, **127**(1), 123-132, (1988).

[18] J. B. Lawrie and I. D. Abrahams, "Acoustic radiation from two opposed semi-infinite coaxial cylindrical wavesguides. II: separated ducts", Wave Motion, **19**, 83-109, (1994).

[19] A. D. Sahasrabudhe and M. L. Munjal, "Analysis of inertance due to the higher order mode effects in a sudden area discontinuity", Journal of Sound and Vibration, **185**(3), 515-529, (1995).

[20] R. Kirby, "A comparison between analytic and numerical methods for modelling automative dissipative silencers with mean flow", Journal of Sound and Vibration, **325**, 565-582, (2009).

[21] D. Homentcovschi and R. N. Miles, "Re-expansion method for circular waveguide discontinuities: application to concentric expansion chambers", Journal of the Acoustical Society of America, **131**(2), 1158-1171, (2012).

[22] S. Föller and W. Polifke, "Identification of aero-acoustic scattering matrices from large eddy simulation. Application to a sudden area expansion of a duct", Journal of Sound and Vibration, **331**, 3096-3113, (2012).

[23] J. Smagorinsky, "General circulation experiments with the primitive equations", Monthly Weather Review, **91**(3), 99164, (1963).

[24] E. Perrey-Debain, R. Maréchal, J. M. Ville, "Side-branch resonators modelling with Green's function methods", Journal of Sound and Vibration, **333**, 4458-4472, (2014).

[25] A. W. Leissa "Vibration of Shells", NASA, SP-288 (1973).

[26] C. B. Burroughs, "Acoustic radiation from fluid-loaded infinite circular cylinders with doubly periodic ring supports", Journal of the Acoustical Society of America, **75**(3), 715-722, (1984).

[27] E. H. Kennard, "The new approach to shell theory: circular cylinders", Journal of Applied Mechanics, **20**, 33-40, (1953).

[28] J. B. Lawrie, "Vibrations of a heavily loaded, semi-infinite, cylindrical elastic shell. I", Proceeedings of the Royal Society of London, **408**, 103-128, (1986).

[29] J. B. Lawrie, "An infinite, elastic, cylindrical shell with a finite number of ring constraints", Journal of Sound and Vibration, **130**(2), 189-206, (1989).

[30] M.C. Junger and D. Feit "Sound, structures, and their interaction", MIT Press, (1972).

[31] P. Stepanishen and R. A. Touga, Jr. "Transient acoustic pressure radiated from a finite duct", Journal of the Acoustical Society of America, **93**(6), 3074-3084, (1993).

[32] B. Zhang and I. D. Abrahams, "The radiation of sound from a finite ring-forced cylindrical elastic shell", Proceedings of the Royal Society A **450**, 89-108, (1995).

[33] E. A. Skelton, "Line force receptance of an elastic cylindrical shell with heavy exterior fluid loading", Journal of Sound and Vibration, **256**(1), 131-153, (2001).

[34] E. A. Skelton, "Acoustic scattering by a cylindrical shell with symmetirc line constraints in the heavy fluid-loading limit", Journal of the Acoustical Society of America, **113**(1), 299-308, (2003).

[35] E. J. Brambley and N. Peake, "Stability and acoustic scattering in a cylindrical thin shell containing compressible mean flow", Journal of Fluid Mechanics, **602**, 403-426, (2008).

[36] M. Caresta and N.J. Kessissoglou, "Structural and acoustic responses of a fluid-loaded cylindrical hull with structural discontinuities, *Applied Acoustics*, **70**(7), 954-963, (2009).

[37] R. Kirby, Z. Zlatev and P. Mudge, "On the scattering of longitudinal elastic waves from axisymmetric defects in coated pipes, *Journal of Sound and Vibration*, **332**, 5040-5058, (2013).

[38] M. Xie, J. Ih, T. Kim and Y. Li, "Prediction of Acoustic Power Transmission of Fluid-Filled Thin Pipe Based on Impedance-Mobility Approach", International Journal of Aerospace Lightweight Structures, 135-151, (2013).

[39] Z. Y. Cao, "Vibration theory of plates and shells", China Railway Publishing House, Beijing, (1983).

[40] H. Lee and M. K. Kwak, "Free vibration analysis of a circular cylindrical shell using the Raleigh-Ritz method and comparison of different shell theories", Journal of Sound and Vibration, **353**, 344-377, (2015).

[41] M. Abramowitz and I. A. Stegun "Handbook of Mathematical Functions", Dover Publications, 9th edition, (1964).

[42] D. G. Crighton, A. P. Dowling, J. E. Ffowcs Williams, M. A. Heckl, F. A. Leppington, "Modern Methods in Analytical Acoustics", Springer-Verlag, (1992).

[43] D. P. Warren, J.B. Lawrie and I.M. Mohamed "Acoustic scattering in waveguides that are discontinuous in geometry and material property", Wave Motion **36**, 119-142 (2002).

[44] J. B. Lawrie "Comments on a class of orthogonality relations relevant to fluid-struture interaction", Springer, (2006).

[45] R. Nawaz and J.B. Lawrie, "Scattering of a fluid-structure coupled wave at a flanged junction between two flexible waveguides, *Journal of the Acoustical Society of America*, **134**(3), 1939-1949, (2013).

[46] J. B. Lawrie "On eigenfunction expansions associated with wave propagation along ducts with wave-bearing boundaries", IMA Journal of Applied Mathematics, 376-394, (2007).

[47] J.W. Brown and R.V. Churchill, "Fourier series and Boundary value problems", McGraw Hill, 241-297, (2008).

[48] J. B. Lawrie and I.D. Abrahams, "An orthogonality relation for a class of problems with high-order boundary conditions; applications in sound-structure interaction", The Quarterly Journal of Mechanics and Applied Mathematics, 161-181, (1999).

[49] J. B. Lawrie, "On acoustic propagation in three-dimensional rectangular ducts with flexible walls and porous linings, *Journal of the Acoustical Society of America*, **131**(3), 1890-1901, (2012).

[50] J. B. Lawrie, "Analytic mode-matching for acoustic scattering in three dimensional waveguides with flexible walls: Application to a triangular duct, *Wave Motion*, **50**, 542-557, (2013).

[51] R .M. Pullen and J. B. Lawrie, "Reflection and transmission at the junction between two sections of circular cylindrical shell", ICSV21, Beijing, China, 1-7, (2014).